T.R.

GEBZE TECHNICAL UNIVERSITY

GRADUATE SCHOOL OF NANOTECHNOLOGY

HIGH-THROUGHPUT COMPUTATIONAL SCREENING OF MXENE FOR CO_2 CAPTURE FROM SYNGAS AND THE EFFECT OF INTERLAYER DISTANCE ON IDEAL GAS SEPARATION

ŞİRİN MASSOUMILARİ

A THESIS SUBMITTED FOR THE DEGREE OF

MASTER OF SCIENCE

DEPARTMENT OF NANOSCIENCE AND NANOENGINEERING

GEBZE

2022

T.R.

GEBZE TECHNICAL UNIVERSITY

GRADUATE SCHOOL OF NANOTECHNOLOGY

HIGH-THROUGHPUT COMPUTATIONAL SCREENING OF MXENE FOR CO_2 CAPTURE FROM SYNGAS AND THE EFFECT OF INTERLAYER DISTANCE ON IDEAL GAS SEPARATION

ŞİRİN MASSOUMILARİ

A THESIS SUBMITTED FOR THE DEGREE OF MASTER OF SCIENCE

DEPARTMENT OF NANOSCIENCE AND NANOENGINEERING

THESIS SUPERVISOR

ASSISTANT PROFESSOR SADİYE VELİOĞLU

GEBZE

2022

T.C.
GEBZE TEKNİK ÜNİVERSİTESİ
NANOTEKNOLOJİ ENSTİTÜSÜ

SENTEZ GAZINDAN CO_2 YAKALANMASI İÇİN MXENE'LERİN ADSORPSİYON PERFORMANSLARININ YÜKSEK VERİMLİ HESAPLAMALI YÖNTEM İLE TARANMASI VE ARA KATMAN MESAFESİNİN İDEAL GAZ AYRIMI ÜZERİNDEKİ ETKİSİ

ŞİRİN MASSOUMILARİ

YÜKSEK LİSANS TEZİ
NANOBİLİM VE NANOMÜHENDİSLİK ANABİLİM DALI

DANIŞMANI
DR. ÖĞRETİM ÜYESİ SADİYE VELİOĞLU

GEBZE
2022

GEBZE TEKNİK ÜNİVERSİTESİ	YÜKSEK LİSANS JÜRİ ONAY FORMU

GTÜ Nanoteknoloji Enstitüsü Yönetim Kurulu'nun 19/01/2022 tarih ve 2022/02 sayılı kararıyla oluşturulan jüri tarafından 20/01/2022 tarihinde tez savunma sınavı yapılan Şirin Massoumilari'nin tez çalışması Nanobilim ve Nanomühendislik Anabilim Dalında YÜKSEK LİSANS tezi olarak kabul edilmiştir.

JÜRİ

ÜYE
(TEZ DANIŞMANI) : Dr. Öğretim Üyesi Sadiye VELİOĞLU

ÜYE : Dr. Öğretim Üyesi İlknur ERUÇAR FINDIKÇI

ÜYE : Dr. Öğretim Üyesi Osman EKSİK

ONAY

Gebze Teknik Üniversitesi Nanoteknoloji Enstitüsü Yönetim Kurulu'nun
…..…/…..…/..…..… tarih ve ……/…….. sayılı kararı.

İMZA/MÜHÜR

SUMMARY

The use of fossil fuels accounts for 90% of global energy consumption. However, as its usage increases, greenhouse gases such as CO_2 accumulates in the atmosphere resulting in global warming. Besides to the increments of sea levels all over the world, this also leads a breakage of ecological chain irreversibly. In this sense, it is crucial to separate CO_2, which is generated during syngas production, from H_2, especially considering the decreasing energy resources. Although different separation processes are available, adsorption is mostly preferred due to its reversibility, and high separation performance. In this thesis, adsorption-based separation performances of novel MXene nanomaterials for CO_2/H_2 separation are investigated. MXene database is created and some of its members are optimized. CO_2 and H_2 uptakes are examined by grand canonical Monte Carlo simulation and several adsorbent metrics are computed. To identify the effect of interlayer spacing of MXenes on the adsorption selectivity, after interlayer distance is enhanced, simulations are repeated. The promising 10 MXene structures for Pressure Swing Adsorption (PSA) and Vacuum Swing Adsorption (VSA) processes were revealed according to some metrics. Among the MXenes with short interlayer distance, four MXene structures, $Ti_{0.4}Nb_{1.6}C$, $V_2Ti_2C_3$, Ti_2VC_2, $Ti_{1.2}Nb_{0.8}C$, containing double metal, and unsaturated surface are noteworthy for both PSA and VSA. After enhancement of interlayer distance, MXenes containing double metal and bulky functional groups of $–(NCS_2)$ stand out for both processes. In general, after increasing the interlayer distance for PSA, the CO_2 working capacity increased, while the adsorption selectivity decreased. The results obtained from this thesis will lead to the use of MXene family as a novel adsorbent material and to guide the experimental studies.

Keywords: MXene Nanomaterials, Adsorption Process, CO_2/H_2 Separation, GCMC Simulations.

ÖZET

Fosil yakıtların kullanımı, küresel enerji tüketiminin %90'ını oluşturmaktadır. Ancak fosil yakıt kullanımı arttıkça CO_2 gibi sera gazları atmosferde birikerek küresel ısınmaya neden olmaktadır. Tüm dünyada deniz seviyelerinin yükselmesinin yanı sıra bu aynı zamanda ekolojik zincirin geri dönüşü olmayan bir şekilde kırılmasına da yol açacaktır. Bu anlamda, özellikle de azalan enerji kaynakları göz önüne alındığında H_2 üretimi sırasında ortaya çıkan CO_2'in H_2'den ayrılması önem arz etmektedir. Bunun için farklı ayırma prosesleri kullanılsa da işlemin geri dönüşümlü olması ve yüksek ayırma sağlayabilmesinden dolayı en çok adsorpsiyon tercih edilmektedir. Bu tezde, yeni ve özgün bir malzeme ailesi olan MXene'lerin adsorpsiyon temelli CO_2/H_2 ayırma için performanslarının incelenmesi hedeflenmiştir. Öncelikle geniş malzeme çeşidine sahip kütüphane oluşturulup, bazı fertlerinin yapısı optimize edilmiştir. Monte Carlo simülasyonu yardımıyla CO_2 ve H_2 adsorpsiyon kapasiteleri hesaplanmış ve bunlar kullanılarak çeşitli gaz adsorbent ölçütleri irdelenmiştir. Ayrıca, MXene' nin katmanlar arası mesafesinin adsorpsiyon seçiciliğine etkisini belirlemek için, ara katman mesafesinin arttırılması sonrası simülasyonlar tekrar yapılmıştır. Hem basınç salınımlı adsorpsiyon hem de vakum salınımlı adsorpsiyon için en iyi performans sergileyen 10 MXene yapısı sıralanmıştır. Ara katman mesafesi dar olan MXene'ler için her iki proseste de Titanyum elementi içeren ve yüzeyi doyurulmamış 4 MXene, $Ti_{0.4}Nb_{1.6}C$, $V_2Ti_2C_3$, Ti_2VC_2, $Ti_{1.2}Nb_{0.8}C$, yapısı dikkati çekmektedir. Ara katman mesafesi arttırıldıktan sonra ise çift metal içeren ve $-(NCS_2)$ gibi büyük fonksiyonel grupları içeren MXene yapıları her iki adsorpsiyon işlemi için öne çıkmaktadır. Genel anlamda, basınç salınımlı adsorpsiyon işlemi için ara katman mesafesinin artması sonrasında CO_2 çalışma kapasitesi artarken adsorpsiyon seçiciliği azalmıştır. Bu tezden elde edilen sonuçlar MXene ailesinin yeni bir adsorbent malzemesi olarak kullanımına vesile olacak ve deneysel çalışmaların ilerlemesine ışık tutacaktır.

Anahtar Kelimeler: MXene Nanomalzemesi, Adsorpsiyon Prosesi, CO_2/H_2 Ayırma, Monte Carlo Simülasyonu.

ACKNOWLEDGEMENTS

I would like to present my sincere thanks to my esteemed advisor Dr. Sadiye VELİOĞLU for providing all kinds of support and opportunities since I started my postgraduate program at Institute of Nanotechnology, Gebze Technical University. She was very patient guiding me to study the molecular simulation. I consider myself lucky to have met her.

I would like to thank research assistant, Tuğba BAYSAL, not only contribution to my thesis but also for always being by my side and encouraging me. I would like to thank research assistant, Mehmet Emre AKÖZ for his kindly support. I would like to thank Melih DOĞANCI for his help and support in my thesis.

I would like to express my gratitude to my dear mother, and especially my precious sister for her support when I started postgraduate program.

Finally, I would like to thank my friends in MEM-CES for kindly supports.

All numerical calculations in this thesis have been carried out at TUBITAK ULAKBIM, High Performance and Grid Computing Center using TRUBA resources. Financial support by the Scientific and Technological Research Council of Turkey (TUBITAK, Grant No. 120M180) is acknowledged.

TABLE of CONTENTS

LIST of ABBREVIATIONS and ACRONYMS

Abbreviations and Acronyms		Explanations
ΔH	:	Enthalpy change
ΔG	:	Gibbs free energy change
ΔS	:	Entropy change
P	:	Pressure
T	:	Temperature
q_e	:	Amount of adsorbate at equilibrium
K_{HE}	:	Henry's adsorption constant
C_e	:	Equilibrium concentration of the adsorbate on the adsorbent
K_{FE}	:	Freundlich isotherm constant
n	:	Isotherm type
1/n	:	Heterogeneity of surface
K_L	:	Ratio of adsorption and desorption rates
q_m	:	Maximum adsorption capacity
a_T	:	Toth constant
1/t	:	Heterogeneity of adsorption system
v	:	Volt
t	:	Time
U	:	Potential energy
N	:	Fixed number of atoms
V	:	Volume
E	:	Energy
μ	:	Chemical potential
F_i	:	Force of i_{th} particle
V_i	:	Velocity of i_{th} particle
M_i	:	Mass of i_{th} particle
a_i	:	Acceleration of i_{th} particle
r_i	:	Position of i_{th} particle
Ω	:	Partition function of micro canonical ensemble
Q	:	Partition function of canonical ensemble

Δ	:	Partition function of isothermal-isobaric ensemble
Ξ	:	Partition function of grand canonical ensemble
α_{ads}	:	Adsorption selectivity of one gas to another
α_{des}	:	Desorption selectivity of one gas to another
N_{ads}	:	Gas adsorption capacity
N_{des}	:	Gas desorption capacity
A	:	Gas type
y	:	Gas concentration in the feed stream
AC	:	Activated Carbon
AFM	:	Adsorbent Figure of Merit
APS	:	Adsorbent Performance Score
CCS	:	Carbon Capture Sequestration
C2DB	:	Computational 2D Materials Database
COF	:	Covalent Organic Framework
CoRE COF	:	Computation-Ready Experimental Covalent Organic Framework
CoRE MOF	:	Computation-Ready Experimental Metal Organic Framework
CMS	:	Carbon Molecular Sieve
CNT	:	Carbon Nano Tube
CSD	:	Cambridge Structural Database
CVD	:	Chemical Vapor Deposition
DDEC	:	Density Derived Electrostatic and Chemical Charges
DFT	:	Density Functional Theory
DMSO	:	Dimethyl Sulfoxide
DND	:	Double Numerical plus-D function
ESA	:	Electrical Swing Adsorption
ESP	:	Electrostatic Potential
fcc	:	Face-centered cubic
FTIR	:	Fourier Transform Infrared Spectroscopy
GAW	:	Global Atmosphere Watch
GCMC	:	Grand Canonical Monte Carlo
GHGs	:	Green House Gases
hcp	:	Hexagonal closest packed
HMM	:	Hybrid Material Metric

HTCS	:	High-Throughput Computational Screening
IFMM	:	Intrinsic Functional Material Metric
ISMM	:	Intrinsic Structural Material Metric
LJ	:	Lennard-Jones
MC	:	Monte Carlo
MD	:	Molecular Dynamics
MOF	:	Metal Organic Framework
MSA	:	Mean-Squared Displacement
NMR	:	Nuclear Magnetic Resonance
PAF	:	Porous Aromatic Framework
POC	:	Porous Organic Cage
PSA	:	Pressure swing adsorption
PTSA	:	Pressure temperature swing adsorption
R%	:	Percent regenerability
RFG	:	Recycled Flue Gas
RPSA	:	Rapid Pressure Swing Adsorption
QEq	:	Charge Equilibration
SCC	:	Spearman Correlation Coefficient
SRCC	:	Binary Spearman Correlation Coefficients
SSA	:	Specific surface area
SSP	:	Sorbent Selection Parameter
Syngas	:	Synthesis gas
ToBaCCo	:	Topologically Based Crystal Constructor
TraPPE	:	Transferable Potentials for Phase Equilibria
TSA	:	Temperature swing adsorption
UFF	:	Universal force field
US DOE	:	United States Department of Energy
vdW	:	Van der Waals
VSA	:	Vacuum swing adsorption
VTSA	:	Vacuum temperature swing adsorption

LIST of FIGURES

LIST of TABLES

1. INTRODUCTION

With rapid industrialization, global warming has become the most important problem for the humanity. As the amount of the greenhouse gases in the atmosphere increase, increment of temperature will reach to 1.9°C, and sea level also rise about 3.8 meter all over the world by the year 2100 [1]. In addition to the industry, greenhouse gases are also emitted from agriculture and human activity by naturally [2]. The primary Greenhouse Gases (GHGs) are carbon dioxide (CO_2), methane (CH_4), nitrous oxide (NO_2), and ozone (O_3). GHGs can absorb infrared radiation and trap heat energy. CO_2 level has been increased due to the combustion of fossil fuel such as coal, oil, and natural gas directly to meet the energy demands increasing day by day. Moreover, average CO_2 residence time in the atmosphere is found as 4 years [3]. Globally averaged abundances and alterations of CO_2, CH_4, and N_2O in 2020 are listed at Table 1.1. According to Table 1.1, global mean abundance of CO_2 was 413.2 ± 0.2 ppm in 2020 with the highest increase rate of 2.40 ppm/year over the last ten years [4].

Table 1.1. Global annual surface mean abundances (2020) and trends of key GHGs from the Global Atmosphere Watch (GAW) in situ observational network.

	CO_2	CH_4	N_2O
2020 global mean abundance	413.2±0.2 ppm	1889±2 ppb	333.2±0.1 ppb
2019-2020 absolute increase	2.5 ppm	11 ppb	1.2 ppb
2019-2020 relative increase	0.61%	0.59%	0.36%
Mean annual absolute increase over the last 10 years	2.40 ppm/year	8.0 ppb/year	0.99 ppb/year

Three main CO_2 emission sources such as power plants, natural gas, and industrial gas exit [5]. Natural gas streams generally contain CH_4, CO_2, N_2, and higher molecular weight hydrocarbons. Depending on its source, CO_2 amount in natural gas varies between 5-50% and, it must be separated from CH_4 due to its corrosive effect in pipelines and reducing energy efficiency. Considering the coal power plant, steam is created by burning coal in air and this steam is used to run a turbine/generator to produce electricity. However, combustion gases mainly contain N_2 and CO_2, which should be separated from other gases.

Carbon Capture and Sequestration (CCS) technologies was used at power plants and industrial facilities to trap CO_2 in order to reduce its emissions. The main CCS

technologies are pre-combustion, post-combustion, and oxy-fuel combustion carbon capture [6]. For all combustion processes, CO_2 is separated from the other gases by various separation methods. Mainly used separation methods are absorption, adsorption, membrane-based separation, and cryogenic distillation. Considering separation methods, adsorption-based separation is emerged as an efficient method with high adsorption efficiency of CO_2 above 85%. In addition, this method is reversible, and adsorbent can be recycled [7]. For CO_2 adsorption, different materials are examined such as zeolites, silica, Metal-Organic Frameworks (MOFs), activated carbon (AC), Covalent Organic Frameworks (COFs), ordered porous carbon, Carbon Molecular Sieve (CMS), etc. [8].

MXenes have a formula of $M_{n+1}X_nT_x$, M is an early transition metal, X is C or N, T_x shows surface terminations [9]. They become very popular among two dimensional nanomaterials due to its many excellent properties since first discovery in 2011. Some of their important features are large surface area, hydrophilicity, high melting point, and electrical and thermal conductivity. MXenes are examined for various applications such as environmental remediation, catalysis, energy storage, biomedical, sensors, etc. In the last few years, only one MXene type ($Ti_3C_2T_x$) has been tested and successfully used in adsorption studies. Given that MXenes are a large family, we have the chance to design several types of MXenes that will outperform currently being tested ones. However, their experimental synthesis and testing for the separation applications is a very challenging process. Therefore, as an effective tool, molecular simulation methods are started to be applied frequently.

Therefore, the purpose of this thesis is to investigate the CO_2 and H_2 adsorption-based separation potential of MXenes at molecular level which ensures rapidly identification of the promising adsorbent materials. In this thesis, MXene library were created which includes both existing and hypothetical MXene structures, and optimized. CO_2 and H_2 adsorption performance of all optimized MXenes were examined by molecular simulation technique named as Grand Canonical Monte Carlo (GCMC). Single gas adsorption capacities of MXenes were evaluated in according to the performance evaluation metrics. The high-throughput computational screening allows us to investigate all MXene types to determine their adsorption-based separation performance with a cost and time-effective manner. Definition of top performing MXene types for separation of CO_2 from H_2 will guide and support the experimental studies that will be carried out in the future. MXene library created in

this thesis will support the researchers to enlarge the library more resulted in more sophisticated MXene database in the future.

2. CO_2 CAPTURE AND SEQUESTRATION

CO_2 capture and sequestration (CCS) is emerged as one of the most important issue to combat global climate changes. The usage of renewable energy sources such as solar, wind or nuclear energy is emerged as an alternative way to reduce the accumulation of CO_2 in the atmosphere. However, CCS is the most effective solution to mitigate emissions of greenhouse gases.

CCS is consisted of emissions of greenhouse gases produced by industrial power plants and industrial facilities capture, transportation and storage in geological sites. Three main CO_2 capture processes are,

- Pre-Combustion Capture,
- Post-Combustion Capture,
- Oxy-fuel Combustion.

In this section, firstly main sources for CO_2 emissions will be provided. Then, adsorption-based separation processes that are highly used for CCS will be discussed. Finally, frequently encountered adsorption isotherm types and preferred models are going to be given.

2.1. Sources for CO_2 Emissions

2.1.1. Pre-combustion

The fuel such as coal or natural gas first oxidized in steam and mixed with air. Syngas (synthesis gas) is obtained at high temperature including mixture of CO, H_2, CO_2, and low amount of CH_4. This process is named as gasification. Following gasification, CO_2 and H_2 are obtained via water-gas shift reaction by conversion of carbon monoxide and water with the addition of steam and reduction of temperature as depicted in Figure 2.1 [10-12]. After pre-combustion method, CO_2 is captured from

mixture and purified H_2 is used for different areas as clean fuel. Concentrated CO_2 gas is removed at high pressure before combustion of H_2 by water-gas shift reaction.

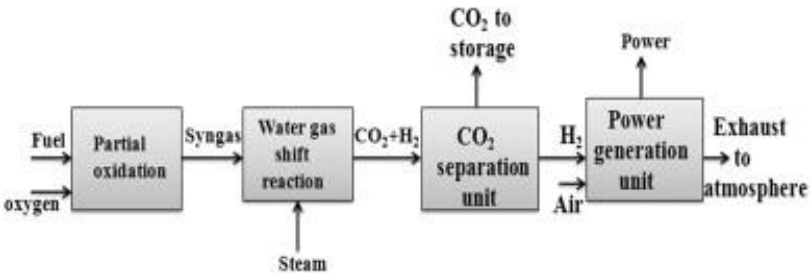

Figure 2.1: Principle of pre-combustion CO_2 capture.

2.1.2. Post-combustion

Different from pre-combustion, removal of CO_2 takes place after combustion process as shown in Figure 2.2 [10-12]. Generally, power plants preferred post-combustion processes that use air and produce a flue gas at atmospheric pressure. This flue gas includes low CO_2 concentration such as 13-15% for coal fired power plant or 7-8% gas fired power plant [13, 14]. Even CO_2 exists at low concentration, high cost and large equipment are required to handle more CO_2. Add to the CO_2, larger amounts of dust, CO, SO_x, and NO_x are also present in the flue gas mixture, which degrade the capture materials.

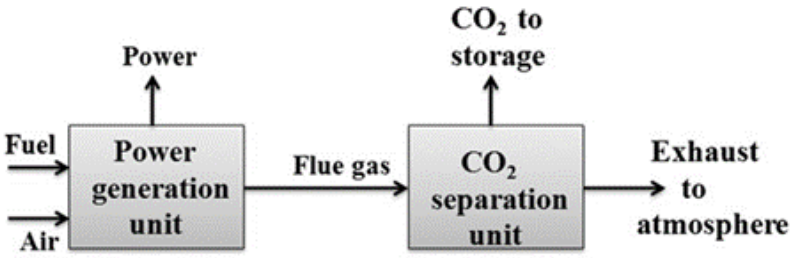

Figure 2.2: Principle of post-combustion CO_2 capture

2.1.3. Oxy-fuel combustion

Fossil fuel is added into a chamber at atmospheric conditions as pictured in Figure 2.3 [1]. The fuel gas is mixed with O_2 having purity of >95% for combustion. Flue gas mixture from the combustion process mostly consists of CO_2 and H_2O. CO_2

is separated via physical separation and compression process while water is deported by condensation [1]. Purity of CO_2 is generally varied between 70-95% related to the fuel quality, process type, and amount of O_2. However, the power consumption of this unit is high, and it requires the use of Recycled Flue Gas (RFG).

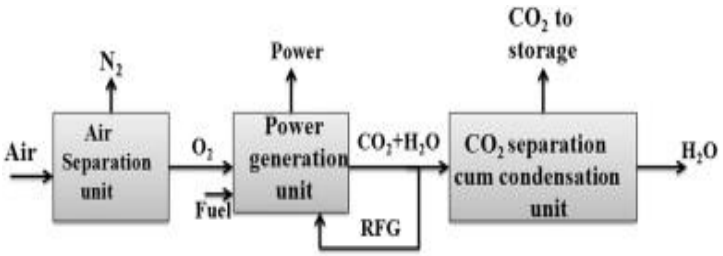

Figure 2.3: Principle of oxy-fuel combustion CO_2 capture

Each CO_2 capture process has its own advantages and disadvantages. Main advantage and disadvantages of three processes are listed comparatively at Table 2.1 [5].

Table 2.1: Comparison of CO_2 capture processes.

Method	Advantages	Disadvantages
Pre-combustion	High CO_2 levels, easy separation	Complicated process, high cost
Post-combustion	Simple process, more branches	Low CO_2 levels
Oxy-fuel combustion	High CO_2 levels, low cost of separation	High cost of oxygen supply

2.2. Adsorption-Based CO_2 Separation

Expectation from available CCS technology is to remove 90% of CO_2 with a purity of 95% [15]. However, considering combustion steps of three CCS methods, CO_2 is fed to the separation unit with other gases together. Within the scope of this thesis, pre-combustion process which includes CO_2 and H_2 gases are aimed to be investigated. The main technologies for the separation of CO_2 from H_2 are absorption, adsorption, chemical looping combustion, membrane separation and cryogenic distillation. Absorption is the most mature process for CO_2 separation. However, process efficiency depends on the CO_2 concentration. Absorbent regeneration is required high amount of heat [16-18]. Development for chemical looping combustion

process is still ongoing, and there is not any large-scale application [19]. Membrane separation is suffered from operational problems such as low flux and fouling [18, 20, 21]. Although cryogenic distillation is adopted for many years in industry, it is effective only at high CO_2 concentration (>90% v/v) [22, 23]. In the end, adsorption is appeared suitable for large plants compared to the other separation methods.

Adsorption is the removal of components from either gas or liquid stream by solid adsorbents. Adsorption was emerged as an alternative approach against to the common solvent based carbon capture process. Since early 1990's, adsorption process continues to grow. The first advantage of adsorption-based separation is that the process is reversible. The second advantage is the adsorbent can be recycled in the process [24-27]. With this process, high adsorption efficiency of above 85% was reached [24-27]. However, requirements of high energy and adsorbents with high resistance to heat are the main disadvantages. Temperature, partial pressure, and adsorbent structure affect the adsorption capacity of adsorbents for components. Intermolecular forces between gases such as CO_2 and surface of solid adsorbents are formed the basis of separation. Adsorption process is carried out by the consecutive two basic steps; adsorption and desorption which are illustrated in Figure 2.4 [28]. Adsorption step is governed by the technical efficiency whereas desorption provides economical sustainability. The balance between adsorption and desorption steps dominates the success of this separation process.

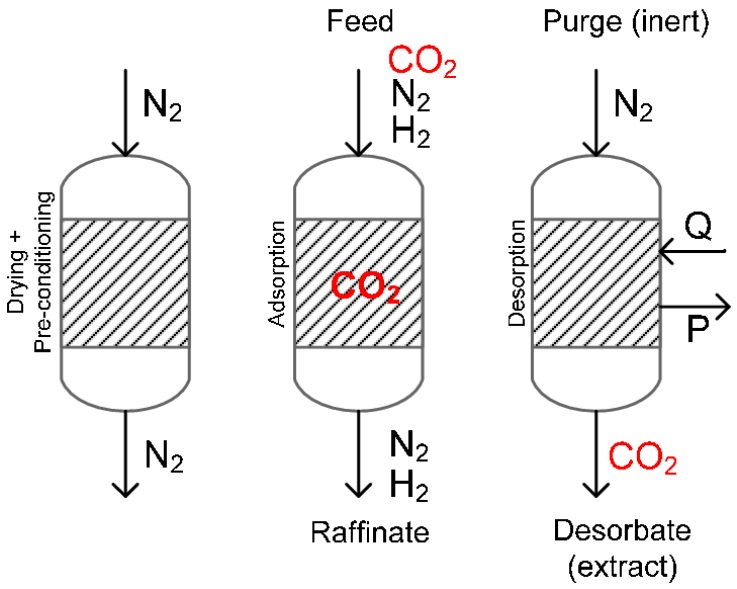

Figure 2.4: Sketch of the adsorption-desorption cycle configuration.

Adsorption is mainly classified as chemical (chemisorption) and physical adsorption (physisorption) according to the adsorption mechanism. In chemical adsorption, chemical reaction is occurred between adsorbate (gas) and surface atoms of the adsorbent and new chemical bond is form altering chemical structure of the atom or molecule as seen at Figure 2.5 [29]. At the chemisorption, adsorption occurs only one monolayer because of the irreversible chemical bonds. Therefore, to reverse the reaction, it requires high temperature.

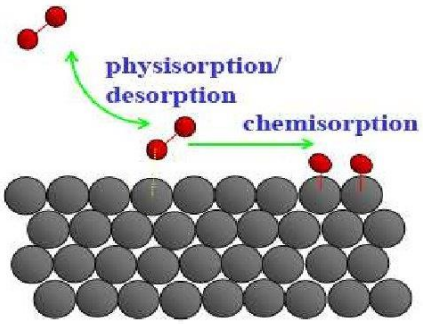

Figure 2.5: Irreversible chemisorption and reversible physisorption.

Unlike chemisorption, physical adsorption is depended on a physical interaction between adsorbate and adsorbent which is reversible and dominated by van der Waals forces and electrostatic interactions. Mainly, it is occurred when the intermolecular attractive forces between adsorbate and adsorbent exceeds the attractive forces between adsorbates. The enthalpy change is followed the equation below:

$$\Delta H=\Delta G+T\Delta S \tag{2.1}$$

Entropy (ΔS) change is commonly negative owing to the steady manner of adsorbed state and Gibbs free energy (ΔG) change is also negative, so the enthalpy change is resulted in negative which means that physisorption is an exothermic process. When the temperature increased in physical adsorption process, decrement in adsorption capacity is observed. Therefore, physisorption is the best choice to separate CO_2 effectively due to its reversibility, low energy requirement, and easily adsorbent regenerability.

The main principle of adsorption-based separation is the diversity of interaction between gas or liquid mixture components and solid adsorbent. This diversity helps us to discriminate adsorption-based separation process under three mechanism; Kinetic separation (diffusion of gas molecules through adsorbent with different rates); Molecular sieving (one gas molecule is bulkier and reside into the pores of the adsorbent while other molecule permeates through the sorbent); equilibrium separation (some molecules form strong interaction with adsorbent by intermolecular interactions) [15]. Adsorption-based separation processes applied in the industry are mostly composed of these three important mechanisms. However, some major technical challenges such as the requirement of effective and low-cost regeneration process are existing in the CO_2 capture. Besides the improvements in the design of effective adsorbents, adsorption process developments are also progressed for CO_2 capture. Several cyclic processes have been designed to obtain successful adsorbent regeneration using temperature, vacuum, moisture, or their combinations. Based on separation conditions, adsorption-based separation can be categorized into four processes:

- Pressure Swing Adsorption (PSA)
- Vacuum Swing Adsorption (VSA)
- Temperature Swing Adsorption (TSA)
- Electrical Swing Adsorption (ESA)

2.2.1. Pressure Swing Adsorption (PSA)

PSA is an effective and economical cyclic process. It requires lower regeneration time and easily resides into a small area [30-34]. In this process, CO_2 is adsorbed on the surface of the adsorbent and separated from the mixture components at higher pressure than the atmospheric pressure. When the pressure drops to atmospheric pressure, CO_2 is desorbed from the adsorbent and release to the stream with an efficiency of higher than 85%.

PSA was set up generally either single- or multi-bed processes depending on the performance of adsorbents. Single-bed PSA displays shorter cycle time and larger

pressure drop and named as Rapid Pressure Swing Adsorption (RPSA) [35]. However, multi-bed PSA contains interconnected two or more beds that operate simultaneously. Thereby, it provides continuous product supply, and feed flows without high pressure differences. For instance, Figure 2.6 [36] illustrates the two-bed PSA system where cyclic operation takes place including four basic steps [35].

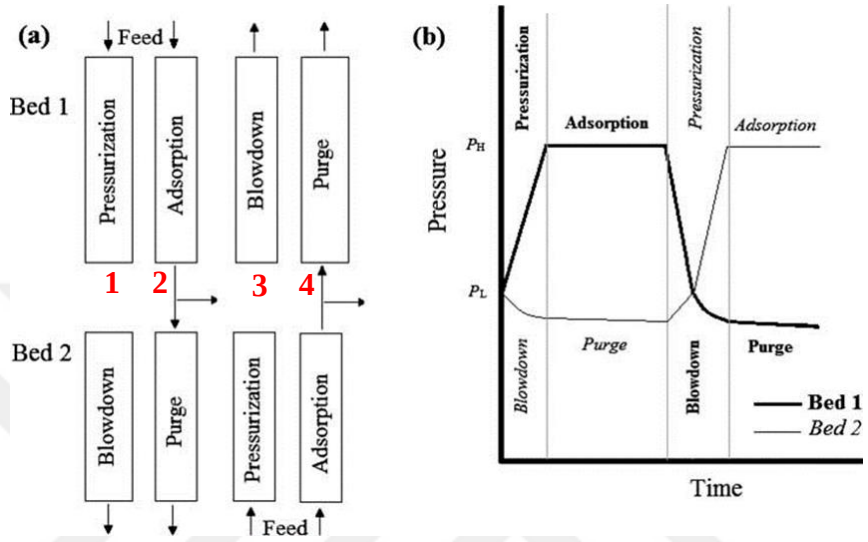

Figure 2.6: Two-bed PSA: a) operating principle, and b) pressure with time evolution.

First step is the pressurization of feed stream in bed 1 at elevated pressure and low temperature. Second step is the adsorption of CO_2 and its separation preferentially from other components. Less adsorbable components are concentrated in the product stream. Some of the CO_2 lean gas is applied to bed 2 to purge it, and the remaining one is stored. At the third step, pressure is decreased (blow downed) with constant outlet flow rate (F_{blow}) of the extract for a time (t_{blow}) with no inlet stream. Fourth step is purging part of the product stream which comes from bed 2 within adsorption step at low inlet pressure. At the end of the purging, emitted gas is the waste and recycled. After regeneration, beds can be used for another adsorption cycle.

2.2.2. Vacuum Swing Adsorption (VSA)

VSA process is directed between atmospheric and low vacuum pressures. Atmospheric pressure is the highest pressure where the adsorption is occurred during

process. Adsorbed CO_2 is desorbed at moderate or low vacuum. PSA and VSA are cyclic processes however, VSA is performed at near ambient temperature and pressures [36].

2.2.3. Temperature Swing Adsorption (TSA)

In TSA, regeneration which means releasing of adsorbed CO_2 is attained by increasing temperature via hot air or steam injection. Since adsorption from the gas phase is exothermic process, higher temperature is going to shift the equilibrium to lower loadings CO_2 named as desorption [15]. Although longer regeneration time is required, purity and recovery rate of CO_2 is above 95 and 80%, respectively [26]. TSA is more expensive process than PSA because of the extra heat demand, however, it provides greater working capacity than PSA as depicted in Figure 2.7.

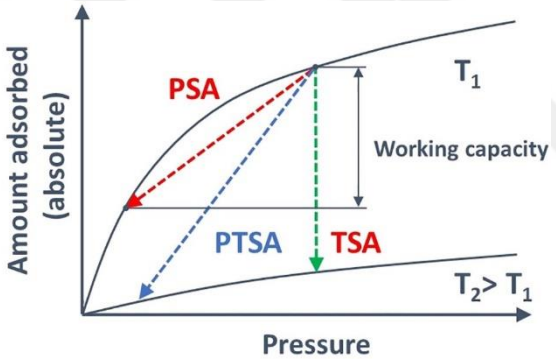

Figure 2.7: Representation of adsorption and desorption conditions in PSA/PTSA/TSA processes via equilibrium gas adsorption isotherms.

With the appropriate combination of pressure and temperature, different processes are also proposed as Pressure and Temperature Swing Adsorption (PTSA), and Vacuum and Temperature Swing Adsorption (VTSA). When modified 13X Zeolite which shows higher adsorption capacity for CO_2 than the commercial 13X Zeolites under steam condition was tested experimentally in the VTSA process for CO_2 separation from flue gas, CO_2 purity was observed as 93.6% with the recovery rate of 92.2% at 110°C, 0.1 bar [37]. They applied different regeneration conditions, temperatures (110, 130, 150, and 170°C), and vacuum pressures (0.03, and 0.1 bar) to modified 13X Zeolite in the VTSA process. The CO_2 recovery and purity rates were determined above 91% as experimentally. However, recovery rate of CO_2 was only

78.1% with purity of 91.6 in TSA process (170°C). This highlighted the importance of hybrid processes such as VTSA using heating and vacuum to regenerate adsorbent on adsorption performance. At another study, Vacuum, and Pressure Swing Adsorption (VPSA) simulations are performed using Zeolite 5A for CO_2 separation from flue gas containing mixture with CO_2/N_2:85/15%. To improve CO_2 purity, more beds and cycles were applied in two-stage VPSA process. CO_2 purity reached to 96% from 70% (one bed) indicating that the hybrid processes could also be improved [38].

2.2.4. Electrical Swing Adsorption (ESA)

ESA is an alternative adsorption process where rapidly heating adsorbents are used. Electric current with low voltage is supplied through the adsorbent so that heat is generated [39]. It seems to be a derivative form of the TSA with the help of in-situ heating approach; however, additional heat requirement is eliminated. Compared with PSA and TSA, it has several advantages such as fast heating, less energy demand, independent of gas and heat flow rates [40]. But the important issue for ESA is the property of adsorbent and design of system. Adsorbent should be conductive, and configuration of system should be designed suitable for the continuous electrical flow.

2.3. Types of Adsorption Isotherm

Adsorption isotherm represents the amount of adsorbate (namely gas in our case) on the adsorbent as a function of pressure or concentration at a constant temperature. Amount of adsorbed adsorbate is expressed as a function of two parameters, equilibrium pressure (P) of bulk phase of adsorbate and temperature (T) as defined following.

$$X_a = f(P)_T \tag{2.2}$$

Physical adsorption occurs at solid-liquid, liquid-gas, or solid-gas interface. Gas adsorption on solid adsorbent which we are particularly interested displays various isotherm types. International Union of Pure and Applied Chemistry (IUPAC) describes adsorption isotherms under six types of isotherms as shown in Figure 2.8 [41]. The

amount of adsorbed gas is represented in any unit such as grams, moles, volume per unit area at standard temperature and pressure (STP) or per gram of the adsorbent. P/P^0 represents the relative pressure.

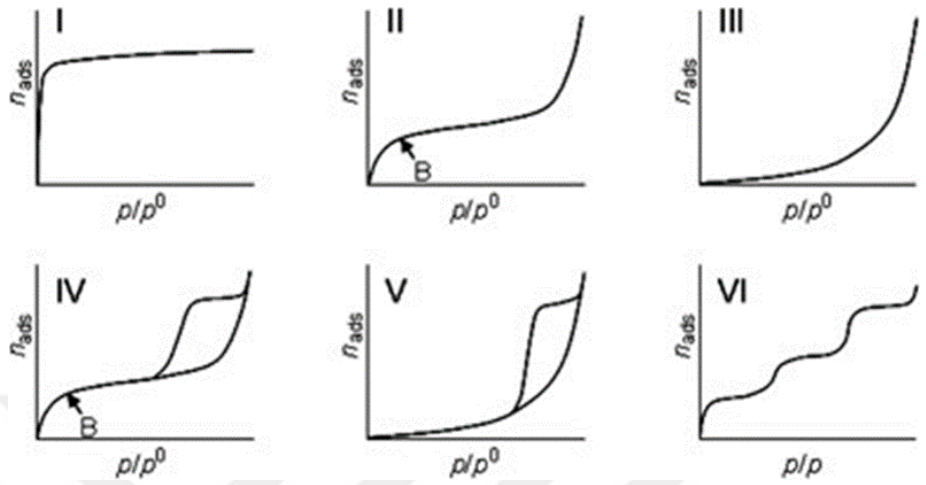

Figure 2.8: Types of physisorption isotherms.

- Type I isotherm**:** They are used to represent adsorption on microporous adsorbent. Adsorption occurred at relatively low pressure and a monolayer form on the adsorbent surface. Isotherm becomes smooth due to the lack of external surface area. Type I isotherms are characterized using Langmuir model.

- Type II isotherm: For the initial phase, type I and II isotherms are similar. Unlike type I isotherm, amount of adsorbed gas does not reach saturation. B shows the starting point of adsorption. After monolayer is formed on sorbent surface, adsorption continues to progress because of the strong adsorbent-adsorbate interaction resulting in multilayer adsorption. These isotherms are typical for non-porous or macro-porous solid sorbents. Reversible adsorption is also represented by this isotherm.

- Type III isotherm: Type III isotherm takes place after the adsorbate-adsorbate interaction exceeds the adsorbent-adsorbate interaction. Although initial adsorption is very low, after starting the adsorption of molecules, as same as multilayer adsorption, progressive adsorption is easily obtained. This type of isotherm is also reversible and applied to describe gases which have very low affinity towards to the adsorbent.

- Type IV isotherm: Adsorption of mesoporous solid materials with pore width between 2-50 nm are defined by this isotherm. Hysteresis is occurred between desorption and adsorption branches because of the capillary condensation. Initially, type IV isotherm resembles type I isotherm however, multilayer formation is observed as the pores are filled up.

- Type V isotherm: Type V isotherm takes place when the interaction between adsorbent and adsorbate is very weak. This isotherm is uncommon and associated with type III isotherms.

- Type VI isotherm: Type VI isotherm is also not common. It exhibits layer-by-layer adsorption on a regular non-porous adsorbent surface. The steps of this isotherm display multilayer adsorbates which indicate the presence of groups of different sized pores.

2.4. Adsorption Isotherm Models

When adsorbate contact to the adsorbent for a sufficient time, adsorption is established under the dynamic balance between interface concentration and the adsorbate concentration. This adsorbed amount onto the adsorbent is measured depending on pressure (for gases) or concentration (for liquids) at constant temperature. For the prediction of the adsorption capacity of the adsorbent at other pressures or concentrations, we utilized from specific models based on linear or non-linear analysis as an alternative mathematical approach [42]. Since interaction between adsorbate and adsorbent shows variations, many adsorption isotherms models have been implemented such as Henry [43], Langmuir [44, 45], Freundlich [46], and Flory-Huggins model [47].

Henry's adsorption isotherm model is linear model which means that adsorption capacity of gases on the adsorbent is a linear function of pressure. So, when the pressure increases, adsorption capacity of gases also increases proportionally as following.

$$q_e = K_{HE} C_e \tag{2.3}$$

The amount of adsorbate at equilibrium (mg/g) is represented by q_e, K_{HE} is the Henry's adsorption constant (l/g), and C_e is the equilibrium concentration of the adsorbate on the adsorbent (mg/l). In according to this model, pressure is low (less than 10 bar) and coverage of the adsorbent surface is only 10%. Thus, this model displays monolayer adsorption in the case of low initial adsorbate concentration. Non-ideal and reversible adsorption is described by Freundlich model with the following equation [43, 48].

$$q_e = K_F C_e^{\frac{1}{n}} \tag{2.4}$$

In according to this model, surface energy of solid adsorbent is not same. Each adsorbed molecule can be filled in one adsorption center. Isotherm type is reported by the value of n, and parameters of K_F and n are dependent on temperature. K_F is Freundlich isotherm constant (l/mg) indicating adsorption capacity, n is the adsorption intensity. Heterogeneity of surface is showed by 1/n. Adsorption is favorable when 1/n is greater than zero. If it is above 1, adsorption is unfavorable. If it is equal to 1, adsorption is irreversible and simplified to the Henry model. Solid surface monolayer adsorption model was proposed by Langmuir kinetic model [44]. The main hypotheses are 1) monolayer adsorption as same as Freundlich exists, 2) adsorption sites are distributed homogeneously, 3) there is no interaction between adsorbate molecules, and 4) adsorption and desorption rates are equal.

$$q_e = \frac{q_m K_L C_e}{1 + K_L C_e} \tag{2.5}$$

K_L (L/mg) is the ratio of adsorption and desorption rates, C_e is the adsorbate concentration (mg/L), q_m (mg/g) is the maximum adsorption capacity which is predicted using Langmuir model. Toth model is the extended form of Langmuir model to decrease the errors between experimental and estimated values [42]. It is implemented to describe the heterogeneity of adsorption systems. Toth isotherm model can define the data at the low and high adsorbate concentrations using the following equations:

.

$$q_e = \frac{K_T C_e}{(a_T + C_e)^{\frac{1}{t}}} \quad (2.6)$$

K_T (mg/g) is a function of the monolayer saturation pressure like q_m which has the same meaning in the Langmuir equation [49]. Toth constant is a_T (mg/L). Heterogeneity of adsorption system is displayed by t. As temperature increases, a_T increases owing to the relation between temperature and t which is independent from temperature. Toth model turns out to the Langmuir isotherm model at t=1. Heterogeneous manner of the adsorption system is observed at t much greater than 1 [50].

Add to the mostly used adsorption isotherm models, many different models have been formulated up to date and summarized at Table 2.2 [51]. Table 2.2 tabulates the names of all isotherm models along with their linear and non-linear equations, and variables used in the plots. Over the years, due to the shortcoming of existing models, many new models were proposed. For instance, since Henry and Langmuir isotherm models were not valid at high pressure [51, 52], Toth isotherm model was proposed [53]. When Toth model was unsuccessful for the explanation of transition to the saturation region, Jaroniec and Marczewksi model was emerged [54-56]. Another model, Dubinin-Radushkevich model performs well at high pressure while ineffective under low pressure [57, 58]. To compare the prediction performance of these models, Wang and colleagues [59] analyzed the adsorption characteristics of a pure gas in a shale reservoir. The comparison of different models is depicted at Figure 2.9 [59]. Henry model displays large error due to the linear model fitting whereas Langmuir and Langmuir-Freundlich models revealed small error with good fitting effect. The fitting results between experimental data and models are decreased from low to high errors as in the following order: Langmuir-Freundlich > Toth > Langmuir > Radke-Prausnitz > Freundlich > Dubinin-Radushkevich > Henry model.

Table 2.2: Lists of adsorption isotherm models.

Isotherm	Nonlinear form	Linear form	Plot
Langmuir	$q_e=\frac{Q_O\, bC_e}{1+bC_e}$	$\frac{C_e}{q_e}=\frac{1}{bQ_O}+\frac{C_e}{Q_O}$	$\frac{C_e}{q_e}$ vs C_e
	-	$\frac{1}{q_e}=\frac{1}{Q_O}+\frac{1}{bQ_OC_e}$	$\frac{1}{q_e}$ vs $\frac{1}{C_e}$
	-	$q_e=Q_O-\frac{q_e}{bC_e}$	q_e vs $\frac{q_e}{bC_e}$
	-	$\frac{q_e}{C_e}=bQ_O-bq_e$	$\frac{q_e}{C_e}$ vs q_e
Freundlich	$q_e=K_F{C_e}^{1/n}$	$\log q_e=\log K_F+\frac{1}{n}\log C_e$	$\log q_e$ vs $\log C_e$
Dubinin-Radushkevich	$q_e=(q_S)\exp(-k_{ad}\varepsilon^2)$	$\ln(q_e)=\ln(q_S)-k_{ad}\varepsilon^2$	$\ln(q_e)$ vs ε^2
Tempkin	$q_e=\frac{RT}{b_T}\ln A_TC_e$	$q_e=\frac{RT}{b_T}\ln A_T+\left(\frac{RT}{b_T}\right)\ln C_e$	q_e vs $\ln C_e$
Flory-Huggins	$\frac{\theta}{C_O}=K_{FH}(1-\theta)^{n_{FH}}$	$\log\left(\frac{\theta}{C_O}\right)=\log(K_{FH})+n_{FH}\log(1-\theta)$	$\log\left(\frac{\theta}{C_O}\right)$ vs $\log(1-\theta)$
Hill	$q_e=\frac{q_{S_H}{C_e}^{n_H}}{K_D+{C_e}^{n_H}}$	$\log\left(\frac{q_e}{q_{S_H}-q_e}\right)=n_H\log(C_e)-\log(K_D)$	$\log\left(\frac{q_e}{q_{S_H}-q_e}\right)$ vs $\log(C_e)$
Redlich-Peterson	$q_e=\frac{K_RC_e}{1+a_R{C_e}^g}$	$\ln\left(K_R\frac{C_e}{q_e}-1\right)=g\ln(C_e)+\ln(a_R)$	$\ln\left(K_R\frac{C_e}{q_e}-1\right)$ vs $\ln(C_e)$
Sips	$q_e=\frac{K_S{C_e}^{\beta_S}}{1+a_S{C_e}^{\beta_S}}$	$\beta_S\ln(C_e)=-\ln\left(\frac{K_S}{q_e}\right)+\ln(a_S)$	$\ln\left(\frac{K_S}{q_e}\right)$ vs $\ln(C_e)$
Toth	$q_e=\frac{K_TC_e}{(a_T+C_e)^{1/t}}$	$\ln\left(\frac{q_e}{K_T}\right)=\ln(C_e)-\frac{1}{t}\ln(a_T+C_e)$	$\ln\left(\frac{q_e}{K_T}\right)$ vs $\ln(C_e)$
Koble-Corrigan	$q_e=\frac{A{C_e}^n}{1+B{C_e}^n}$	$\frac{1}{q_e}=\frac{1}{A{C_e}^n}+\frac{B}{A}$	-
Khan	$q_e=\frac{q_Sb_KC_e}{(1+b_KC_e)^{a_K}}$	-	-
Radke-Prausnitz	$q_e=\frac{a_{RP}r_R{C_e}^{B_R}}{a_{RP}+r_R{C_e}^{B_R-1}}$	-	-
BET	$q_e=\frac{q_SC_{BET}C_e}{(C_S-C_e)[1+(C_{BET}-1)(C_e/C_S)]}$	$\frac{C_e}{q_e(C_S-C_e)}=\frac{1}{q_SC_{BET}}+\frac{(C_{BET}-1)}{q_SC_{BET}}\frac{C_e}{C_S}$	$\frac{C_e}{q_e(C_S-C_e)}$ vs $\frac{C_e}{C_s}$
FHH	$\ln\left(\frac{C_e}{C_S}\right)=-\frac{\alpha}{RT}\left(\frac{q_S}{{q_e}^d}\right)^r$	-	-
MET	$q_e=q_S\left(\frac{k}{\ln(C_S/C_e)}\right)^{1/3}$	-	-

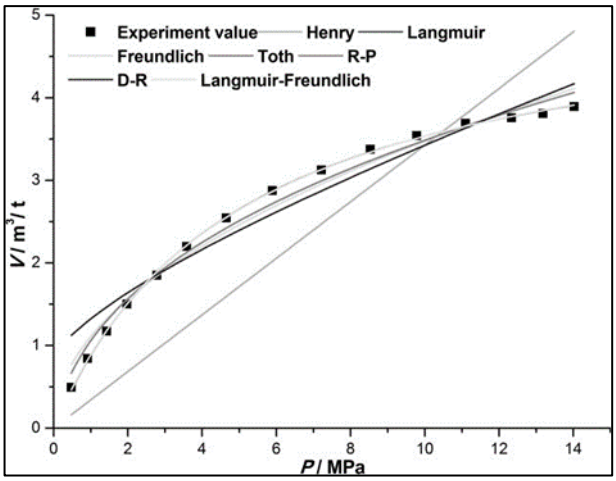

Figure 2.9: Comparison of different models fitting with adsorption manner of Barnett shale gas.

3. ADSORBENTS FOR GAS SEPARATION

Adsorbents with high adsorption capacity and selectivity are desired for efficient adsorption-based separation processes. Moreover, adsorbents should maintain their structure after several adsorption-desorption cycles. They must have thermal and mechanical stability to withstand with process conditions. [60, 61]. To determine the real adsorption behavior of adsorbents against to the conditions, adsorbents should be examined under actual process conditions with different configurations by experimentally and theoretically. Up to date, different types of adsorbents are notified in the literature for physical and chemical adsorption. Adsorbents used in physical adsorption process are classified under two main titles, carbonaceous and non-carbonaceous adsorbents. Carbonaceous materials are consisted of AC, Carbon Nano Tube (CNT), graphene, and CMS. Silica, zeolites, and MOFs compose the non-carbonaceous adsorbents. In this section, commonly used adsorbents for gas separation will be mentioned.

ACs are synthesized from different raw materials by chemical and physical activations, or combination of these two processes. They have different forms such as powder, granular, spherical, bead, and fiber [62, 63]. They have various shapes of pores (cylindrical, rectangular, or irregular) with size ranging from 0.8 to 2000 nm [64]. The properties of ACs are dominantly affected from the raw precursor material and activation technique that used in the synthesis. High surface area is obtained which is ranging between 700-1800 m^2/g [65, 66]. The main advantages of ACs are low energy cost, easy regeneration, and high thermal stability. However, when partial pressure increased, adsorption capacity decreased owing to the impurities such as NO_x, SO_x, and H_2O [67, 68]. In addition, ACs are soft and tend to cause deterioration in the beds. Therefore, instead of AC, CNT, graphene, and CMS have been used as adsorbents.

Graphene is single layer sheet of sp^2 hybridized carbon atoms which is arranged in a hexagonal honeycomb lattice [69]. Large surface area of ~ 2600 m^2/g, tunable and expendable layer structures [70-72]are the main advantages of graphene for the CO_2 adsorption process. Since it has been discovered by Iijima in 1991, CNTs are the famous members of fullerene family with dimensions ranging from 1-10 nm diameter and 200-500 nm in length [73, 74]. They are mechanically strongest and hardest fibers

because of their C-C bond. They have also thermal stability at vacuum and air which makes them suitable for CO_2 separation [75]. CMSs are another member of carbonaceous materials with molecular dimensions. They have a narrow pore size distribution. Molecules can be easily separated depending on their sizes and shape [76]. CMSs provide high adsorption capacity and selectivity for different molecules such as SO_2 and CO_2 [77].

Silica is the first adsorbent used as a non-carbonaceous material due to its abundance in the world as quartz. [78]. Mesoporous silica materials are favorable for CO_2 adsorption because they have large surface area, chemical and thermal stability, tunable pore diameter [79]. However, low hydrothermal stability in the presence of water or stream is the main disadvantages of silica materials [80]. Therefore, zeolites and MOFs have been emerged as an alternative adsorbent to the silica materials. Zeolites are a class of porous crystalline materials that existing naturally. The advantages are tunable physical properties such as high surface area, uniform porosity, and interconnected channels with regular pore sizes in range of between 0.5-1.2 nm [81, 82]. Strong dipole-quadrupole interactions between CO_2 and alkali metal cations of zeolites makes them favorable for adsorption [83]. However, CO_2 adsorption performance of zeolites are affected from the process conditions such as temperature, pressure, and moisture [84, 85]. MOFs are hybrid materials produced by the combination of metal containing clusters and organic linkers with pore size reaching up to 150 nm [86, 87]. High surface area of more than 10000 m^2/g, tunable pore size and geometry provide improved CO_2 adsorption and selectivity [88, 89]. However, CO_2 adsorption capacity decreased at low CO_2 partial pressure [90] and the presence of high-water vapor [91]. MOFs tend to be sensitive to water vapor and thermal treatment which may lead to their degradation. Thus, they have poor stability and mechanical strength towards to the moisture.

Transition metal carbides are emerged recently especially for CO_2 adsorption due to their outstanding properties such as high surface area, thermal and chemical stability, surface chemistry and tunable interlayer distance. Transition metal carbides and transition metal nitrides named collectively “MXenes” which have become more popular material since their first discovery in 2011 [9].

4. MXENE NANOMATERIALS

MXenes are rapidly growing member of two-dimensional materials including transition-metal carbides, nitrides, and carbonitrides. MXene structure is derived from its three-dimensional counterpart named as MAX phase which is formulated $M_{n+1}AX_n$ (M = early transition metal(s), containing Sc, Y, Ti, Zr, Hf, V, Nb, Ta, Cr, Mo, W, and Mn; n = 1, 2, 3, 4; A = IIIA or IVA group elements such as Al; X = C and N) [92-94]. M atoms of MAX phase are closed pack with X atoms into the hexagonal lattice (hcp) and X atoms fills their octahedral spaces. With the extraction of A atoms from MAX phase, M_nX_{n-1} thin layer is obtained with a horizontal arrangement [95, 96]. To extract A atoms for the synthesis of MXene, MAX phase is immersed into the acid commonly hydrofluoric acid (HF) which demolish the bonds between transition metals and A elements. This step is named as etching. Final two-dimensional M_nX_{n-1} layer is terminated with T_x groups including hydroxyl, oxygen, fluoride and/or chloride groups and the ultimate MXene structure is formulated as $M_{n+1}X_nT_x$.

MXenes are categorized under several groups depending on composition and arrangement which are illustrated in Figure 4.1 [9]. The first group is mono-transition-metal MXenes which M layers are composed of a single type of transition metal such as Ti_2CT_x or $Nb_4C_3T_x$. The second group is double transition-metal MXenes. They consist of two separate transition metals, colored by blue and pink representing their coordination within MXene layer. Two separate transition metals may reside specific sites of M layers described as in-plane order or out-of-plane order. In-plane ordered MXenes, two separate transition metals are organized alternately in each M layer atomic plane. Unlike, in out-of-plane MXenes, transition metals are ordered in separate atomic planes. For solid solution MXenes, transition metals are randomly distributed within all M layers and carbon and nitrogen atoms similarly randomly oriented within X layers. Finally, ordered vacancy MXenes are composed of mono-transition metals such as Mo, W, Cr and only $Mo_{1.33}C$ and $W_{1.33}C$ have been synthesized experimentally while $Cr_{1.33}C$ was designed by theoretically. The composition of the ordered vacancy structure is ~33 atom % in the M layers.

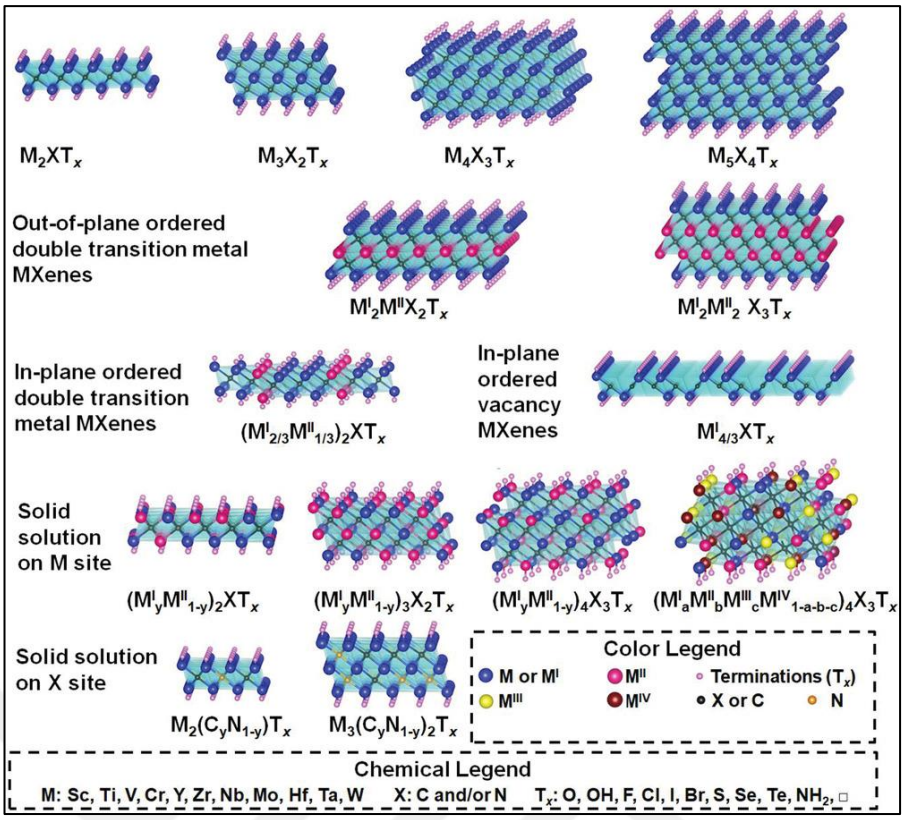

Figure 4.1: Typical MXene structures and compositions reported up to date.

There were only 70 different MAX phases at the discovery of Ti_3C_2 in 2011. Today, this number reached to 150 and will continue to increase in the near future [9]. However, unfortunately, few kinds of MXene structures have been synthesized. Thanks to the power of computational science which predicted recently many possible MXene compositions that have never been synthesized yet. Since ordered MXenes were first synthesized in 2014 and reported in 2015 [92], about 50 new ordered double transition metal MXenes and infinite number of solid solutions have been added to the MXene family [97]. Besides, studies continue to produce two dimensional "borides" to add another X element [92]. While MXene family has increased its members since 2011, another advance has been recorded for the MXene synthesis approaches. New synthesis methods are examined which provide to obtain new MXene compositions.

4.1. MXene Synthesis

Various MXene types and forms were fabricated due to the discovery of various synthesis techniques since 2011. Vital properties of MXenes such as surface

chemistry, hydrophilicity, stability, and tunable interlayer spacing can be tailored by the synthesis methods. Two basic approaches used for the synthesis of MXenes: top-down and bottom-up approaches. Basically, at the top-down strategy, bulky MAX phase is exfoliated to the thin MXene nanosheets while bottom-up synthesis focuses on the production of MXenes from atoms or molecules [98, 99]. Mostly used top-down approaches are selective etching of MAX phases such as wet acid, molten-salt, Lewis-acid, and electrochemical etching, as well as chemical transformation containing ammonization, carburization, de-oxygenation-carburization [99].

4.1.1. Selective Etching

First MXene type, Ti_3C_2 was synthesized via immersing MAX phase (Ti_3AlC_2) into the HF for two hours at ambient conditions by Naguib et al. [100, 101]. The reaction is summarized as follows:

$$M_{n+1}AX_n + 3HF = M_{n+1}X_n(s) + AF_3 + 1.5H_2(g) \quad (4.1)$$

$$M_{n+1}X_n(s) + 2HF = M_{n+1}X_n F_2 + H_2(g) \quad (4.2)$$

HF utilized to remove A layer from MAX phase. H_2 and Al/Si-based fluorides are produced, and accordion-like structure is observed. Synthesized MXene terminated with several functional groups such as hydroxyl, oxygen, fluoride, etc. From the Al/Si-based MAX precursors such as Ti_2AlC, Ti_3SiC_2, Nb_2AlC, Ti_3AlCN, $Zr_3Al_3C_5$, different MXenes have been fabricated using HF etching. Since HF is highly toxic, alternative etchants such as fluoride salts (LiF, KF, NH_4HF_2, and NH_4F) and hydrofluoric acid mixtures has been examined for etching. With the use of these alternative etchants, some cations have been easily intercalated into the interlayer spacing of MXene.

Besides to the carbide MXenes, nitrite MXenes, $Ti_4N_3T_x$, was synthesized via molten-salt etching technique [102]. A ternary eutectic molten fluoride salt (LiF/NaF/KF = 29/12/59, weight ratio) mixture was used as an etchant. Salt mixture and Ti_4AlN_3 MAX powders mixed and heated at 550°C for 30 minutes. After mixed with tetrabutylammonium hydroxide (TBAOH) and centrifuged, $Ti_4N_3T_x$ layers

(T_x=hydroxyl, fluoride) were obtained with poorer crystallinity than the $Ti_3C_2T_x$ which was synthesized with HF etching [102].

Two main challenges emerge during the MXene synthesis: (i) first to apply non-toxic synthesis method, and (ii) second to fabricate more new MAX phase precursors. Li et al. [103] created various MXenes such as Ti_2C, Ti_3C_2, Ti_4N_3, Ti_3CN, Nb_2C, Ta_2C, Zr_3C_2, and Hf_3C_2 using various MAX phases and salts via Lewis- acid etching method. For example, Ti_3SiC_2 MAX phase was soaked into the $CuCl_2$ Lewis molten salt, NaCl, and KCl at 750°C. $Ti_3C_2Cl_2$ MXene powder and Cu^{++} metals were produced and then they were soaked into the ammonium persulfate ($(NH_4)_2S_2O_8$) solution. $Ti_3C_2T_x$ (T_x=oxygen, and chloride) was obtained as the final material. Not only chloride but also other surface termination groups were achievable such as (oxygen, sulfur, selenium, and bromine groups) for MXene which was synthesized by Lewis-acid etching method [103]. This method allows the tailoring of surface chemistry of MXene according to the application of interest.

Alternative to the acid usage, electrochemical etching method was developed by Yang et al. [104]. The etching process was implemented in a two-electrode system, where two bulk Ti_3AlC_2 were used as anode and cathode, respectively. When a low potential of 5 V is applied, anode was progressively delaminated in a mix of 1M NH_4Cl and 0.2M tetramethylammonium hydroxide (TMA.OH) (pH > 9) at room temperature. After etching was completed, the sediment and suspended $Ti_3C_2T_x$ powders were grinded and put into the 25% w/w TMA.OH for delamination. Using this method, Yang et al. [104] obtained single and double MXene layers of more than 90% amount with average lateral size above 2 μm that was higher than the obtained values by traditional HF etching method. In addition, $Ti_3C_2T_x$ layers did not contain fluorine terminal groups.

4.1.2. Chemical Transformation

Chemical transformation processes are classified under three in-situ chemical reaction topics: ammonization, carburization-involved chemical conversion, and de-oxygenation-carburization. Etching method using HF is effective way to obtain carbide-based MXenes whereas nitride-based MXenes are suffered from instability in aqueous HF solution. Urbankowski et al. [105] examined Mo_2CT_x and V_2CT_x powders

and delaminated films at 600°C for 1 hour with heating rate of 10°C/h in the presence of ammonia flow. Carbon atoms were replaced with nitrogen atoms which is named as nitridation during ammonization reaction. Nitride-based MXenes, Mo_2N and V_2N, with different crystal structure due to the ammonization process were obtained from carbide precursors [105].

Molybdenum carbides were synthesized by several methods, however controllable synthesis method for low-dimensional structures has not been reported yet. Jeon et al. [106] fabricated Mo_2C sheets which are derived from Mo_2S via chemical conversion in the presence of H_2 and CH_4 at 820°C. Combination of thermal annealing with consecutive steps named as hydro-desulfurization, carburization, and chemical conversion, Mo_2C nanosheets with controllable thickness (3-100 nm) and lateral size (100 μm) were obtained [106]. Differently, Lin et al. [107] attained two different phases of molybdenum carbides (MoC as fcc and Mo_2C as hcp) using different carbon sources such as sucrose and carbon films by the combination of de-oxygenation and carburization processes. Molybdenum peroxide hydrate precursor and its dissolved form in sucrose were dropped onto the carbon film and then heated up to 1200°C with the rate of 20°C/min. Mo_2C (hcp) was produced from carbon film while the origin of MoC (fcc) was carbon of sucrose. Depending on the carbon sources and process temperature, phase and facet of molybdenum carbides can be altered [107].

4.1.3. Bottom-Up Construction

Although top-down approaches are commonly used for MXene synthesis, few types of MXene such as Ti_4C_3, W_2N have been fabricated by bottom-up construction methods. Mostly used bottom-up construction methods are Chemical Vapor Deposition (CVD) and salt-templated growth. Ultrathin α-Mo_2C nanocrystals were fabricated via CVD by Xu et al. [108] for the first time. They benefitted from bilayer substrate composed of Cu foil reside top of the Mo foil and CH_4 as a carbon source. During CVD, heat was increased above 1085°C and Mo-Cu alloy was created at the liquid Cu/Mo interface. Mo_2C crystals with large lateral size approximately 100 nm and thickness of 3-20 nm were formed [108]. After study of Xu et al. [108], CVD process started to be used widely for MXene family.

Another method for the bottom-up construction of MXene is growing 2D MXene on the surface of inorganic salts such as NaCl, KCl. Xiao et al. [109] used KCl salt as a template to synthesize Mn_3N_2 layers via salt-templated growth. First, $MnCl_2$@KCl powder was obtained using manganese chloride solution in ethanol, which was coated onto the surface of KCl template and dried in the oven. Second, this powder was treated with high temperature under ammonia flow. After ammonization, 2D Mn_3N_2@KCl was formed. Third, KCl salt template was washed with deionized water, and Mn_3N_2 layers were observed. Thanks to the closely matched lattice parameters between Mn_3N_2 and KCl resulted in magnetic metal nitride at room temperature. Considering the Mn_3N_2 is the first magnetic metal nitride produced by this method, more studies should be done to produce other magnetic metal nitrides using room temperature ferromagnetism.

4.2. MXenes as Adsorbents

Due to their unique properties such as high specific surface area, high surface energy, book-like structure and adjustable interlayer spacing, MXenes have started to gain importance for adsorption studies. However, there are few experimental studies showing the gas adsorption performance of MXenes up to date. Liu et al. [110] investigated CH_4 adsorption capacity of Ti_2C, both theoretically and experimentally. Ti_2C etched with HCl and LiF was exfoliated by intercalation using $NH_3.H_2O$ in order to obtain MXene with larger interlayer spacing. For the intercalated Ti_2C with $NH_3.H_2O$, adsorption amount of CH_4 was reported as 16.81 cm^3 (STP)/g at 25°C and 50 bar which was greater than as-synthesized MXene due to large interlayer spacing. With the increase in temperature to 50°C, adsorption amount of CH_4 reached to 52.76 cm^3(STP)/g for the intercalated Ti_2C. Most importantly, theoretical (22.9 wt.%) and experimental (28.8 wt.%) CH_4 adsorption capacities agreed well with each other. They revealed that the physical adsorption was dominated by the oxygen functional groups on the surface of Ti_2C. Moreover, although Ti_2C is less stable than Ti_3C_2, Ti_2C was offered as a promising MXene type for the CH_4 adsorption by Liu and colleagues [110]. In another study, Liu et al. [111] fabricated two different MXene types, $Ti_3C_2T_x$ and Ti_2CT_x, by etching with different salts such as LiF, sodium fluoride (NaF), potassium fluoride (KF) and ammonium fluoride (NH_4F) to determine CH_4 adsorption

capacity. Highest CH_4 adsorption capacities were reported as 8.5 cm^3/g for Ti_3C_2 etched with LiF and 11.6 cm^3/g for Ti_2C etched with KF at 60 bar. Since Li^+ ion was smaller than the other ions used for etching, it was easily adsorbed and kept on the surface of the MXene layers. On the other hand, MXenes exfoliated by NaF and KF released greater amount of adsorbed CH_4 in desorption process compared to MXenes exfoliated by LiF. Because few Na^+ and K^+ ions were located on the surface of the MXene layers, leading to easily release of CH_4 molecules due to the weak interaction with surface structure of MXene ($Ti_2C(F/OH/O)_x$).

In addition to CH_4 adsorption measurements, Wang et al. [112] investigated the CO_2 adsorption performance of two kinds of MXenes, $Ti_3C_2T_x$ and V_2CT_x. MXenes were delaminated by the intercalation of dimethyl sulfoxide (DMSO). Interlayer spacing of as-synthesized $Ti_3C_2T_x$ and V_2CT_x increased from 23.4Å to 27.6Å and 21.9Å to 23.7Å after intercalation of DMSO, respectively. Similarly, after intercalation, Specific Surface Area (SSA) of $Ti_3C_2T_x$ increased from 21 m^2/g to 66 m^2/g and SSA of V_2CT_x reached to 19 m^2/g from 9 m^2/g which is crucial for the gas adsorption performances. Amount of adsorbed CO_2 increased from 1.33 to 5.79 mmol/g for $Ti_3C_2T_x$ and from 0.52 to 0.77 mmol/g for V_2CT_x under 40 bar at room temperature (25°C). However, theoretical SSA of V_2CT_x was higher than $Ti_3C_2T_x$ meaning that the challenge in the exfoliation of V_2CT_x should be handled properly. In order to enhance adsorption capacity, they suggested that preparation of V_2CT_x as a multi-layer rather than single layer form. Moreover, they highlighted the importance of synthesizing MXene as 100% exfoliated to obtain enhanced CO_2 adsorption performance. Because the theoretical CO_2 adsorption capacity was calculated as 44.2 mmol/g for fully exfoliated $Ti_3C_2T_x$ with a surface area of 496 m^2/g. Besides to the experimental studies, Garcia et al. [113] theoretically examined MXenes formulated as M_2C (M = Ti, Zr, HF, V, Nb, Ta, Cr, Mo, and W) to determine CO_2 adsorption performance. CO_2 capture increased along the series of MXenes following the order of W_2C, Ta_2C, Hf_2C, Mo_2C, Nb_2C, Zr_2C, V_2C, and Ti_2C. Carbide MXenes exhibited high CO_2 adsorption capacity ranging from 2.34-8.25 mol/kg at 25°C and 1 bar in according to adsorption bonding energies between CO_2 and M_2C calculated using quantum mechanics simulations. Compared to the common adsorbents as zeolites (Ca-X, 13X), graphene oxides, and metal oxides, 2D M_2C MXenes were proposed as potential adsorbents for CO_2 capture by Garcia et al. [113].

H_2 storage capacity was identified by Liu et al. [114] for Ti_2CT_x which had a bell-mouth shape like interlayer spacing of 6.8 Å with remaining Al atoms. Compared to the other room-temperature H_2 storage materials, Ti_2CT_x exhibited higher H_2 adsorption amounts of 4.2, 5.7, and 8.8 wt.% at 20, 40, and 60 bar and room temperature, respectively. Additionally, hydrogenated MXene, which was stored under 50 bar H_2, lost only its H_2 content of 0.5, 4.1, 10.1, and 9.3% after a period of 1, 7, 10, and 14 days prior to the release, respectively. These results also met recent and 2020 US DOE target of 10% [114]. By adjusting pressure, desorption speed was tailored and by adjusting temperature, desorbed H_2 amount can be increased which proved that the release of H_2 can be controlled easily. Since H_2 adsorption of single Ti_2CT_x layer was very low as 0.02 wt.%, the increase in interlayer spacing from 6.8 to 13.5 Å lead to the dramatic decrease in H_2 uptake from 8.43 to 0.44 wt.%. This evidently proves the importance of narrow interlayer spacing for nanopump effect of multi-layered MXenes. Furthermore, they proved using NMR and FTIR analysis as well as DFT calculations that -F functional groups were responsible for the reversible H_2 due to the weak chemisorption, and -O functional groups were responsible for irreversible H_2 capacity due to the strong physical adsorption. Although these pioneering studies help researchers to the develop MXenes with enhanced gas adsorption performances, more studies should be done experimentally also theoretically concurrently.

5. MOLECULAR SIMULATION TECHNIQUES

Adsorption based separation and purification technologies mostly focus on modelling approaches to identify the adsorption mechanism. Although several models for adsorption isotherm exist, they don't use the information of solid structure. However, molecular simulation techniques can be applied for adsorption predictions by using this information effectively. We can screen various materials to determine the best performing one for adsorption-based separation. Considering the big development of computer science and hardware technology, adsorption as well as transport properties of nanoporous materials are easily determined on a nanoscale by molecular simulation techniques. Two major simulation methods are mostly used: Molecular Dynamics (MD) and Monte Carlo (MC). In this section, molecular simulation methods will be explained firstly. Then, force field and ensembles used in molecular simulations will be mentioned. Finally, history of computational screening of porous materials is going to be provided.

5.1. Molecular Dynamics Simulation

Molecular dynamics (MD) simulation uses Newton's equation of motion with respect to time. Each particle in the system interacts with others and environment, and force acting on the system is evaluated by this equation [115, 116]:

$$F_i(t)= m_i a_i(t)=m_i \frac{dV_i}{dt}=m_i \frac{d^2 r_i}{dt^2}=-\nabla_i U(r_i) \qquad i=1,2,3,\ldots, N \tag{5.1}$$

Force, velocity, mass, acceleration, and position of the i^{th} particle are represented by F_i, v_i, m_i, a_i, and r_i, respectively. U and t represent the potential energy of the system and time. To integrate equation of motion easily, several numerical integration algorithms were developed in the literature such as Verlet, Leapfrog, and Velocity Verlet. Before setting up molecular dynamics simulation, ensemble is chosen that will represent macroscopic conditions of our system. The common ensembles are micro-canonical, canonical, isothermal-isobaric, and grand canonical ensembles. For micro-canonical ensemble, energy, volume, and number of particles are constant, while in

canonical ensemble, temperature, volume, and number of particles are constant. In isothermal-isobaric ensemble, temperature, pressure, and number of particles are constant and last ensemble for grand canonical ensemble, temperature, volume, and chemical potential are constant. Depending on the last system that we want to obtain and our problem that we want to solve, selection of ensemble type may change. First step in molecular dynamics simulation is defining initial velocities and configurations of the system. The information about positions is usually taken from the crystal structure data or optimized geometries whereas velocities are determined randomly. Second step is describing interatomic interactions of all particles using force fields besides to the other simulation parameters such as time step, pressure, and temperature. Molecular dynamics simulation acts as engine that produce time-dependent trajectories including primary and secondary properties such as mean-squared displacement (MSA), thermal and transport properties.

5.2. Monte Carlo Simulation

Monte Carlo (MC) simulation is based on the creation of the configuration sum using statistical methods with the distribution in the desired probability without solving Newton's equation of motion [117]. This method computes thermodynamic properties using averaging of ensemble. It has no time-dependency therefore dynamic properties are not be able to be measured [118]. Since new conformations are formed at the random walk-in phase space by defining random displacements to the internal degrees of freedom, bonds, angles and torsions, all conformations have not same probability resulting in sampling bias [119]. Several sampling approaches were proposed in Monte Carlo approaches such as simple sampling, importance sampling, Metropolis sampling, etc. The Metropolis algorithm provides the determination of the configurations that will make the most contribution. It counts each configuration equally by making random choices based on $\exp[-\beta E(r^N)]$ probability [120]. According to Metropolis algorithm, whether the randomly generated configuration is accepted or not, is determined using equation 5.2.

$$P(\text{old}\rightarrow\text{new})=\min(1,\exp(-\beta(U_{new}-U_{old}))) \quad (5.2)$$

The steps summarized below are followed by Metropolis algorithm [121]:

- At the initial state, potential energy (U_{old}) is calculated.
- Random molecule is selected within a regular random distribution.
- Potential energy of the new state (U_{new}) is calculated.
- If U_{old} is greater than U_{new}, move is accepted.
- If U_{new} is greater than U_{old}, random value (q) is picked altering between 0-1. If $\exp(-\beta(U_{new}-U_{old})) > q$, move is accepted. If not, the steps between 2-5 is repeated.

Microstate represents the system including a certain number molecules with their positions**.** These microstates are formed with respect to the Boltzmann probability distribution. During the formation of microstates, state of the system is perturbed via movement of the molecules resulting in position changing. Changing of the system state is named as Monte Carlo moves. These moves are translation, rotation, insertion, and deletion. Common moves are illustrated in Figure 5.1 [122].

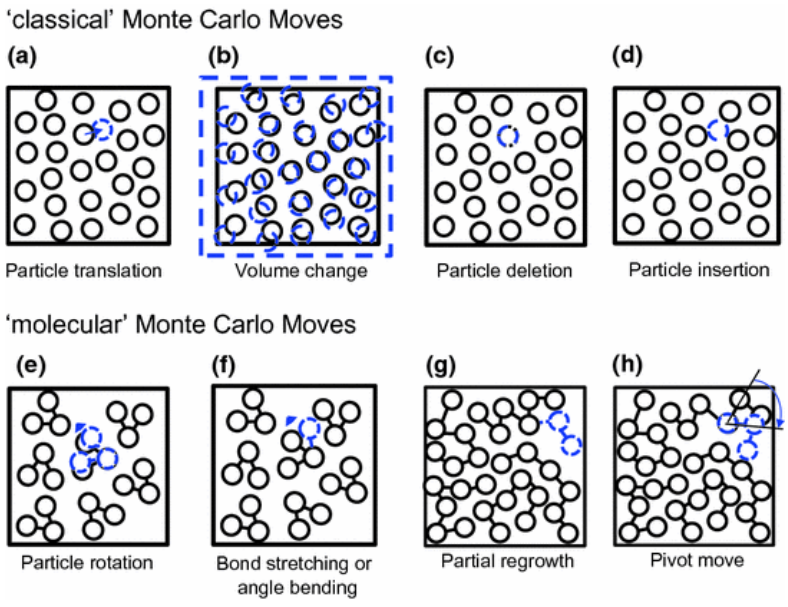

Figure 5.1: Classical and Molecular Monte Carlo Moves.

5.3. Force Field

Force field is a mathematical formulation of the system energy depending on the coordinates of particles [123]. It includes inter-atomic and intra-atomic potential energies. The parameters in force field are provided either from quantum mechanical calculations or via fitting to experimental data such as X-ray diffraction, NMR and Raman spectroscopy, etc. To evaluate the system behavior easily, force field should be simple but at the same time complicated enough to reproduce the properties for system that we interest. General representation for force field is provided in equation 5.3. At this equation, first four terms indicate intra-molecular interactions including bond stretching, angle bending, dihedral, and improper torsions, while last two terms represent inter-molecular interactions including van der Waals (by means of a 12-6 Lennard-Jones potential) and Coulombic interactions.

$$U=\Sigma_{bonds}\frac{1}{2}k_b(r-r_0)^2+\Sigma_{angles}\frac{1}{2}k_a(\theta-\theta_0)^2+\Sigma_{torsions}\frac{V_n}{2}[1+\cos(n\phi-\delta)]+\Sigma_{improper}V_{imp}+$$
$$\Sigma_{LJ}4\epsilon_{ij}\left(\frac{\sigma_{ij}^{12}}{r_{ij}^{12}}-\frac{\sigma_{ij}^{6}}{r_{ij}^{6}}\right)+\Sigma_{elec}\frac{q_i\,q_j}{r_{ij}} \qquad (5.3)$$

Bond stretching is usually demonstrated with a simple harmonic function which controls the length of covalent bonds. Although trigonometric potential is preferred for some cases, angle bending is also indicated by a harmonic potential. When the molecule contain more than four atoms, dihedral or torsional terms should be included. Torsional motions are less strict than bond stretching motions and must provide the accurate degree of molecule rigidity. In addition, they should reproduce the major conformational alterations owing to the bond's rotations. Torsional energy is demonstrated via cosine function at the equation 5.3. To provide planarity of some groups such as sp^2 hybridized carbons in carbonyl groups or aromatic rings, improper torsion terms are required to describe the positive contribution of out-of-plane motions to the system energy. Improper torsion is expressed as the following equations, where improper angle (deviation from planarity) is shown by ω.

$$U_{imp}=\Sigma_{impropers}\frac{k_{imp}}{2}[1+\cos(2\omega-\pi)] \qquad (5.4)$$

$$U_{imp}=\Sigma_{impropers}\frac{k_{imp}}{2}(\omega-\omega_0)^2 \quad (5.5)$$

Van der Waals (vdW) interactions are derived from the balance between repulsive and attractive forces. The Lennard Jones (LJ) 12-6 potential is the mostly used to show these interactions. This potential was first offered to calculate interaction between two particles by Lennard-Jones in 1931. In LJ potential, particles are sphere and rotation of particle has no effect on this potential. If we clarify the rotational motions, other potentials should be considered. Potential energy is computed via equation 5.6 [15].

$$U_{LJ,ij}=4\varepsilon_{ij}\left[\left(\frac{\sigma_{ij}}{r_{ij}}\right)^{12}-\left(\frac{\sigma_{ij}}{r_{ij}}\right)^{6}\right] \quad (5.6)$$

Distance parameter is represented as σ, and ε is the parameter defining the strength of the interaction [124]. Lennard-Jones potential is altered depending on the distance between two particles as illustrated in Figure 5.2 [118].

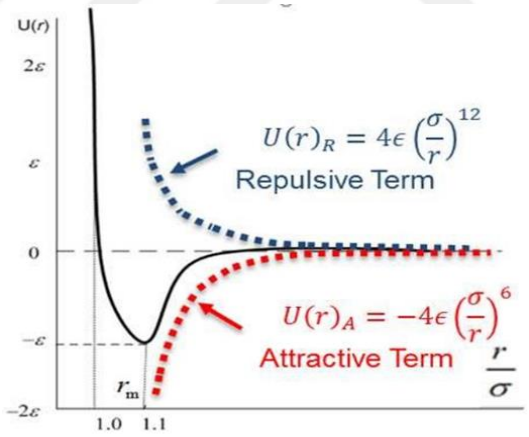

Figure 5.2: Lennard-Jones potential relation to the distance between two particles.

The polar interactions are mostly caught via locating partial charges on the center of specified atoms of the molecule. Using Coulomb equation, the interaction between partial charges is calculated.

$$U_{Coul,ij}=\frac{q_i q_j}{4\pi\varepsilon_0 r_{ij}} \quad (5.7)$$

Partial charges of atoms are labelled as q_i and q_j .Vacuum electrical permittivity is represented by ε_0 . The total dispersion and electrostatic interaction energy of system is calculated via the summation of all binary terms in according to the equation 5.6 and 5.7. Most importantly, these equations are evaluated within a specified cut-off distance for each particle with another in the system [125]. For LJ potential (short-range interactions), small errors can be observed related to the cut-off distance, however, this is not the issue for the long-range Coulombic interactions. Improved techniques such as the Ewald summations were used to overcome this issue in coulomb potential.

Although many force fields were developed and applied to various bio and nanomaterials, Universal Force Field (UFF) is commonly used for calculating intermolecular energies of porous inorganic nanomaterials at gas adsorption simulations [126]. Partial charges for atoms were not provided in UFF, therefore several different charge assignment approaches were proposed in the literature such as either empirical methods as QEq or quantum-mechanical calculations as Mulliken Population Analyses [127], Density Derived Electrostatic and Chemical charges (DDEC) [128], ChelpG [129], etc.

5.4. Ensembles

An ensemble consists of collection of all probable systems with various microscopic states but definitely identical thermodynamic state. All ensembles demonstrate a state which is probably exist in a time. In other words, ensemble exhibits probability distribution. Common ensembles are micro-canonical, canonical, isothermal-isobaric, and grand canonical, and their probability distributions are listed in Table 5.1 [118].

Table 5.1: Common ensembles.

All States of	Probability Distribution
Microcanonical (NEV)	$\pi_i = \frac{1}{\Omega}$
Canonical (NVT)	$\pi(E_i) = \frac{1}{Q} e^{-\beta E_i}$
Isothermal-isobaric (NPT)	$\pi_i(E_i, V_i) = \frac{1}{\Delta} e^{-\beta(E_{i+} PV_i)}$
Grand Canonical (μVT)	$\pi_i(E_i, N_i) = \frac{1}{\Xi} e^{-\beta(E_{i+} \mu N_i)}$

Normalization constant of probability distribution functions or in other terms partition functions are labelled as Ω, Q, Δ, and Ξ for micro canonical, canonical, isothermal-isobaric, and grand canonical ensembles, respectively. Partition functions gives us statistical properties of our system in thermodynamic equilibrium. For micro canonical ensemble, thermodynamic state described by fixed number of atoms (N), volume (V) and energy (E). Partition function is equal to 1 because of the one energy level. For canonical ensemble, it is characterized by fixed number of atoms, volume, and temperature (T). This ensemble is located into the heat bath, so heat transfer is allowed with constant number of particles. Isobaric-isothermal ensemble is highly used ensemble for the equilibration of systems. In this ensemble, atom numbers, temperature, and pressure (P) are fixed and various states with different energy levels and volumes are obtained. In grand canonical ensemble, chemical potential (μ), volume, and temperature are fixed, however atom numbers are not constant. Partition function of this ensemble is related to its chemical potential and system energy. All these ensemble characteristics are depicted in Figure 5.3 in detail [118].

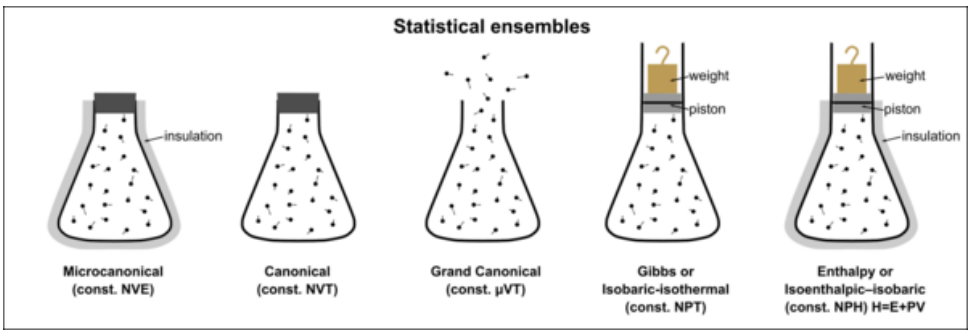

Figure 5.3: Illustration of the Ensembles.

Grand canonical ensemble is convenient and preferable in MC simulation for simulating phase-equilibrium systems such as adsorption due to the fugacity coefficient, Gibbs free energy. Rigid porous materials are examined using this approach since no significant changes in the volume are not observed during adsorption and desorption of quest molecules. However, for flexible materials, a part of the MOF family, more complicated simulation methods should be applied such as Osmotic Ensemble or Gibbs Ensemble [130]. Generally, four types of molecular movements were included in the use of grand canonical ensemble for adsorption simulations. These movements are rotation, translation, deletion, and insertion as illustrated in Figure 5.4 [118].

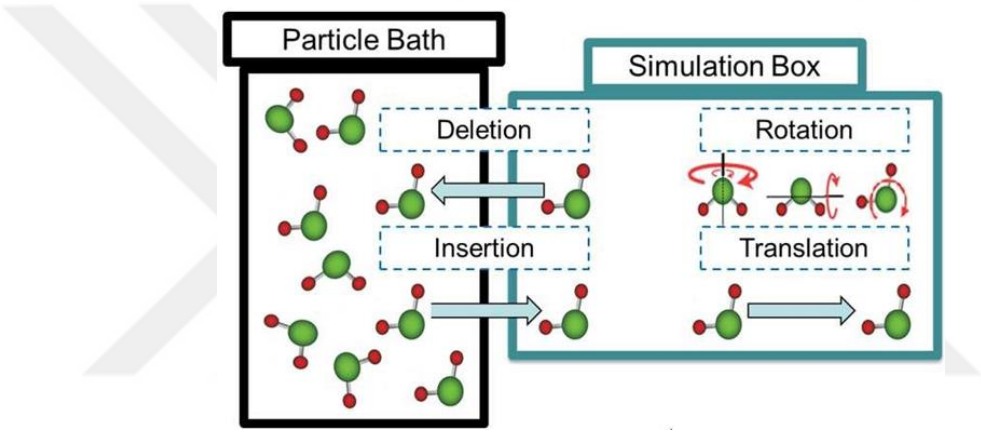

Figure 5.4: Summary of molecular movements used in grand canonical ensemble in CO_2 adsorption simulation.

During simulation, number and position of molecules change and a set of microstates are generated over the average properties of system. These microstates are named as trajectory which is the main output of the Monte Carlo and Molecular Dynamics. Using these trajectories, primary and secondary properties of the system can be easily calculated. For adsorption studies, average number of molecules that exist in the system is the most important property. GCMC simulation generates an averaged adsorbed gas density for the specific fugacity or chemical potential value. With increasing chemical potentials or fugacity, a serial of simulations creates an adsorption isotherm. Important point is the difference between absolute and excess amount adsorbed gases [131]. The absolute amount of adsorbed gas reveals the real number of molecules existing in the micropores of adsorbent at the certain fugacity. Excess amount is the quantity determined in a gravimetric or volumetric adsorption

experiment. It is the difference between the amount of gases in the system and the amount that would be present in the absence of adsorption at the same temperature and pressure [131]. Experimental studies mostly display excess amount adsorbed whereas Monte Carlo simulations show absolute amount adsorbed which is correct for the adsorption studies of microporous materials [131]. Besides to the written data, GCMC simulations produce visual information about the adsorption process on a molecular level such as images, movies, and density maps. With the help of the visual outputs, crucial information about adsorption such as specific binding sites and molecule distribution within the structure of interest can be determined effectively.

5.5. Computational Screening of Porous Materials

Conventionally, to design a new process or device, researchers focused on a small number of materials that can be experimentally explored. However, over 20-30 years, many new and novel material families have been revealed including lots of members. To experimentally test all these materials is required so many efforts and cost [15]. Screening of large number of materials via computational approaches before carrying out experimental study has emerged as a promising strategy. Therefore, High-Throughput Computational Screening (HTCS) approaches and theoretical performance evaluation metrics were explored to identify the best performing materials for the target application or process. To perform HTCS approaches, firstly, material database is generated by collecting several materials either synthesized or hypothetical ones. Secondly, each member in the material family is tested for their performance of interest via computational approaches. Finally, the most promising candidates considering their performance were determined. The materials that have performance meet with targets examined experimentally [15]. According to the output of the experimental studies, the specific functionality in material database resulting in more advance process performance can be investigated in detail by computational approaches, specifically creating several hypothetical functionalities and screening them. The HTCS workflow specific for gas adsorption predictions is depicted in Figure 5.5 [15]. Initially, database for MOFs is created. Then, GCMC simulations are applied to obtain gas adsorption isotherms. To mimic real adsorption processes such as PSA,

VSA, or TSA, simulations are performed under different conditions (temperature, pressure). Finally, output of the simulations is evaluated using several adsorption metrics.

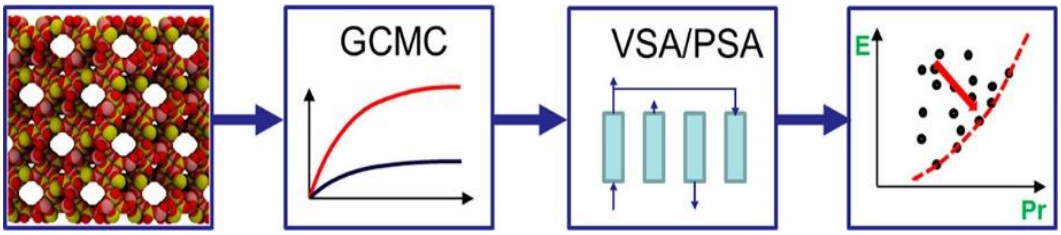

Figure 5.5: Multiscale workflow.

Heart of an adsorption process is the use of an efficient adsorbent with proper characteristics. Pore sizes and distribution, shapes of porous materials make them crucial for the adsorption process [132]. For example, zeolite with uniform micropores can easily separate molecules in according to their sizes. Thereby, requirement to fabricate porous materials with uniform pore size, shape, and volume has been increased in the recent years. Moreover, adsorption process efficiency not only depends on the adsorbent property but also interactions between structure of adsorbents as well as process configuration [15]. Many different porous materials have been synthesized that include diverse range of chemistry, network, and physical properties such as MOFs, Zeolitic Imidazolate Frameworks (ZIFs), COFs, Porous Organic Cages (POCs), Porous Aromatic Frameworks (PAFs), etc. [133]. At the initial single simulation studies, researchers mainly focused on the structural and functional properties of few porous materials for some special application [134]. However, with growing number of new materials, single simulation studies have been evolved to the HTCS for the identification of property of interest [134].

HTCS has emerged as a star research method to determine the relationship between structure and performance of materials for various applications such as carbon capture and sequestration, energy storage, batteries, etc. [134]. By using HTCS, dozens of materials can be examined easily at the same time [134]. For example, synthesizing, characterizing, and testing a new MOF can continue months even under optimal condition [133]. Comparing with the experimental studies, HTCS is faster, cheaper, and more effective method. Considering the gas adsorption or separation, to analyze thousands or dozens of materials provide us advantages in terms of identifying

adsorption behavior of such extensive material pool and their structure-performance relationship. Outputs of HTCS gives crucial information at the atomic scale to support the effective design of next-generation materials for adsorption.

Up to date, many HTCS studies have been performed for various porous materials to identify the best performing adsorbents. Especially MOFs, COFs and zeolites have been emerged among other materials because of their structural properties for adsorption and separation of gas mixtures. During HTCS studies, large number of materials were screened. These materials are either derived from experimental studies or created by hypothetically. The first pioneering material screening study has been reported 11 years ago by Krishna and Van Baten et al. [135] who examined adsorption, diffusion, and permeation selectivities of a few experimentally synthesized Zeolite, MOF, ZIF and CNT structures for CO_2/H_2, CO_2/CH_4, CO_2/N_2, CH_4/N_2, and CH_4/H_2 separation. Snurr and colleagues [136] studied with nearly 5000 MOFs taken from Computation-Ready Experimental MOF (CoRE MOF) database to investigate CH_4 storage capacity. Qiao et al. [137] also used CoRE-MOFs database and investigated CO_2 separation performance from flue and natural gas for 4764 MOFs. Differently, Avcı and coworkers [138] identified binary CO_2/H_2 separation of 3857 experimentally synthesized MOFs taken directly from Cambridge Structural Database (CSD) for PSA and VSA processes. Burns et al. [139] investigated post-combustion CO_2 capture performance of 5000 MOFs with experimentally characterized. Unlike MOFs, Tong and colleagues [140] studied with COFs. Almost 46 different COF were collected from experimental studies and their separation performance of gas mixtures, CH_4/H_2, CO_2/H_2, and CO_2/CH_4 were examined. In their second study, 187 COFs provided from CoRE COF database (computation-ready experimental COF database) were screened for adsorption-based noble gas (Kr, Ar, Xe, Rn) separation [141].

Computational screening took another forward step by the studies of Snurr and co-workers. Snurr and co-workers [142] examined 137953 hypothetical MOFs for CH_4 storage. At the second study [143], they simulated adsorption of CO_2, CH_4, and N_2 using same database. These studies were the first examples for computational screening which was applied to a large group of hypothetical MOFs. Hypothetical Zeolites (119661), and ZIFs (1031) were also investigated for post-combustion CO_2 capture by Balashankar and Rajendran [144]. Yang et al. [145] built 169898 ZIF structures from 84949 hypothetical zeolite networks and determined their CO_2 capture

from flue gas. Li et al. [146] created nearly 10000 multivariate MOFs, with mixed linkers and functional groups hypothetically, for defining CO_2 capture performance and CO_2/N_2 selectivity. Anderson et al. [147] created a set of MOFs containing 31 main MOF structures and their derivatives using Topologically Based Crystal Constructor (ToBaCCo) and computed their adsorption performances of pure CO_2 and CO_2/H_2 and CO_2/N_2 mixture. Pardakhti et al. [148] tested 130938 MOFs for CH_4 adsorption performance. They took MOFs from the database of hypothetical MOFs provided by the Snurr group. To predict high CO_2 working capacity and CO_2/H_2 selectivity for pre-combustion carbon capture process, Dureckova et al. [149] used 358,400 hypothetical MOFs. Likewise, large number of COFs were also hypothetically created for the screening study. For example, Mercado et al. [150] designed huge number of novel COFs nearly 69000 to screen CH_4 storage capacity. Differently, Martin et al. [151] created 4147 three dimensional COFs to investigate the CH_4 adsorption capacity. Considering HTCS studies with examining large data sets, a huge amount of data is accumulated. Most importantly, the accurate and effective evaluation of these large datasets is located at the center of the high-throughput screening studies. Therefore, the crucial point is to select proper performance indicator, in other terms, metrics for porous materials.

Effective performance indicator for adsorption should quantify properly the separation performance. Metrics were classified at several groups according to their evaluation parameters such as Intrinsic Structural (ISMM), Intrinsic Functional (IFMM), or Hybrid (HMM) Material Metrics. ISMM includes specific structural characteristics of materials which are observed from experimental or computational characterization results. IFMM includes functional properties of materials such as adsorption selectivity, working capacity and regenerability [152]. Third metric group combines different metrics in order to distinguish adsorbents correctly which have various performances. For example, Adsorbent Figure of Merit (AFM) [153], Sorbent Selection Parameter (SSP) [154], and Adsorbent Performance Score (APS) [155] combine working capacity and adsorption selectivity. Evaluation metrics are generally compared with each other using Spearman Correlation Coefficient (SCC) by means of the range of best performing materials. Adsorption metrics that is going to be used in the thesis for H_2/CO_2 separation are summarized at Table 5.2 [152-155].

Table 5.2: Performance evaluation metrics for adsorption-base separation.

Metric Class	Screening Metric	Definition
IFMM	Ideal gas adsorption selectivity	$\alpha_{ads.,\,CO_2/H_2}^{Ideal}=\frac{N_{CO_2}}{N_{H_2}}$
IFMM	Working capacity	$\Delta N_A=N_{ads.,A}-N_{des.,A}$
IFMM	Regenerability	$\%R=\frac{\Delta N_{CO_2}}{N_{ads.,\,CO_2}}\times 100\%$
HMM	Adsorbent figure of merit	$AFM=\Delta N_{CO_2}\times\frac{\left(\alpha_{ads.,\,CO_2/H_2}\right)^2}{\alpha_{des.,\,CO_2/H_2}}$
HMM	Sorbent selection parameter	$SSP=\alpha_{ads.,\,CO_2/H_2}\times\frac{\Delta N_{CO_2}}{\Delta N_{H_2}}$
HMM	Adsorbent performance score	$APS=\alpha_{ads.,\,CO_2/H_2}\times\Delta N_{CO_2}$

6. SIMULATION METHODOLOGY

In this section, molecular simulation methodology followed in the thesis will be provided. Specifically, initially the compiled MXene database will be explained. Then, structure optimization and charge assignment method for MXene structures will be given. Finally, simulation method used for the identification of single CO_2 and H_2 adsorption capacities is going to be discussed.

6.1 Compiling MXene Database

All MXene studies that have been identified for different applications are searched in the literature with the help of the Gebze Technical University library. A total of discrete 730 MXene structures identified from different areas are included in the database. Initially, 123 MXene structures of 730 are taken from the database created by the "Materials Theory and Simulations Group" (http://anant.mrc.iisc.ac.in/) belonging to the Professor Abhishek in the Institute of Science of India. Secondly, 222 MXene structures of 730 are taken from the database built by the group of Professor Thygesen named as "Computational 2D Materials Database (C2DB)" (https://cmrdb.fsyik.dtu.dk/c2db/). C2DB database includes several different 2D materials, not only MXene structure. Thirdly, the crystallographic files of 88 MXene structures of 730 are downloaded from supporting information files of four different articles (see Appendix A for the list of these studies) [156-160]. Finally, the rest of 297 MXene structures are compiled from different articles which did not provide their crystallographic files. For these 297 MXene structures obtained from literature, the relevant atom types are changed by using the crystallographic files of MXene structures provided in the literature.

6.2. Optimization and Charge Assignment

All prepared MXene structures are optimized using "Forcite module" of Material Studio 2017 version. Geometry optimization task of Forcite module is used to observe the structure with the minimized total energy. Hence, optimized structure represents

the minimum state in the potential energy surface. Various algorithms are proposed in Material studio software for geometry optimization such as steepest descent, conjugate gradient, Quasi-Newton, adjusted basis set Newton-Raphson (ABNR) and smart. Smart is used which combines algorithms of steepest-descent, ABNR, and quasi-Newton methods. Therefore, first, primitive structure of all MXene structures is examined for geometry optimization as non-periodic system and their cartesian atomic coordinates were optimized accordingly. The observed lattice parameters of MXene structures after optimization are compared with those taken from literature. The percent difference is shown in Figure 6.1 as a histogram. Accordingly, difference in Bravais lattice parameters was mainly < 5%. The population of the structures having the difference greater than 6% was too less, proving that optimized structures can be safely used for gas adsorption analyses.

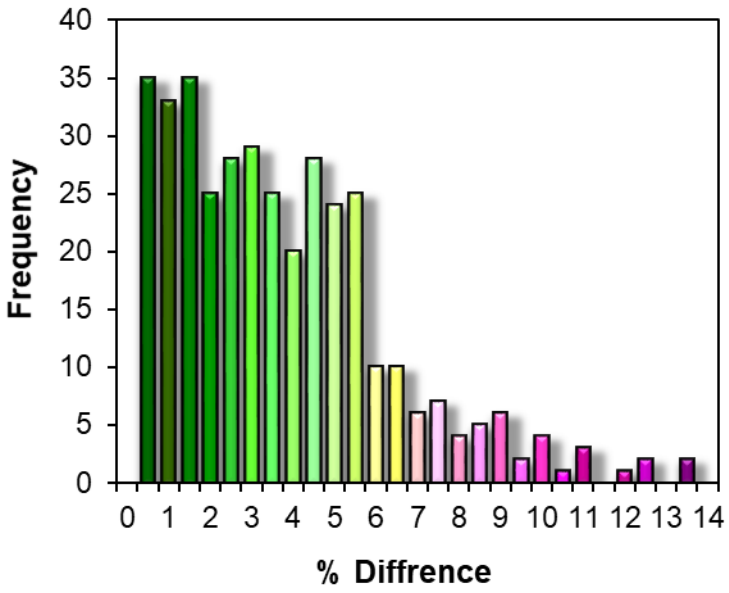

Figure 6.1: Population analyses of percentage difference in Bravais lattice parameters of MXene structures optimized within the thesis and reported in the literature.

As atomic partial charges are crucial for the identification of interactions between MXene structures and gases, quantum mechanics approach is applied to assign partial charges for all optimized MXene structures instead of QEq. Density Functional Theory (DFT) is used as a quantum mechanics approach which provides modelling electronic structures and energies of solids and surfaces accurately. DMol3 module of Materials Studio (version 2017) is used for DFT simulations to assign

partial charges for atoms of MXene structures. Various systems such as organic, inorganic molecules, molecular crystals, covalent solids, metallic solids, and surfaces of a materials were studied in the literature using DMol3 module. DMol3 produces accurate results and keep the computational cost low as an ab initio method. B3LYP (Becke 3-parameter Lee Yang Parr) [161, 162] is chosen as a nonlocal hybrid function (gradient-corrected functionals) for DMol3 to increase the accuracy of the predicted energies and structures. That kind of hybrid functions is utilized for improving the exchange-correlation energy function. Double Numerical plus-d function (DND) is selected as a basis set. DND includes a polarization d-function on all non-H_2 atoms. This basis set ensures reasonable accuracy for DFT simulations. Electrostatic potential (ESP) charges which are the atomic-centered charges that best reproduce the DFT Coulomb potential [163] were calculated with DND basis set.

6.3. Structure Arrangement

After charge assignment process, MXene structures were formed as periodic structures and their symmetry systems are imposed. Last step before carrying out simulations is to determine the interlayer distance of optimized MXene structures. In order to adjust interlayer distance of MXene structures, experimental studies in the literature are complied. D-spacing and interlayer distance of MXene structures taken from experimental studies [110, 112, 114, 164-171] are summarized in Table 6.1.

Table 6.1: Interlayer distance of MXenes used in experimental gas separation studies (* represents d-spacing).

$M_{n+1}X_nT_x$	Distance (Å)	$M_{n+1}X_nT_x$	Distance (Å)
$Ti_3C_2T_x$	11.4*	Ti_2CT_x	2.3-2.8
V_2CT_x	11.9*	$Ti_3C_2T_x$	3.4
$Ti_3C_2T_x$	12.9*	$Ti_3C_2T_x$	3.4
$Ti_3C_2T_x$	13.5*	$Ti_3C_2T_x$	4.0
$Ti_3C_2T_x$	13.8*	Ti_2CT_x	6.8-8.7
$Ti_3C_2T_x$	15.0*	$Ti_3C_2T_x$	9.3

Considering the data tabulated in Table 6.1, interlayer distance was adjusted to be 3.5 Å for all MXene structures. Since kinetic diameters of CO_2 and H_2 are 2.89 and 3.3 Å, respectively, gases are expected to enter between MXene layers easily. Since high-throughput screening is aimed to be applied for the 730 MXene structures, one specific interlayer distance is chosen for all MXene structures rather than setting different d-spacing values one by one for all structures considering the bulkiness of functional groups. Interlayer distance is adjusted by fixing the z-axis length of the crystal lattice without including the volume of the functional group. Considering the chemical formula of MXene as $M_{n+1}X_nT_x$, the lengths of z-axis are determined as 14, 15, 18, 20, 21, 23, 25, 28, and 30 Å when n+1 was 2, 3, 4, 5, 6, 7, 8, 9, and 10, respectively. Exceptionally, interlayer distance is set to 17 Å for MXene structures with n+1=2 and having bulky functional groups such as -NCS, -OCN, -SCN, -NCO, and -CN. Additionally, to determine the effect of interlayer distance on ideal gas separation, pre-defined interlayer distances are enlarged 3 Å more for all MXene structures and MXene structures with large interlayer distance are observed. Unit cells having x, y, and z lengths lower than 26 Å are redesigned to be close to each other by creating super cells. Lengths of z-axis of unit cell, cut-off distance, and enhancement factor from each length of unit cell are listed in Table 6.2.

Table 6.2: Set up parameters of MXene structures

Layers	C length (Å)	Cut-off (Å)	Enhancement
MXene structures with short interlayer distance			
2	14	13.5	9×9×2
2*	17	16.5	10×10×2
3	15	14	10×10×2
4	18	17	12×12×2
5	20	19	13×13×2
6	21	20	14×14×2
7	23	22	15×15×2
8	25	24	17×17×2
9	28	13.5	9×9×1
10	30	14.9	10×10×1
MXene structures with large interlayer distance			
2	17	16.5	11×11×2
2*	20	19	13×13×2
3	18	17	12×12×2
4	21	20	14×14×2
5	23	22	15×15×2
6	24	23	16×16×2
7	26	13	8×8×1
8	28	13.5	9×9×1
9	31	15	10×10×1
10	33	16	11×11×1

*MXene structures including bulky functional groups

6.4. Molecular Simulation Details for Gas Adsorption

Single gas adsorption capacities of CO_2 and H_2 are measured using GCMC simulation. Total 730 MXene structures with both short and large interlayer distances are used for adsorption analysis. To describe the pair interactions, partial charges are calculated using DFT method as explained in the section of 6.2, and vdW interactions of LJ 12-6 potential are taken from the UFF. All MXene structures are kept fixed

during GCMC simulations and applied periodic boundary conditions. For CO_2 and H_2 molecules, the rigid body model of Transferable Potentials for Phase Equilibria (TraPPE) is used, since TraPPE describes well the vapor-liquid and liquid-solid equilibria of CO_2 [172]. CO_2 is modelled as a rigid molecule including three atomic centers whereas H_2 is modeled as single atom of LJ site. The bond length of C-O is fixed at 1.16 Å and O-C-O bond angle is fixed at 180° for CO_2 [172]. The LJ interactions between pairs are calculated from Lorentz-Berthlot mixing rules [173]. Cut-off is determined as the half of the c length (z) of the unit cell for each MXene structure, which are listed in Table 6.2.

GCMC simulations are performed using RASPA simulation software (version 2.0.41) [174] to define single CO_2 and H_2 adsorption capacities of MXene structures. Equilibration and production cycles are 50,000 and 250,000 for CO_2 while those are 5,000 and 20,000 for H_2. The cycle numbers are defined based on the least deviation by testing different cycles for each gas and for three different MXene structures. All simulations are carried out at 35°C and 0.1, 1, and 10 bar. The input file including all parameters and RASPA commands for Ti_2CO_2 is shown in Figure 6.2.

```
SimulationType                  MonteCarlo
NumberOfCycles                  250000
NumberOfInitializationCycles    50000
PrintEvery                      10000
CutOff                          13.5
UseChargesFromCifFile           yes

Framework                       0
FrameworkName                   Ti2CO2
UnitCells                       9 9 2
ExternalTemperature             308.0
ExternalPressure                10000 100000 1000000

Component 0 MoleculeName                CO2
            TranslationProbability      0.5
            WidomProbability            1.0
            RotationProbability         0.5
            ReinsertionProbability      0.5
            SwapProbability             1.0
            CreateNumberOfMolecules     0
```

Figure 6.2: Input file of Ti_2CO_2 for RASPA

PSA and VSA emerge as mostly used adsorption processes at the industry. Adsorption is generally occurred at 10 bar, and pressure should be decreased to 1 bar in PSA process for desorption. However, in VSA process, system is reduced to low

pressures using vacuum for desorption of the adsorbed gases under ambient conditions. To simulate these conditions, adsorption and desorption pressures used for PSA are 10 and 1 bar, and for VSA are 1 and 0.1 bar, respectively. Accordingly, after the corresponding single CO_2 and H_2 adsorption capacities are computed, adsorbent metrics provided in Table 5.2 are calculated. Since recently, regenerability become an important metric in the selection of suitable adsorbent for industrial applications, rather than using selectivity metric, APS and R% are used together for the selection of top performing MXene structures. Therefore, simply ignoring the predefined R% criteria for MOF adsorbents [138, 175, 176], MXenes having R% > 90% are focused on this thesis. Following this criterion, the remaining MXene structures are ranked based on their APSs. Top 10 MXenes with the highest APSs for CO_2/H_2 separation are determined both for MXene structures having short and large interlayer distances.

7. RESULTS AND DISCUSSION

In this section, firstly single gas (CO_2 and H_2) adsorption measurements of MXenes having short and large interlayer distances will be evaluated in according to the APS and working capacity. Then, correlation between adsorption metrics for MXenes will be explained, again considering MXenes both having short and large interlayer distances. Finally, based on regenerability (R%) criteria (>90%) and ranking using APS, AFM and SSP as separate metrics, top 10 MXene lists will be observed for PSA and VSA processes.

7.1. Relationship between APS and Working Capacity

GCMC simulations of 730 MXene structures for single CO_2 and H_2 adsorption were carried out at 35°C and 0.1, 1, and 10 bar. Adsorption capacities of MXenes at three different pressures were listed in Appendix B for MXenes with short interlayer spacing, and Appendix C for MXenes with large interlayer spacing along with all adsorption metrics (Table 5.2) that we aimed to identify. These adsorption metrics were identified in Section 5, but to summarize them briefly again, adsorption selectivity is expressed by the ratio of highly adsorbing gas (CO_2) to the least adsorbing gas (H_2). Working capacity is defined by the difference between gas adsorption uptakes at adsorption and desorption pressures which are 10 and 1 bar for PSA and 1 and 0.1 bar for VSA, respectively. High selectivity indicates highly purified gas stream while high working capacity remarks great efficiency for the adsorbents. However, adsorbents with high selectivity generally exhibit low working capacity and vice versa. To determine the effect of adsorption selectivity and working capacity, adsorption performance score (APS) is used to include the effects of these two parameters by multiplying them. In this thesis, calculated APS, adsorption selectivity and working capacity for each MXene structure with short interlayer spacing are depicted in Figure 7.1 for PSA and VSA processes and used to reveal the adsorption performance of MXene family.

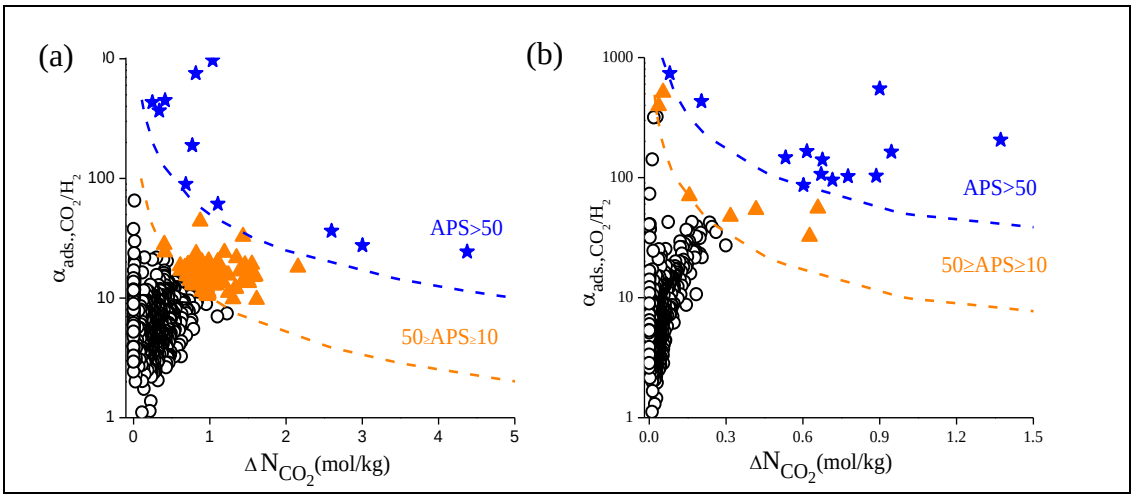

Figure 7.1: Relation between adsorption selectivity, working capacity, and APS of MXenes having short interlayer distance for CO_2/H_2 separation at (a) PSA and (b) VSA conditions. Black empty circles, orange triangles, and blue stars represent MXenes with APS < 10, 10 < APS < 50, APS > 50 mol/kg, respectively.

Up to date, the upper and lower limits of APS and adsorption selectivities of CO_2/H_2 were revealed for MOFs, COFs, and Zeolites in different research. For example, Avcı and colleagues [138] reported the upper limits of APS as 6,339 and 2,365 mol/kg for VSA and PSA, respectively for 3,857 MOF structures. Adsorption selectivity of CO_2/H_2 was in range of 2 to 25,000 for PSA and 2 to 85,000 for VSA. However, the highest regenerability was determined as 86.76 and 88.05% for PSA and VSA, respectively. After two years, the same group [177] increased the number of MOF structures from 3,857 to 10,221 and investigated their CO_2/H_2 separation performances. Although APS and CO_2/H_2 adsorption selectivity reached to 9,834 mol/kg and 119,000 under VSA condition, respectively, regenerability values were not improved and almost same as their previous study. Unlike MOFs, COFs which were taken from CoRE COF database and screened by Aksu et al. [178] displayed lower APS ranging between 0.1 and 802 mol/kg for VSA. The highest adsorption selectivity of CO_2/H_2 was observed as 1,000 for VSA condition. Regenerability for 288 COF structures varied between 86-90%. On the other hand, 3,184 hypothetical COF structures were examined for CO_2/H_2 separation by Aksu et al. [179]. They reported maximum APS as 3,736 mol/kg and adsorption selectivity as 954 for VSA conditions. Finally, Shi et al. [180] studied 2,625 hypothetical aluminosilicate Zeolites for CO_2/N_2 separation. The highest APS was calculated as 671 mol/kg for VSA with adsorption selectivity of 5,473 and 1,313 for PSA and VSA, respectively. However, the highest

regenerability ratio was recorded as 66.37% which was lower than those of MOFs and COFs.

For PSA and VSA conditions, the upper limit of APS was calculated as 50 mol/kg for MXene structures having short interlayer distance. MXene displayed lower APS and adsorption selectivity compared to the other 2D nano materials such as MOFs and COFs previously reported in the literature [138, 177-179]. MXene with APS values above 50 mol/kg are shown with blue circles in Figure 7.1 (a) and (b), respectively. Accordingly, MXene structures with high APS values display either high ideal adsorption selectivity (>100 for both PSA and VSA) or high working capacity (>2 mol/kg for PSA and >0.5 mol/kg for VSA). Examining MXene structures in according to the highest APS value (>50 mol/kg), 11 and 13 types of MXene structures are available for PSA and VSA, respectively. For PSA process, APS performance of these 11 MXene structures, which consist of two different metals and are un-functionalized, is governed by mainly high adsorption selectivity. However, considering VSA process, APS performance of 13 MXene structures are governed by great working capacity and comparable adsorption selectivity. These MXene structures are the ones with functionalized with bulky groups such as T_x = -$(NCS)_2$. Thanks to these bulky groups, desorption of CO_2 is facilitated and high CO_2 working capacity is observed. In addition, sulphur element in the bulky groups provides higher affinity towards to the CO_2 than H_2 resulting in enhanced adsorption selectivity for these MXene structures. Anderson and colleagues [147] have examined several MOFs for the effect of different functional groups on CO_2 adsorption. The binding energies of examined functional groups for CO_2 were calculated as follows: -$(NH_2)_2$ > -$(CN)_4$ > -$(SH)_2$ > -$(NO)_2$ > -$(OH)_2$ > -$(CN)_2$ > -$(F)_4$ > -$(Br)_2$ > -$(CF)_3$ > -$(F)_2$ > -$(CH)_3$ > -$(H)_4$ > -$(Br)_4$. They emphasized that this arrangement was also same when they were compared according to their binding dipole moments. MOFs' functional groups including S and N elements showed higher CO_2 adsorption capacity whereas MOFs with -Br_2 and -F_2 functional groups exhibited low CO_2 uptake. Additionally, a different analysis, but a similar result was suggested by Daglar et al. [181]. They investigated CO_2, H_2, and CH_4 adsorption performance of MOF structures having different functional groups and aimed to reveal the alteration in gas adsorption with the removal of these functional groups. With the removal of bulky functional groups, great increments in gas adsorption capacities were computed from molecular simulations. However, no change in gas adsorption capacities was recorded with the removal of

small groups like -Cl_2, -F_2, and -Br_2. These studies support our findings and exhibit that the arguments observed for metal containing structures like MOFs may also be valid for MXenes. According to the second criteria of APS values of MXene structures ranked between 10 and 50 mol/kg, there are 93 and 7 MXenes in PSA and VSA conditions, respectively. These structures show both mediocre adsorption selectivities and CO_2 working capacities for PSA process. However, high adsorption selectivities (>50) are observed at these APS range for MXene structures in VSA conditions.

To further examine the effect of interlayer spacing between the layers of 2D MXene structures, their interlayer distances are increased further following the methodology provided in Section 6. There are two important things worth to be noted in relation to the interlayer distance. (i) it was suggested in the literature that due to the smooth surface of 2D nanomaterials, fluid transport through the inner sides of channels is facilitated, and in addition, due to the uniform distribution of adsorption sites on their smooth surface, layered-wise accommodation on their surfaces can take place. All these enhances the gas adsorption on 2D materials. (ii) However, it was observed that large interlayer spacing in these 2D materials hinders the effective adsorption of fluids on their surface due to the loss of interaction with the adsorbents. Therefore, the large increase in interlayer distance does not work in 2D materials, which suggest the need for optimum interlayer distance for better adsorption performance. Since it is aimed in this thesis to screen the performance of all MXene structures, their interlayer distances are fixed as it was detailed in Section 6. However, due to the bulky functional groups on the surface of some MXene structures, gas adsorption is not monitored. By increasing the interlayer distance for all structures, it is aimed to observe the enhancement in adsorption performance of MXenes having bulky functional groups, and to provide the alteration in adsorption performance of MXenes having small functional groups. Similarly, APS, adsorption selectivity and working capacity for each MXene structure with large interlayer spacing are depicted in Figure 7.2 for PSA and VSA processes.

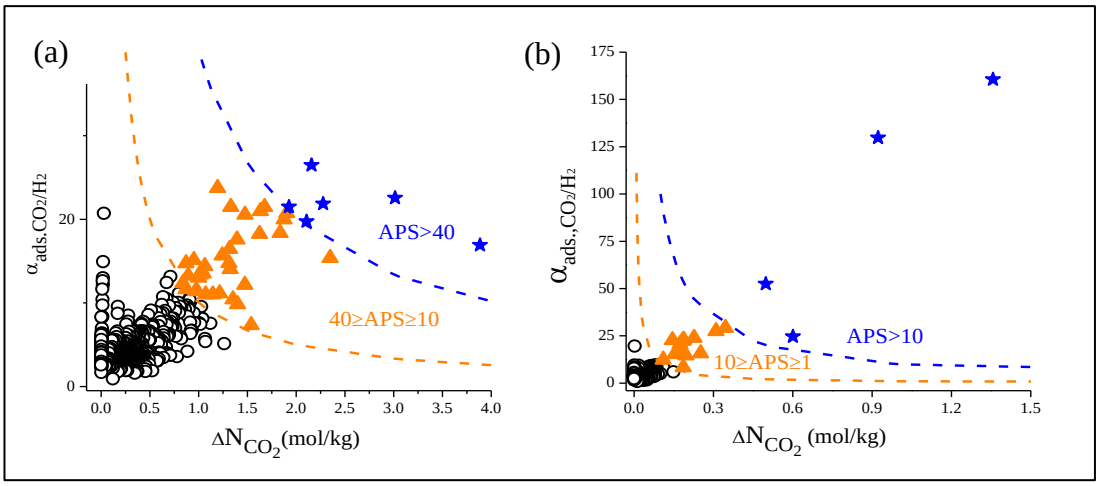

Figure 7.2: Relation between adsorption selectivity, working capacity, and APS of MXenes having large interlayer distance for CO_2/H_2 separation at (a) PSA and (b) VSA conditions. Black empty circles, orange triangles, and blue stars represent MXenes with APS<10 and APS < 1, 10<APS<40 mol/kg and 1<APS<10, APS>40 and APS>10 mol/kg for PSA and VSA, respectively.

According to Figure 7.2 (a) and (b), MXene structures with high APS values display improved adsorption selectivity (>20 for PSA and VSA) and the comparable working capacity (>1.5 mol/kg for PSA and >0.3 mol/kg for VSA). Considering the MXene having APS>40 mol/kg, 6 and 4 different structures are noticed for PSA and VSA, respectively. For PSA process, similarly, MXene structures functionalized with bulky groups of T_x = -$(NCS)_2$ dominate this portion. However, for VSA process, contrarily to the observation gained from MXene structure with short interlayer spacing, in-plane ordered vacancy MXenes such as $W_{1.33}C$ and $Nb_{1.33}C$ are revealed the greatest APS values after interlayer distance enhancement. This is not surprising due to the fact that MXenes with vacancies have an open metal site which can be easily accessible by gas molecules, and the enhancement in interlayer spacing does not lead to the loss in interaction with MXene surface and bring them to the first place in APS by improving both selectivity and working capacity. Finally, compared to the MXene structures with short interlayer distance, CO_2 working capacity increased whereas adsorption selectivity decreased for PSA and VSA conditions with the enhancement in interlayer spacing. This can be attributed to the fact that both gases can find a place to be adsorbed by leading the decrease in adsorption selectivity. To specifically elaborate this observation, the adsorbed coordination of CO_2 and H_2 molecules on the surface of $V_2Ti_2C_3$ MXene, which is chosen as an example, is identified in Figure 7.3. It can be seen that CO_2 molecules are arranged especially on the Ti element and occupy

it. However, H_2 molecules differ from CO_2 by coordinating mostly in the bridge position between C and V elements. The fact that they prefer different adsorption sites on the MXene surface displays that there will not be any competition between them for the same adsorption site. However, it should be noted that since the metals are very close to each other in MXene structure, due to the bulkiness of CO_2, after the enhancement in interlayer spacing, CO_2 adsorption capacity of MXenes at the specific pressure will not much further improve as H_2 uptake, leading to the decrease in ideal adsorption selectivity.

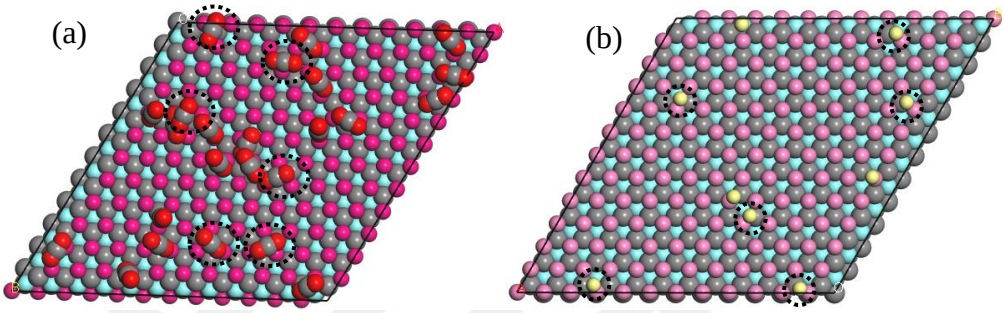

Figure 7.3: Coordination of (a) CO_2 and (b) H_2 on the surface of $V_2Ti_2C_3$ MXene after adsorption. (V, Ti, C, H and O elements are represented with pink, light blue, grey, yellow, and red colors.)

7.2. Correlation of Performance Metrics

In addition to the APS metric, AFM and SSP metrics are also used to compare the adsorbent performance of adsorbents in the literature. MXene structures having short interlayer distance are ranked based on APS. The first 10 MXenes with greatest APS are defined. Their APS, AFM, and SSP metrics are compared in Figure 7.4 to provide the relation between these metrics.

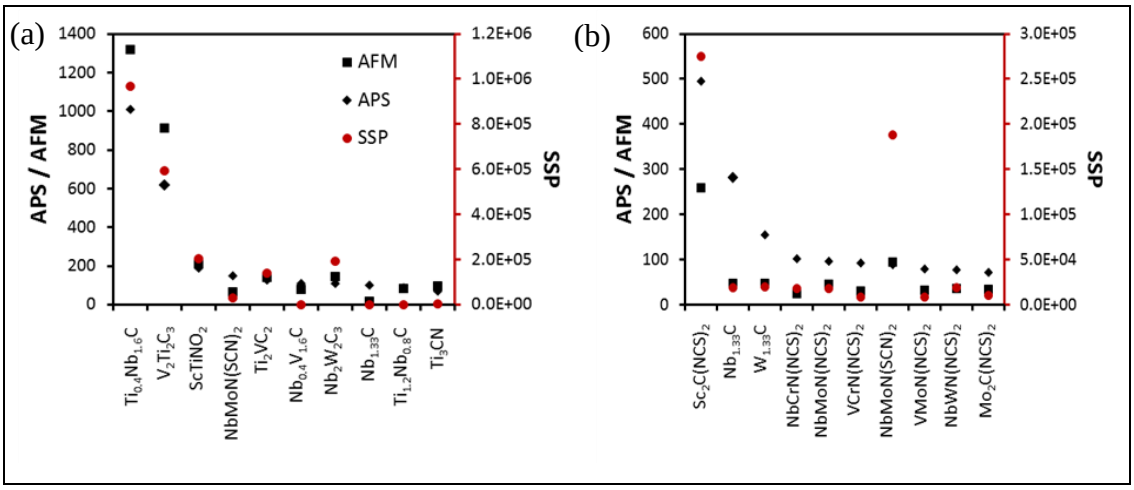

Figure 7.4: For CO_2/H_2 separation, top 10 MXene structures and relationship with APS-AFM-SSP (a) at PSA and (b) VSA conditions.

Considering Figure 7.4, up to fifth and sixth MXene structures, similar ranking in each metric is observed for PSA and VSA. However, there are some discrepancies in the further MXenes. For example, $Nb_2W_2C_3$ is the seventh best MXene structure in PSA process in according to the APS ranking whereas it is fourth MXene for SSP ranking. For VSA condition, $NbMoN(SCN)_2$ is the second MXene ranked according to the SSP while it is ranked as the lowest in both APS and AFM metrics. To apply this ranking analysis for all data set including MXene structures with short and large interlayer distances, Spearman correlation is used in this thesis. Spearman correlation gives us information about how similar the rankings of two different data sets (r_s) are. The r_s value calculated from this correlation varies between -1.0 and +1.0. It becomes unity if the correlation perfectly matches in two independent rankings. The r_s value of 0 represents the lack of correlation. Binary Spearman correlation coefficients for APS, AFM, and SSP parameters are summarized in Table 7.1 for MXene structures with short and large interlayer distances.

Table 7.1: Binary Spearman correlation coefficients (SRCC) of all MXene structures for APS, AFM, and SSP parameters.

	APS-AFM	APS-SSP	AFM-SSP
MXenes with short interlayer distance			
PSA	0.977	0.723	0.683
VSA	0.999	0.765	0.766
MXenes with large interlayer distance			
PSA	0.999	0.594	0.609
VSA	0.999	0.562	0.565

Table 7.1 presents that SRCC values especially between APS and AFM rankings are higher than 0.8, more importantly almost 1, indicating that there is a high correlation between this metrics for MXenes at both PSA and VSA conditions. Similar ranking in APS and AFM metrics suggests us the similarity in the parameters of adsorption and desorption selectivities. However, SRCC is very weak between APS-SSP and AFM-SSP, providing that SSP metric gives us a different the ranking in MXenes both having short and large interlayer distance. In other words, the including H_2 working capacity in SSP metric differs the ranking considerably for MXenes. On the other hand, almost all correlations are hindered with the enhancement of interlayer spacing, except the one between APS and AFM.

7.3. Regenerability and Promising 10 MXene

Percent regenerability (R%) is the ratio between CO_2 working capacity and adsorption capacity [178]. Relation between R% and APS for PSA and VSA processes are given in Figure 7.5 for MXene structures with short interlayer distance. Considering MOFs and COFs [138, 177-179], percent regenerability reached to the 88% while the lowest regenerability was reported as 66% for Zeolites. Therefore R% criterion was preferred as 85% in literature [138, 175]. In this thesis, R% criterion is accepted as 90% for MXene structures.

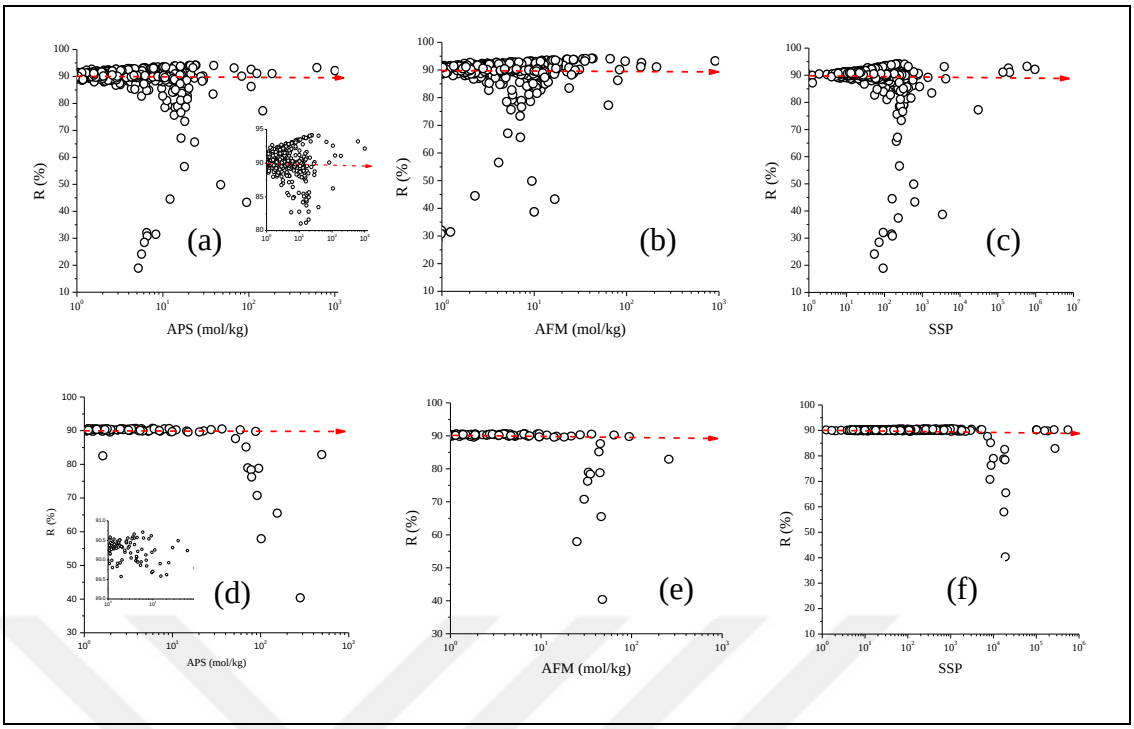

Figure 7.5: Relation between R% and APS, AFM and SSP of MXenes having short interlayer distance for CO_2/H_2 separation at (a, b, c) PSA and (d, e, f) VSA conditions, respectively. Red dotted lines show the minimum desired R% = 90%.

The highest R% values are obtained as 94.1% and 92.3% for PSA and VSA conditions, respectively. Almost 64% of total MXene structures revealed R%>90% for PSA process while it is much greater as 84% for VSA. On the other hand, MXene structures with R%<85% are very few such as 42 for PSA and 10 for VSA. These results demonstrate that MXenes can be easily reused several times in the consecutive adsorption-desorption cycles. With considering the criteria of R%>90%, ranges of APS, AFM, and SSP metrics for the best 10 MXenes are between 10-1006, 12-1320, and 240-966 mol/kg, respectively for PSA. However, those values sharply decrease for VSA process. Similar relation is also drawn in Figure 7.6 for MXene structures with large interlayer distances in PSA and VSA conditions.

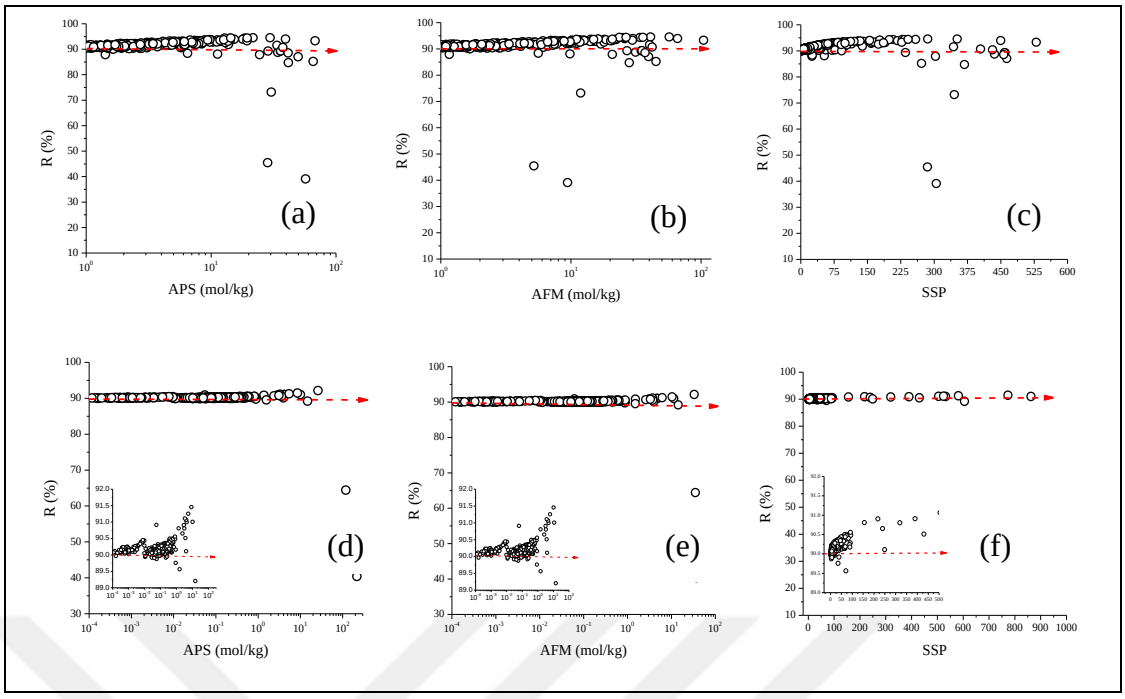

Figure 7.6: Relation between R% and APS, AFM, and SSP of MXenes having large interlayer distance for CO_2/H_2 separation at (a, b, c) PSA and (d, e, f) VSA conditions, respectively. Red dotted lines show the minimum desired R% = 90%.

The highest R% are obtained as 94.5% and 92.1% for PSA and VSA conditions, respectively, which are almost same with the performance of MXenes with short interlayer distance. This evidently displays that interlayer enhancement does not influence the regenerability performance of MXenes. The number of MXene structures with R%>90% is reached to 98% and 95% of total MXenes for PSA and VSA, respectively. For PSA and VSA processes, the number of MXenes with R%<85% is only 4 and 2, respectively. However, the upper values of APS and AFM, are below 100 mol/kg for PSA compared to the promising MXenes with short interlayer distance. The highest and lowest values of SSP are 530 and 155. For VSA process, the upper limits of APS and AFM decreased below 50 mol/kg as same as MXenes with short interlayer distance. Importantly, the highest SSP value surpasses 1000 and reaches to 2818 mol/kg. This is explained by the effect of enhanced interlayer distance on H_2 working capacity. Finally, promising 10 MXene lists are prepared, initially considering R%>90%, and then ranking APS, AFM, and SSP metrics for MXene structures having short and large interlayer distances, separately. For MXene structures having short interlayer distance, promising 10 MXene structures are given in Table 7.2.

Table 7.2: Promising 10 MXene structures derived from each adsorbent metric (APS, AFM, and SSP) for PSA and VSA processes. Please note that this list is obtained considering the short interlayer distance of MXene structures.

PSA			VSA		
APS	**AFM**	**SSP**	**APS**	**AFM**	**SSP**
$Ti_{0.4}Nb_{1.6}C$	$Ti_{0.4}Nb_{1.6}C$	$Ti_{0.4}Nb_{1.6}C$	$Ti_{0.4}Nb_{1.6}C$	$Ti_{0.4}Nb_{1.6}C$	$Ti_{0.4}Nb_{1.6}C$
$V_2Ti_2C_3$	$V_2Ti_2C_3$	$V_2Ti_2C_3$	Cr_2CS_2	Cr_2CS_2	$V_2Ti_2C_3$
$ScTiNO_2$	$ScTiNO_2$	$ScTiNO_2$	$V_2Ti_2C_3$	$V_2Ti_2C_3$	Ti_2VC_2
Ti_2VC_2	$Nb_2W_2C_3$	$Nb_2W_2C_3$	$NbCrN(NCO)_2$	$NbCrN(NCO)_2$	$Nb_2W_2C_3$
$Nb_2W_2C_3$	Ti_2VC_2	Ti_2VC_2	Ti_2VC_2	Ti_2VC_2	$TaCrN(OCN)_2$
$Ti_{1.2}Nb_{0.8}C$	Ti_3CN	Ti_3CN	$VCrNBr_2$	$VCrNBr_2$	$NbCrN(NCO)_2$
Ti_3CN	$Ti_{1.2}Nb_{0.8}C$	Ti_2C	$Ti_{1.2}Nb_{0.8}C$	$Ti_{1.2}Nb_{0.8}C$	Cr_2CS_2
$Ti_{0.8}Nb_{1.2}C$	$Ti_{0.8}Nb_{1.2}C$	$Ti_{1.2}Nb_{0.8}C$	$Cr_3N_2(OH)_2$	$Cr_3N_2(OH)_2$	Ti_3CN
$NbCrNCl_2$	Cr_2TiCN	$TiCrCO_2$	$VMoNBr_2$	$NbCrNBr_2$	$TaMoNBr_2$
Cr_2TiCN	Cr_2VCN	$NbCrNCl_2$	$NbCrNBr_2$	$VMoNBr_2$	$TaCrNBr_2$

Considering Table 7.2, $Ti_{0.4}Nb_{1.6}C$ is emerged at the first order in according to all performance metrics both at PSA, and VSA conditions. The CO_2/H_2 adsorption selectivities of $Ti_{0.4}Nb_{1.6}C$ are 678, 739, and 970 at 0.1, 1, and 10 bar, respectively. R% values of $Ti_{0.4}Nb_{1.6}C$ are 92.1 and 90.2% for PSA and VSA, respectively. For PSA conditions, first, second and third MXene structures are same in each adsorption metric and the rest of promising MXene structures are almost same with only alteration in their rankings in the list of adsorption metrics. For VSA conditions, promising MXene structures ranked according to the APS and AFM are the same however according to SSP metric, different promising MXene structures are observed such as $TaCrN(OCN)_2$, $NbCrN(NCO)_2$, $TaMoNBr_2$, and $TaCrNBr_2$. This evidently reveals that introduction of the H_2 working capacity as a parameter in the adsorption metric considerably changes the promising adsorbent material in MXene structures, especially at VSA conditions.

Promising MXene structures for PSA mostly include two types of metal and no functional groups. These types of MXenes are also seen within the promising structures for VSA. However, for all adsorption metrics, functionalized MXene structures generally become prominent at VSA process such as the one having bulky functional groups, $–(OCN)_2$, $–(NCO)_2$ or small functional groups such as $-Br_2$, $-S_2$ and $-OH_2$. Considering APS, AFM, and SSP, four MXene structures are observed as common for both conditions. These MXenes are $Ti_{0.4}Nb_{1.6}C$, $V_2Ti_2C_3$, Ti_2VC_2, and $Ti_{1.2}Nb_{0.8}C$. Their common features are comprising of two types of metal, being un-

functionalized, and including Ti element accompanying the other metal type. Therefore, since metal atoms are unsaturated on the MXene surfaces, they can easily interact with gas molecules. There are other studies that supports this observation. For example, Qiao and co-workers [137] studied 4764 MOFs for CO_2 separation from flue gas and natural gas. Best performing MOF structures for CO_2 adsorption were mostly contained unsaturated metals. Moreover, they proposed that MOFs which contain second metal besides to the transition metal had high separation performance for CO_2. Sun et al. [182] synthesized bimetallic MOF structures and investigated their adsorption performances of 1-hexene and n-hexane. Bimetallic MOF structures exhibited high adsorption selectivities of 1-hexene/n-hexane than the others containing only one metal. Collectively, it is not surprising to observe $Ti_{0.4}Nb_{1.6}C$, V_2TiC_3, Ti_2VC_2, and $Ti_{1.2}Nb_{0.8}C$ structures as promising MXene types for CO_2/H_2 separation.

Similarly, for MXene structures having large interlayer distance, promising 10 MXene structures are provided in Table 7.3. Accordingly, Cr_2CS_2 takes the first place in rankings based on all adsorbent metrics for PSA, while first place belongs to $NbCrN(NCS)_2$ for VSA. The CO_2/H_2 adsorption selectivities of Cr_2CS_2 are 13, 15, and 23 for 0.1, 1, and 10 bar, respectively. R% value of Cr_2CS_2 is 93.3 for PSA. The CO_2/H_2 adsorption selectivities of $NbCrN(NCS)_2$ are 42, 52, and 21 for 0.1, 1, and 10 bar, respectively. Regenerability ratio of $NbCrN(NCS)_2$ was 92.1% for VSA. For PSA conditions, based on ranking of APS and AFM, promising MXene structures are almost same with minor changes in their ordering. Tantalum metal including MXene structures, $TaMoN(NCS)_2$ and $TaCrNBr_2$, are emerged in the promising 10 MXene structures ranked according to the SSP. Commonly, MXene structures with bromine and sulfur containing functional groups become prominent for PSA. Surprisingly, only MXene structures in the form of M_2XT_x (two metal layer) are caught from each metric. Adsorption capacity of CO_2 increased more than H_2 owing to the strong interaction CO_2 and metals. Thus, CO_2/H_2 adsorption selectivity improved especially at 10 bar for MXenes containing double metals. For VSA conditions, again similar type of MXene structures is observed based on each metric but there is considerable alteration in their ordering after the sixth MXene structure. Nearly all promising MXene structures ranked based on each metric in VSA have double metals and bulky functional group of $–(NCS)_2$. Since adsorption of H_2 increases as much as CO_2 adsorption, CO_2/H_2 adsorption selectivity also decreases. Moreover, the presence of sulphur element also made them efficient for VSA process. The only MXene in the promising 10 lists

ranked according to all three-performance metrics for PSA and VSA processes is $YCrC(NCS)_2$.

Table 7.3: Promising 10 MXene structures derived from each adsorbent metric (APS, AFM, and SSP) for PSA and VSA processes. Please note that this list is obtained considering the large interlayer distance of MXene structures.

PSA			**VSA**		
APS	**AFM**	**SSP**	**APS**	**AFM**	**SSP**
Cr_2CS_2	Cr_2CS_2	Cr_2CS_2	$NbCrN(NCS)_2$	$NbCrN(NCS)_2$	$NbCrN(NCS)_2$
Mo_2CS_2	Mo_2CS_2	Mo_2CS_2	$Sc_2C(NCS)_2$	$Sc_2C(NCS)_2$	$Sc_2C(NCS)_2$
$YCrC(NCS)_2$	$VCrNBr_2$	$TaMoN(NCS)_2$	$VCrN(NCS)_2$	$VCrN(NCS)_2$	$VCrN(NCS)_2$
$ScYC(NCS)_2$	$YCrC(NCS)_2$	$YCrC(NCS)_2$	$VMoN(NCS)_2$	$VMoN(NCS)_2$	$VMoN(NCS)_2$
$VCrNBr_2$	$NbCrNBr_2$	$VCrNBr_2$	$Mo_2C(NCS)_2$	$Mo_2C(NCS)_2$	$Mo_2C(NCS)_2$
$NbCrNBr_2$	$ScYC(NCS)_2$	$ScYC(NCS)_2$	$NbMoN(NCS)_2$	$NbMoN(NCS)_2$	$NbWN(NCS)_2$
$VMoNBr_2$	$VMoNBr_2$	$NbCrNBr_2$	$Ti_{1.2}Nb_{0.8}C$	$Ti_{1.2}Nb_{0.8}C$	$NbMoN(NCS)_2$
$VCrN(SCN)_2$	Cr_2CBr_2	$VMoNBr_2$	$Y_2C(NCS)_2$	$NbWN(NCS)_2$	$Y_2C(NCS)_2$
Cr_2CBr_2	$Sc_2C(OCl)_2$	$VWNBr_2$	$NbWN(NCS)_2$	$Y_2C(NCS)_2$	$TaMoN(NCS)_2$
$Sc_2C(OCl)_2$	$VCrN(SCN)_2$	$TaCrNBr_2$	$YCrC(NCS)_2$	$YCrC(NCS)_2$	$YCrC(NCS)_2$

8. CONCLUSIONS AND RECOMMENDATIONS

In this thesis, it is aimed to investigate CO_2 adsorption-based separation performances of different MXene structures whose crystal structure information are collected from various databases and literature. Some of structure are created and their geometries are optimized and hence, I am ended up with totally 730 MXene structures. To compute gas adsorption capacities of MXenes, grand canonical Monte Carlo simulation method has been applied and the computed adsorption capacities are evaluated according to several adsorbent performance metrics. To identify the effect of interlayer distance on gas adsorption performance of MXenes, their interlayer spacing is enhanced and the same simulation methodology is followed for them.

Relationship between CO_2 working capacity and CO_2/H_2 adsorption selectivity of all MXene structures having both short and large interlayer distances is investigated for PSA and VSA. Considering MXene structures having short interlayer distances, ones having the highest APSs exhibited high adsorption selectivity or high working capacity for PSA and VSA. However, slight decrement is observed in adsorption selectivities at VSA conditions compared to PSA.

Considering the structures having each interlayer distance, MXenes containing double metals with unfunctionalized form displayed high APS performance in PSA process. It is suggested that the absence of functional groups in the MXenes made them more susceptible towards CO_2 leading to the strong interaction between metals and CO_2. However, especially MXenes functionalized with bulky groups such as $–(NCS)_2$ are emerged for VSA process according to only APS ranking. With these results, it is revealed that bulky groups including Sulphur element improve CO_2 working capacity and also facilitate desorption.

In general, enhancement of interlayer distance caused to the improved CO_2 working capacity and decrease in adsorption selectivity for PSA. However, both parameters are hindered for VSA with the interlayer alteration, revealing the considerably decreased CO_2 adsorption capacities (589 out of 730 structures) and slightly increased H_2 adsorption capacities. Since the adsorption sites on MXene structures are different for each gas, it is expected to observe enhanced gas uptakes. However, the more interact gas molecule as CO_2 is highly coordinated in the hindered

interlayer distance due to the smooth surface of MXene and hence this leads to great CO_2 uptake for MXene having short interlayer distances.

The relationship between mostly used performance metrics such as APS, AFM, and SSP are revealed by calculating SRCC. High correlation between APS-AFM brought us similar MXene ranking while low correlation of AFM-SSP caused changes in rankings of MXenes for PSA and VSA due to the contribution of H_2 working capacity as a parameter in SSP.

The lower limit of R% is determined as 90% for all MXenes at each condition. The highest R% values are observed as 94% and 92% for PSA and VSA, respectively. These results indicate that MXenes can be used repeatedly as an adsorbent for gas separation.

Promising structures are revealed using the criteria firstly R%>90% and then APS ranking for PSA and VSA for MXenes with short and large interlayer distances. For both processes and all performance metrics, MXenes containing double different metals are emerged in the performing lists. However, the best performing MXenes with short interlayer distance had no functional group for PSA conditions whereas some MXenes contained small and large functional groups such as -(OH), -$(NCO)_2$ for VSA. Contrarily, evaluating MXenes with large interlayer distance, bulky functional groups dominated adsorption performances especially in VSA conditions. Small functional group such as -(Br_2) is noteworthy for PSA. Accordingly, for further studies, some recommendations are proposed as follows:

- To carry out more systematic research, the number of MXenes should be increased by constructing all possible MXene structure combinations.

- Since charge calculation is important for MXene-gas interactions, different partial charge assignment methods can be applied for point charges of atoms on MXene structure.

- To highlight the performance limit of promising MXenes for gas adsorption, their gas uptakes should be investigated at severe conditions: high temperature or pressure, binary or ternary gas compositions, humid gas stream, etc.

- To identify the possible processes, the performance of MXene structures can be identified for TSA, PTSA, or VTSA processes.

- In addition to CO_2/H_2 separation, investigations for different gas pair separations should be carried out considering the MXene database.

Since this is the first study identifying the performance of MXene adsorbents for CO_2/H_2 separation, it starts from examining the ideal case as single gas adsorption for specifically concentrating on only PSA and VSA processes. However, with the proposed further studies, the advantages of MXene family in adsorption-based gas separation will be revealed completely and hope, this will be ended up with the contribution of new and novel adsorbents to the separation technology.

REFERENCES

[1] Mondal M. K., Balsora H. K., Varshney P., (2012), "Progress and trends in CO_2 capture/separation technologies: A review", Energy, 46 (1), 431-441.

[2] Sood A., Vyas S., (2017). "Carbon capture and sequestration-a review", IOP Conference Series: Earth and Environmental Science, 012024.

[3] Harde H., (2017), "Scrutinizing the carbon cycle and CO_2 residence time in the atmosphere", Global Planetary Change, 152, 19-26.

[4] Zhongming Z., Linong L., Wangqiang Z., Wei L., (2021), "Greenhouse Gas Bulletin: Another Year Another Record".

[5] Yuan P., Qiu Z., Liu J., (2017). "Recent enlightening strategies for CO_2 capture: a review", IOP Conference Series: Earth and Environmental Science, 012046.

[6] Cannone S. F., Lanzini A., Santarelli M., (2021), "A Review on CO_2 Capture Technologies with Focus on CO_2-Enhanced Methane Recovery from Hydrates", Energies, 14 (2), 387.

[7] Leung D. Y., Caramanna G., Maroto-Valer M. M., (2014), "An overview of current status of carbon dioxide capture and storage technologies", Renewable Sustainable Energy Reviews, 39, 426-443.

[8] Lai J. Y., Ngu L. H., Hashim S. S., (2021), "A review of CO_2 adsorbents performance for different carbon capture technology processes conditions", Greenhouse Gases: Science Technology, 11 (5), 1076-1117.

[9] Naguib M., Barsoum M. W., Gogotsi Y., (2021), "Ten years of progress in the synthesis and development of MXenes", Advanced Materials, 33 (39), 2103393.

[10] Figueroa J. D., Fout T., Plasynski S., McIlvried H., Srivastava R. D., (2008), "Advances in CO_2 capture technology—the US Department of Energy's Carbon Sequestration Program", International Journal of Greenhouse Gas Control, 2 (1), 9-20.

[11] Damen K., van Troost M., Faaij A., Turkenburg W., (2006), "A comparison of electricity and hydrogen production systems with CO_2 capture and storage. Part A: Review and selection of promising conversion and capture technologies", Progress in Energy Combustion Science, 32 (2), 215-246.

[12] Blomen E., Hendriks C., Neele F., (2009), "Capture technologies: improvements and promising developments", Energy Procedia, 1 (1), 1505-1512.

[13] Solomon S., Qin D., Manning M., Chen Z., Marquis M., Averyt K., Tignor M., Miller H., (2007), "Summary for policymakers", Climate change : The Physical Science Basis. Contribution of Working Group I to the Fourth Assessment Report of the Intergovernmental Panel on Climate Change, 1-18.

[14] Car A., Stropnik C., Yave W., Peinemann K.-V., (2008), "Pebax®/polyethylene glycol blend thin film composite membranes for CO_2 separation: Performance with mixed gases", Separation Purification Technology, 62 (1), 110-117.

[15] Farmahini A. H., Krishnamurthy S., Friedrich D., Brandani S., Sarkisov L., (2021), "Performance-based screening of porous materials for carbon capture", Chemical Reviews, 121 (17), 10666-10741.

[16] Bhown A. S., Freeman B. C., (2011), "Analysis and status of post-combustion carbon dioxide capture technologies", Environmental Science Technology, 45 (20), 8624-8632.

[17] Hendriks C., (1995), "Energy conversion: CO_2 removal from coal-fired power plant", 1st Edition, Kluwer Academic Publishers.

[18] Aaron D., Tsouris C., (2005), "Separation of CO_2 from flue gas: a review", Separation Science Technology, 40 (1-3), 321-348.

[19] Erlach B., Schmidt M., Tsatsaronis G., (2011), "Comparison of carbon capture IGCC with pre-combustion decarbonisation and with chemical-looping combustion", Energy, 36 (6), 3804-3815.

[20] Gielen D., (2003). "The energy policy consequences of future CO_2 capture and sequestration technologies", Proceedings of the 2nd Annual Conference on Carbon Sequestration. Alexandria, VA, 5-8.

[21] Chiaramonte L., Zoback M., Friedmann J., Stamp V., Zahm C., (2011), "Fracture characterization and fluid flow simulation with geomechanical constraints for a CO_2–EOR and sequestration project Teapot Dome Oil Field, Wyoming, USA", Energy Procedia, 4, 3973-3980.

[22] Sun D., Englezos P., (2014), "Storage of CO_2 in a partially water saturated porous medium at gas hydrate formation conditions", International Journal of Greenhouse Gas Control, 25, 1-8.

[23] Tuinier M., van Sint Annaland M., Kramer G. J., Kuipers J., (2010), "Cryogenic CO_2 capture using dynamically operated packed beds", Chemical Engineering Science, 65 (1), 114-119.

[24] Takamura Y., Aoki J., Uchida S., Narita S., (2001), "Application of high-pressure swing adsorption process for improvement of CO_2 recovery system from flue gas", The Canadian Journal of Chemical Engineering, 79 (5), 812-816.

[25] McKee B., (2002), "Solutions for 21st century, Zero emissions technologies for fossil fuels, Technology Status report", International Energy Agency Working Party on Fossil Fuels, 1-47.

[26] Clausse M., Merel J., Meunier F., (2011), "Numerical parametric study on CO_2 capture by indirect thermal swing adsorption", International Journal of Greenhouse Gas Control, 5 (5), 1206-1213.

[27] Ritter J. A., (2004), "Radically new adsorption cycles for carbon dioxide sequestration", Idea, 2, 2.

[28] Garcia S., Gil M., Martín C., Pis J., Rubiera F., Pevida C., (2011), "Breakthrough adsorption study of a commercial activated carbon for pre-combustion CO_2 capture", Chemical Engineering Journal, 171 (2), 549-556.

[29] Griffiths H., (2012), "Layered double hydroxides: structure, synthesis and catalytic applications", University of Huddersfield.

[30] Cavalcante C., (2000), "Industrial adsorption separation processes: Fundamentals, modeling and applications", Latin American Applied Research, 30 (4), 357-364.

[31] Reijers H. T. J., Valster-Schiermeier S. E., Cobden P. D., Van Den Brink R. W., (2006), "Hydrotalcite as CO_2 sorbent for sorption-enhanced steam reforming of methane", Industrial Engineering Chemistry Research, 45 (8), 2522-2530.

[32] Sircar S., (2006), "Basic research needs for design of adsorptive gas separation processes", Industrial Engineering Chemistry Research, 45 (16), 5435-5448.

[33] Ho M. T., Allinson G. W., Wiley D. E., (2008), "Reducing the cost of CO_2 capture from flue gases using pressure swing adsorption", Industrial Engineering Chemistry Research, 47 (14), 4883-4890.

[34] Zhang J., Webley P. A., Xiao P., (2008), "Effect of process parameters on power requirements of vacuum swing adsorption technology for CO_2 capture from flue gas", Energy Conversion Management, 49 (2), 346-356.

[35] Wiheeb A., Helwani Z., Kim J., Othman M., (2016), "Pressure swing adsorption technologies for carbon dioxide capture", Separation Purification Reviews, 45 (2), 108-121.

[36] Hasan M. F., Baliban R. C., Elia J. A., Floudas C. A., (2012), "Modeling, simulation, and optimization of postcombustion CO_2 capture for variable feed concentration and flow rate. 2. Pressure swing adsorption and vacuum swing adsorption processes", Industrial Engineering Chemistry Research, 51 (48), 15665-15682.

[37] Wang L., Liu Z., Li P., Yu J., Rodrigues A. E., (2012), "Experimental and modeling investigation on post-combustion carbon dioxide capture using

zeolite 13X-APG by hybrid VTSA process", Chemical Engineering Journal, 197, 151-161.

[38] Liu Z., Grande C. A., Li P., Yu J., Rodrigues A. E., (2011), "Multi-bed vacuum pressure swing adsorption for carbon dioxide capture from flue gas", Separation Purification Technology, 81 (3), 307-317.

[39] Olajire A. A., (2010), "CO_2 capture and separation technologies for end-of-pipe applications–A review", Energy, 35 (6), 2610-2628.

[40] An H., Feng B., Su S., (2011), "CO_2 capture by electrothermal swing adsorption with activated carbon fibre materials", International Journal of Greenhouse Gas Control, 5 (1), 16-25.

[41] Dube T. C., (2020), "Experimental and Modeling Study of Gas Adsorption in Metal-Organic Framework Coated on 3D Printed Plastics".

[42] Al-Ghouti M. A., Da'ana D. A., (2020), "Guidelines for the use and interpretation of adsorption isotherm models: A review", Journal of Hazardous Materials, 393, 122383.

[43] Ayawei N., Ebelegi A. N., Wankasi D., (2017), "Modelling and interpretation of adsorption isotherms", Journal of Chemistry, 2017, 1-11.

[44] Langmuir I., (1916), "The constitution and fundamental properties of solids and liquids. Part I. Solids", Journal of the American Chemical Society, 38 (11), 2221-2295.

[45] Langmuir I., (1918), "The adsorption of gases on plane surfaces of glass, mica and platinum", Journal of the American Chemical Society, 40 (9), 1361-1403.

[46] Freundlich H., (1906), "Over the adsorption in solution", Journal of Physical Chemistry, 57 (385471), 1100-1107.

[47] Almalike L. B., (2017), "Equations adsorption isotherms for biuret on soils, paper and cortex plant application of the Freundlich, Langmuir, Temkin, Elovich, flory-huggins, Halsey, and harkins-jura", Parameters, 4 (S3), S2.

[48] Do D. D., (1998), "Adsorption analysis: Equilibria and kinetics (with cd containing computer MATLAB programs)", 1st Edition, World Scientific.

[49] Ladshaw A., Yiacoumi S., Tsouris C., DePaoli D., (2015), "Generalized gas–solid adsorption modeling: Single-component equilibria", Fluid Phase Equilibria, 388, 169-181.

[50] Rudzinski W., Everett D. H., (2012), "Adsorption of gases on heterogeneous surfaces", 1st Edition, Academic Press.

[51] Foo K. Y., Hameed B. H., (2010), "Insights into the modeling of adsorption isotherm systems", Chemical Engineering Journal, 156 (1), 2-10.

[52] Vijayaraghavan K., Rangabhashiyam S., Ashokkumar T., Arockiaraj J., (2016), "Mono-and multi-component biosorption of lead (II), cadmium (II), copper (II) and nickel (II) ions onto coco-peat biomass", Separation Science Technology, 51 (17), 2725-2733.

[53] Tóth J., (1994), "Thermodynamical correctness of gas/solid adsorption isotherm equations", Journal of Colloid Interface Science, 163 (2), 299-302.

[54] Marczewski A. W., Jaroniec M., (1983), "A new isotherm equation for single-solute adsorption from dilute solutions on energetically heterogeneous solids", Monatshefte für Chemie/Chemical Monthly, 114 (6), 711-715.

[55] Jaroniec M., Marczewski A. W., (1984), "Physical adsorption of gases on energetically heterogeneous solids II. Theoretical extension of a generalizedLangmuir equation and its application for analysing adsorption data", Monatshefte für Chemie/Chemical Monthly, 115 (8-9), 1013-1038.

[56] Tóth J., (1981), "A uniform interpretation of gas/solid adsorption", Journal of Colloid Interface Science, 79 (1), 85-95.

[57] Dubinin M., Astakhov V., (1971), "Development of the concepts of volume filling of micropores in the adsorption of gases and vapors by microporous adsorbents", Bulletin of the Academy of Sciences of the USSR, Division of Chemical Science, 20 (1), 8-12.

[58] Bering B., Gordeeva V., Dubinin M., Efimova L., Serpinskii V., (1971), "Development of concepts of the volume filling of micropores in the adsorption of gases and vapors by microporous adsorbents", Bulletin of the Academy of Sciences of the USSR, Division of Chemical Science, 20 (1), 17-22.

[59] Wang Z., Li Y., Guo P., Meng W., (2016), "Analyzing the adaption of different adsorption models for describing the shale gas adsorption law", Chemical Engineering Technology, 39 (10), 1921-1932.

[60] Chaffee A. L., Knowles G. P., Liang Z., Zhang J., Xiao P., Webley P. A., (2007), "CO_2 capture by adsorption: materials and process development", International Journal of Greenhouse Gas Control, 1 (1), 11-18.

[61] Helwani Z., Wiheeb A., Kim J., Othman M., (2012), "Improved carbon dioxide capture using metal reinforced hydrotalcite under wet conditions", International Journal of Greenhouse Gas Control, 7, 127-136.

[62] Ooi C.-H., Lee T., Pung S.-Y., Yeoh F.-Y., (2015), "Activated carbon fiber derived from single step carbonization-activation process", ASEAN Engineering Journal, 4 (1), 40-50.

[63] Dodevski V., Janković B., Stojmenović M., Krstić S., Popović J., Pagnacco M. C., Popović M., Pašalić S., (2017), "Plane tree seed biomass used for preparation of activated carbons (AC) derived from pyrolysis. Modeling the

activation process", Colloids Surfaces A: Physicochemical Engineering Aspects, 522, 83-96.

[64] McDougall G., (1991), "The physical nature and manufacture of activated carbon", Journal of the Southern African Institute of Mining Metallurgy, 91 (4), 109-120.

[65] Manocha S. M., (2003), "Porous carbons", Sadhana, 28 (1-2), 335-348.

[66] Jeguirim M., Belhachemi M., Limousy L., Bennici S., (2018), "Adsorption/reduction of nitrogen dioxide on activated carbons: textural properties versus surface chemistry–a review", Chemical Engineering Journal, 347, 493-504.

[67] Tong L., Yue T., Zuo P., Zhang X., Wang C., Gao J., Wang K., (2017), "Effect of characteristics of KI-impregnated activated carbon and flue gas components on Hg^0 removal", Fuel, 197, 1-7.

[68] Wang J., Huang L., Yang R., Zhang Z., Wu J., Gao Y., Wang Q., O'Hare D., Zhong Z., (2014), "Recent advances in solid sorbents for CO_2 capture and new development trends", Energy Environmental Science, 7 (11), 3478-3518.

[69] Abd A. A., Naji S. Z., Hashim A. S., Othman M. R., (2020), "Carbon dioxide removal through physical adsorption using carbonaceous and non-carbonaceous adsorbents: a review", Journal of Environmental Chemical Engineering, 8 (5), 104142.

[70] Chen Y., Zhang B., Liu G., Zhuang X., Kang E.-T., (2012), "Graphene and its derivatives: switching ON and OFF", Chemical Society Reviews, 41 (13), 4688-4707.

[71] Stoller M. D., Park S., Zhu Y., An J., Ruoff R. S., (2008), "Graphene-based ultracapacitors", Nano Letters, 8 (10), 3498-3502.

[72] Gadipelli S., Guo Z. X., (2015), "Graphene-based materials: Synthesis and gas sorption, storage and separation", Progress in Materials Science, 69, 1-60.

[73] Iijima S., (1991), "Helical microtubules of graphitic carbon", Nature, 354 (6348), 56-58.

[74] Songolzadeh M., Ravanchi M. T., Soleimani M., (2012), "Carbon Dioxide Capture and Storage: A General Review on Adsorbents", Proceedings of World Academy of Science, Engineering and Technology, 6, 225-232.

[75] Wang Y., Yeow J. T., (2009), "A review of carbon nanotubes-based gas sensors", Journal of Sensors, 2009, 1-24.

[76] Yang R. T., (1997), "Gas separation by adsorption processes", 1st Edition, World Scientific.

[77] Bae Y.-S., Lee C.-H., (2005), "Sorption kinetics of eight gases on a carbon molecular sieve at elevated pressure", Carbon, 43 (1), 95-107.

[78] Pardakhti M., Jafari T., Tobin Z., Dutta B., Moharreri E., Shemshaki N. S., Suib S., Srivastava R., (2019), "Trends in solid adsorbent materials development for CO_2 capture", ACS Applied Materials Interfaces, 11 (38), 34533-34559.

[79] Kumar S., Malik M., Purohit R., (2017), "Synthesis methods of mesoporous silica materials", Materials Today: Proceedings, 4 (2), 350-357.

[80] Chew T.-L., Ahmad A. L., Bhatia S., (2010), "Ordered mesoporous silica (OMS) as an adsorbent and membrane for separation of carbon dioxide (CO_2)", Advances in Colloid Interface Science, 153 (1-2), 43-57.

[81] Ullah R., Saad M. A. H. S., Aparicio S., Atilhan M., (2018), "Adsorption equilibrium studies of CO_2, CH_4 and N_2 on various modified zeolites at high pressures up to 200 bars", Microporous Mesoporous Materials, 262, 49-58.

[82] Hunger M. (2009), "Solid-state NMR Spectroscopy". "Zeolite characterization and catalysis", 1st Edition, Springer.

[83] Zhang J., Singh R., Webley P. A., (2008), "Alkali and alkaline-earth cation exchanged chabazite zeolites for adsorption based CO_2 capture", Microporous Mesoporous Materials, 111 (1-3), 478-487.

[84] Harlick P. J., Sayari A., (2006), "Applications of pore-expanded mesoporous silicas. 3. Triamine silane grafting for enhanced CO_2 adsorption", Industrial Engineering Chemistry Research, 45 (9), 3248-3255.

[85] Brandani F., Ruthven D. M., (2004), "The effect of water on the adsorption of CO_2 and C_3H_8 on type X zeolites", Industrial Engineering Chemistry Research, 43 (26), 8339-8344.

[86] Liu Y., Wang Z. U., Zhou H. C., (2012), "Recent advances in carbon dioxide capture with metal-organic frameworks", Greenhouse Gases: Science Technology, 2 (4), 239-259.

[87] Huang L., Wang H., Chen J., Wang Z., Sun J., Zhao D., Yan Y., (2003), "Synthesis, morphology control, and properties of porous metal–organic coordination polymers", Microporous Mesoporous Materials, 58 (2), 105-114.

[88] Farha O. K., Eryazici I., Jeong N. C., Hauser B. G., Wilmer C. E., Sarjeant A. A., Snurr R. Q., Nguyen S. T., Yazaydın A. O. z. r., Hupp J. T., (2012), "Metal–organic framework materials with ultrahigh surface areas: is the sky the limit?", Journal of the American Chemical Society, 134 (36), 15016-15021.

[89] Furukawa H., Ko N., Go Y. B., Aratani N., Choi S. B., Choi E., Yazaydin A. Ö., Snurr R. Q., O'Keeffe M., Kim J., (2010), "Ultrahigh porosity in metal-organic frameworks", Science, 329 (5990), 424-428.

[90] Lee S.-Y., Park S.-J., (2015), "A review on solid adsorbents for carbon dioxide capture", Journal of Industrial Engineering Chemistry, 23, 1-11.

[91] Liu J., Wang Y., Benin A. I., Jakubczak P., Willis R. R., LeVan M. D., (2010), "CO_2/H_2O adsorption equilibrium and rates on metal− organic frameworks: HKUST-1 and Ni/DOBDC", Langmuir, 26 (17), 14301-14307.

[92] Gogotsi Y., Anasori B., (2019), "The rise of MXenes", ACS Nano, 13 (8), 8491-8494.

[93] Deysher G., Shuck C. E., Hantanasirisakul K., Frey N. C., Foucher A. C., Maleski K., Sarycheva A., Shenoy V. B., Stach E. A., Anasori B., (2019), "Synthesis of Mo_4VAlC_4 MAX phase and two-dimensional Mo_4VC_4 MXene with five atomic layers of transition metals", ACS Nano, 14 (1), 204-217.

[94] Zheng L., Wang J., Lu X., Li F., Wang J., Zhou Y., (2010), "$(Ti_{0.5}Nb_{0.5})_5AlC_4$: A New-Layered Compound Belonging to MAX Phases", Journal of the American Ceramic Society, 93 (10), 3068-3071.

[95] Barsoum M. W., (2013), "MAX phases: properties of machinable ternary carbides and nitrides", 1st Edition, John Wiley & Sons.

[96] Wang Z., (2021). "A Review on MXene: Synthesis, Properties and Applications on Alkali Metal Ion Batteries", IOP Conference Series: Earth and Environmental Science, 042030.

[97] Hong W., Wyatt B. C., Nemani S. K., Anasori B., (2020), "Double transition-metal MXenes: Atomistic design of two-dimensional carbides and nitrides", Materials Research Society Bulletin, 45 (10), 850-861.

[98] Tao Q., Dahlqvist M., Lu J., Kota S., Meshkian R., Halim J., Palisaitis J., Hultman L., Barsoum M. W., Persson P. O., (2017), "Two-dimensional $Mo_{1.33}C$ MXene with divacancy ordering prepared from parent 3D laminate with in-plane chemical ordering", Nature Communications, 8 (1), 1-7.

[99] Zhan X., Si C., Zhou J., Sun Z., (2020), "MXene and MXene-based composites: synthesis, properties and environment-related applications", Nanoscale Horizons, 5 (2), 235-258.

[100] Naguib M., Kurtoglu M., Presser V., Lu J., Niu J., Heon M., Hultman L., Gogotsi Y., Barsoum M. W., (2011), "Two-dimensional nanocrystals produced by exfoliation of Ti_3AlC_2", Advanced Materials, 23 (37), 4248-4253.

[101] Wu Y., Nie P., Wang J., Dou H., Zhang X., (2017), "Few-layer MXenes delaminated via high-energy mechanical milling for enhanced sodium-ion batteries performance", ACS Applied Materials Interfaces, 9 (45), 39610-39617.

[102] Urbankowski P., Anasori B., Makaryan T., Er D., Kota S., Walsh P. L., Zhao M., Shenoy V. B., Barsoum M. W., Gogotsi Y., (2016), "Synthesis of two-dimensional titanium nitride Ti_4N_3(MXene)", Nanoscale, 8 (22), 11385-11391.

[103] Li Y., Shao H., Lin Z., Lu J., Liu L., Duployer B., Persson P. O., Eklund P., Hultman L., Li M., (2020), "A general Lewis acidic etching route for preparing MXenes with enhanced electrochemical performance in non-aqueous electrolyte", Nature Materials, 19 (8), 894-899.

[104] Yang S., Zhang P., Wang F., Ricciardulli A. G., Lohe M. R., Blom P. W., Feng X., (2018), "Fluoride-free synthesis of two-dimensional titanium carbide (MXene) using a binary aqueous system", Angewandte Chemie, 130 (47), 15717-15721.

[105] Urbankowski P., Anasori B., Hantanasirisakul K., Yang L., Zhang L., Haines B., May S. J., Billinge S. J., Gogotsi Y., (2017), "2D molybdenum and vanadium nitrides synthesized by ammoniation of 2D transition metal carbides (MXenes)", Nanoscale, 9 (45), 17722-17730.

[106] Jeon J., Park Y., Choi S., Lee J., Lim S. S., Lee B. H., Song Y. J., Cho J. H., Jang Y. H., Lee S., (2018), "Epitaxial synthesis of molybdenum carbide and formation of a Mo_2C/MoS_2 hybrid structure via chemical conversion of molybdenum disulfide", ACS Nano, 12 (1), 338-346.

[107] Lin Z., Cai L., Lu W., Chai Y., (2017), "Phase and facet control of molybdenum carbide nanosheet observed by in situ TEM", Small, 13 (35), 1700051.

[108] Xu C., Wang L., Liu Z., Chen L., Guo J., Kang N., Ma X.-L., Cheng H.-M., Ren W., (2015), "Large-area high-quality 2D ultrathin Mo_2C superconducting crystals", Nature Materials, 14 (11), 1135-1141.

[109] Xiao X., Urbankowski P., Hantanasirisakul K., Yang Y., Sasaki S., Yang L., Chen C., Wang H., Miao L., Tolbert S. H., (2019), "Scalable Synthesis of Ultrathin Mn_3N_2 Exhibiting Room-Temperature Antiferromagnetism", Advanced Functional Materials, 29 (17), 1809001.

[110] Liu F., Zhou A., Chen J., Zhang H., Cao J., Wang L., Hu Q., (2016), "Preparation and methane adsorption of two-dimensional carbide Ti_2C", Adsorption, 22 (7), 915-922.

[111] Liu F., Zhou A., Chen J., Jia J., Zhou W., Wang L., Hu Q., (2017), "Preparation of Ti_3C_2 and Ti_2C MXenes by fluoride salts etching and methane adsorptive properties", Applied Surface Science, 416, 781-789.

[112] Wang B., Zhou A., Liu F., Cao J., Wang L., Hu Q., (2018), "Carbon dioxide adsorption of two-dimensional carbide MXenes", Journal of Advanced Ceramics, 7 (3), 237-245.

[113] Morales-García Á., Fernández-Fernández A., Viñes F., Illas F., (2018), "CO_2 abatement using two-dimensional MXene carbides", Journal of Materials Chemistry A, 6 (8), 3381-3385.

[114] Liu S., Liu J., Liu X., Shang J., Xu L., Yu R., Shui J., (2021), "Hydrogen storage in incompletely etched multilayer Ti_2CT_x at room temperature", Nature Nanotechnology, 16 (3), 331-336.

[115] Gubbins K. E., Liu Y.-C., Moore J. D., Palmer J. C., (2011), "The role of molecular modeling in confined systems: impact and prospects", Physical Chemistry Chemical Physics, 13 (1), 58-85.

[116] Verlet L., (1967), "Computer" experiments" on classical fluids. I. Thermodynamical properties of Lennard-Jones molecules", Physical review, 159 (1), 98.

[117] McDonald I., (1972), "NpT-ensemble Monte Carlo calculations for binary liquid mixtures", Molecular Physics, 23 (1), 41-58.

[118] Coskuner Y. B., (2018), "A Grand Canonical Monte Carlo Simulation Model for Phase Behavior of Confined Hydrocarbons", Phd Thesis, Colorado School of Mines.

[119] Genheden S., Reymer A., Saenz-Méndez P., Eriksson L. A., (2017), "Computational chemistry and molecular modelling basics", Computational Tools for Chemical Biology.

[120] Ray J. R., (1991), "Microcanonical ensemble monte carlo method", Physical Review A, 44 (6), 4061.

[121] Evans J. D., Fraux G., Gaillac R., Kohen D., Trousselet F., Vanson J.-M., Coudert F.-X., (2016), "Computational chemistry methods for nanoporous materials", Chemistry of Materials, 29 (1), 199-212.

[122] Raabe G., (2017), "Molecular Simulation Studies on Thermophysical Properties ; With Application to Working Fluids", 1st Edition, Springer.

[123] González M., (2011), "Force fields and molecular dynamics simulations", École Thématique de la Société Française de la Neutronique, 12, 169-200.

[124] MAGHFIROH C. Y., MISTO M., MAULINA W., ARKUNDATO A., "Parameters (σ, ε) of Lennard-Jones for Fe, Ni, Pb for Potential and Cr based on Melting Point Values Using the Molecular Dynamics Method of the Lammps Program".

[125] Allen M. P., Tildesley D. J., (2017), "Computer Simulation of Liquids", 2nd Edition, Oxford University Press.

[126] Getman R. B., Bae Y.-S., Wilmer C. E., Snurr R. Q., (2012), "Review and analysis of molecular simulations of methane, hydrogen, and acetylene storage in metal–organic frameworks", Chemical Reviews, 112 (2), 703-723.

[127] Mulliken R. S., (1955), "Electronic population analysis on LCAO–MO molecular wave functions. ", The Journal of Chemical Physics, 23 (10), 1833-1840.

[128] Manz T. A., Sholl D. S., (2010), "Chemically meaningful atomic charges that reproduce the electrostatic potential in periodic and nonperiodic materials", Journal of Chemical Theory Computation, 6 (8), 2455-2468.

[129] Breneman C. M., Wiberg K. B., (1990), "Determining atom-centered monopoles from molecular electrostatic potentials. The need for high sampling density in formamide conformational analysis", Journal of Computational Chemistry, 11 (3), 361-373.

[130] Farmahini A. H., Opletal G., Bhatia S. K., (2013), "Structural modelling of silicon carbide-derived nanoporous carbon by hybrid reverse Monte Carlo simulation", The Journal of Physical Chemistry C, 117 (27), 14081-14094.

[131] Brandani S., Mangano E., Sarkisov L., (2016), "Net, excess and absolute adsorption and adsorption of helium", Adsorption, 22 (2), 261-276.

[132] Huo Q. (2011), "Synthetic chemistry of the inorganic ordered porous materials". "Modern Inorganic Synthetic Chemistry", 2nd Edition, Elsevier.

[133] Boyd P. G., Lee Y., Smit B., (2017), "Computational development of the nanoporous materials genome", Nature Reviews Materials, 2 (8), 1-15.

[134] Yan Y., Zhang L., Li S., Liang H., Qiao Z., (2021), "Adsorption behavior of metal-organic frameworks: From single simulation, high-throughput computational screening to machine learning", Computational Materials Science, 110383.

[135] Krishna R., van Baten J. M., (2010), "In silico screening of zeolite membranes for CO_2 capture", Journal of Membrane Science, 360 (1-2), 323-333.

[136] Chung Y. G., Camp J., Haranczyk M., Sikora B. J., Bury W., Krungleviciute V., Yildirim T., Farha O. K., Sholl D. S., Snurr R. Q., (2014), "Computation-ready, experimental metal–organic frameworks: A tool to enable high-throughput screening of nanoporous crystals", Chemistry of Materials, 26 (21), 6185-6192.

[137] Qiao Z., Zhang K., Jiang J., (2016), "In silico screening of 4764 computation-ready, experimental metal–organic frameworks for CO_2 separation", Journal of Materials Chemistry A, 4 (6), 2105-2114.

[138] Avci G., Velioglu S., Keskin S., (2018), "High-throughput screening of MOF adsorbents and membranes for H_2 purification and CO_2 capture", ACS Applied Materials Interfaces, 10 (39), 33693-33706.

[139] Burns T. D., Pai K. N., Subraveti S. G., Collins S. P., Krykunov M., Rajendran A., Woo T. K., (2020), "Prediction of MOF performance in vacuum swing adsorption systems for postcombustion CO_2 capture based on integrated molecular simulations, process optimizations, and machine learning models", Environmental Science Technology, 54 (7), 4536-4544.

[140] Tong M., Yang Q., Zhong C., (2015), "Computational screening of covalent organic frameworks for CH_4/H_2, CO_2/H_2 and CO_2/CH_4 separations", Microporous Mesoporous Materials, 210, 142-148.

[141] Tong M., Lan Y., Yang Q., Zhong C., (2017), "Exploring the structure-property relationships of covalent organic frameworks for noble gas separations", Chemical Engineering Science, 168, 456-464.

[142] Wilmer C. E., Leaf M., Lee C. Y., Farha O. K., Hauser B. G., Hupp J. T., Snurr R. Q., (2012), "Large-scale screening of hypothetical metal–organic frameworks", Nature Chemistry, 4 (2), 83-89.

[143] Wilmer C. E., Farha O. K., Bae Y.-S., Hupp J. T., Snurr R. Q., (2012), "Structure–property relationships of porous materials for carbon dioxide separation and capture", Energy Environmental Science, 5 (12), 9849-9856.

[144] Subramanian Balashankar V., Rajendran A., (2019), "Process Optimization-Based Screening of Zeolites for Post-Combustion CO_2 Capture by Vacuum Swing Adsorption", ACS Sustainable Chemistry Engineering, 7 (21), 17747-17755.

[145] Yang L., Shi C., Li L., Li Y., (2020), "High-throughput model-building and screening of zeolitic imidazolate frameworks for CO_2 capture from flue gas", Chinese Chemical Letters, 31 (1), 227-230.

[146] Li S., Chung Y. G., Simon C. M., Snurr R. Q., (2017), "High-Throughput Computational Screening of Multivariate Metal–Organic Frameworks (MTV-MOFs) for CO_2 Capture", The Journal of Physical Chemistry Letters, 8 (24), 6135-6141.

[147] Anderson R., Rodgers J., Argueta E., Biong A., Gómez-Gualdrón D. A., (2018), "Role of pore chemistry and topology in the CO_2 capture capabilities of MOFs: From molecular simulation to machine learning", Chemistry of Materials, 30 (18), 6325-6337.

[148] Pardakhti M., Moharreri E., Wanik D., Suib S. L., Srivastava R., (2017), "Machine learning using combined structural and chemical descriptors for prediction of methane adsorption performance of metal organic frameworks (MOFs)", ACS Combinatorial Science, 19 (10), 640-645.

[149] Dureckova H., Krykunov M., Aghaji M. Z., Woo T. K., (2019), "Robust machine learning models for predicting high CO_2 working capacity and CO_2/H_2 selectivity of gas adsorption in metal organic frameworks for precombustion carbon capture", The Journal of Physical Chemistry C, 123 (7), 4133-4139.

[150] Mercado R., Fu R.-S., Yakutovich A. V., Talirz L., Haranczyk M., Smit B., (2018), "In silico design of 2D and 3D covalent organic frameworks for methane storage applications", Chemistry of Materials, 30 (15), 5069-5086.

[151] Martin R. L., Simon C. M., Medasani B., Britt D. K., Smit B., Haranczyk M., (2014), "In silico design of three-dimensional porous covalent organic frameworks via known synthesis routes and commercially available species", The Journal of Physical Chemistry C, 118 (41), 23790-23802.

[152] Bae Y. S., Snurr R. Q., (2011), "Development and evaluation of porous materials for carbon dioxide separation and capture", Angewandte Chemie International Edition, 50 (49), 11586-11596.

[153] Baksh M. S. A., Notaro F., (1998), "Method for Production of Nitrogen using Oxygen Selective Adsorbents".

[154] Rege S. U., Yang R. T., (2001), "A simple parameter for selecting an adsorbent for gas separation by pressure swing adsorption", Separation Science Technology, 36 (15), 3355-3365.

[155] Chung Y. G., Gómez-Gualdrón D. A., Li P., Leperi K. T., Deria P., Zhang H., Vermeulen N. A., Stoddart J. F., You F., Hupp J. T., (2016), "In silico discovery of metal-organic frameworks for precombustion CO_2 capture using a genetic algorithm", Science Advances, 2 (10), e1600909.

[156] Zhou L., Zhang Y., Zhuo Z., Neukirch A. J., Tretiak S., (2018), "Interlayer-decoupled Sc-based MXene with high carrier mobility and strong light-harvesting ability", The Journal of Physical Chemistry Letters, 9 (23), 6915-6920.

[157] Zeng Z., Chen X., Weng K., Wu Y., Zhang P., Jiang J., Li N., (2021), "Computational screening study of double transition metal carbonitrides $M'_2M''CNO_2$-MXene as catalysts for hydrogen evolution reaction", Nature Partner Journals Computational Materials, 7 (1), 1-7.

[158] Khazaei M., Arai M., Sasaki T., Estili M., Sakka Y., (2014), "Two-dimensional molybdenum carbides: potential thermoelectric materials of the MXene family", Physical Chemistry Chemical Physics, 16 (17), 7841-7849.

[159] Khazaei M., Ranjbar A., Arai M., Yunoki S., (2016), "Topological insulators in the ordered double transition metals $M_2'M''C_2$ MXenes (M′= Mo, W; M ″= Ti, Zr, Hf)", Physical Review B, 94 (12), 125152.

[160] Khazaei M., Arai M., Sasaki T., Chung C. Y., Venkataramanan N. S., Estili M., Sakka Y., Kawazoe Y., (2013), "Novel electronic and magnetic properties of two-dimensional transition metal carbides and nitrides", Advanced Functional Materials, 23 (17), 2185-2192.

[161] Stephens P. J., Devlin F. J., Chabalowski C. F., Frisch M. J., (1994), "Ab initio calculation of vibrational absorption and circular dichroism spectra using density functional force fields", The Journal of Physical Chemistry, 98 (45), 11623-11627.

[162] Beck A. D., (1993), "Density-functional thermochemistry. III. The role of exact exchange", The Journal of Chemical Physics, 98 (7), 5648-5646.

[163] Delley B., (1990), "An all-electron numerical method for solving the local density functional for polyatomic molecules", The Journal of Chemical Physics, 92 (1), 508-517.

[164] Fan Y., Li J., Wang S., Meng X., Jin Y., Yang N., Meng B., Li J., Liu S., (2021), "Nickel (II) ion-intercalated MXene membranes for enhanced H_2/CO_2 separation", Frontiers of Chemical Science Engineering, 15 (4), 882-891.

[165] Lin H., Gong K., Hykys P., Chen D., Ying W., Sofer Z., Yan Y., Li Z., Peng X., (2021), "Nanoconfined deep eutectic solvent in laminated MXene for efficient CO_2 separation", Chemical Engineering Journal, 405, 126961.

[166] Ding L., Wei Y., Li L., Zhang T., Wang H., Xue J., Ding L.-X., Wang S., Caro J., Gogotsi Y., (2018), "MXene molecular sieving membranes for highly efficient gas separation", Nature Communications, 9 (1), 1-7.

[167] Shen J., Liu G., Ji Y., Liu Q., Cheng L., Guan K., Zhang M., Liu G., Xiong J., Yang J., (2018), "2D MXene nanofilms with tunable gas transport channels", Advanced Functional Materials, 28 (31), 1801511.

[168] Jin Y., Fan Y., Meng X., Zhang W., Meng B., Yang N., Liu S., (2019), "Theoretical and experimental insights into the mechanism for gas separation through nanochannels in 2D laminar MXene membranes", Processes, 7 (10), 751.

[169] Fan Y., Wei L., Meng X., Zhang W., Yang N., Jin Y., Wang X., Zhao M., Liu S., (2019), "An unprecedented high-temperature-tolerance 2D laminar MXene membrane for ultrafast hydrogen sieving", Journal of Membrane Science, 569, 117-123.

[170] Qu K., Dai L., Xia Y., Wang Y., Zhang D., Wu Y., Yao Z., Huang K., Guo X., Xu Z., (2021), "Self-crosslinked MXene hollow fiber membranes for H_2/CO_2 separation", Journal of Membrane Science, 638, 119669.

[171] Guan W., Yang X., Dong C., Yan X., Zheng W., Xi Y., Ruan X., Dai Y., He G., (2021), "Prestructured MXene fillers with uniform channels to enhance

CO_2 selective permeation in mixed matrix membranes", Journal of Applied Polymer Science, 138 (8), 49895.

[172] Potoff J. J., Siepmann J. I., (2001), "Vapor–liquid equilibria of mixtures containing alkanes, carbon dioxide, and nitrogen", American Institute of Chemical Engineers Journal, 47 (7), 1676-1682.

[173] Allen M., Tildesley D., (1989), "Computer Simulation of Liquids", 2nd Edition, Oxford University Press.

[174] Dubbeldam D., Calero S., Ellis D. E., Snurr R. Q., (2016), "RASPA: molecular simulation software for adsorption and diffusion in flexible nanoporous materials", Molecular Simulation, 42 (2), 81-101.

[175] Altintas C., Avci G., Daglar H., Nemati Vesali Azar A., Velioglu S., Erucar I., Keskin S., (2018), "Database for CO_2 separation performances of MOFs based on computational materials screening", ACS Applied Materials Interfaces, 10 (20), 17257-17268.

[176] Altintas C., Erucar I., Keskin S., (2018), "High-throughput computational screening of the metal organic framework database for CH_4/H_2 separations", ACS Applied Materials Interfaces, 10 (4), 3668-3679.

[177] Avci G., Erucar I., Keskin S., (2020), "Do new MOFs perform better for CO_2 capture and H_2 purification? Computational screening of the updated MOF database", ACS Applied Materials Interfaces, 12 (37), 41567-41579.

[178] Aksu G. O., Daglar H., Altintas C., Keskin S., (2020), "Computational Selection of High-Performing Covalent Organic Frameworks for Adsorption and Membrane-Based CO_2/H_2 Separation", The Journal of Physical Chemistry C, 124 (41), 22577-22590.

[179] Aksu G. O., Erucar I., Haslak Z. P., Keskin S., (2022), "Accelerating discovery of COFs for CO_2 capture and H_2 purification using structurally guided computational screening", Chemical Engineering Journal, 427, 131574.

[180] Shi C., Li L., Li Y., (2020), "High-throughput screening of hypothetical aluminosilicate zeolites for CO2 capture from flue gas", Journal of CO2 Utilization, 42, 101346.

[181] Daglar H., Gulbalkan H. C., Avci G., Aksu G. O., Altundal O. F., Altintas C., Erucar I., Keskin S., (2021), "Effect of Metal–Organic Framework (MOF) Database Selection on the Assessment of Gas Storage and Separation Potentials of MOFs", Angewandte Chemie, 133 (14), 7907-7916.

[182] Sun H., Ren D., Kong R., Wang D., Jiang H., Tan J., Wu D., Chen S., Shen B., (2019), "Tuning 1-hexene/n-hexane adsorption on MOF-74 via constructing Co-Mg bimetallic frameworks", Microporous Mesoporous Materials, 284, 151-160.

BIOGRAPHY

Sirin Massoumilari completed her high school education in the College of Fevziye Schools Foundation. She graduated from the Biology Department at Istanbul University in 1994. She started her first Masters of Science degree in the Institute of Health Science, Kadir Has University and completed in 2004. She started her second Masters of Science degree in the Institute of Nanotechnology at Gebze Technical University. As a part of her Master of Science education, she awarded with a scholarship by TÜBİTAK in the project which is numbered as 120M180 and has a title of "Molecular Investigation of Hydrogen Separation Potential of MXene Nanomaterials for Efficient and Economical Energy Production".

APPENDIX

APPENDIX A: MXene Types Whose Crystal Structures are Available in the Literature

MXene Type	Article Title	Author List	Journal Name, Issue, Date, and Page
$Cr_2C(OH)_2$	Two -dimensional molybdenum carbides: Potential thermoelectric materials in MXenes	Mohammad Khazaei, Masao Arai, Taizo Sasaki, Mehdi Estili, Yoshio Sakka	Physical Chemistry Chemical Physics, 16, 2014, 7841-7888
Cr_2CBr_2	Two- dimensional molybdenum carbides: Potential thermoelectric materials in MXenes	Mohammad Khazaei, Masao Arai, Taizo Sasaki, Mehdi Estili, Yoshio Sakka	Physical Chemistry Chemical Physics, 16, 2014, 7841-7887
Cr_2CCl_2	Two- dimensional molybdenum carbides: Potential thermoelectric materials in MXenes	Mohammad Khazaei, Masao Arai, Taizo Sasaki, Mehdi Estili, Yoshio Sakka	Physical Chemistry Chemical Physics, 16, 2014, 7841-7886
Cr_2CF_2	Two -dimensional molybdenum carbides: Potential thermoelectric materials in MXenes	Mohammad Khazaei, Masao Arai, Taizo Sasaki, Mehdi Estili, Yoshio Sakka	Physical Chemistry Chemical Physics, 16, 2014, 7841-7885
Cr_2CO_2	Two -dimensional molybdenum carbides: Potential thermoelectric materials in MXenes	Mohammad Khazaei, Masao Arai, Taizo Sasaki, Mehdi Estili, Yoshio Sakka	Physical Chemistry Chemical Physics, 16, 2014, 7841-7889
Cr_2CS_2	Two- dimensional molybdenum carbides: Potential thermoelectric materials in MXenes	Mohammad Khazaei, Masao Arai, Taizo Sasaki, Mehdi Estili, Yoshio Sakka	Physical Chemistry Chemical Physics, 16, 2014, 7841-7890
Cr_2HfCN	Computational screening study of double transition metal carbonitrides $M'_2M''CNO_2$-MXene as catalysts for hydrogen evolution reaction	Zhoulan Zeng, Xingzhu Chen, Kaiyi Weng, Yang Wu, Peng Zhang, Jizhou Jiang and Neng L	npj Computational Materials, 7, 2021, 80
Cr_2HfCNO_2	Computational screening study of double transition metal carbonitrides $M'_2M''CNO_2$-MXene as catalysts for hydrogen evolution reaction	Zhoulan Zeng, Xingzhu Chen, Kaiyi Weng, Yang Wu, Peng Zhang, Jizhou Jiang and Neng L	npj Computational Materials, 7, 2021, 80
$Cr_2N(OH)_2$	Novel electronic and magnetic properties of two-dimensional transition metal carbides and nitrides	Mohammad Khazaei, Masao Arai, Taizo Sasaki, Chan-Yeup Chung, Natarajan S. Venkataramanan, Mehdi Estili, Yoshio Sakka, Yoshiyuki Kawazoe	Advanced Functional Materials, 23(17), 2013, 2185-2213
Cr_2NF_2	Novel electronic and magnetic properties of two-dimensional transition metal carbides and nitrides	Mohammad Khazaei, Masao Arai, Taizo Sasaki, Chan-Yeup Chung, Natarajan S. Venkataramanan, Mehdi Estili, Yoshio Sakka, Yoshiyuki Kawazoe	Advanced Functional Materials, 23(17), 2013, 2185-2192
Cr_2NO_2	Novel electronic and magnetic properties of two-dimensional transition metal carbides and nitrides	Mohammad Khazaei, Masao Arai, Taizo Sasaki, Chan-Yeup Chung, Natarajan S. Venkataramanan, Mehdi Estili, Yoshio Sakka, Yoshiyuki Kawazoe	Advanced Functional Materials, 23(17), 2013, 2185-2203
Cr_2NbCN	Computational screening study of double transition metal carbonitrides $M'_2M''CNO_2$-MXene as catalysts for hydrogen evolution reaction	Zhoulan Zeng, Xingzhu Chen, Kaiyi Weng, Yang Wu, Peng Zhang, Jizhou Jiang and Neng L	npj Computational Materials, 7, 2021, 80
Cr_2NbCNO_2	Computational screening study of double transition metal carbonitrides $M'_2M''CNO_2$-MXene as catalysts for hydrogen evolution reaction	Zhoulan Zeng, Xingzhu Chen, Kaiyi Weng, Yang Wu, Peng Zhang, Jizhou Jiang and Neng L	npj Computational Materials, 7, 2021, 80
Cr_2TaCN	Computational screening study of double transition metal carbonitrides $M'_2M''CNO_2$-MXene as catalysts for hydrogen evolution reaction	Zhoulan Zeng, Xingzhu Chen, Kaiyi Weng, Yang Wu, Peng Zhang, Jizhou Jiang and Neng L	npj Computational Materials, 7, 2021, 80

Cr_2TaCNO_2	Computational screening study of double transition metal carbonitrides $M'_2M''CNO_2$-MXene as catalysts for hydrogen evolution reaction	Zhoulan Zeng, Xingzhu Chen, Kaiyi Weng, Yang Wu, Peng Zhang, Jizhou Jiang and Neng L	npj Computational Materials, 7, 2021, 80
Cr_2TiCN	Computational screening study of double transition metal carbonitrides $M'_2M''CNO_2$-MXene as catalysts for hydrogen evolution reaction	Zhoulan Zeng, Xingzhu Chen, Kaiyi Weng, Yang Wu, Peng Zhang, Jizhou Jiang and Neng L	npj Computational Materials, 7, 2021, 80
Cr_2TiCNO_2	Computational screening study of double transition metal carbonitrides $M'_2M''CNO_2$-MXene as catalysts for hydrogen evolution reaction	Zhoulan Zeng, Xingzhu Chen, Kaiyi Weng, Yang Wu, Peng Zhang, Jizhou Jiang and Neng L	npj Computational Materials, 7, 2021, 80
Cr_2VCN	Computational screening study of double transition metal carbonitrides $M'_2M''CNO_2$-MXene as catalysts for hydrogen evolution reaction	Zhoulan Zeng, Xingzhu Chen, Kaiyi Weng, Yang Wu, Peng Zhang, Jizhou Jiang and Neng L	npj Computational Materials, 7, 2021, 80
Cr_2VCNO_2	Computational screening study of double transition metal carbonitrides $M'_2M''CNO_2$-MXene as catalysts for hydrogen evolution reaction	Zhoulan Zeng, Xingzhu Chen, Kaiyi Weng, Yang Wu, Peng Zhang, Jizhou Jiang and Neng L	npj Computational Materials, 7, 2021, 80
Cr_2ZrCN	Computational screening study of double transition metal carbonitrides $M'_2M''CNO_2$-MXene as catalysts for hydrogen evolution reaction	Zhoulan Zeng, Xingzhu Chen, Kaiyi Weng, Yang Wu, Peng Zhang, Jizhou Jiang and Neng L	npj Computational Materials, 7, 2021, 80
Cr_2ZrCNO_2	Computational screening study of double transition metal carbonitrides $M'_2M''CNO_2$-MXene as catalysts for hydrogen evolution reaction	Zhoulan Zeng, Xingzhu Chen, Kaiyi Weng, Yang Wu, Peng Zhang, Jizhou Jiang and Neng L	npj Computational Materials, 7, 2021, 80
$Hf_2C(OH)_2$	Two- dimensional molybdenum carbides: Potential thermoelectric materials in MXenes	Mohammad Khazaei, Masao Arai, Taizo Sasaki, Mehdi Estili, Yoshio Sakka	Physical Chemistry Chemical Physics, 16, 2014, 7841-7851
Hf_2CF_2	Two- dimensional molybdenum carbides: Potential thermoelectric materials in MXenes	Mohammad Khazaei, Masao Arai, Taizo Sasaki, Mehdi Estili, Yoshio Sakka	Physical Chemistry Chemical Physics, 16, 2014, 7841-7849
Hf_2CO_2	Two -dimensional molybdenum carbides: Potential thermoelectric materials in MXenes	Mohammad Khazaei, Masao Arai, Taizo Sasaki, Mehdi Estili, Yoshio Sakka	Physical Chemistry Chemical Physics, 16, 2014, 7841-7850
Hf_2CrCN	Computational screening study of double transition metal carbonitrides $M'_2M''CNO_2$-MXene as catalysts for hydrogen evolution reaction	Zhoulan Zeng, Xingzhu Chen, Kaiyi Weng, Yang Wu, Peng Zhang, Jizhou Jiang and Neng L	npj Computational Materials, 7, 2021, 80
Hf_2CrCNO_2	Computational screening study of double transition metal carbonitrides $M'_2M''CNO_2$-MXene as catalysts for hydrogen evolution reaction	Zhoulan Zeng, Xingzhu Chen, Kaiyi Weng, Yang Wu, Peng Zhang, Jizhou Jiang and Neng L	npj Computational Materials, 7, 2021, 80
Hf_2MoCN	Computational screening study of double transition metal carbonitrides $M'_2M''CNO_2$-MXene as catalysts for hydrogen evolution reaction	Zhoulan Zeng, Xingzhu Chen, Kaiyi Weng, Yang Wu, Peng Zhang, Jizhou Jiang and Neng L	npj Computational Materials, 7, 2021, 80
Hf_2MoCNO_2	Computational screening study of double transition metal carbonitrides $M'_2M''CNO_2$-MXene as catalysts for hydrogen evolution reaction	Zhoulan Zeng, Xingzhu Chen, Kaiyi Weng, Yang Wu, Peng Zhang, Jizhou Jiang and Neng L	npj Computational Materials, 7, 2021, 80
$Hf_2N(OH)_2$	Two- dimensional molybdenum carbides: Potential thermoelectric materials in MXenes	Mohammad Khazaei, Masao Arai, Taizo Sasaki, Mehdi Estili, Yoshio Sakka	Physical Chemistry Chemical Physics, 16, 2014, 7841-7854
Hf_2NF_2	Two- dimensional molybdenum carbides: Potential thermoelectric materials in MXenes	Mohammad Khazaei, Masao Arai, Taizo Sasaki, Mehdi Estili, Yoshio Sakka	Physical Chemistry Chemical Physics, 16, 2014, 7841-7852
Hf_2NO_2	Two -dimensional molybdenum carbides: Potential thermoelectric materials in MXenes	Mohammad Khazaei, Masao Arai, Taizo Sasaki, Mehdi Estili, Yoshio Sakka	Physical Chemistry Chemical Physics, 16, 2014, 7841-7853
Hf_2NbCN	Computational screening study of double transition metal carbonitrides $M'_2M''CNO_2$-MXene as catalysts for hydrogen evolution reaction	Zhoulan Zeng, Xingzhu Chen, Kaiyi Weng, Yang Wu, Peng Zhang, Jizhou Jiang and Neng L	npj Computational Materials, 7, 2021, 80
Hf_2NbCNO_2	Computational screening study of double transition metal carbonitrides $M'_2M''CNO_2$-MXene as catalysts for hydrogen evolution reaction	Zhoulan Zeng, Xingzhu Chen, Kaiyi Weng, Yang Wu, Peng Zhang, Jizhou Jiang and Neng L	npj Computational Materials, 7, 2021, 80
Hf_2TaCN	Computational screening study of double transition metal carbonitrides $M'_2M''CNO_2$-MXene as catalysts for hydrogen evolution reaction	Zhoulan Zeng, Xingzhu Chen, Kaiyi Weng, Yang Wu, Peng Zhang, Jizhou Jiang and Neng L	npj Computational Materials, 7, 2021, 80
Hf_2TaCNO_2	Computational screening study of double transition metal carbonitrides $M'_2M''CNO_2$-MXene as catalysts for hydrogen evolution reaction	Zhoulan Zeng, Xingzhu Chen, Kaiyi Weng, Yang Wu, Peng Zhang, Jizhou Jiang and Neng L	npj Computational Materials, 7, 2021, 80

Hf_2TiCN	Computational screening study of double transition metal carbonitrides $M'_2M''CNO_2$-MXene as catalysts for hydrogen evolution reaction	Zhoulan Zeng, Xingzhu Chen, Kaiyi Weng, Yang Wu, Peng Zhang, Jizhou Jiang and Neng L	npj Computational Materials, 7, 2021, 80
Hf_2TiCNO_2	Computational screening study of double transition metal carbonitrides $M'_2M''CNO_2$-MXene as catalysts for hydrogen evolution reaction	Zhoulan Zeng, Xingzhu Chen, Kaiyi Weng, Yang Wu, Peng Zhang, Jizhou Jiang and Neng L	npj Computational Materials, 7, 2021, 80
Hf_2VCN	Computational screening study of double transition metal carbonitrides $M'_2M''CNO_2$-MXene as catalysts for hydrogen evolution reaction	Zhoulan Zeng, Xingzhu Chen, Kaiyi Weng, Yang Wu, Peng Zhang, Jizhou Jiang and Neng L	npj Computational Materials, 7, 2021, 80
Hf_2VCNO_2	Computational screening study of double transition metal carbonitrides $M'_2M''CNO_2$-MXene as catalysts for hydrogen evolution reaction	Zhoulan Zeng, Xingzhu Chen, Kaiyi Weng, Yang Wu, Peng Zhang, Jizhou Jiang and Neng L	npj Computational Materials, 7, 2021, 80
Hf_2ZrCN	Computational screening study of double transition metal carbonitrides $M'_2M''CNO_2$-MXene as catalysts for hydrogen evolution reaction	Zhoulan Zeng, Xingzhu Chen, Kaiyi Weng, Yang Wu, Peng Zhang, Jizhou Jiang and Neng L	npj Computational Materials, 7, 2021, 80
Hf_2ZrCNO_2	Computational screening study of double transition metal carbonitrides $M'_2M''CNO_2$-MXene as catalysts for hydrogen evolution reaction	Zhoulan Zeng, Xingzhu Chen, Kaiyi Weng, Yang Wu, Peng Zhang, Jizhou Jiang and Neng L	npj Computational Materials, 7, 2021, 80
$Mo_2C(OH)_2$	Two- dimensional molybdenum carbides: Potential thermoelectric materials in MXenes	Mohammad Khazaei, Masao Arai, Taizo Sasaki, Mehdi Estili, Yoshio Sakka	Physical Chemistry Chemical Physics, 16, 2014, 7841-7882
Mo_2CBr_2	Two- dimensional molybdenum carbides: Potential thermoelectric materials in MXenes	Mohammad Khazaei, Masao Arai, Taizo Sasaki, Mehdi Estili, Yoshio Sakka	Physical Chemistry Chemical Physics, 16, 2014, 7841-7881
Mo_2CCl_2	Two- dimensional molybdenum carbides: Potential thermoelectric materials in MXenes	Mohammad Khazaei, Masao Arai, Taizo Sasaki, Mehdi Estili, Yoshio Sakka	Physical Chemistry Chemical Physics, 16, 2014, 7841-7880
Mo_2CF_2	Two- dimensional molybdenum carbides: Potential thermoelectric materials in MXenes	Mohammad Khazaei, Masao Arai, Taizo Sasaki, Mehdi Estili, Yoshio Sakka	Physical Chemistry Chemical Physics, 16, 2014, 7841-7879
Mo_2CO_2	Two- dimensional molybdenum carbides: Potential thermoelectric materials in MXenes	Mohammad Khazaei, Masao Arai, Taizo Sasaki, Mehdi Estili, Yoshio Sakka	Physical Chemistry Chemical Physics, 16, 2014, 7841-7883
Mo_2CS_2	Two- dimensional molybdenum carbides: Potential thermoelectric materials in MXenes	Mohammad Khazaei, Masao Arai, Taizo Sasaki, Mehdi Estili, Yoshio Sakka	Physical Chemistry Chemical Physics, 16, 2014, 7841-7884
$Mo_2Hf_2C_3O_2$	Topological insulators in ordered double transition metals $M'_2M''C_2$ (M'= Mo, W; M"= Ti, Zr, Hf) MXenes	Mohammad Khazaei, Ahmad Ranjbar, Masao Arai, Seiji Yunoki	Physical Review B, 94, 2016, 125160
$Mo_2HfC_2O_2$	Topological insulators in ordered double transition metals $M'_2M''C_2$ (M'= Mo, W; M"= Ti, Zr, Hf) MXenes	Mohammad Khazaei, Ahmad Ranjbar, Masao Arai, Seiji Yunoki	Physical Review B, 94, 2016, 125154
Mo_2HfCN	Computational screening study of double transition metal carbonitrides $M'_2M''CNO_2$-MXene as catalysts for hydrogen evolution reaction	Zhoulan Zeng, Xingzhu Chen, Kaiyi Weng, Yang Wu, Peng Zhang, Jizhou Jiang and Neng L	npj Computational Materials, 7, 2021, 80
Mo_2HfCNO_2	Computational screening study of double transition metal carbonitrides $M'_2M''CNO_2$-MXene as catalysts for hydrogen evolution reaction	Zhoulan Zeng, Xingzhu Chen, Kaiyi Weng, Yang Wu, Peng Zhang, Jizhou Jiang and Neng L	npj Computational Materials, 7, 2021, 80
Mo_2NbCN	Computational screening study of double transition metal carbonitrides $M'_2M''CNO_2$-MXene as catalysts for hydrogen evolution reaction	Zhoulan Zeng, Xingzhu Chen, Kaiyi Weng, Yang Wu, Peng Zhang, Jizhou Jiang and Neng L	npj Computational Materials, 7, 2021, 80
Mo_2NbCNO_2	Computational screening study of double transition metal carbonitrides $M'_2M''CNO_2$-MXene as catalysts for hydrogen evolution reaction	Zhoulan Zeng, Xingzhu Chen, Kaiyi Weng, Yang Wu, Peng Zhang, Jizhou Jiang and Neng L	npj Computational Materials, 7, 2021, 80
$Mo_2Ti_2C_3O_2$	Topological insulators in ordered double transition metals $M'_2M''C_2$ (M'= Mo, W; M"= Ti, Zr, Hf) MXenes	Mohammad Khazaei, Ahmad Ranjbar, Masao Arai, Seiji Yunoki	Physical Review B, 94, 2016, 125158
$Mo_2TiC_2O_2$	Topological insulators in ordered double transition metals $M'_2M''C_2$ (M'= Mo, W; M"= Ti, Zr, Hf) MXenes	Mohammad Khazaei, Ahmad Ranjbar, Masao Arai, Seiji Yunoki	Physical Review B, 94, 2016, 125152
Mo_2TiCN	Computational screening study of double transition metal carbonitrides $M'_2M''CNO_2$-MXene as catalysts for hydrogen evolution reaction	Zhoulan Zeng, Xingzhu Chen, Kaiyi Weng, Yang Wu, Peng Zhang, Jizhou Jiang and Neng L	npj Computational Materials, 7, 2021, 80

Mo_2TiCNO_2	Computational screening study of double transition metal carbonitrides $M'_2M''CNO_2$-MXene as catalysts for hydrogen evolution reaction	Zhoulan Zeng, Xingzhu Chen, Kaiyi Weng, Yang Wu, Peng Zhang, Jizhou Jiang and Neng L	npj Computational Materials, 7, 2021, 80
Mo_2VCN	Computational screening study of double transition metal carbonitrides $M'_2M''CNO_2$-MXene as catalysts for hydrogen evolution reaction	Zhoulan Zeng, Xingzhu Chen, Kaiyi Weng, Yang Wu, Peng Zhang, Jizhou Jiang and Neng L	npj Computational Materials, 7, 2021, 80
Mo_2VCNO_2	Computational screening study of double transition metal carbonitrides $M'_2M''CNO_2$-MXene as catalysts for hydrogen evolution reaction	Zhoulan Zeng, Xingzhu Chen, Kaiyi Weng, Yang Wu, Peng Zhang, Jizhou Jiang and Neng L	npj Computational Materials, 7, 2021, 80
$Mo_2Zr_2C_3O_2$	Topological insulators in ordered double transition metals $M'_2M''C_2$ (M'= Mo, W; M"= Ti, Zr, Hf) MXenes	Mohammad Khazaei, Ahmad Ranjbar, Masao Arai, Seiji Yunoki	Physical Review B, 94, 2016, 125159
$Mo_2ZrC_2O_2$	Topological insulators in ordered double transition metals $M'_2M''C_2$ (M'= Mo, W; M"= Ti, Zr, Hf) MXenes	Mohammad Khazaei, Ahmad Ranjbar, Masao Arai, Seiji Yunoki	Physical Review B, 94, 2016, 125153
Mo_2ZrCN	Computational screening study of double transition metal carbonitrides $M'_2M''CNO_2$-MXene as catalysts for hydrogen evolution reaction	Zhoulan Zeng, Xingzhu Chen, Kaiyi Weng, Yang Wu, Peng Zhang, Jizhou Jiang and Neng L	npj Computational Materials, 7, 2021, 80
Mo_2ZrCNO_2	Computational screening study of double transition metal carbonitrides $M'_2M''CNO_2$-MXene as catalysts for hydrogen evolution reaction	Zhoulan Zeng, Xingzhu Chen, Kaiyi Weng, Yang Wu, Peng Zhang, Jizhou Jiang and Neng L	npj Computational Materials, 7, 2021, 80
$Nb_2C(OH)_2$	Two -dimensional molybdenum carbides: Potential thermoelectric materials in MXenes	Mohammad Khazaei, Masao Arai, Taizo Sasaki, Mehdi Estili, Yoshio Sakka	Physical Chemistry Chemical Physics, 16, 2014, 7841-7857
Nb_2CF_2	Two -dimensional molybdenum carbides: Potential thermoelectric materials in MXenes	Mohammad Khazaei, Masao Arai, Taizo Sasaki, Mehdi Estili, Yoshio Sakka	Physical Chemistry Chemical Physics, 16, 2014, 7841-7855
Nb_2CO_2	Two -dimensional molybdenum carbides: Potential thermoelectric materials in MXenes	Mohammad Khazaei, Masao Arai, Taizo Sasaki, Mehdi Estili, Yoshio Sakka	Physical Chemistry Chemical Physics, 16, 2014, 7841-7856
Nb_2CrCN	Computational screening study of double transition metal carbonitrides $M'_2M''CNO_2$-MXene as catalysts for hydrogen evolution reaction	Zhoulan Zeng, Xingzhu Chen, Kaiyi Weng, Yang Wu, Peng Zhang, Jizhou Jiang and Neng L	npj Computational Materials, 7, 2021, 80
Nb_2CrCNO_2	Computational screening study of double transition metal carbonitrides $M'_2M''CNO_2$-MXene as catalysts for hydrogen evolution reaction	Zhoulan Zeng, Xingzhu Chen, Kaiyi Weng, Yang Wu, Peng Zhang, Jizhou Jiang and Neng L	npj Computational Materials, 7, 2021, 80
Nb_2HfCN	Computational screening study of double transition metal carbonitrides $M'_2M''CNO_2$-MXene as catalysts for hydrogen evolution reaction	Zhoulan Zeng, Xingzhu Chen, Kaiyi Weng, Yang Wu, Peng Zhang, Jizhou Jiang and Neng L	npj Computational Materials, 7, 2021, 80
Nb_2HfCNO_2	Computational screening study of double transition metal carbonitrides $M'_2M''CNO_2$-MXene as catalysts for hydrogen evolution reaction	Zhoulan Zeng, Xingzhu Chen, Kaiyi Weng, Yang Wu, Peng Zhang, Jizhou Jiang and Neng L	npj Computational Materials, 7, 2021, 80
Nb_2MoCN	Computational screening study of double transition metal carbonitrides $M'_2M''CNO_2$-MXene as catalysts for hydrogen evolution reaction	Zhoulan Zeng, Xingzhu Chen, Kaiyi Weng, Yang Wu, Peng Zhang, Jizhou Jiang and Neng L	npj Computational Materials, 7, 2021, 80
Nb_2MoCNO_2	Computational screening study of double transition metal carbonitrides $M'_2M''CNO_2$-MXene as catalysts for hydrogen evolution reaction	Zhoulan Zeng, Xingzhu Chen, Kaiyi Weng, Yang Wu, Peng Zhang, Jizhou Jiang and Neng L	npj Computational Materials, 7, 2021, 80
Nb_2TaCN	Computational screening study of double transition metal carbonitrides $M'_2M''CNO_2$-MXene as catalysts for hydrogen evolution reaction	Zhoulan Zeng, Xingzhu Chen, Kaiyi Weng, Yang Wu, Peng Zhang, Jizhou Jiang and Neng L	npj Computational Materials, 7, 2021, 80
Nb_2TaCNO_2	Computational screening study of double transition metal carbonitrides $M'_2M''CNO_2$-MXene as catalysts for hydrogen evolution reaction	Zhoulan Zeng, Xingzhu Chen, Kaiyi Weng, Yang Wu, Peng Zhang, Jizhou Jiang and Neng L	npj Computational Materials, 7, 2021, 80
Nb_2TiCN	Computational screening study of double transition metal carbonitrides $M'_2M''CNO_2$-MXene as catalysts for hydrogen evolution reaction	Zhoulan Zeng, Xingzhu Chen, Kaiyi Weng, Yang Wu, Peng Zhang, Jizhou Jiang and Neng L	npj Computational Materials, 7, 2021, 80
Nb_2TiCNO_2	Computational screening study of double transition metal carbonitrides $M'_2M''CNO_2$-MXene as catalysts for hydrogen evolution reaction	Zhoulan Zeng, Xingzhu Chen, Kaiyi Weng, Yang Wu, Peng Zhang, Jizhou Jiang and Neng L	npj Computational Materials, 7, 2021, 80
Nb_2VCN	Computational screening study of double transition metal carbonitrides $M'_2M''CNO_2$-MXene as catalysts for hydrogen evolution reaction	Zhoulan Zeng, Xingzhu Chen, Kaiyi Weng, Yang Wu, Peng Zhang, Jizhou Jiang and Neng L	npj Computational Materials, 7, 2021, 80

Nb_2VCNO_2	Computational screening study of double transition metal carbonitrides $M'_2M''CNO_2$-MXene as catalysts for hydrogen evolution reaction	Zhoulan Zeng, Xingzhu Chen, Kaiyi Weng, Yang Wu, Peng Zhang, Jizhou Jiang and Neng L	npj Computational Materials, 7, 2021, 80
Nb_2ZrCN	Computational screening study of double transition metal carbonitrides $M'_2M''CNO_2$-MXene as catalysts for hydrogen evolution reaction	Zhoulan Zeng, Xingzhu Chen, Kaiyi Weng, Yang Wu, Peng Zhang, Jizhou Jiang and Neng L	npj Computational Materials, 7, 2021, 80
Nb_2ZrCNO_2	Computational screening study of double transition metal carbonitrides $M'_2M''CNO_2$-MXene as catalysts for hydrogen evolution reaction	Zhoulan Zeng, Xingzhu Chen, Kaiyi Weng, Yang Wu, Peng Zhang, Jizhou Jiang and Neng L	npj Computational Materials, 7, 2021, 80
Nb_3CNO_2	Computational screening study of double transition metal carbonitrides $M'_2M''CNO_2$-MXene as catalysts for hydrogen evolution reaction	Zhoulan Zeng, Xingzhu Chen, Kaiyi Weng, Yang Wu, Peng Zhang, Jizhou Jiang and Neng L	npj Computational Materials, 7, 2021, 80
$Nb_4C_3(OH)_2$	Novel electronic and magnetic properties of two-dimensional transition metal carbides and nitrides	Mohammad Khazaei, Masao Arai, Taizo Sasaki, Chan-Yeup Chung, Natarajan S. Venkataramanan, Mehdi Estili, Yoshio Sakka, Yoshiyuki Kawazoe	Advanced Functional Materials, 23(17), 2013, 2185-2214
$Nb_4C_3F_2$	Novel electronic and magnetic properties of two-dimensional transition metal carbides and nitrides	Mohammad Khazaei, Masao Arai, Taizo Sasaki, Chan-Yeup Chung, Natarajan S. Venkataramanan, Mehdi Estili, Yoshio Sakka, Yoshiyuki Kawazoe	Advanced Functional Materials, 23(17), 2013, 2185-2193
$Nb_4C_3O_2$	Novel electronic and magnetic properties of two-dimensional transition metal carbides and nitrides	Mohammad Khazaei, Masao Arai, Taizo Sasaki, Chan-Yeup Chung, Natarajan S. Venkataramanan, Mehdi Estili, Yoshio Sakka, Yoshiyuki Kawazoe	Advanced Functional Materials, 23(17), 2013, 2185-2204
$Nb_5C_4(OH)_2$	Novel electronic and magnetic properties of two-dimensional transition metal carbides and nitrides	Mohammad Khazaei, Masao Arai, Taizo Sasaki, Chan-Yeup Chung, Natarajan S. Venkataramanan, Mehdi Estili, Yoshio Sakka, Yoshiyuki Kawazoe	Advanced Functional Materials, 23(17), 2013, 2185-2215
$Nb_5C_4F_2$	Novel electronic and magnetic properties of two-dimensional transition metal carbides and nitrides	Mohammad Khazaei, Masao Arai, Taizo Sasaki, Chan-Yeup Chung, Natarajan S. Venkataramanan, Mehdi Estili, Yoshio Sakka, Yoshiyuki Kawazoe	Advanced Functional Materials, 23(17), 2013, 2185-2194
$Nb_5C_4O_2$	Novel electronic and magnetic properties of two-dimensional transition metal carbides and nitrides	Mohammad Khazaei, Masao Arai, Taizo Sasaki, Chan-Yeup Chung, Natarajan S. Venkataramanan, Mehdi Estili, Yoshio Sakka, Yoshiyuki Kawazoe	Advanced Functional Materials, 23(17), 2013, 2185-2205
$Sc_2C(OH)_2$	Two -dimensional molybdenum carbides: Potential thermoelectric materials in MXenes	Mohammad Khazaei, Masao Arai, Taizo Sasaki, Mehdi Estili, Yoshio Sakka	Physical Chemistry Chemical Physics, 16, 2014, 7841-7860
Sc_2CCl_2	Interlayer-decoupled Sc-based MXene with high carrier mobility and strong light-harvesting ability	Liujiang Zhou, Yu Zhang, Zhiwen Zhuo, Amanda J. Neukirch, Sergei Tretiak	Jornal of Physical Chemistry Letters, 9(23), 2018, 6915–6920
Sc_2CF_2	Two -dimensional molybdenum carbides: Potential thermoelectric materials in MXenes	Mohammad Khazaei, Masao Arai, Taizo Sasaki, Mehdi Estili, Yoshio Sakka	Physical Chemistry Chemical Physics, 16, 2014, 7841-7858
Sc_2CO_2 - (model3)	Two -dimensional molybdenum carbides: Potential thermoelectric materials in MXenes	Mohammad Khazaei, Masao Arai, Taizo Sasaki, Mehdi Estili, Yoshio Sakka	Physical Chemistry Chemical Physics, 16, 2014, 7841-7859
$Ta_2C(OH)_2$	Two- dimensional molybdenum carbides: Potential thermoelectric materials in MXenes	Mohammad Khazaei, Masao Arai, Taizo Sasaki, Mehdi Estili, Yoshio Sakka	Physical Chemistry Chemical Physics, 16, 2014, 7841-7863
Ta_2CF_2	Two- dimensional molybdenum carbides: Potential thermoelectric materials in MXenes	Mohammad Khazaei, Masao Arai, Taizo Sasaki, Mehdi Estili, Yoshio Sakka	Physical Chemistry Chemical Physics, 16, 2014, 7841-7861
Ta_2CO_2	Two -dimensional molybdenum carbides: Potential thermoelectric materials in MXenes	Mohammad Khazaei, Masao Arai, Taizo Sasaki, Mehdi Estili, Yoshio Sakka	Physical Chemistry Chemical Physics, 16, 2014, 7841-7862
Ta_2CrCN	Computational screening study of double transition metal carbonitrides $M'_2M''CNO_2$-MXene as catalysts for hydrogen evolution reaction	Zhoulan Zeng, Xingzhu Chen, Kaiyi Weng, Yang Wu, Peng Zhang, Jizhou Jiang and Neng L	npj Computational Materials, 7, 2021, 80

Ta_2CrCNO_2	Computational screening study of double transition metal carbonitrides $M'_2M''CNO_2$-MXene as catalysts for hydrogen evolution reaction	Zhoulan Zeng, Xingzhu Chen, Kaiyi Weng, Yang Wu, Peng Zhang, Jizhou Jiang and Neng L	npj Computational Materials, 7, 2021, 80
Ta_2HfCN	Computational screening study of double transition metal carbonitrides $M'_2M''CNO_2$-MXene as catalysts for hydrogen evolution reaction	Zhoulan Zeng, Xingzhu Chen, Kaiyi Weng, Yang Wu, Peng Zhang, Jizhou Jiang and Neng L	npj Computational Materials, 7, 2021, 80
Ta_2HfCNO_2	Computational screening study of double transition metal carbonitrides $M'_2M''CNO_2$-MXene as catalysts for hydrogen evolution reaction	Zhoulan Zeng, Xingzhu Chen, Kaiyi Weng, Yang Wu, Peng Zhang, Jizhou Jiang and Neng L	npj Computational Materials, 7, 2021, 80
Ta_2MoCN	Computational screening study of double transition metal carbonitrides $M'_2M''CNO_2$-MXene as catalysts for hydrogen evolution reaction	Zhoulan Zeng, Xingzhu Chen, Kaiyi Weng, Yang Wu, Peng Zhang, Jizhou Jiang and Neng L	npj Computational Materials, 7, 2021, 80
Ta_2MoCNO_2	Computational screening study of double transition metal carbonitrides $M'_2M''CNO_2$-MXene as catalysts for hydrogen evolution reaction	Zhoulan Zeng, Xingzhu Chen, Kaiyi Weng, Yang Wu, Peng Zhang, Jizhou Jiang and Neng L	npj Computational Materials, 7, 2021, 80
Ta_2NbCN	Computational screening study of double transition metal carbonitrides $M'_2M''CNO_2$-MXene as catalysts for hydrogen evolution reaction	Zhoulan Zeng, Xingzhu Chen, Kaiyi Weng, Yang Wu, Peng Zhang, Jizhou Jiang and Neng L	npj Computational Materials, 7, 2021, 80
Ta_2NbCNO_2	Computational screening study of double transition metal carbonitrides $M'_2M''CNO_2$-MXene as catalysts for hydrogen evolution reaction	Zhoulan Zeng, Xingzhu Chen, Kaiyi Weng, Yang Wu, Peng Zhang, Jizhou Jiang and Neng L	npj Computational Materials, 7, 2021, 80
Ta_2TiCN	Computational screening study of double transition metal carbonitrides $M'_2M''CNO_2$-MXene as catalysts for hydrogen evolution reaction	Zhoulan Zeng, Xingzhu Chen, Kaiyi Weng, Yang Wu, Peng Zhang, Jizhou Jiang and Neng L	npj Computational Materials, 7, 2021, 80
Ta_2TiCNO_2	Computational screening study of double transition metal carbonitrides $M'_2M''CNO_2$-MXene as catalysts for hydrogen evolution reaction	Zhoulan Zeng, Xingzhu Chen, Kaiyi Weng, Yang Wu, Peng Zhang, Jizhou Jiang and Neng L	npj Computational Materials, 7, 2021, 80
Ta_2VCN	Computational screening study of double transition metal carbonitrides $M'_2M''CNO_2$-MXene as catalysts for hydrogen evolution reaction	Zhoulan Zeng, Xingzhu Chen, Kaiyi Weng, Yang Wu, Peng Zhang, Jizhou Jiang and Neng L	npj Computational Materials, 7, 2021, 80
Ta_2VCNO_2	Computational screening study of double transition metal carbonitrides $M'_2M''CNO_2$-MXene as catalysts for hydrogen evolution reaction	Zhoulan Zeng, Xingzhu Chen, Kaiyi Weng, Yang Wu, Peng Zhang, Jizhou Jiang and Neng L	npj Computational Materials, 7, 2021, 80
Ta_2ZrCN	Computational screening study of double transition metal carbonitrides $M'_2M''CNO_2$-MXene as catalysts for hydrogen evolution reaction	Zhoulan Zeng, Xingzhu Chen, Kaiyi Weng, Yang Wu, Peng Zhang, Jizhou Jiang and Neng L	npj Computational Materials, 7, 2021, 80
Ta_2ZrCNO_2	Computational screening study of double transition metal carbonitrides $M'_2M''CNO_2$-MXene as catalysts for hydrogen evolution reaction	Zhoulan Zeng, Xingzhu Chen, Kaiyi Weng, Yang Wu, Peng Zhang, Jizhou Jiang and Neng L	npj Computational Materials, 7, 2021, 80
$Ta_3C_2(OH)_2$	Novel electronic and magnetic properties of two-dimensional transition metal carbides and nitrides	Mohammad Khazaei, Masao Arai, Taizo Sasaki, Chan-Yeup Chung, Natarajan S. Venkataramanan, Mehdi Estili, Yoshio Sakka, Yoshiyuki Kawazoe	Advanced Functional Materials, 23(17), 2013, 2185-2216
$Ta_3C_2F_2$	Novel electronic and magnetic properties of two-dimensional transition metal carbides and nitrides	Mohammad Khazaei, Masao Arai, Taizo Sasaki, Chan-Yeup Chung, Natarajan S. Venkataramanan, Mehdi Estili, Yoshio Sakka, Yoshiyuki Kawazoe	Advanced Functional Materials, 23(17), 2013, 2185-2195
$Ta_3C_2O_2$	Novel electronic and magnetic properties of two-dimensional transition metal carbides and nitrides	Mohammad Khazaei, Masao Arai, Taizo Sasaki, Chan-Yeup Chung, Natarajan S. Venkataramanan, Mehdi Estili, Yoshio Sakka, Yoshiyuki Kawazoe	Advanced Functional Materials, 23(17), 2013, 2185-2206
Ta_3CNO_2-1	Computational screening study of double transition metal carbonitrides $M'_2M''CNO_2$-MXene as catalysts for hydrogen evolution reaction	Zhoulan Zeng, Xingzhu Chen, Kaiyi Weng, Yang Wu, Peng Zhang, Jizhou Jiang and Neng L	npj Computational Materials, 7, 2021, 80
$Ta_4C_3(OH)_2$	Novel electronic and magnetic properties of two-dimensional transition metal carbides and nitrides	Mohammad Khazaei, Masao Arai, Taizo Sasaki, Chan-Yeup Chung, Natarajan S. Venkataramanan, Mehdi Estili, Yoshio Sakka, Yoshiyuki Kawazoe	Advanced Functional Materials, 23(17), 2013, 2185-2217
$Ta_4C_3F_2$	Novel electronic and magnetic properties of two-dimensional transition metal carbides and nitrides	Mohammad Khazaei, Masao Arai, Taizo Sasaki, Chan-Yeup Chung, Natarajan S. Venkataramanan, Mehdi Estili, Yoshio Sakka, Yoshiyuki Kawazoe	Advanced Functional Materials, 23(17), 2013, 2185-2196

$Ta_4C_3O_2$	Novel electronic and magnetic properties of two-dimensional transition metal carbides and nitrides	Mohammad Khazaei, Masao Arai, Taizo Sasaki, Chan-Yeup Chung, Natarajan S. Venkataramanan, Mehdi Estili, Yoshio Sakka, Yoshiyuki Kawazoe	Advanced Functional Materials, 23(17), 2013, 2185-2207
$Ti_2C(OH)_2$	Two- dimensional molybdenum carbides: Potential thermoelectric materials in MXenes	Mohammad Khazaei, Masao Arai, Taizo Sasaki, Mehdi Estili, Yoshio Sakka	Physical Chemistry Chemical Physics, 16, 2014, 7841-7866
Ti_2CF_2	Two- dimensional molybdenum carbides: Potential thermoelectric materials in MXenes	Mohammad Khazaei, Masao Arai, Taizo Sasaki, Mehdi Estili, Yoshio Sakka	Physical Chemistry Chemical Physics, 16, 2014, 7841-7864
Ti_2CO_2	Two -dimensional molybdenum carbides: Potential thermoelectric materials in MXenes	Mohammad Khazaei, Masao Arai, Taizo Sasaki, Mehdi Estili, Yoshio Sakka	Physical Chemistry Chemical Physics, 16, 2014, 7841-7865
$Ti_2N(OH)_2$	Two -dimensional molybdenum carbides: Potential thermoelectric materials in MXenes	Mohammad Khazaei, Masao Arai, Taizo Sasaki, Mehdi Estili, Yoshio Sakka	Physical Chemistry Chemical Physics, 16, 2014, 7841-7869
Ti_2NF_2	Two- dimensional molybdenum carbides: Potential thermoelectric materials in MXenes	Mohammad Khazaei, Masao Arai, Taizo Sasaki, Mehdi Estili, Yoshio Sakka	Physical Chemistry Chemical Physics, 16, 2014, 7841-7867
Ti_2NO_2	Two -dimensional molybdenum carbides: Potential thermoelectric materials in MXenes	Mohammad Khazaei, Masao Arai, Taizo Sasaki, Mehdi Estili, Yoshio Sakka	Physical Chemistry Chemical Physics, 16, 2014, 7841-7868
Ti_2CrCN	Computational screening study of double transition metal carbonitrides $M'_2M''CNO_2$-MXene as catalysts for hydrogen evolution reaction	Zhoulan Zeng, Xingzhu Chen, Kaiyi Weng, Yang Wu, Peng Zhang, Jizhou Jiang and Neng L	npj Computational Materials, 7, 2021, 80
Ti_2CrCNO_2	Computational screening study of double transition metal carbonitrides $M'_2M''CNO_2$-MXene as catalysts for hydrogen evolution reaction	Zhoulan Zeng, Xingzhu Chen, Kaiyi Weng, Yang Wu, Peng Zhang, Jizhou Jiang and Neng L	npj Computational Materials, 7, 2021, 80
Ti_2HfCN	Computational screening study of double transition metal carbonitrides $M'_2M''CNO_2$-MXene as catalysts for hydrogen evolution reaction	Zhoulan Zeng, Xingzhu Chen, Kaiyi Weng, Yang Wu, Peng Zhang, Jizhou Jiang and Neng L	npj Computational Materials, 7, 2021, 80
Ti_2HfCNO_2	Computational screening study of double transition metal carbonitrides $M'_2M''CNO_2$-MXene as catalysts for hydrogen evolution reaction	Zhoulan Zeng, Xingzhu Chen, Kaiyi Weng, Yang Wu, Peng Zhang, Jizhou Jiang and Neng L	npj Computational Materials, 7, 2021, 80
Ti_2MoCN	Computational screening study of double transition metal carbonitrides $M'_2M''CNO_2$-MXene as catalysts for hydrogen evolution reaction	Zhoulan Zeng, Xingzhu Chen, Kaiyi Weng, Yang Wu, Peng Zhang, Jizhou Jiang and Neng L	npj Computational Materials, 7, 2021, 80
Ti_2MoCNO_2	Computational screening study of double transition metal carbonitrides $M'_2M''CNO_2$-MXene as catalysts for hydrogen evolution reaction	Zhoulan Zeng, Xingzhu Chen, Kaiyi Weng, Yang Wu, Peng Zhang, Jizhou Jiang and Neng L	npj Computational Materials, 7, 2021, 80
Ti_2NbCN	Computational screening study of double transition metal carbonitrides $M'_2M''CNO_2$-MXene as catalysts for hydrogen evolution reaction	Zhoulan Zeng, Xingzhu Chen, Kaiyi Weng, Yang Wu, Peng Zhang, Jizhou Jiang and Neng L	npj Computational Materials, 7, 2021, 80
Ti_2NbCNO_2	Computational screening study of double transition metal carbonitrides $M'_2M''CNO_2$-MXene as catalysts for hydrogen evolution reaction	Zhoulan Zeng, Xingzhu Chen, Kaiyi Weng, Yang Wu, Peng Zhang, Jizhou Jiang and Neng L	npj Computational Materials, 7, 2021, 80
Ti_2VCN	Computational screening study of double transition metal carbonitrides $M'_2M''CNO_2$-MXene as catalysts for hydrogen evolution reaction	Zhoulan Zeng, Xingzhu Chen, Kaiyi Weng, Yang Wu, Peng Zhang, Jizhou Jiang and Neng L	npj Computational Materials, 7, 2021, 80
Ti_2VCNO_2	Computational screening study of double transition metal carbonitrides $M'_2M''CNO_2$-MXene as catalysts for hydrogen evolution reaction	Zhoulan Zeng, Xingzhu Chen, Kaiyi Weng, Yang Wu, Peng Zhang, Jizhou Jiang and Neng L	npj Computational Materials, 7, 2021, 80
Ti_2ZrCN	Computational screening study of double transition metal carbonitrides $M'_2M''CNO_2$-MXene as catalysts for hydrogen evolution reaction	Zhoulan Zeng, Xingzhu Chen, Kaiyi Weng, Yang Wu, Peng Zhang, Jizhou Jiang and Neng L	npj Computational Materials, 7, 2021, 80
Ti_2ZrCNO_2	Computational screening study of double transition metal carbonitrides $M'_2M''CNO_2$-MXene as catalysts for hydrogen evolution reaction	Zhoulan Zeng, Xingzhu Chen, Kaiyi Weng, Yang Wu, Peng Zhang, Jizhou Jiang and Neng L	npj Computational Materials, 7, 2021, 80
$Ti_3C_2(OH)_2$	Novel electronic and magnetic properties of two-dimensional transition metal carbides and nitrides	Mohammad Khazaei, Masao Arai, Taizo Sasaki, Chan-Yeup Chung, Natarajan S. Venkataramanan, Mehdi Estili, Yoshio Sakka, Yoshiyuki Kawazoe	Advanced Functional Materials, 23(17), 2013, 2185-2218

$Ti_3C_2F_2$	Novel electronic and magnetic properties of two-dimensional transition metal carbides and nitrides	Mohammad Khazaei, Masao Arai, Taizo Sasaki, Chan-Yeup Chung, Natarajan S. Venkataramanan, Mehdi Estili, Yoshio Sakka, Yoshiyuki Kawazoe	Advanced Functional Materials, 23(17), 2013, 2185-2197
$Ti_3C_2O_2$	Novel electronic and magnetic properties of two-dimensional transition metal carbides and nitrides	Mohammad Khazaei, Masao Arai, Taizo Sasaki, Chan-Yeup Chung, Natarajan S. Venkataramanan, Mehdi Estili, Yoshio Sakka, Yoshiyuki Kawazoe	Advanced Functional Materials, 23(17), 2013, 2185-2208
$Ti_4C_3(OH)_2$	Novel electronic and magnetic properties of two-dimensional transition metal carbides and nitrides	Mohammad Khazaei, Masao Arai, Taizo Sasaki, Chan-Yeup Chung, Natarajan S. Venkataramanan, Mehdi Estili, Yoshio Sakka, Yoshiyuki Kawazoe	Advanced Functional Materials, 23(17), 2013, 2185-2219
$Ti_4C_3F_2$	Novel electronic and magnetic properties of two-dimensional transition metal carbides and nitrides	Mohammad Khazaei, Masao Arai, Taizo Sasaki, Chan-Yeup Chung, Natarajan S. Venkataramanan, Mehdi Estili, Yoshio Sakka, Yoshiyuki Kawazoe	Advanced Functional Materials, 23(17), 2013, 2185-2198
$Ti_4C_3O_2$	Novel electronic and magnetic properties of two-dimensional transition metal carbides and nitrides	Mohammad Khazaei, Masao Arai, Taizo Sasaki, Chan-Yeup Chung, Natarajan S. Venkataramanan, Mehdi Estili, Yoshio Sakka, Yoshiyuki Kawazoe	Advanced Functional Materials, 23(17), 2013, 2185-2209
$Ti_4N_3(OH)_2$	Novel electronic and magnetic properties of two-dimensional transition metal carbides and nitrides	Mohammad Khazaei, Masao Arai, Taizo Sasaki, Chan-Yeup Chung, Natarajan S. Venkataramanan, Mehdi Estili, Yoshio Sakka, Yoshiyuki Kawazoe	Advanced Functional Materials, 23(17), 2013, 2185-2220
$Ti_4N_3F_2$	Novel electronic and magnetic properties of two-dimensional transition metal carbides and nitrides	Mohammad Khazaei, Masao Arai, Taizo Sasaki, Chan-Yeup Chung, Natarajan S. Venkataramanan, Mehdi Estili, Yoshio Sakka, Yoshiyuki Kawazoe	Advanced Functional Materials, 23(17), 2013, 2185-2199
$Ti_4N_3O_2$	Novel electronic and magnetic properties of two-dimensional transition metal carbides and nitrides	Mohammad Khazaei, Masao Arai, Taizo Sasaki, Chan-Yeup Chung, Natarajan S. Venkataramanan, Mehdi Estili, Yoshio Sakka, Yoshiyuki Kawazoe	Advanced Functional Materials, 23(17), 2013, 2185-2200
$Ti_5C_4(OH)_2$	Novel electronic and magnetic properties of two-dimensional transition metal carbides and nitrides	Mohammad Khazaei, Masao Arai, Taizo Sasaki, Chan-Yeup Chung, Natarajan S. Venkataramanan, Mehdi Estili, Yoshio Sakka, Yoshiyuki Kawazoe	Advanced Functional Materials, 23(17), 2013, 2185-2221
$Ti_5C_4F_2$	Novel electronic and magnetic properties of two-dimensional transition metal carbides and nitrides	Mohammad Khazaei, Masao Arai, Taizo Sasaki, Chan-Yeup Chung, Natarajan S. Venkataramanan, Mehdi Estili, Yoshio Sakka, Yoshiyuki Kawazoe	Advanced Functional Materials, 23(17), 2013, 2185-2200
$Ti_5C_4O_2$	Novel electronic and magnetic properties of two-dimensional transition metal carbides and nitrides	Mohammad Khazaei, Masao Arai, Taizo Sasaki, Chan-Yeup Chung, Natarajan S. Venkataramanan, Mehdi Estili, Yoshio Sakka, Yoshiyuki Kawazoe	Advanced Functional Materials, 23(17), 2013, 2185-2210
$V_2C(OH)_2$	Two- dimensional molybdenum carbides: Potential thermoelectric materials in MXenes	Mohammad Khazaei, Masao Arai, Taizo Sasaki, Mehdi Estili, Yoshio Sakka	Physical Chemistry Chemical Physics, 16, 2014, 7841-7872
V_2CF_2	Two- dimensional molybdenum carbides: Potential thermoelectric materials in MXenes	Mohammad Khazaei, Masao Arai, Taizo Sasaki, Mehdi Estili, Yoshio Sakka	Physical Chemistry Chemical Physics, 16, 2014, 7841-7870
V_2CO_2	Two -dimensional molybdenum carbides: Potential thermoelectric materials in MXenes	Mohammad Khazaei, Masao Arai, Taizo Sasaki, Mehdi Estili, Yoshio Sakka	Physical Chemistry Chemical Physics, 16, 2014, 7841-7871
V_2CrCN	Computational screening study of double transition metal carbonitrides $M'_2M''CNO_2$-MXene as catalysts for hydrogen evolution reaction	Zhoulan Zeng, Xingzhu Chen, Kaiyi Weng, Yang Wu, Peng Zhang, Jizhou Jiang and Neng L	npj Computational Materials, 7, 2021, 80
V_2CrCNO_2	Computational screening study of double transition metal carbonitrides $M'_2M''CNO_2$-MXene as catalysts for hydrogen evolution reaction	Zhoulan Zeng, Xingzhu Chen, Kaiyi Weng, Yang Wu, Peng Zhang, Jizhou Jiang and Neng L	npj Computational Materials, 7, 2021, 80

V_2HfCN	Computational screening study of double transition metal carbonitrides $M'_2M''CNO_2$-MXene as catalysts for hydrogen evolution reaction	Zhoulan Zeng, Xingzhu Chen, Kaiyi Weng, Yang Wu, Peng Zhang, Jizhou Jiang and Neng L	npj Computational Materials, 7, 2021, 80
V_2HfCNO_2	Computational screening study of double transition metal carbonitrides $M'_2M''CNO_2$-MXene as catalysts for hydrogen evolution reaction	Zhoulan Zeng, Xingzhu Chen, Kaiyi Weng, Yang Wu, Peng Zhang, Jizhou Jiang and Neng L	npj Computational Materials, 7, 2021, 80
V_2MoCN	Computational screening study of double transition metal carbonitrides $M'_2M''CNO_2$-MXene as catalysts for hydrogen evolution reaction	Zhoulan Zeng, Xingzhu Chen, Kaiyi Weng, Yang Wu, Peng Zhang, Jizhou Jiang and Neng L	npj Computational Materials, 7, 2021, 80
V_2MoCNO_2	Computational screening study of double transition metal carbonitrides $M'_2M''CNO_2$-MXene as catalysts for hydrogen evolution reaction	Zhoulan Zeng, Xingzhu Chen, Kaiyi Weng, Yang Wu, Peng Zhang, Jizhou Jiang and Neng L	npj Computational Materials, 7, 2021, 80
V_2NbCN	Computational screening study of double transition metal carbonitrides $M'_2M''CNO_2$-MXene as catalysts for hydrogen evolution reaction	Zhoulan Zeng, Xingzhu Chen, Kaiyi Weng, Yang Wu, Peng Zhang, Jizhou Jiang and Neng L	npj Computational Materials, 7, 2021, 80
V_2NbCNO_2	Computational screening study of double transition metal carbonitrides $M'_2M''CNO_2$-MXene as catalysts for hydrogen evolution reaction	Zhoulan Zeng, Xingzhu Chen, Kaiyi Weng, Yang Wu, Peng Zhang, Jizhou Jiang and Neng L	npj Computational Materials, 7, 2021, 80
V_2TiCN	Computational screening study of double transition metal carbonitrides $M'_2M''CNO_2$-MXene as catalysts for hydrogen evolution reaction	Zhoulan Zeng, Xingzhu Chen, Kaiyi Weng, Yang Wu, Peng Zhang, Jizhou Jiang and Neng L	npj Computational Materials, 7, 2021, 80
V_2TiCNO_2	Computational screening study of double transition metal carbonitrides $M'_2M''CNO_2$-MXene as catalysts for hydrogen evolution reaction	Zhoulan Zeng, Xingzhu Chen, Kaiyi Weng, Yang Wu, Peng Zhang, Jizhou Jiang and Neng L	npj Computational Materials, 7, 2021, 80
V_2ZrCN	Computational screening study of double transition metal carbonitrides $M'_2M''CNO_2$-MXene as catalysts for hydrogen evolution reaction	Zhoulan Zeng, Xingzhu Chen, Kaiyi Weng, Yang Wu, Peng Zhang, Jizhou Jiang and Neng L	npj Computational Materials, 7, 2021, 80
V_2ZrCNO_2	Computational screening study of double transition metal carbonitrides $M'_2M''CNO_2$-MXene as catalysts for hydrogen evolution reaction	Zhoulan Zeng, Xingzhu Chen, Kaiyi Weng, Yang Wu, Peng Zhang, Jizhou Jiang and Neng L	npj Computational Materials, 7, 2021, 80
$V_3C_2(OH)_2$	Novel electronic and magnetic properties of two-dimensional transition metal carbides and nitrides	Mohammad Khazaei, Masao Arai, Taizo Sasaki, Chan-Yeup Chung, Natarajan S. Venkataramanan, Mehdi Estili, Yoshio Sakka, Yoshiyuki Kawazoe	Advanced Functional Materials, 23(17), 2013, 2185-2222
$V_3C_2F_2$	Novel electronic and magnetic properties of two-dimensional transition metal carbides and nitrides	Mohammad Khazaei, Masao Arai, Taizo Sasaki, Chan-Yeup Chung, Natarajan S. Venkataramanan, Mehdi Estili, Yoshio Sakka, Yoshiyuki Kawazoe	Advanced Functional Materials, 23(17), 2013, 2185-2201
$V_3C_2O_2$	Novel electronic and magnetic properties of two-dimensional transition metal carbides and nitrides	Mohammad Khazaei, Masao Arai, Taizo Sasaki, Chan-Yeup Chung, Natarajan S. Venkataramanan, Mehdi Estili, Yoshio Sakka, Yoshiyuki Kawazoe	Advanced Functional Materials, 23(17), 2013, 2185-2211
$V_4C_3(OH)_2$	Novel electronic and magnetic properties of two-dimensional transition metal carbides and nitrides	Mohammad Khazaei, Masao Arai, Taizo Sasaki, Chan-Yeup Chung, Natarajan S. Venkataramanan, Mehdi Estili, Yoshio Sakka, Yoshiyuki Kawazoe	Advanced Functional Materials, 23(17), 2013, 2185-2223
$V_4C_3F_2$	Novel electronic and magnetic properties of two-dimensional transition metal carbides and nitrides	Mohammad Khazaei, Masao Arai, Taizo Sasaki, Chan-Yeup Chung, Natarajan S. Venkataramanan, Mehdi Estili, Yoshio Sakka, Yoshiyuki Kawazoe	Advanced Functional Materials, 23(17), 2013, 2185-2202
$V_4C_3O_2$	Novel electronic and magnetic properties of two-dimensional transition metal carbides and nitrides	Mohammad Khazaei, Masao Arai, Taizo Sasaki, Chan-Yeup Chung, Natarajan S. Venkataramanan, Mehdi Estili, Yoshio Sakka, Yoshiyuki Kawazoe	Advanced Functional Materials, 23(17), 2013, 2185-2212
$W_2Hf_2C_3O_2$	Topological insulators in ordered double transition metals $M'_2M''C_2$ (M'= Mo, W; M"= Ti, Zr, Hf) MXenes	Mohammad Khazaei, Ahmad Ranjbar, Masao Arai, Seiji Yunoki	Physical Review B, 94, 2016, 125163
$W_2HfC_2O_2$	Topological insulators in ordered double transition metals $M'_2M''C_2$ (M'= Mo, W; M"= Ti, Zr, Hf) MXenes	Mohammad Khazaei, Ahmad Ranjbar, Masao Arai, Seiji Yunoki	Physical Review B, 94, 2016, 125157

$W_2Ti_2C_3O_2$	Topological insulators in ordered double transition metals M'$_2$M"C_2 (M'= Mo, W; M"= Ti, Zr, Hf) MXenes	Mohammad Khazaei, Ahmad Ranjbar, Masao Arai, Seiji Yunoki	Physical Review B, 94, 2016, 125161
$W_2TiC_2O_2$	Topological insulators in ordered double transition metals M'$_2$M"C_2 (M'= Mo, W; M"= Ti, Zr, Hf) MXenes	Mohammad Khazaei, Ahmad Ranjbar, Masao Arai, Seiji Yunoki	Physical Review B, 94, 2016, 125155
$W_2Zr_2C_3O_2$	Topological insulators in ordered double transition metals M'$_2$M"C_2 (M'= Mo, W; M"= Ti, Zr, Hf) MXenes	Mohammad Khazaei, Ahmad Ranjbar, Masao Arai, Seiji Yunoki	Physical Review B, 94, 2016, 125162
$W_2ZrC_2O_2$	Topological insulators in ordered double transition metals M'$_2$M"C_2 (M'= Mo, W; M"= Ti, Zr, Hf) MXenes	Mohammad Khazaei, Ahmad Ranjbar, Masao Arai, Seiji Yunoki	Physical Review B, 94, 2016, 125156
$Zr_2C(OH)_2$	Two- dimensional molybdenum carbides: Potential thermoelectric materials in MXenes	Mohammad Khazaei, Masao Arai, Taizo Sasaki, Mehdi Estili, Yoshio Sakka	Physical Chemistry Chemical Physics, 16, 2014, 7841-7875
Zr_2CF_2	Two -dimensional molybdenum carbides: Potential thermoelectric materials in MXenes	Mohammad Khazaei, Masao Arai, Taizo Sasaki, Mehdi Estili, Yoshio Sakka	Physical Chemistry Chemical Physics, 16, 2014, 7841-7873
Zr_2CO_2	Two- dimensional molybdenum carbides: Potential thermoelectric materials in MXenes	Mohammad Khazaei, Masao Arai, Taizo Sasaki, Mehdi Estili, Yoshio Sakka	Physical Chemistry Chemical Physics, 16, 2014, 7841-7874
Zr_2CrCN	Computational screening study of double transition metal carbonitrides $M'_2M''CNO_2$-MXene as catalysts for hydrogen evolution reaction	Zhoulan Zeng, Xingzhu Chen, Kaiyi Weng, Yang Wu, Peng Zhang, Jizhou Jiang and Neng L	npj Computational Materials, 7, 2021, 80
Zr_2CrCNO_2	Computational screening study of double transition metal carbonitrides $M'_2M''CNO_2$-MXene as catalysts for hydrogen evolution reaction	Zhoulan Zeng, Xingzhu Chen, Kaiyi Weng, Yang Wu, Peng Zhang, Jizhou Jiang and Neng L	npj Computational Materials, 7, 2021, 80
Zr_2HfCN	Computational screening study of double transition metal carbonitrides $M'_2M''CNO_2$-MXene as catalysts for hydrogen evolution reaction	Zhoulan Zeng, Xingzhu Chen, Kaiyi Weng, Yang Wu, Peng Zhang, Jizhou Jiang and Neng L	npj Computational Materials, 7, 2021, 80
Zr_2HfCNO_2	Computational screening study of double transition metal carbonitrides $M'_2M''CNO_2$-MXene as catalysts for hydrogen evolution reaction	Zhoulan Zeng, Xingzhu Chen, Kaiyi Weng, Yang Wu, Peng Zhang, Jizhou Jiang and Neng L	npj Computational Materials, 7, 2021, 80
Zr_2MoCN	Computational screening study of double transition metal carbonitrides $M'_2M''CNO_2$-MXene as catalysts for hydrogen evolution reaction	Zhoulan Zeng, Xingzhu Chen, Kaiyi Weng, Yang Wu, Peng Zhang, Jizhou Jiang and Neng L	npj Computational Materials, 7, 2021, 80
Zr_2MoCNO_2	Computational screening study of double transition metal carbonitrides $M'_2M''CNO_2$-MXene as catalysts for hydrogen evolution reaction	Zhoulan Zeng, Xingzhu Chen, Kaiyi Weng, Yang Wu, Peng Zhang, Jizhou Jiang and Neng L	npj Computational Materials, 7, 2021, 80
$Zr_2N(OH)_2$	Two-dimensional molybdenum carbides: Potential thermoelectric materials in MXenes	Mohammad Khazaei, Masao Arai, Taizo Sasaki, Mehdi Estili, Yoshio Sakka	Physical Chemistry Chemical Physics, 16, 2014, 7841-7878
Zr_2NF_2	Two- dimensional molybdenum carbides: Potential thermoelectric materials in MXenes	Mohammad Khazaei, Masao Arai, Taizo Sasaki, Mehdi Estili, Yoshio Sakka	Physical Chemistry Chemical Physics, 16, 2014, 7841-7876
Zr_2NO_2	Two -dimensional molybdenum carbides: Potential thermoelectric materials in MXenes	Mohammad Khazaei, Masao Arai, Taizo Sasaki, Mehdi Estili, Yoshio Sakka	Physical Chemistry Chemical Physics, 16, 2014, 7841-7877
Zr_2NbCN	Computational screening study of double transition metal carbonitrides $M'_2M''CNO_2$-MXene as catalysts for hydrogen evolution reaction	Zhoulan Zeng, Xingzhu Chen, Kaiyi Weng, Yang Wu, Peng Zhang, Jizhou Jiang and Neng L	npj Computational Materials, 7, 2021, 80
Zr_2NbCNO_2	Computational screening study of double transition metal carbonitrides $M'_2M''CNO_2$-MXene as catalysts for hydrogen evolution reaction	Zhoulan Zeng, Xingzhu Chen, Kaiyi Weng, Yang Wu, Peng Zhang, Jizhou Jiang and Neng L	npj Computational Materials, 7, 2021, 80
Zr_2TaCN	Computational screening study of double transition metal carbonitrides $M'_2M''CNO_2$-MXene as catalysts for hydrogen evolution reaction	Zhoulan Zeng, Xingzhu Chen, Kaiyi Weng, Yang Wu, Peng Zhang, Jizhou Jiang and Neng L	npj Computational Materials, 7, 2021, 80
Zr_2TaCNO_2	Computational screening study of double transition metal carbonitrides $M'_2M''CNO_2$-MXene as catalysts for hydrogen evolution reaction	Zhoulan Zeng, Xingzhu Chen, Kaiyi Weng, Yang Wu, Peng Zhang, Jizhou Jiang and Neng L	npj Computational Materials, 7, 2021, 80
Zr_2TiCN	Computational screening study of double transition metal carbonitrides $M'_2M''CNO_2$-MXene as catalysts for hydrogen evolution reaction	Zhoulan Zeng, Xingzhu Chen, Kaiyi Weng, Yang Wu, Peng Zhang, Jizhou Jiang and Neng L	npj Computational Materials, 7, 2021, 80

Zr_2TiCNO_2	Computational screening study of double transition metal carbonitrides $M'_2M''CNO_2$-MXene as catalysts for hydrogen evolution reaction	Zhoulan Zeng, Xingzhu Chen, Kaiyi Weng, Yang Wu, Peng Zhang, Jizhou Jiang and Neng L	npj Computational Materials, 7, 2021, 80
Zr_2VCN	Computational screening study of double transition metal carbonitrides $M'_2M''CNO_2$-MXene as catalysts for hydrogen evolution reaction	Zhoulan Zeng, Xingzhu Chen, Kaiyi Weng, Yang Wu, Peng Zhang, Jizhou Jiang and Neng L	npj Computational Materials, 7, 2021, 80
Zr_2VCNO_2	Computational screening study of double transition metal carbonitrides $M'_2M''CNO_2$-MXene as catalysts for hydrogen evolution reaction	Zhoulan Zeng, Xingzhu Chen, Kaiyi Weng, Yang Wu, Peng Zhang, Jizhou Jiang and Neng L	npj Computational Materials, 7, 2021, 80

APPENDIX B : Adsorption Capacities and Calculated Performance Metrics of MXenes with Short Interlayer Distance at 35°C and 0.1, 1, and 10 bar

MXene Type	CO_2 Adsorption Capacity (mol/kg)			CO_2/H_2 Selectivity			CO_2 Working Capacity		Regenerability (%)		APS		AFM		SSP	
	0.1 bar	1 bar	10 bar	0.1 bar	1 bar	10 bar	PSA	VSA	PSA	VSA	PSA	VSA	PSA	VSA	PSA	VSA
$(CrV)_3C_2$	0.006	0.058	0.734	5.72	5.99	7.81	0.675	0.053	92.03	90.28	5.27	0.32	6.87	0.33	62.57	36.09
$(Mo_{0.66}Y_{0.33})_2CO_2$	0.003	0.030	0.329	4.20	4.19	4.69	0.299	0.027	91.01	90.10	1.41	0.11	1.58	0.11	22.30	17.54
$(TiV)_3C_2$	0.006	0.064	0.755	6.28	6.46	7.48	0.691	0.058	91.49	90.15	5.17	0.37	5.98	0.39	56.79	41.90
$(TiV)C(OH)_2$	0.006	0.064	0.698	6.60	6.73	7.42	0.633	0.058	90.79	90.04	4.70	0.39	5.18	0.40	55.59	45.46
$(TiV)CF_2$	0.004	0.041	0.467	3.47	3.53	4.15	0.427	0.037	91.31	90.16	1.77	0.13	2.08	0.13	17.50	12.51
$(TiV)CO_2$	0.004	0.044	0.494	4.02	4.09	4.66	0.450	0.039	91.17	90.14	2.10	0.16	2.39	0.16	22.00	16.73
$(W_{0.66}Y_{0.33})_2CO_2$	0.007	0.072	0.477	24.92	25.41	16.93	0.406	0.065	84.97	89.91	6.87	1.64	4.58	1.67	270.67	647.08
Cr_2C	0.005	0.046	0.515	2.86	2.82	3.21	0.468	0.042	91.00	90.04	1.50	0.12	1.71	0.12	10.45	7.93
$Cr_2C(OH)_2$	0.006	0.056	0.580	6.46	6.53	6.76	0.524	0.050	90.35	90.05	3.54	0.33	3.67	0.33	45.86	42.65
Cr_2CBr_2	0.019	0.201	1.335	24.10	24.50	16.71	1.134	0.182	84.94	90.57	18.95	4.46	12.93	4.53	264.46	601.13
Cr_2CCl_2	0.017	0.178	1.685	15.39	15.94	15.48	1.507	0.161	89.42	90.44	23.33	2.57	22.67	2.66	238.91	254.92
Cr_2CF_2	0.003	0.032	0.346	2.84	3.20	3.52	0.315	0.028	90.89	90.08	1.11	0.09	1.22	0.10	12.52	10.35
Cr_2CFCl	0.005	0.049	0.597	4.82	5.01	6.26	0.548	0.044	91.75	90.29	3.43	0.22	4.28	0.23	40.03	25.24
Cr_2CH_2	0.003	0.025	0.257	2.27	2.41	2.52	0.232	0.023	90.20	90.02	0.59	0.05	0.61	0.06	6.40	5.86
Cr_2CO_2	0.005	0.050	0.594	5.80	5.54	6.78	0.544	0.045	91.59	90.18	3.69	0.25	4.52	0.24	46.99	30.58
Cr_2CS_2	0.069	0.727	2.119	56.14	55.60	16.82	1.392	0.658	65.67	90.49	23.42	36.60	7.09	36.24	207.45	3088.02
Cr_2HfCN	0.004	0.044	0.640	6.17	6.80	9.90	0.596	0.040	93.11	90.32	5.90	0.27	8.60	0.30	101.53	46.68
Cr_2HfCNO_2	0.006	0.062	0.600	13.32	13.31	13.63	0.538	0.056	89.64	90.27	7.33	0.75	7.51	0.75	186.18	177.05
Cr_2MoCN	0.007	0.070	1.128	7.65	7.75	12.82	1.058	0.064	93.78	90.53	13.56	0.49	22.43	0.50	171.67	60.12
Cr_2MoCNO_2	0.008	0.086	0.831	13.01	14.54	14.30	0.745	0.077	89.71	90.30	10.66	1.12	10.48	1.26	204.10	214.24
Cr_2N	0.003	0.028	0.298	2.23	2.14	2.37	0.270	0.025	90.66	90.17	0.64	0.05	0.71	0.05	5.66	4.56
$Cr_2N(OH)_2$	0.005	0.049	0.513	5.66	5.97	6.22	0.464	0.044	90.37	90.06	2.88	0.27	3.00	0.28	38.80	35.84
$Cr_2Nb_2C_3$	0.004	0.038	0.540	5.63	5.64	8.02	0.502	0.035	92.89	90.28	4.02	0.20	5.72	0.20	66.48	31.83
Cr_2NbCN	0.007	0.071	1.158	7.74	7.96	12.94	1.087	0.065	93.84	90.47	14.06	0.51	22.84	0.53	174.51	63.62
Cr_2NbCNO_2	0.009	0.090	0.857	14.13	14.99	14.61	0.767	0.081	89.52	90.39	11.21	1.22	10.92	1.29	212.75	226.04
Cr_2NF_2	0.002	0.025	0.266	2.80	2.86	3.06	0.241	0.022	90.62	90.00	0.74	0.06	0.79	0.07	9.45	8.17
Cr_2NH_2	0.003	0.025	0.256	2.86	2.76	2.81	0.231	0.023	90.22	89.97	0.65	0.06	0.66	0.06	7.92	7.59
Cr_2NO_2	0.003	0.035	0.393	3.62	3.60	4.09	0.358	0.032	91.01	90.21	1.46	0.11	1.66	0.11	16.94	12.95
$Cr_2Ta_2C_3$	0.000	0.000	0.004	4.70	4.92	6.46	0.004	0.000	92.27	90.19	0.02	0.00	0.03	0.00	42.91	24.36
Cr_2TaC_2	0.000	0.000	0.003	2.76	2.77	3.15	0.003	0.000	90.90	90.03	0.01	0.00	0.01	0.00	10.05	7.70
Cr_2TaCN	0.000	0.001	0.013	6.79	7.49	11.76	0.012	0.001	93.58	90.37	0.14	0.01	0.22	0.01	144.02	56.71
Cr_2TaCNO_2	0.000	0.001	0.012	13.50	14.19	14.23	0.010	0.001	89.71	90.34	0.15	0.02	0.15	0.02	202.44	202.38
$Cr_2Ti_2C_3$	0.006	0.060	0.897	6.46	6.28	9.64	0.838	0.054	93.36	90.31	8.07	0.34	12.40	0.33	96.59	39.28
Cr_2TiC_2	0.003	0.032	0.362	3.30	3.32	3.83	0.330	0.029	91.19	90.11	1.27	0.10	1.46	0.10	14.89	10.99
$Cr_2TiC_2(OH)_2$	0.011	0.114	0.789	21.43	20.06	14.39	0.675	0.102	85.57	90.00	9.71	2.05	6.97	1.92	197.62	399.53
$Cr_2TiC_2F_2$	0.010	0.100	1.191	11.00	12.57	15.46	1.091	0.090	91.63	90.44	16.88	1.13	20.75	1.30	244.19	160.55

$Cr_2TiC_2O_2$	0.009	0.092	0.919	12.69	13.06	13.29	0.827	0.083	90.03	90.37	10.99	1.08	11.19	1.11	177.08	171.07
Cr_2TiCN	0.009	0.099	1.696	8.07	8.62	15.26	1.597	0.090	94.15	90.53	24.36	0.77	43.14	0.83	244.53	74.79
Cr_2TiCNO_2	0.011	0.114	1.078	14.87	15.62	15.13	0.964	0.103	89.40	90.47	14.58	1.62	14.12	1.70	227.97	245.36
$Cr_2V_2C_3$	0.006	0.060	0.914	6.15	6.54	10.23	0.855	0.054	93.49	90.37	8.75	0.35	13.68	0.37	109.00	43.13
Cr_2VC_2	0.003	0.031	0.354	3.35	3.34	3.81	0.323	0.028	91.16	89.99	1.23	0.09	1.40	0.09	14.69	11.17
Cr_2VCN	0.009	0.098	1.676	8.69	8.63	15.13	1.577	0.089	94.13	90.50	23.87	0.77	41.83	0.76	240.23	74.49
Cr_2VCNO_2	0.011	0.111	1.062	15.25	15.24	15.01	0.951	0.101	89.51	90.40	14.27	1.53	14.05	1.53	224.87	232.35
Cr_2ZrCN	0.006	0.065	0.972	6.90	7.03	10.88	0.908	0.058	93.36	90.41	9.87	0.41	15.28	0.42	123.17	49.53
Cr_2ZrCNO_2	0.008	0.087	0.834	13.37	14.63	14.07	0.747	0.079	89.52	90.29	10.50	1.15	10.10	1.26	196.96	216.18
Cr_3C_2	0.004	0.044	0.528	4.00	4.02	4.87	0.484	0.040	91.68	90.18	2.36	0.16	2.85	0.16	24.14	16.20
$Cr_3C_2(OH)_2$	0.006	0.060	0.517	11.22	11.78	10.11	0.456	0.054	88.37	89.99	4.62	0.64	3.96	0.67	100.41	139.59
$Cr_3C_2F_2$	0.003	0.029	0.304	5.62	5.51	5.80	0.275	0.026	90.40	90.02	1.59	0.14	1.67	0.14	33.78	30.31
$Cr_3C_2H_2$	0.004	0.038	0.405	5.63	5.99	6.51	0.367	0.034	90.57	90.16	2.39	0.21	2.59	0.22	42.71	36.19
$Cr_3C_2O_2$	0.004	0.045	0.467	6.87	7.35	8.01	0.422	0.040	90.46	90.18	3.38	0.30	3.69	0.32	64.82	54.48
Cr_3CN	0.009	0.092	1.530	7.86	8.30	14.02	1.438	0.083	93.98	90.40	20.16	0.69	34.03	0.73	205.48	69.33
Cr_3CNO_2	0.012	0.122	1.170	15.99	16.52	16.34	1.048	0.111	89.55	90.51	17.11	1.83	16.92	1.89	266.48	274.02
Cr_3N_2	0.002	0.021	0.237	3.02	2.91	3.23	0.215	0.019	91.01	89.95	0.70	0.06	0.77	0.05	10.53	8.44
$Cr_3N_2(OH)_2$	0.022	0.224	1.042	35.17	34.63	16.86	0.818	0.202	78.52	90.12	13.79	6.99	6.71	6.88	249.11	1197.52
$Cr_3N_2H_2$	0.004	0.044	0.494	5.66	6.41	7.52	0.450	0.039	91.17	90.31	3.39	0.25	3.97	0.29	57.52	41.66
$Cr_3N_2O_2$	0.004	0.044	0.440	9.55	9.25	9.36	0.395	0.040	89.92	90.12	3.70	0.37	3.74	0.36	87.70	85.24
Cr_4C_3	0.004	0.039	0.467	4.60	4.36	5.26	0.428	0.035	91.70	90.23	2.25	0.15	2.71	0.14	28.15	18.89
$Cr_4C_3(OH)_2$	0.004	0.043	0.421	9.03	9.33	9.15	0.378	0.039	89.71	90.16	3.46	0.36	3.39	0.38	83.46	87.43
$Cr_4C_3F_2$	0.002	0.023	0.243	4.37	4.52	4.94	0.221	0.020	90.73	90.05	1.09	0.09	1.19	0.09	24.59	20.48
$Cr_4C_3H_2$	0.003	0.028	0.301	4.71	5.16	5.74	0.274	0.025	90.86	90.10	1.57	0.13	1.75	0.14	33.31	26.92
$Cr_4C_3O_2$	0.003	0.034	0.373	6.46	6.76	7.37	0.339	0.031	90.92	90.23	2.50	0.21	2.72	0.22	54.77	45.86
Cr_4N_3	0.002	0.023	0.247	2.67	2.76	3.04	0.224	0.020	90.84	90.11	0.68	0.06	0.75	0.06	9.33	7.64
$Cr_4N_3(OH)_2$	0.003	0.035	0.341	7.54	7.86	7.87	0.306	0.031	89.77	90.08	2.40	0.25	2.41	0.26	61.89	61.98
$Cr_4N_3F_2$	0.002	0.018	0.189	3.78	3.83	4.12	0.171	0.016	90.57	90.11	0.71	0.06	0.76	0.06	17.15	14.69
$Cr_4N_3H_2$	0.002	0.021	0.233	4.28	4.22	4.88	0.212	0.019	91.06	90.16	1.04	0.08	1.20	0.08	24.21	17.83
$Cr_4N_3O_2$	0.002	0.024	0.263	5.26	5.08	5.57	0.239	0.022	90.72	90.03	1.33	0.11	1.46	0.11	31.29	25.70
$CrMoCF_2$	0.003	0.031	0.353	3.32	3.58	4.17	0.322	0.028	91.27	90.09	1.34	0.10	1.56	0.11	17.66	12.96
$CrWCF_2$	0.002	0.024	0.280	4.19	4.12	4.77	0.256	0.021	91.49	90.09	1.22	0.09	1.41	0.09	23.05	16.90
Hf_2C	0.002	0.017	0.191	2.88	2.78	3.12	0.174	0.015	91.01	90.13	0.54	0.04	0.61	0.04	9.88	7.72
$Hf_2C(OH)_2$	0.002	0.020	0.197	5.52	6.01	6.06	0.177	0.018	89.86	89.99	1.07	0.11	1.08	0.12	36.74	36.55
Hf_2CF_2	0.001	0.013	0.143	3.39	3.39	3.72	0.129	0.012	90.62	90.05	0.48	0.04	0.53	0.04	13.95	11.46
Hf_2CF_2 -(model2)	0.002	0.015	0.167	3.67	3.46	3.97	0.152	0.014	90.97	89.96	0.60	0.05	0.69	0.04	15.96	11.88
Hf_2CF_2 -(model3)	0.002	0.019	0.215	3.13	3.02	3.42	0.196	0.017	91.10	90.05	0.67	0.05	0.76	0.05	11.82	9.07
Hf_2CF_2 -(model4)	0.002	0.017	0.188	3.03	2.95	3.33	0.171	0.015	91.01	90.08	0.57	0.04	0.64	0.04	11.25	8.67
Hf_2CO_2	0.002	0.020	0.234	4.41	4.48	5.36	0.214	0.018	91.32	90.08	1.15	0.08	1.38	0.08	29.33	20.09
Hf_2CO_2 -(model2)	0.001	0.013	0.139	3.85	3.84	4.11	0.126	0.012	90.46	90.07	0.52	0.05	0.55	0.05	17.02	14.73
Hf_2CO_2 -(model3)	0.002	0.018	0.202	3.07	3.26	3.64	0.184	0.016	91.00	90.16	0.67	0.05	0.75	0.06	13.40	10.71
Hf_2CO_2 -(model4)	0.002	0.020	0.234	3.46	3.47	4.00	0.214	0.018	91.28	90.13	0.86	0.06	0.99	0.06	16.26	12.05
Hf_2CrCN	0.002	0.023	0.294	4.78	4.88	6.34	0.271	0.021	92.07	90.21	1.72	0.10	2.23	0.10	41.25	23.85

Hf_2CrCNO_2	0.003	0.027	0.263	10.69	9.94	9.74	0.235	0.024	89.66	90.12	2.29	0.24	2.25	0.23	94.74	98.05
Hf_2MoCN	0.002	0.020	0.237	4.53	4.64	5.70	0.218	0.018	91.74	90.16	1.24	0.08	1.53	0.08	33.21	21.59
Hf_2MoCNO_2	0.002	0.025	0.234	10.44	10.08	9.88	0.210	0.022	89.42	90.03	2.07	0.23	2.03	0.22	97.34	101.26
Hf_2N	0.001	0.013	0.146	2.50	2.35	2.60	0.133	0.012	90.79	90.02	0.34	0.03	0.38	0.03	6.81	5.48
$Hf_2N(OH)_2$	0.002	0.021	0.201	7.59	7.36	7.19	0.180	0.019	89.58	89.97	1.29	0.14	1.26	0.13	51.57	54.04
Hf_2NbCN	0.002	0.020	0.236	4.63	4.58	5.56	0.216	0.018	91.73	90.17	1.20	0.08	1.46	0.08	31.57	20.94
Hf_2NbCNO_2	0.002	0.025	0.236	9.06	10.05	9.80	0.212	0.022	89.53	90.17	2.07	0.22	2.02	0.25	95.81	102.13
Hf_2NF_2	0.001	0.011	0.119	3.59	3.57	3.84	0.107	0.010	90.44	90.03	0.41	0.04	0.44	0.04	14.90	12.72
Hf_2NF_2 -(model2)	0.001	0.015	0.165	4.42	4.42	4.97	0.150	0.013	90.95	89.98	0.74	0.06	0.84	0.06	25.01	19.57
Hf_2NF_2 -(model4)	0.003	0.026	0.309	4.09	4.17	5.07	0.283	0.023	91.66	90.14	1.43	0.10	1.74	0.10	26.19	17.40
Hf_2NO_2	0.002	0.017	0.193	4.09	4.12	4.65	0.176	0.016	91.09	90.21	0.82	0.06	0.92	0.06	21.87	16.96
Hf_2TaCN	0.000	0.001	0.006	4.59	4.50	5.46	0.006	0.000	91.69	90.17	0.03	0.00	0.04	0.00	30.38	20.17
Hf_2TaCNO_2	0.000	0.001	0.006	10.80	10.28	9.80	0.006	0.001	89.29	90.04	0.06	0.01	0.05	0.01	95.50	105.19
Hf_2TiCN	0.002	0.023	0.277	4.74	4.74	5.78	0.254	0.020	91.82	90.21	1.47	0.10	1.79	0.10	34.06	22.48
Hf_2TiCNO_2	0.003	0.027	0.259	9.53	9.64	9.40	0.232	0.024	89.67	90.08	2.18	0.23	2.13	0.23	88.13	93.06
Hf_2VCN	0.002	0.022	0.271	4.71	4.64	5.75	0.248	0.020	91.80	90.29	1.43	0.09	1.77	0.09	33.75	21.50
Hf_2VCNO_2	0.003	0.027	0.260	9.88	9.78	9.68	0.233	0.024	89.72	90.13	2.26	0.24	2.23	0.23	93.57	95.45
Hf_2ZrCN	0.002	0.019	0.218	4.08	4.20	5.07	0.199	0.017	91.48	90.12	1.01	0.07	1.22	0.07	26.25	17.69
Hf_2ZrCNO_2	0.002	0.024	0.230	9.81	9.71	9.56	0.206	0.022	89.45	90.01	1.97	0.21	1.94	0.21	91.32	94.23
Hf_3C_2	0.002	0.016	0.181	4.35	3.99	4.69	0.165	0.014	91.36	90.04	0.77	0.06	0.91	0.05	22.33	15.79
$Hf_3C_2(OH)_2$	0.001	0.012	0.108	7.41	7.77	7.29	0.096	0.011	89.04	89.93	0.70	0.08	0.66	0.09	52.67	60.78
$Hf_3C_2F_2$	0.001	0.012	0.123	6.10	5.86	5.91	0.110	0.011	90.01	90.07	0.65	0.06	0.66	0.06	35.01	34.16
$Hf_3C_2H_2$	0.000	0.004	0.038	2.97	3.10	3.06	0.034	0.004	89.62	90.01	0.10	0.01	0.10	0.01	9.34	9.68
$Hf_3C_2O_2$	0.002	0.021	0.210	8.36	8.67	8.85	0.189	0.019	90.05	90.15	1.67	0.16	1.71	0.17	78.46	75.48
Hf_3CN	0.002	0.015	0.177	4.01	4.03	4.78	0.162	0.014	91.39	90.04	0.77	0.06	0.91	0.06	23.21	16.26
Hf_3CNO_2	0.002	0.023	0.234	8.96	9.06	9.54	0.212	0.021	90.28	90.12	2.02	0.19	2.13	0.19	91.56	82.18
Hf_3N_2	0.001	0.010	0.112	3.14	3.25	3.67	0.102	0.009	90.95	90.12	0.37	0.03	0.42	0.03	13.65	10.59
$Hf_3N_2(OH)_2$	0.001	0.007	0.062	6.42	6.09	5.71	0.055	0.006	89.29	90.03	0.32	0.04	0.30	0.03	32.36	36.85
$Hf_3N_2F_2$	0.001	0.010	0.093	5.43	5.82	5.60	0.084	0.009	89.73	90.05	0.47	0.05	0.45	0.05	31.27	34.19
$Hf_3N_2H_2$	0.001	0.006	0.057	4.63	4.50	4.45	0.051	0.005	89.56	89.92	0.23	0.02	0.22	0.02	19.81	20.19
$Hf_3N_2O_2$	0.002	0.017	0.173	7.44	7.57	7.64	0.156	0.015	90.16	90.10	1.19	0.12	1.20	0.12	58.45	57.40
Hf_4C_3	0.001	0.009	0.093	3.26	3.36	3.65	0.084	0.008	90.64	90.03	0.31	0.03	0.33	0.03	13.46	11.36
$Hf_4C_3(OH)_2$	0.001	0.014	0.129	7.36	7.09	6.84	0.115	0.012	89.49	90.06	0.79	0.09	0.76	0.08	46.55	50.03
$Hf_4C_3F_2$	0.001	0.010	0.105	6.28	5.93	6.04	0.095	0.009	90.13	90.11	0.57	0.06	0.58	0.05	36.55	35.00
$Hf_4C_3H_2$	0.000	0.005	0.045	4.57	4.30	4.11	0.040	0.004	89.60	90.00	0.17	0.02	0.16	0.02	16.83	18.35
$Hf_4C_3O_2$	0.002	0.017	0.183	8.50	8.59	9.37	0.166	0.016	90.62	90.15	1.56	0.13	1.70	0.13	88.55	73.91
Hf_4N_3	0.001	0.008	0.090	3.09	3.19	3.55	0.082	0.007	90.96	90.09	0.29	0.02	0.33	0.02	12.75	10.20
$Hf_4N_3(OH)_2$	0.001	0.012	0.105	8.25	8.96	7.99	0.093	0.011	88.70	89.90	0.74	0.10	0.66	0.10	63.01	81.09
$Hf_4N_3F_2$	0.001	0.008	0.083	5.18	5.11	5.23	0.075	0.007	90.18	90.04	0.39	0.04	0.40	0.04	27.44	26.04
$Hf_4N_3H_2$	0.000	0.005	0.044	4.44	3.98	3.84	0.040	0.004	89.68	89.92	0.15	0.02	0.15	0.01	14.71	15.70
$Hf_4N_3O_2$	0.001	0.013	0.140	6.58	7.02	7.55	0.127	0.012	90.51	90.15	0.96	0.08	1.03	0.09	57.46	49.64
$HfCrNO_2$	0.002	0.021	0.230	4.19	4.11	4.62	0.209	0.019	90.93	90.11	0.96	0.08	1.08	0.08	21.58	16.85
Mn_2C	0.005	0.046	0.506	2.88	2.88	3.15	0.461	0.041	90.97	90.04	1.45	0.12	1.59	0.12	10.01	8.26

$Mn_2C(OH)_2$	0.005	0.052	0.542	6.01	6.08	6.58	0.490	0.047	90.47	90.04	3.23	0.28	3.49	0.29	43.70	37.00
Mn_2CF_2	0.003	0.028	0.297	3.24	3.17	3.49	0.269	0.025	90.62	90.10	0.94	0.08	1.03	0.08	12.33	10.05
Mn_2CO_2	0.004	0.039	0.441	4.49	4.02	4.65	0.402	0.035	91.18	90.03	1.87	0.14	2.16	0.13	21.91	15.98
Mn_2N	0.002	0.025	0.266	1.95	2.16	2.31	0.241	0.022	90.63	90.13	0.56	0.05	0.59	0.05	5.35	4.70
$Mn_2N(OH)_2$	0.004	0.040	0.413	4.37	4.59	4.96	0.373	0.036	90.39	90.05	1.85	0.16	2.00	0.17	24.78	21.23
Mn_2NF_2	0.002	0.024	0.249	2.76	2.70	2.93	0.225	0.021	90.55	89.96	0.66	0.06	0.72	0.06	8.67	7.27
Mn_2NO_2	0.003	0.033	0.367	3.44	3.80	4.17	0.334	0.030	90.97	90.13	1.39	0.11	1.53	0.13	17.60	14.59
Mn_3C_2	0.004	0.043	0.514	4.03	4.07	5.06	0.471	0.039	91.67	90.29	2.38	0.16	2.96	0.16	26.20	16.62
$Mn_3C_2(OH)_2$	0.006	0.062	0.523	11.98	12.22	10.91	0.460	0.056	88.09	89.93	5.02	0.68	4.48	0.70	117.38	149.77
$Mn_3C_2F_2$	0.003	0.028	0.289	5.15	5.40	5.67	0.262	0.025	90.41	90.05	1.48	0.13	1.55	0.14	32.26	29.36
$Mn_3C_2O_2$	0.004	0.042	0.442	6.88	7.17	7.87	0.400	0.038	90.56	90.08	3.15	0.27	3.45	0.28	62.54	51.61
Mn_3N_2	0.003	0.030	0.334	2.76	2.90	3.23	0.304	0.027	90.99	90.15	0.98	0.08	1.09	0.08	10.53	8.47
$Mn_3N_2(OH)_2$	0.005	0.051	0.435	11.59	12.29	10.16	0.384	0.046	88.35	89.99	3.90	0.56	3.23	0.59	100.93	152.16
$Mn_3N_2F_2$	0.002	0.022	0.232	4.52	4.28	4.68	0.210	0.020	90.37	90.14	0.98	0.09	1.08	0.08	22.17	18.23
Mn_4C_3	0.004	0.037	0.449	4.29	4.23	5.35	0.412	0.034	91.72	90.20	2.20	0.14	2.79	0.14	29.33	17.86
$Mn_4C_3(OH)_2$	0.005	0.048	0.433	11.66	11.05	10.55	0.386	0.043	89.03	89.99	4.07	0.47	3.88	0.45	110.63	121.31
$Mn_4C_3F_2$	0.002	0.022	0.234	5.08	5.04	5.45	0.212	0.020	90.57	90.08	1.15	0.10	1.25	0.10	29.95	25.35
$Mn_4C_3O_2$	0.003	0.030	0.334	5.98	6.10	6.78	0.304	0.027	90.98	90.20	2.06	0.17	2.29	0.17	46.54	37.30
Mn_4N_3	0.002	0.020	0.223	3.74	3.66	4.13	0.203	0.018	91.05	90.05	0.84	0.07	0.94	0.06	17.23	13.37
$Mn_4N_3(OH)_2$	0.004	0.040	0.373	9.94	10.12	9.75	0.333	0.036	89.17	90.05	3.24	0.37	3.12	0.37	94.55	102.60
$Mn_4N_3O_2$	0.002	0.023	0.247	5.22	5.01	5.43	0.224	0.021	90.73	90.09	1.22	0.10	1.32	0.10	29.71	25.02
$Mo_{1.33}C$	0.007	0.069	0.762	4.44	4.36	4.86	0.693	0.062	90.94	90.17	3.37	0.27	3.76	0.27	23.92	18.97
Mo_2C	0.003	0.034	0.392	3.53	3.23	3.78	0.358	0.031	91.23	90.18	1.35	0.10	1.58	0.09	14.50	10.35
$Mo_2C(NCS)_2$	0.179	0.849	1.250	228.17	106.69	16.20	0.401	0.671	32.06	78.98	6.49	71.57	0.99	33.46	93.76	9968.73
$Mo_2C(OCN)_2$	0.011	0.112	0.925	17.77	18.24	15.88	0.813	0.101	87.89	90.37	12.90	1.85	11.23	1.89	247.70	333.61
$Mo_2C(OH)_2$	0.003	0.032	0.326	4.69	4.98	5.32	0.294	0.028	90.32	90.19	1.57	0.14	1.67	0.15	28.56	25.02
$Mo_2C(SCN)_2$	0.021	0.206	0.976	39.39	39.35	19.27	0.770	0.185	78.92	89.84	14.83	7.27	7.26	7.27	326.65	1548.55
Mo_2CBr_2	0.014	0.141	0.968	22.76	23.29	16.24	0.827	0.127	85.45	90.34	13.43	2.96	9.36	3.03	250.67	543.83
Mo_2CCl_2	0.010	0.107	1.028	13.98	14.00	13.85	0.921	0.096	89.63	90.28	12.76	1.35	12.62	1.35	191.58	196.08
Mo_2CF_2	0.002	0.022	0.237	2.98	3.11	3.41	0.215	0.020	90.78	90.18	0.73	0.06	0.80	0.06	11.73	9.71
Mo_2CF_2 -(model4)	0.004	0.038	0.460	3.79	4.13	4.92	0.422	0.035	91.67	90.28	2.08	0.14	2.48	0.16	24.66	17.22
Mo_2CO_2	0.003	0.031	0.344	5.56	5.65	6.20	0.313	0.028	90.96	90.06	1.94	0.16	2.13	0.16	38.86	31.97
Mo_2CO_2 -(model4)	0.003	0.026	0.291	3.53	3.72	4.29	0.265	0.024	91.01	90.18	1.14	0.09	1.31	0.09	18.65	13.94
Mo_2CrCN	0.005	0.052	0.784	6.68	6.89	10.65	0.733	0.047	93.39	90.30	7.80	0.32	12.06	0.33	117.92	47.61
Mo_2CrCNO_2	0.006	0.059	0.603	10.42	11.58	12.28	0.544	0.053	90.24	90.35	6.68	0.62	7.09	0.68	151.91	135.64
Mo_2CS_2	0.047	0.464	1.410	56.65	54.16	17.22	0.947	0.417	67.12	89.93	16.30	22.58	5.18	21.59	222.18	2918.84
$Mo_2Hf_2C_3O_2$	0.002	0.019	0.189	9.38	9.10	9.05	0.170	0.017	89.89	90.11	1.54	0.16	1.53	0.15	81.91	82.57
Mo_2HfC_2	0.001	0.011	0.123	2.50	2.59	2.77	0.112	0.010	90.69	90.08	0.31	0.03	0.33	0.03	7.71	6.75
$Mo_2HfC_2O_2$	0.003	0.030	0.277	9.72	10.42	9.89	0.247	0.027	89.31	90.11	2.45	0.28	2.32	0.30	97.31	109.45
Mo_2HfCN	0.003	0.028	0.354	5.39	5.38	7.16	0.327	0.025	92.19	90.30	2.34	0.13	3.11	0.13	52.75	28.98
Mo_2HfCNO_2	0.004	0.039	0.392	9.77	11.35	11.56	0.353	0.035	90.00	90.21	4.07	0.40	4.15	0.47	133.80	131.06
Mo_2N	0.002	0.022	0.246	2.75	2.75	3.12	0.224	0.020	90.98	90.17	0.70	0.05	0.79	0.05	9.87	7.55
$Mo_2N(OH)_2$	0.006	0.058	0.486	13.86	13.46	11.56	0.428	0.052	88.10	90.04	4.95	0.70	4.26	0.68	131.22	180.64

$Mo_2Nb_2C_3$	0.003	0.026	0.340	4.78	4.95	6.55	0.314	0.024	92.32	90.23	2.06	0.12	2.73	0.12	44.13	24.56
Mo_2NbC_2	0.001	0.015	0.165	2.54	2.72	3.00	0.150	0.014	90.78	90.21	0.45	0.04	0.50	0.04	9.09	7.43
Mo_2NbCN	0.004	0.038	0.515	5.63	6.42	8.49	0.477	0.034	92.59	90.27	4.05	0.22	5.35	0.25	74.04	41.86
Mo_2NbCNO_2	0.005	0.051	0.506	11.69	11.54	12.02	0.455	0.046	90.00	90.21	5.47	0.53	5.70	0.52	145.19	133.03
Mo_2NF_2	0.002	0.021	0.217	4.82	5.03	5.16	0.196	0.019	90.40	90.03	1.01	0.09	1.04	0.10	26.74	25.42
Mo_2NO_2	0.003	0.028	0.300	5.21	5.10	5.84	0.273	0.025	90.83	90.12	1.59	0.13	1.83	0.12	34.65	25.93
Mo_2ScC_2	0.002	0.019	0.203	2.70	2.73	3.09	0.185	0.017	90.81	90.07	0.57	0.05	0.64	0.05	9.65	7.47
$Mo_2ScC_2O_2$	0.004	0.040	0.381	9.24	9.94	9.62	0.341	0.036	89.42	90.10	3.28	0.36	3.18	0.39	92.28	99.60
$Mo_2Ta_2C_3$	0.000	0.000	0.004	4.69	4.65	5.97	0.003	0.000	92.02	90.18	0.02	0.00	0.02	0.00	36.55	21.65
Mo_2TaC_2	0.000	0.000	0.003	2.59	2.69	2.86	0.002	0.000	90.68	90.14	0.01	0.00	0.01	0.00	8.24	7.25
Mo_2TaCN	0.000	0.001	0.009	5.68	5.79	7.94	0.008	0.001	92.58	90.29	0.06	0.00	0.09	0.00	64.97	33.64
Mo_2TaCNO_2	0.000	0.001	0.009	11.14	11.12	11.41	0.008	0.001	90.08	90.25	0.09	0.01	0.10	0.01	130.55	123.62
$Mo_2Ti_2C_3$	0.004	0.038	0.533	5.29	5.64	7.96	0.495	0.034	92.87	90.30	3.94	0.19	5.56	0.21	65.50	32.08
$Mo_2Ti_2C_3(OH)_{1.5}F_{0.5}$	0.005	0.052	0.479	13.43	13.34	12.77	0.427	0.047	89.14	90.19	5.45	0.63	5.21	0.62	162.13	177.80
$Mo_2Ti_2C_3O_{1.5}F_{0.5}$	0.003	0.032	0.356	7.22	7.63	8.75	0.324	0.029	91.07	90.19	2.84	0.22	3.25	0.23	77.60	58.52
$Mo_2Ti_2C_3O_2$	0.003	0.032	0.327	8.30	8.66	9.05	0.295	0.029	90.24	90.14	2.67	0.25	2.79	0.26	82.35	75.35
Mo_2TiC_2	0.002	0.019	0.208	3.06	2.94	3.22	0.189	0.017	90.91	90.10	0.61	0.05	0.67	0.05	10.48	8.59
$Mo_2TiC_2(O_{1.5}F_{0.5})$	0.007	0.068	0.470	16.13	15.11	10.70	0.402	0.061	85.57	89.95	4.30	0.92	3.05	0.86	109.18	226.72
$Mo_2TiC_2(OH)_2$	0.007	0.073	0.541	17.55	18.38	13.54	0.468	0.066	86.45	89.99	6.33	1.21	4.66	1.27	176.02	339.44
$Mo_2TiC_2F_2$	0.005	0.056	0.717	8.53	9.10	11.71	0.661	0.050	92.22	90.38	7.74	0.46	9.96	0.49	140.49	83.39
$Mo_2TiC_2O_2$	0.004	0.042	0.415	9.27	9.59	9.60	0.374	0.038	89.94	90.10	3.59	0.36	3.59	0.37	92.24	92.34
Mo_2TiCN	0.005	0.049	0.712	6.09	6.38	9.45	0.663	0.045	93.08	90.35	6.27	0.28	9.28	0.30	92.64	40.97
Mo_2TiCNO_2	0.006	0.058	0.592	11.63	11.86	11.99	0.534	0.053	90.13	90.26	6.40	0.63	6.46	0.64	143.90	141.03
$Mo_2V_2C_3$	0.004	0.037	0.520	5.73	5.64	8.04	0.483	0.034	92.84	90.23	3.88	0.19	5.54	0.19	66.88	31.72
Mo_2VC_2	0.002	0.019	0.206	3.07	2.89	3.25	0.187	0.017	90.92	90.21	0.61	0.05	0.69	0.05	10.70	8.30
Mo_2VCN	0.005	0.049	0.705	5.95	6.44	9.59	0.657	0.044	93.09	90.34	6.30	0.28	9.37	0.31	95.37	41.85
Mo_2VCNO_2	0.006	0.057	0.583	11.34	11.40	12.03	0.527	0.051	90.28	90.18	6.33	0.58	6.68	0.59	145.45	130.12
$Mo_2Zr_2C_3O_2$	0.003	0.027	0.260	9.01	9.03	9.03	0.233	0.024	89.76	90.15	2.11	0.22	2.11	0.22	81.59	81.48
Mo_2ZrC_2	0.001	0.015	0.162	2.63	2.58	2.89	0.147	0.014	90.74	90.14	0.43	0.03	0.48	0.03	8.45	6.63
$Mo_2ZrC_2O_2$	0.004	0.039	0.397	9.83	9.52	9.94	0.358	0.035	90.14	90.18	3.56	0.34	3.71	0.33	99.18	90.32
Mo_2ZrCN	0.004	0.037	0.482	5.43	5.63	7.58	0.445	0.033	92.38	90.25	3.37	0.19	4.55	0.19	59.19	31.78
Mo_2ZrCNO_2	0.005	0.049	0.499	11.44	11.47	11.64	0.450	0.045	90.09	90.18	5.24	0.51	5.32	0.51	135.81	131.52
Mo_3C_2	0.003	0.029	0.359	4.99	5.06	6.47	0.331	0.026	91.98	90.23	2.14	0.13	2.74	0.13	42.91	25.60
$Mo_3C_2(OH)_2$	0.000	0.004	0.036	3.79	3.45	3.24	0.032	0.003	89.46	89.88	0.10	0.01	0.10	0.01	10.44	11.75
$Mo_3C_2F_2$	0.002	0.021	0.195	7.79	8.38	8.15	0.174	0.019	89.23	89.96	1.42	0.16	1.38	0.17	66.25	70.75
$Mo_3C_2H_2$	0.003	0.031	0.309	8.30	8.38	8.52	0.277	0.028	89.85	90.02	2.36	0.24	2.40	0.24	72.70	70.31
$Mo_3C_2O_2$	0.004	0.045	0.397	12.92	13.20	11.88	0.352	0.041	88.63	90.13	4.18	0.54	3.76	0.55	139.35	174.73
Mo_3CN	0.004	0.036	0.482	5.40	5.66	7.63	0.446	0.033	92.46	90.31	3.40	0.19	4.59	0.19	59.89	32.19
Mo_3N_2	0.002	0.017	0.199	3.94	3.75	4.40	0.182	0.016	91.22	90.18	0.80	0.06	0.94	0.06	19.68	13.99
$Mo_3N_2(OH)_2$	0.000	0.000	0.003	0.60	0.64	0.62	0.003	0.000	89.65	89.87	0.00	0.00	0.00	0.00	0.38	0.42
$Mo_3N_2F_2$	0.002	0.017	0.157	7.88	8.19	7.79	0.140	0.015	89.20	89.96	1.09	0.12	1.04	0.13	60.39	67.42
$Mo_3N_2H_2$	0.002	0.020	0.208	5.38	5.05	5.62	0.188	0.018	90.58	90.04	1.06	0.09	1.17	0.08	31.90	25.35
$Mo_3N_2O_2$	0.003	0.032	0.274	12.48	11.75	10.66	0.242	0.028	88.48	89.96	2.58	0.33	2.34	0.31	112.33	137.24

Mo_4C_3	0.003	0.028	0.366	4.83	5.02	6.83	0.339	0.025	92.42	90.26	2.31	0.13	3.15	0.13	48.07	25.32
$Mo_4C_3(OH)_2$	0.003	0.028	0.242	10.61	10.42	9.29	0.214	0.025	88.62	90.01	1.99	0.26	1.77	0.25	85.04	108.39
$Mo_4C_3F_2$	0.002	0.016	0.167	5.27	5.43	5.63	0.151	0.015	90.32	90.11	0.85	0.08	0.88	0.08	31.83	29.54
$Mo_4C_3O_2$	0.002	0.025	0.266	7.69	7.60	8.40	0.241	0.023	90.60	90.19	2.02	0.17	2.23	0.17	71.36	57.74
Mo_4N_3	0.002	0.016	0.180	3.50	3.53	4.10	0.164	0.014	91.26	90.06	0.67	0.05	0.78	0.05	17.04	12.45
$Mo_4N_3(OH)_2$	0.002	0.021	0.199	6.57	6.89	6.77	0.179	0.019	89.68	90.05	1.21	0.13	1.19	0.13	45.69	47.74
$Mo_4N_3F_2$	0.001	0.013	0.142	3.79	3.98	4.31	0.129	0.012	90.54	90.03	0.56	0.05	0.60	0.05	18.78	15.95
$Mo_4N_3H_2$	0.001	0.010	0.103	4.32	4.40	4.58	0.093	0.009	90.15	90.15	0.42	0.04	0.44	0.04	21.07	19.45
$Mo_4N_3O_2$	0.002	0.018	0.195	4.66	4.73	5.36	0.178	0.016	90.97	90.11	0.95	0.08	1.08	0.08	29.09	22.39
MoCrC	0.003	0.028	0.304	2.09	2.21	2.39	0.276	0.026	90.69	90.15	0.66	0.06	0.71	0.06	5.75	4.92
$MoCrCO_2$ -(model4)	0.003	0.035	0.411	4.19	4.31	5.12	0.375	0.032	91.38	90.15	1.92	0.14	2.28	0.14	26.63	18.64
MoWC	0.002	0.015	0.164	2.19	2.10	2.30	0.148	0.014	90.61	90.06	0.34	0.03	0.37	0.03	5.36	4.40
$MoWC(NCO)_2$	0.007	0.073	0.655	15.45	15.46	14.34	0.582	0.066	88.87	90.30	8.35	1.02	7.75	1.02	203.90	239.09
$MoWC(OCN)_2$	0.008	0.085	0.715	16.63	18.38	15.83	0.630	0.077	88.06	90.38	9.97	1.42	8.59	1.57	246.03	341.51
$MoWC(SCN)_2$	0.016	0.160	0.774	37.23	36.72	18.60	0.613	0.144	79.27	89.86	11.41	5.29	5.78	5.22	306.39	1346.02
$MoWCCl_2$	0.009	0.093	0.937	14.32	14.97	15.54	0.844	0.084	90.04	90.46	13.12	1.26	13.62	1.32	242.50	225.08
$MoWCF_2$	0.001	0.012	0.125	1.11	1.12	1.11	0.112	0.011	89.97	90.19	0.12	0.01	0.12	0.01	1.23	1.25
$MoWCO_2$-(model2)	0.002	0.021	0.243	4.21	4.57	5.30	0.222	0.019	91.31	90.15	1.18	0.09	1.36	0.09	28.57	21.05
$Nb_{0.4}V_{1.6}C$	0.072	0.698	5.075	36.34	32.37	24.39	4.376	0.626	86.24	89.62	106.74	20.26	80.41	18.05	572.31	1035.00
$Nb_{0.8}V_{1.2}C$	0.021	0.205	1.819	11.55	10.67	9.75	1.614	0.184	88.73	89.57	15.74	1.96	14.38	1.81	94.01	112.76
$Nb_{1.2}V_{0.8}C$	0.011	0.107	1.209	6.16	6.20	7.02	1.102	0.096	91.15	90.18	7.73	0.60	8.75	0.60	49.87	38.41
$Nb_{1.33}C$	2.027	3.399	5.995	1214.01	205.51	36.33	2.596	1.372	43.31	40.37	94.33	282.02	16.68	47.74	635.30	18965.08
$Nb_{1.6}V_{0.4}C$	0.006	0.064	0.694	3.96	4.05	4.34	0.630	0.058	90.80	90.22	2.73	0.23	2.93	0.24	18.96	16.46
Nb_2C	0.003	0.033	0.377	3.18	3.02	3.40	0.343	0.030	91.12	89.97	1.17	0.09	1.32	0.09	11.73	9.04
$Nb_2C(OH)_2$	0.004	0.035	0.351	6.05	6.31	6.25	0.315	0.032	89.94	90.03	1.97	0.20	1.96	0.21	39.08	40.03
Nb_2CF_2	0.002	0.022	0.239	3.18	3.43	3.74	0.217	0.020	90.66	90.07	0.81	0.07	0.88	0.07	14.08	11.90
Nb_2CO_2	0.003	0.032	0.363	4.45	4.44	5.13	0.331	0.029	91.20	90.14	1.70	0.13	1.96	0.13	26.70	19.72
Nb_2CrCN	0.005	0.053	0.796	6.65	6.70	10.36	0.743	0.048	93.30	90.40	7.70	0.32	11.90	0.33	111.77	44.92
Nb_2CrCNO_2	0.006	0.058	0.558	11.94	12.80	12.43	0.500	0.052	89.66	90.19	6.22	0.67	6.04	0.71	154.08	165.25
Nb_2HfCN	0.003	0.029	0.368	5.08	5.39	6.99	0.340	0.026	92.26	90.27	2.37	0.14	3.08	0.15	50.08	29.28
Nb_2HfCNO_2	0.004	0.036	0.343	11.96	11.15	11.01	0.307	0.032	89.55	90.08	3.38	0.36	3.34	0.34	120.98	123.33
Nb_2MoCN	0.004	0.041	0.566	6.08	6.20	8.55	0.525	0.037	92.76	90.30	4.49	0.23	6.19	0.23	75.25	38.51
Nb_2MoCNO_2	0.005	0.048	0.458	12.24	12.11	11.84	0.410	0.043	89.53	90.15	4.86	0.52	4.75	0.52	139.87	146.37
Nb_2N	0.003	0.026	0.279	2.36	2.43	2.62	0.253	0.023	90.81	90.18	0.67	0.06	0.72	0.06	6.94	5.93
$Nb_2N(OH)_2$	0.005	0.047	0.425	9.51	10.09	9.36	0.378	0.042	88.95	90.04	3.53	0.43	3.28	0.45	86.82	102.45
Nb_2NF_2	0.002	0.021	0.217	3.40	3.15	3.44	0.196	0.019	90.40	89.94	0.68	0.06	0.74	0.05	11.94	9.85
Nb_2NH_2	0.002	0.015	0.156	3.16	3.30	3.36	0.140	0.014	90.12	90.06	0.47	0.05	0.48	0.05	11.32	10.94
Nb_2NO_2	0.003	0.028	0.320	3.36	3.90	4.46	0.292	0.026	91.12	90.32	1.30	0.10	1.49	0.12	20.22	15.43
$Nb_2Ta_2C_3$	0.000	0.000	0.004	0.04	0.04	0.05	0.003	0.000	91.96	90.22	0.00	0.00	0.00	0.00	0.00	0.00
Nb_2TaCN	0.000	0.001	0.009	5.97	5.89	8.16	0.008	0.001	92.61	90.29	0.07	0.00	0.10	0.00	68.70	34.61
Nb_2TaCNO_2	0.000	0.001	0.009	11.79	11.62	11.72	0.008	0.001	89.74	90.15	0.09	0.01	0.09	0.01	137.48	134.85
Nb_2TiCN	0.005	0.050	0.718	5.97	6.16	9.17	0.668	0.045	93.03	90.30	6.12	0.28	9.11	0.29	87.23	38.03
Nb_2TiCNO_2	0.006	0.058	0.547	12.36	13.08	12.56	0.489	0.053	89.33	90.19	6.14	0.69	5.90	0.73	156.92	172.11

Nb_2VCN	0.005	0.049	0.696	5.96	6.32	9.07	0.646	0.044	92.93	90.36	5.86	0.28	8.42	0.30	85.10	40.17
Nb_2VCNO_2	0.005	0.055	0.535	12.12	11.92	11.97	0.480	0.050	89.69	90.29	5.74	0.59	5.77	0.58	143.29	141.94
$Nb_2W_2C_3$	0.002	0.020	0.267	303.98	317.45	431.91	0.247	0.018	92.59	90.27	106.71	5.67	145.18	5.92	192095.67	101259.50
$Nb_2Zr_2C_3$	0.003	0.027	0.336	7.03	7.08	9.05	0.310	0.024	92.11	90.23	2.80	0.17	3.58	0.17	83.87	50.15
Nb_2ZrCN	0.004	0.038	0.501	5.24	5.35	7.45	0.463	0.034	92.41	90.25	3.45	0.18	4.80	0.19	57.29	28.65
Nb_2ZrCNO_2	0.004	0.044	0.425	11.03	10.85	10.92	0.381	0.040	89.63	90.07	4.16	0.43	4.18	0.42	119.30	117.48
Nb_3C_2	0.003	0.031	0.372	5.33	5.63	6.72	0.341	0.028	91.71	90.12	2.29	0.16	2.74	0.17	45.94	31.92
$Nb_3C_2(OH)_2$	0.003	0.025	0.228	3.66	3.54	3.31	0.203	0.023	88.94	89.87	0.67	0.08	0.63	0.08	10.90	12.49
$Nb_3C_2F_2$	0.002	0.021	0.218	8.71	8.33	8.47	0.196	0.019	90.12	90.04	1.66	0.16	1.69	0.15	71.85	69.02
$Nb_3C_2H_2$	0.001	0.015	0.145	4.06	4.30	4.24	0.130	0.013	89.72	90.04	0.55	0.06	0.55	0.06	17.97	18.62
$Nb_3C_2O_2$	0.004	0.036	0.367	12.25	13.07	12.80	0.330	0.032	90.17	90.13	4.23	0.42	4.14	0.45	163.41	172.04
Nb_3CN	0.004	0.037	0.491	8.83	9.00	11.98	0.453	0.034	92.36	90.30	5.43	0.30	7.22	0.31	147.50	81.12
Nb_3CNO_2	0.005	0.047	0.456	11.65	11.82	11.64	0.409	0.043	89.62	90.19	4.76	0.50	4.69	0.51	135.14	139.85
Nb_3N_2	0.002	0.018	0.202	2.49	2.59	2.99	0.184	0.016	91.08	90.03	0.55	0.04	0.63	0.04	9.10	6.76
$Nb_3N_2(OH)_2$	0.000	0.001	0.009	0.16	0.18	0.17	0.008	0.001	89.57	90.50	0.00	0.00	0.00	0.00	0.03	0.03
$Nb_3N_2F_2$	0.002	0.017	0.163	23.72	24.52	21.90	0.145	0.016	89.30	89.91	3.18	0.38	2.84	0.40	473.76	603.56
$Nb_3N_2H_2$	0.002	0.018	0.176	7.42	8.27	7.89	0.158	0.016	89.85	90.05	1.25	0.13	1.19	0.15	61.90	69.29
$Nb_3N_2O_2$	0.003	0.030	0.300	9.55	10.21	10.05	0.270	0.027	89.98	90.11	2.71	0.28	2.67	0.30	100.76	105.11
Nb_4C_3	0.002	0.024	0.297	6.42	6.65	8.41	0.273	0.022	91.89	90.27	2.30	0.14	2.91	0.15	72.50	44.42
$Nb_4C_3(OH)_2$	0.002	0.023	0.195	4.26	4.23	3.74	0.173	0.020	88.44	90.03	0.65	0.09	0.57	0.09	13.80	17.88
$Nb_4C_3F_2$	0.002	0.017	0.170	8.07	8.89	8.64	0.153	0.016	89.78	89.95	1.32	0.14	1.28	0.15	74.39	79.96
$Nb_4C_3H_2$	0.001	0.012	0.123	4.84	4.80	4.90	0.111	0.011	89.98	90.04	0.54	0.05	0.55	0.05	24.04	22.97
$Nb_4C_3O_2$	0.003	0.028	0.287	10.73	11.22	11.71	0.260	0.025	90.38	90.19	3.04	0.28	3.17	0.29	137.81	126.63
Nb_4N_3	0.002	0.017	0.191	4.75	5.08	5.81	0.174	0.015	91.12	90.16	1.01	0.08	1.16	0.08	34.29	26.00
$Nb_4N_3(OH)_2$	0.002	0.022	0.206	4.39	4.45	4.14	0.183	0.020	89.06	90.00	0.76	0.09	0.70	0.09	16.97	19.87
$Nb_4N_3F_2$	0.001	0.014	0.147	5.13	5.13	5.59	0.133	0.013	90.37	90.18	0.74	0.07	0.81	0.07	31.55	26.37
$Nb_4N_3O_2$	0.002	0.021	0.228	6.88	6.91	7.56	0.207	0.019	90.66	90.20	1.57	0.13	1.71	0.13	57.74	47.81
$Nb_5C_4(OH)_2$	0.000	0.002	0.021	0.64	0.66	0.62	0.019	0.002	89.51	89.87	0.01	0.00	0.01	0.00	0.39	0.43
$Nb_5C_4F_2$	0.001	0.014	0.131	16.88	17.21	16.37	0.117	0.012	89.61	90.02	1.92	0.21	1.83	0.21	266.54	296.90
$Nb_5C_4O_2$	0.002	0.022	0.225	10.70	11.18	11.26	0.202	0.020	90.04	90.13	2.28	0.23	2.29	0.24	126.82	125.69
$NbCrN(NCO)_2$	0.017	0.173	1.049	67.12	70.57	43.85	0.875	0.157	83.46	90.25	38.38	11.05	23.85	11.61	1788.73	5008.24
$NbCrN(NCS)_2$	0.447	1.062	1.310	674.34	165.27	20.97	0.248	0.615	18.91	57.93	5.20	101.70	0.66	24.92	92.73	17641.13
$NbCrN(OCN)_2$	0.013	0.133	1.096	13.66	14.34	12.28	0.963	0.120	87.90	90.42	11.82	1.72	10.12	1.81	147.83	206.84
$NbCrN(SCN)_2$	0.028	0.273	1.123	38.25	38.74	15.99	0.849	0.245	75.64	89.68	13.57	9.50	5.60	9.62	214.91	1503.12
$NbCrNBr_2$	0.019	0.203	1.182	29.19	32.32	19.73	0.978	0.184	82.80	90.71	19.30	5.96	11.78	6.60	360.11	1056.11
$NbCrNCl_2$	0.014	0.148	1.498	19.67	20.67	21.71	1.350	0.134	90.14	90.56	29.31	2.76	30.79	2.90	474.01	429.51
$NbCrNF_2$	0.003	0.032	0.372	3.54	3.43	4.00	0.340	0.029	91.36	89.94	1.36	0.10	1.58	0.10	16.22	11.70
$NbMoN(NCO)_2$	0.008	0.087	0.818	9.36	9.81	9.51	0.731	0.079	89.32	90.38	6.95	0.77	6.73	0.81	90.02	96.71
$NbMoN(NCS)_2$	0.182	0.858	1.252	299.65	140.89	21.05	0.394	0.676	31.46	78.81	8.29	95.24	1.24	44.78	155.32	17376.04
$NbMoN(OCN)_2$	0.000	0.000	0.001	0.01	0.01	0.01	0.001	0.000	89.71	89.28	0.00	0.00	0.00	0.00	0.00	0.00
$NbMoN(SCN)_2$	0.023	0.227	0.997	402.91	431.93	188.75	0.770	0.204	77.24	89.79	145.42	88.02	63.55	94.36	30557.64	188100.72
$NbMoNBr_2$	0.014	0.151	1.046	26.26	28.20	20.07	0.894	0.137	85.51	90.56	17.95	3.87	12.78	4.15	384.25	801.49
$NbMoNCl_2$	0.011	0.111	1.204	16.21	17.26	19.36	1.093	0.100	90.80	90.45	21.17	1.73	23.75	1.84	379.59	299.87

$NbMoN(CN)_2$	0.005	0.049	0.584	5.51	5.89	7.42	0.535	0.044	91.68	90.26	3.97	0.26	5.01	0.28	56.45	34.93
$NbMoNF_2$	0.003	0.029	0.337	4.18	4.19	4.95	0.308	0.026	91.41	90.11	1.52	0.11	1.80	0.11	24.97	17.59
$NbWN(NCO)_2$	0.007	0.069	0.640	9.82	8.76	8.46	0.571	0.062	89.25	90.30	4.83	0.54	4.67	0.49	71.33	75.87
$NbWN(NCS)_2$	0.147	0.679	0.981	327.36	146.95	21.82	0.302	0.532	30.80	78.38	6.59	78.17	0.98	35.09	163.45	18745.27
$NbWN(OCN)_2$	0.007	0.077	0.694	11.43	11.47	11.01	0.617	0.070	88.90	90.37	6.79	0.80	6.52	0.80	120.54	131.49
$NbWN(SCN)_2$	0.017	0.170	0.790	38.70	35.86	17.05	0.621	0.153	78.52	89.95	10.58	5.48	5.03	5.07	254.14	1275.48
$NbWNBr_2$	0.013	0.133	0.845	27.66	29.43	19.08	0.712	0.120	84.28	90.58	13.59	3.54	8.81	3.77	341.60	871.90
$NbWNCl_2$	0.008	0.088	0.916	16.71	17.00	18.19	0.827	0.080	90.35	90.53	15.05	1.36	16.10	1.38	333.23	289.58
$NbWN(CN)_2$	0.003	0.028	0.335	4.34	4.73	5.59	0.306	0.026	91.53	90.23	1.71	0.12	2.02	0.13	31.78	22.56
$NbWNF_2$	0.002	0.022	0.253	3.54	3.80	4.45	0.231	0.020	91.37	90.27	1.03	0.07	1.21	0.08	20.17	14.55
Sc_2C	0.004	0.041	0.433	7.12	6.57	7.20	0.392	0.037	90.48	90.13	2.82	0.24	3.09	0.23	52.37	42.79
$Sc_2C(CN)_2$	0.006	0.061	0.687	2.60	2.84	3.26	0.626	0.055	91.11	90.22	2.04	0.16	2.34	0.17	10.76	8.12
$Sc_2C(NCO)_2$	0.014	0.147	1.181	17.31	18.02	14.81	1.033	0.133	87.51	90.20	15.30	2.40	12.57	2.49	213.76	326.23
$Sc_2C(NCS)_2$	0.186	1.086	1.773	1056.13	550.02	89.51	0.686	0.900	38.72	82.88	61.42	495.16	10.00	257.87	3445.34	275270.11
$Sc_2C(OCI)_2$	0.018	0.197	1.749	20.33	21.51	19.16	1.552	0.178	88.76	90.66	29.75	3.83	26.51	4.06	362.22	465.34
$Sc_2C(OCN)_2$	0.019	0.195	1.243	24.40	24.77	16.02	1.048	0.175	84.34	90.06	16.79	4.34	10.86	4.41	240.79	614.64
$Sc_2C(OH)_2$	0.005	0.049	0.491	22.16	21.05	20.44	0.441	0.044	89.95	90.03	9.02	0.93	8.76	0.89	416.31	440.61
$Sc_2C(SCN)_2$	0.022	0.220	1.463	21.64	23.20	15.62	1.242	0.199	84.93	90.22	19.41	4.62	13.07	4.95	230.75	542.65
Sc_2CBr_2	0.013	0.139	1.253	15.19	16.53	15.21	1.114	0.126	88.87	90.32	16.94	2.08	15.59	2.27	229.10	275.99
Sc_2CCl_2	0.016	0.164	1.626	19.84	18.92	18.94	1.462	0.148	89.90	90.30	27.68	2.81	27.71	2.68	358.74	356.12
Sc_2CF_2	0.003	0.034	0.364	2.83	2.75	3.04	0.330	0.031	90.55	90.00	1.00	0.08	1.11	0.08	9.32	7.51
Sc_2CF_2 -(model2)	0.005	0.051	0.584	4.57	4.49	5.23	0.534	0.046	91.35	90.17	2.79	0.20	3.25	0.20	27.74	20.11
Sc_2CF_2 -(model3)	0.006	0.057	0.656	4.55	4.56	5.41	0.599	0.051	91.32	90.12	3.24	0.23	3.85	0.23	29.78	20.76
Sc_2CF_2 -(model4)	0.007	0.070	0.858	4.40	4.41	5.50	0.787	0.063	91.79	90.16	4.33	0.28	5.40	0.28	30.97	19.50
Sc_2CO_2 -(model3)	0.006	0.058	0.660	3.45	3.54	4.06	0.602	0.052	91.28	90.01	2.44	0.18	2.80	0.19	16.70	12.60
Sc_2CO_2 -(model4)	0.005	0.046	0.517	2.94	3.03	3.30	0.471	0.042	91.03	90.18	1.55	0.13	1.69	0.13	10.96	9.22
Sc_2N	0.003	0.031	0.319	2.54	2.40	2.63	0.288	0.028	90.39	90.11	0.76	0.07	0.83	0.06	7.00	5.75
$Sc_2N(OH)_2$	0.005	0.047	0.477	2.61	2.61	2.64	0.430	0.042	90.18	89.98	1.13	0.11	1.14	0.11	6.95	6.81
Sc_2NF_2	0.003	0.029	0.306	3.16	3.10	3.22	0.276	0.027	90.37	90.28	0.89	0.08	0.92	0.08	10.40	9.59
Sc_2NF_2 -(model3)	0.006	0.059	0.692	5.59	5.70	6.80	0.634	0.053	91.51	90.03	4.31	0.30	5.14	0.31	47.12	32.61
Sc_2NF_2 -(model4)	0.005	0.047	0.536	3.04	3.08	3.55	0.489	0.042	91.27	90.20	1.74	0.13	2.00	0.13	12.79	9.50
Sc_2NO_2	0.004	0.044	0.482	3.51	3.53	3.87	0.439	0.040	90.88	90.10	1.70	0.14	1.86	0.14	15.12	12.50
Sc_2NO_2 -(model2)	0.005	0.047	0.512	3.73	3.78	4.27	0.466	0.042	90.91	90.14	1.99	0.16	2.25	0.16	18.48	14.34
Sc_3C_2	0.004	0.035	0.383	3.40	3.57	3.97	0.348	0.032	90.81	90.06	1.38	0.11	1.54	0.12	15.97	12.78
$Sc_3C_2(OH)_2$	0.004	0.035	0.325	2.71	2.69	2.57	0.290	0.031	89.28	89.89	0.75	0.08	0.71	0.08	6.59	7.23
$Sc_3C_2Br_2$	0.002	0.023	0.228	4.74	4.45	4.51	0.205	0.021	89.85	89.91	0.92	0.09	0.94	0.09	20.36	19.66
$Sc_3C_2F_2$	0.003	0.031	0.308	8.39	8.72	8.71	0.278	0.028	90.06	89.94	2.42	0.24	2.42	0.25	75.94	76.45
$Sc_3C_2O_2$	0.005	0.050	0.556	7.75	8.53	9.55	0.507	0.045	91.03	90.23	4.84	0.38	5.41	0.42	92.26	73.54
Sc_3N_2	0.002	0.023	0.245	2.38	2.39	2.57	0.222	0.021	90.56	90.06	0.57	0.05	0.62	0.05	6.68	5.71
$Sc_3N_2(OH)_2$	0.003	0.034	0.310	3.31	3.18	2.98	0.277	0.030	89.18	90.00	0.83	0.10	0.77	0.09	8.84	10.06
$Sc_3N_2F_2$	0.002	0.025	0.255	5.81	5.67	5.85	0.229	0.023	90.07	90.12	1.34	0.13	1.39	0.13	34.40	32.06
$Sc_3N_2O_2$	0.004	0.039	0.408	6.75	6.90	7.33	0.369	0.035	90.43	90.06	2.70	0.24	2.87	0.25	54.04	47.68
Sc_4C_3	0.003	0.034	0.374	4.92	4.82	5.31	0.340	0.031	90.87	90.19	1.80	0.15	1.99	0.15	28.46	23.14

$Sc_4C_3(OH)_2$	0.003	0.030	0.275	2.89	2.84	2.63	0.245	0.027	88.97	89.96	0.64	0.08	0.60	0.08	6.85	8.03
$Sc_4C_3F_2$	0.003	0.027	0.272	6.51	6.98	7.14	0.245	0.024	90.15	90.03	1.75	0.17	1.79	0.18	51.03	49.12
$Sc_4C_3O_2$	0.004	0.041	0.435	7.97	8.21	8.89	0.393	0.037	90.46	90.08	3.50	0.31	3.78	0.32	79.71	67.66
Sc_4N_3	0.002	0.019	0.198	3.22	3.29	3.42	0.179	0.017	90.59	90.06	0.61	0.06	0.64	0.06	11.73	10.83
$Sc_4N_3(OH)_2$	0.003	0.033	0.301	3.98	4.01	3.62	0.268	0.030	88.92	89.99	0.97	0.12	0.87	0.12	12.93	16.07
$Sc_4N_3F_2$	0.002	0.021	0.217	5.15	4.88	5.24	0.195	0.019	90.28	90.03	1.02	0.09	1.10	0.09	27.66	23.66
$Sc_4N_3O_2$	0.003	0.031	0.329	6.32	6.25	6.79	0.298	0.028	90.49	90.07	2.02	0.18	2.20	0.17	46.56	39.06
$ScCrC(OCN)_2$	0.015	0.159	1.351	26.80	27.21	24.07	1.193	0.144	88.25	90.39	28.71	3.91	25.39	3.97	570.64	741.68
$ScCrC(OH)_2$	0.007	0.068	0.718	7.04	7.56	8.22	0.651	0.061	90.60	90.19	5.35	0.46	5.82	0.49	68.27	57.56
$ScCrCF_2$	0.004	0.041	0.465	4.17	4.40	5.01	0.424	0.037	91.22	90.16	2.12	0.16	2.42	0.17	25.47	19.46
$ScHfN(SCN)_2$	0.015	0.152	0.881	13.45	13.62	7.76	0.729	0.137	82.70	89.92	5.65	1.87	3.22	1.89	55.20	185.66
$ScHfNO_2$	0.002	0.024	0.268	5.05	4.95	5.68	0.244	0.021	91.09	90.12	1.38	0.11	1.58	0.10	32.68	24.49
$ScNbCO_2$	0.004	0.036	0.400	5.53	5.72	6.37	0.364	0.032	91.01	90.12	2.32	0.19	2.58	0.19	41.06	32.81
$ScTaCO_2$	0.000	0.000	0.005	0.05	0.04	0.05	0.004	0.000	91.24	90.07	0.00	0.00	0.00	0.00	0.00	0.00
$ScTiNO_2$	0.004	0.041	0.455	387.20	396.56	449.80	0.414	0.037	91.06	89.90	186.39	14.50	211.41	14.85	205022.11	157684.37
$ScVCO_2$	0.004	0.043	0.468	3.70	3.97	4.46	0.426	0.038	90.90	90.19	1.90	0.15	2.14	0.16	20.18	15.88
$ScYC(CN)_2$	0.005	0.049	0.528	4.65	4.40	4.70	0.479	0.044	90.73	90.17	2.25	0.19	2.41	0.18	22.23	19.22
$ScYC(NCO)_2$	0.009	0.091	0.927	9.36	9.65	9.98	0.836	0.082	90.17	90.30	8.34	0.79	8.63	0.82	99.93	93.49
$ScYC(NCS)_2$	0.085	0.687	1.582	99.09	86.34	19.94	0.895	0.602	56.56	87.63	17.84	52.01	4.12	45.32	249.86	7320.96
$ScYC(OCI)_2$	0.010	0.101	1.176	11.15	11.86	14.14	1.075	0.091	91.43	90.29	15.21	1.08	18.13	1.15	203.67	141.64
$ScYC(OCN)_2$	0.011	0.108	1.040	11.22	11.54	11.30	0.932	0.098	89.60	90.25	10.53	1.13	10.31	1.16	127.40	133.51
$ScYC(OH)_2$	0.005	0.046	0.465	5.73	5.97	6.16	0.419	0.041	90.16	90.09	2.59	0.25	2.67	0.26	38.14	35.81
$ScYC(SCN)_2$	0.019	0.192	1.245	22.99	24.06	15.62	1.053	0.173	84.57	89.98	16.45	4.16	10.68	4.35	229.41	581.82
$ScYCBr_2$	0.013	0.131	1.080	18.68	20.00	16.25	0.949	0.118	87.89	90.24	15.42	2.36	12.53	2.53	257.27	403.23
$ScYCCl_2$	0.010	0.105	1.148	13.31	14.26	15.72	1.042	0.095	90.81	90.34	16.38	1.36	18.06	1.46	249.65	204.81
$ScYCF_2$	0.004	0.038	0.425	3.50	3.62	4.09	0.387	0.034	91.10	90.05	1.58	0.12	1.79	0.13	16.98	13.16
$ScZrN(SCN)_2$	0.023	0.229	1.208	21.43	21.71	11.37	0.979	0.206	81.05	89.96	11.13	4.47	5.83	4.53	116.36	472.08
$ScZrNO_2$	0.004	0.036	0.408	5.39	5.54	6.44	0.372	0.033	91.17	90.15	2.40	0.18	2.79	0.19	42.14	30.76
Ta_2C	0.000	0.000	0.002	0.02	0.02	0.03	0.002	0.000	91.41	90.13	0.00	0.00	0.00	0.00	0.00	0.00
$Ta_2C(OH)_2$	0.000	0.000	0.003	5.12	5.20	4.95	0.003	0.000	89.17	90.05	0.01	0.00	0.01	0.00	24.32	27.13
Ta_2CF_2	0.000	0.000	0.002	4.42	4.68	5.17	0.002	0.000	90.71	90.02	0.01	0.00	0.01	0.00	27.00	22.05
Ta_2CO_2	0.000	0.000	0.003	5.09	5.11	5.93	0.002	0.000	91.23	90.18	0.01	0.00	0.02	0.00	35.71	26.11
Ta_2CrCN	0.000	0.000	0.005	6.11	5.97	8.39	0.004	0.000	92.82	90.30	0.04	0.00	0.05	0.00	72.71	35.56
Ta_2CrCNO_2	0.000	0.000	0.004	11.41	10.74	11.00	0.003	0.000	89.76	90.14	0.04	0.00	0.04	0.00	121.36	114.63
Ta_2HfCN	0.000	0.000	0.003	4.80	4.79	6.05	0.003	0.000	91.88	90.23	0.02	0.00	0.02	0.00	37.47	22.98
Ta_2HfCNO_2	0.000	0.000	0.003	9.56	10.04	9.79	0.003	0.000	89.52	90.16	0.03	0.00	0.03	0.00	95.65	101.46
Ta_2MoCN	0.000	0.000	0.004	5.31	5.46	7.31	0.004	0.000	92.39	90.23	0.03	0.00	0.04	0.00	54.95	29.91
Ta_2MoCNO_2	0.000	0.000	0.004	10.55	10.67	10.54	0.003	0.000	89.65	90.16	0.03	0.00	0.03	0.00	110.92	113.98
Ta_2N	0.000	0.000	0.002	3.49	3.59	4.05	0.002	0.000	91.05	90.13	0.01	0.00	0.01	0.00	16.60	12.90
$Ta_2N(OH)_2$	0.000	0.000	0.003	5.56	5.77	5.20	0.003	0.000	88.57	90.06	0.01	0.00	0.01	0.00	26.68	33.48
Ta_2NbCN	0.000	0.000	0.004	5.24	5.34	7.16	0.004	0.000	92.30	90.36	0.03	0.00	0.04	0.00	52.76	28.56
Ta_2NbCNO_2	0.000	0.000	0.004	10.64	10.24	10.27	0.003	0.000	89.72	90.18	0.03	0.00	0.03	0.00	105.44	104.51
Ta_2NF_2	0.000	0.000	0.002	4.97	5.04	5.54	0.001	0.000	90.35	90.09	0.01	0.00	0.01	0.00	30.99	25.39

Ta_2NH_2	0.000	0.000	0.001	2.95	2.94	3.02	0.001	0.000	90.13	90.03	0.00	0.00	0.00	0.00	9.13	8.62
Ta_2NO_2	0.000	0.000	0.002	4.74	4.61	5.24	0.002	0.000	91.17	90.22	0.01	0.00	0.01	0.00	27.86	21.18
Ta_2TiCN	0.000	0.000	0.004	5.43	5.66	7.64	0.004	0.000	92.50	90.26	0.03	0.00	0.04	0.00	60.05	32.19
Ta_2TiCNO_2	0.000	0.000	0.004	12.24	11.45	10.73	0.003	0.000	89.33	90.12	0.03	0.00	0.03	0.00	114.27	130.25
Ta_2VCN	0.000	0.000	0.004	5.20	5.64	7.45	0.004	0.000	92.47	90.31	0.03	0.00	0.04	0.00	56.94	32.11
Ta_2VCNO_2	0.000	0.000	0.004	10.87	10.09	10.28	0.003	0.000	89.88	90.10	0.03	0.00	0.03	0.00	106.02	100.95
Ta_2ZrCN	0.000	0.000	0.004	5.59	5.08	6.47	0.003	0.000	92.01	90.23	0.02	0.00	0.03	0.00	42.89	25.53
Ta_2ZrCNO_2	0.000	0.000	0.003	10.14	10.06	10.02	0.003	0.000	89.68	90.18	0.03	0.00	0.03	0.00	100.31	101.22
Ta_3C_2	0.000	0.000	0.003	4.44	4.39	5.71	0.002	0.000	92.16	90.26	0.01	0.00	0.02	0.00	33.51	19.24
$Ta_3C_2(OH)_2$	0.000	0.000	0.001	2.72	2.61	2.43	0.001	0.000	89.14	89.82	0.00	0.00	0.00	0.00	5.87	6.76
$Ta_3C_2F_2$	0.000	0.000	0.001	12.32	12.21	11.63	0.001	0.000	89.50	89.97	0.01	0.00	0.01	0.00	134.55	148.83
$Ta_3C_2H_2$	0.000	0.000	0.001	3.43	3.35	3.30	0.001	0.000	89.68	89.77	0.00	0.00	0.00	0.00	10.90	11.18
$Ta_3C_2O_2$	0.000	0.000	0.002	16.65	16.74	16.99	0.002	0.000	90.14	90.19	0.04	0.00	0.04	0.00	289.24	280.29
Ta_3CN	0.000	0.000	0.002	6.44	6.48	7.98	0.002	0.000	91.67	90.14	0.02	0.00	0.02	0.00	65.11	41.95
Ta_3CNO_2	0.000	0.000	0.002	10.26	10.18	10.11	0.002	0.000	89.65	90.02	0.02	0.00	0.02	0.00	102.03	103.62
Ta_3N_2	0.000	0.000	0.001	3.19	3.33	3.91	0.001	0.000	91.34	90.15	0.01	0.00	0.01	0.00	15.57	11.13
$Ta_3N_2(OH)_2$	0.000	0.000	0.000	0.03	0.03	0.03	0.000	0.000	89.62	90.76	0.00	0.00	0.00	0.00	0.00	0.00
$Ta_3N_2F_2$	0.000	0.000	0.001	36.59	40.73	37.83	0.001	0.000	89.18	89.97	0.04	0.00	0.03	0.00	1418.48	1680.04
$Ta_3N_2H_2$	0.000	0.000	0.001	5.67	5.34	5.24	0.001	0.000	89.67	89.88	0.00	0.00	0.00	0.00	27.35	28.28
$Ta_3N_2O_2$	0.000	0.000	0.002	13.29	13.46	13.66	0.002	0.000	89.72	90.09	0.03	0.00	0.03	0.00	186.92	181.49
Ta_4C_3	0.000	0.000	0.002	7.00	7.25	9.46	0.002	0.000	92.48	90.29	0.02	0.00	0.02	0.00	91.81	52.75
$Ta_4C_3(OH)_2$	0.000	0.000	0.002	5.94	6.00	4.98	0.001	0.000	87.88	89.95	0.01	0.00	0.01	0.00	24.25	35.98
$Ta_4C_3F_2$	0.000	0.000	0.001	8.36	8.95	8.96	0.001	0.000	89.72	90.07	0.01	0.00	0.01	0.00	80.35	80.72
$Ta_4C_3H_2$	0.000	0.000	0.001	3.67	3.88	3.89	0.001	0.000	89.83	90.05	0.00	0.00	0.00	0.00	15.15	15.17
$Ta_4C_3O_2$	0.000	0.000	0.002	12.77	14.12	14.63	0.002	0.000	90.73	90.17	0.03	0.00	0.03	0.00	214.96	201.76
Ta_4N_3	0.000	0.000	0.001	5.07	5.13	6.16	0.001	0.000	91.46	90.11	0.01	0.00	0.01	0.00	38.68	26.36
$Ta_4N_3(OH)_2$	0.000	0.000	0.001	5.41	5.12	4.71	0.001	0.000	89.02	89.97	0.01	0.00	0.01	0.00	21.98	26.10
$Ta_4N_3F_2$	0.000	0.000	0.001	5.52	5.36	5.85	0.001	0.000	90.36	90.12	0.01	0.00	0.01	0.00	34.60	28.65
$Ta_4N_3H_2$	0.000	0.000	0.001	2.93	2.85	2.94	0.001	0.000	90.01	89.94	0.00	0.00	0.00	0.00	8.66	8.12
$Ta_4N_3O_2$	0.000	0.000	0.002	10.06	10.88	11.79	0.001	0.000	90.78	90.27	0.02	0.00	0.02	0.00	140.19	119.44
$TaCrN(OCN)_2$	0.000	0.002	0.014	71.05	73.26	65.21	0.012	0.001	88.70	90.36	0.81	0.10	0.72	0.11	4193.24	5384.41
$TaCrN(SCN)_2$	0.000	0.004	0.018	38.64	37.36	19.10	0.014	0.003	79.15	89.95	0.27	0.12	0.14	0.12	323.29	1390.37
$TaCrNBr_2$	0.000	0.004	0.020	36.51	37.34	20.49	0.016	0.003	81.28	90.45	0.33	0.13	0.18	0.13	380.28	1397.85
$TaCrNCl_2$	0.000	0.002	0.017	15.60	16.27	14.95	0.015	0.002	88.61	90.48	0.23	0.03	0.21	0.03	221.33	265.75
$TaCrNF_2$	0.000	0.000	0.004	3.18	3.03	3.53	0.004	0.000	91.18	90.10	0.01	0.00	0.01	0.00	12.64	9.12
$TaMoN(NCO)_2$	0.000	0.001	0.012	12.50	12.86	12.38	0.011	0.001	89.71	90.22	0.13	0.01	0.13	0.01	152.71	166.03
$TaMoN(NCS)_2$	0.002	0.014	0.022	260.51	141.88	23.68	0.008	0.011	37.39	82.53	0.20	1.62	0.03	0.88	234.10	18360.42
$TaMoN(SCN)_2$	0.000	0.002	0.014	15.96	15.64	10.08	0.011	0.002	83.91	89.91	0.12	0.03	0.07	0.03	95.20	244.12
$TaMoNBr_2$	0.000	0.003	0.020	39.83	40.82	29.87	0.017	0.003	85.82	90.44	0.51	0.10	0.37	0.11	854.43	1670.55
$TaMoNCl_2$	0.000	0.002	0.017	11.93	12.69	13.56	0.015	0.001	90.45	90.43	0.20	0.02	0.22	0.02	185.10	162.14
$TaMoNF_2$	0.000	0.000	0.004	3.24	3.17	3.79	0.004	0.000	91.30	90.13	0.02	0.00	0.02	0.00	14.64	10.02
$TaWN(CN)_2$	0.000	0.001	0.006	4.96	4.93	5.76	0.006	0.000	91.13	90.25	0.03	0.00	0.04	0.00	33.68	24.32
$TaWN(NCO)_2$	0.000	0.001	0.012	12.15	11.93	11.66	0.011	0.001	89.76	90.24	0.13	0.01	0.12	0.01	135.66	142.13

$TaWNBr_2$	0.000	0.003	0.020	29.91	31.79	21.41	0.017	0.003	85.18	90.51	0.37	0.09	0.25	0.09	433.85	1017.24
$TaWNCl_2$	0.000	0.002	0.017	14.86	15.00	14.36	0.015	0.002	89.08	90.48	0.22	0.03	0.21	0.03	205.04	225.27
$Ti_{0.4}Nb_{1.6}C$	0.009	0.088	1.126	678.36	738.93	969.86	1.037	0.080	92.16	90.23	1005.99	58.85	1320.39	64.11	966327.31	551337.84
$Ti_{0.8}Nb_{1.2}C$	0.013	0.136	2.292	9.92	10.65	18.11	2.156	0.123	94.07	90.43	39.04	1.31	66.37	1.41	343.06	114.37
$Ti_{1.2}Nb_{0.8}C$	0.031	0.330	3.334	24.29	27.18	27.60	3.004	0.299	90.09	90.54	82.89	8.13	84.17	9.10	762.90	748.04
$Ti_{1.5}Nb_{0.5}C$	0.008	0.078	0.823	5.42	5.77	6.20	0.745	0.070	90.55	90.10	4.62	0.40	4.96	0.43	38.70	33.57
$Ti_{1.6}Nb_{0.4}C$	0.016	0.161	1.387	8.68	8.72	7.44	1.226	0.144	88.42	89.80	9.13	1.26	7.79	1.26	54.35	76.03
$Ti_{10}C_9F_2$	0.003	0.031	0.246	1.48	1.45	1.14	0.214	0.028	87.20	89.84	0.24	0.04	0.19	0.04	1.25	2.10
$Ti_{10}N_9F_2$	0.002	0.017	0.157	8.52	8.86	8.73	0.140	0.015	89.29	90.08	1.23	0.13	1.21	0.14	76.08	78.89
Ti_2C	0.004	0.042	0.445	23.52	25.30	28.08	0.404	0.038	90.63	90.22	11.33	0.95	12.57	1.02	797.32	645.28
$Ti_2C(OH)_2$	0.006	0.059	0.600	3.39	3.31	3.26	0.540	0.053	90.11	90.04	1.76	0.18	1.73	0.17	10.61	10.93
Ti_2CCI_2	0.002	0.024	0.246	2.52	2.59	2.84	0.223	0.021	90.44	89.94	0.63	0.05	0.69	0.06	8.14	6.71
Ti_2CF_2	0.003	0.031	0.328	4.12	3.80	4.09	0.297	0.028	90.56	90.06	1.22	0.11	1.31	0.10	16.86	14.34
Ti_2CF_2-(model2)	0.006	0.061	0.765	6.48	6.34	8.02	0.704	0.055	91.98	90.25	5.65	0.35	7.15	0.34	65.90	40.06
Ti_2CF_2-(model3)	0.007	0.067	0.832	5.57	5.26	6.55	0.765	0.061	91.90	90.21	5.01	0.32	6.24	0.30	43.85	27.45
Ti_2CF_2-(model4)	0.010	0.101	1.408	7.07	6.98	9.86	1.306	0.092	92.80	90.31	12.88	0.64	18.21	0.63	100.53	48.64
$Ti_2CO_{0.11}F_{1.89}$	0.004	0.041	0.472	2.49	2.49	2.87	0.431	0.037	91.27	90.08	1.24	0.09	1.43	0.09	8.36	6.21
$Ti_2CO_{0.44}F_{1.56}$	0.005	0.046	0.529	4.30	4.28	5.06	0.484	0.041	91.38	90.11	2.45	0.18	2.89	0.18	26.08	18.34
$Ti_2CO_{0.67}F_{1.33}$	0.005	0.046	0.537	4.07	4.29	5.11	0.491	0.041	91.43	90.21	2.51	0.18	2.99	0.19	26.57	18.51
$Ti_2CO_{0.89}F_{1.11}$	0.005	0.050	0.587	4.74	4.80	5.58	0.538	0.045	91.57	90.07	3.00	0.21	3.48	0.22	31.55	23.03
$Ti_2CO_{1.33}F_{0.67}$	0.005	0.049	0.576	4.42	4.63	5.50	0.527	0.044	91.45	90.14	2.90	0.21	3.45	0.22	30.82	21.53
Ti_2CO_2	0.004	0.043	0.489	4.13	4.06	4.58	0.445	0.039	91.12	90.00	2.04	0.16	2.30	0.16	21.27	16.44
Ti_2CO_2-(model2)	0.005	0.051	0.597	4.27	4.75	5.42	0.546	0.046	91.49	90.14	2.96	0.22	3.38	0.24	29.77	22.84
Ti_2CO_2-(model3)	0.006	0.057	0.677	4.99	5.12	6.18	0.620	0.052	91.53	90.17	3.83	0.26	4.62	0.27	38.93	26.26
Ti_2CrCN	0.009	0.097	1.607	7.47	8.12	13.46	1.511	0.088	93.98	90.45	20.33	0.71	33.71	0.77	189.14	66.53
Ti_2CrCNO_2	0.010	0.102	0.999	12.81	14.04	14.14	0.898	0.092	89.81	90.31	12.69	1.29	12.77	1.42	199.99	199.22
Ti_2HfCN	0.004	0.043	0.589	6.00	5.94	8.28	0.546	0.039	92.71	90.39	4.52	0.23	6.30	0.23	70.77	35.26
Ti_2HfCNO_2	0.005	0.055	0.549	12.12	12.49	12.47	0.493	0.050	89.90	90.21	6.15	0.62	6.14	0.64	155.55	156.40
Ti_2MoCN	0.006	0.067	1.008	6.44	6.93	10.60	0.941	0.060	93.36	90.32	9.98	0.42	15.27	0.45	116.79	48.36
Ti_2MoCNO_2	0.008	0.078	0.768	12.23	13.59	13.29	0.690	0.071	89.83	90.38	9.17	0.96	8.97	1.07	176.11	186.88
Ti_2N	0.003	0.030	0.316	2.07	2.22	2.32	0.286	0.027	90.46	90.17	0.66	0.06	0.70	0.06	5.41	4.95
$Ti_2N(OH)_2$	0.005	0.052	0.535	3.25	3.18	3.34	0.482	0.047	90.20	90.08	1.61	0.15	1.69	0.15	11.23	10.11
$Ti_2Nb_2C_3$	0.004	0.038	0.516	4.26	4.49	6.03	0.478	0.035	92.58	90.26	2.88	0.16	3.86	0.16	37.36	20.30
Ti_2NbC_2	0.002	0.025	0.271	3.29	3.42	3.84	0.246	0.022	90.94	90.02	0.95	0.08	1.06	0.08	14.93	11.74
Ti_2NbCN	0.007	0.069	1.047	6.88	6.87	10.69	0.978	0.062	93.45	90.39	10.46	0.43	16.27	0.43	118.88	47.15
Ti_2NbCNO_2	0.008	0.080	0.778	12.72	13.05	13.07	0.698	0.072	89.76	90.40	9.12	0.94	9.13	0.96	170.73	170.82
Ti_2NF_2	0.003	0.027	0.285	3.07	3.18	3.41	0.258	0.024	90.51	90.03	0.88	0.08	0.94	0.08	11.71	10.15
Ti_2NF_2-(model2)	0.006	0.060	0.763	5.92	6.42	8.18	0.703	0.054	92.12	90.18	5.75	0.35	7.34	0.38	68.58	41.54
Ti_2NO_2	0.004	0.038	0.414	2.97	3.17	3.45	0.375	0.034	90.78	90.23	1.30	0.11	1.41	0.12	12.02	10.12
Ti_2NO_2-(model4)	0.008	0.086	1.055	8.04	8.33	10.47	0.969	0.077	91.86	90.20	10.15	0.65	12.76	0.67	112.27	69.68
Ti_2NS_2	0.002	0.024	0.251	1.28	1.30	1.37	0.227	0.022	90.43	90.01	0.31	0.03	0.33	0.03	1.89	1.68
$Ti_2Ta_2C_3$	0.000	0.000	0.004	0.04	0.04	0.06	0.004	0.000	92.47	90.21	0.00	0.00	0.00	0.00	0.00	0.00
Ti_2TaC_2	0.000	0.000	0.003	4.50	4.69	5.28	0.003	0.000	90.86	90.10	0.01	0.00	0.02	0.00	28.20	22.06

Ti_2TaCN	0.000	0.001	0.012	6.57	6.68	10.00	0.011	0.001	93.24	90.37	0.11	0.00	0.16	0.00	103.85	44.65
Ti_2TaCNO_2	0.000	0.001	0.010	12.04	12.99	13.08	0.009	0.001	89.89	90.28	0.12	0.01	0.12	0.01	171.20	170.32
Ti_2VC_2	0.003	0.033	0.370	317.06	320.63	368.20	0.337	0.030	91.11	90.19	124.12	9.51	142.53	9.62	137561.99	102929.53
Ti_2VCN	0.009	0.090	1.434	6.90	7.29	12.10	1.344	0.082	93.71	90.36	16.26	0.59	26.99	0.63	153.15	53.43
Ti_2VCNO_2	0.009	0.098	0.975	13.71	13.50	13.58	0.877	0.089	89.90	90.38	11.91	1.20	11.98	1.18	184.66	182.07
Ti_2ZrCN	0.006	0.063	0.890	6.10	6.40	8.99	0.828	0.057	92.95	90.33	7.44	0.36	10.46	0.38	83.43	41.12
Ti_2ZrCNO_2	0.007	0.077	0.750	12.24	12.72	12.86	0.673	0.069	89.79	90.26	8.66	0.88	8.75	0.91	165.54	162.59
Ti_3C_2	0.004	0.037	0.419	3.68	3.61	4.14	0.382	0.033	91.21	90.08	1.58	0.12	1.81	0.12	17.36	13.03
$Ti_3C_2(O_{0.13}F_{0.83}(OH)_{1.04})$	0.014	0.141	0.930	12.18	12.60	8.24	0.789	0.127	84.81	89.83	6.51	1.60	4.26	1.65	64.01	159.27
$Ti_3C_2(O_{0.1}F_{1.1}(OH)_{0.8})$	0.018	0.174	1.070	30.95	29.50	18.55	0.896	0.157	83.72	89.94	16.62	4.62	10.45	4.41	320.83	865.81
$Ti_3C_2(O_{0.7}F_{1.3})$	0.006	0.056	0.601	9.04	9.39	10.29	0.545	0.050	90.69	90.05	5.61	0.47	6.14	0.49	106.84	88.63
$Ti_3C_2(OH)_2$	0.006	0.064	0.539	11.28	10.52	8.81	0.475	0.058	88.11	89.88	4.19	0.61	3.51	0.56	76.02	109.77
$Ti_3C_2Br_2$	0.003	0.027	0.262	5.24	5.89	5.79	0.236	0.024	89.79	90.04	1.37	0.14	1.34	0.16	33.49	35.14
$Ti_3C_2CI_2$	0.003	0.026	0.270	7.33	7.20	7.69	0.244	0.024	90.29	89.87	1.88	0.17	2.00	0.17	59.59	51.79
$Ti_3C_2F_2$	0.003	0.030	0.311	5.83	6.09	6.70	0.281	0.027	90.29	90.10	1.88	0.17	2.07	0.17	45.34	37.30
$Ti_3C_2O_2$	0.005	0.047	0.480	8.07	7.94	8.39	0.433	0.042	90.27	90.18	3.64	0.33	3.85	0.33	70.92	62.87
$Ti_3C_2Se_2$	0.001	0.013	0.129	2.18	1.99	2.02	0.116	0.012	89.72	90.04	0.24	0.02	0.24	0.02	4.10	3.94
$Ti_3C_2Te_2$	0.001	0.008	0.077	2.71	2.72	2.68	0.069	0.007	89.57	89.95	0.18	0.02	0.18	0.02	7.16	7.43
Ti_3CN	0.008	0.082	1.188	38.94	42.71	61.08	1.107	0.074	93.13	90.44	67.60	3.15	96.68	3.46	3852.65	1842.66
Ti_3CNF_2	0.012	0.124	1.370	9.45	9.89	11.13	1.246	0.112	90.95	90.54	13.86	1.11	15.59	1.16	125.36	98.31
Ti_3CNO_2	0.010	0.108	1.071	12.09	12.59	12.90	0.963	0.098	89.92	90.41	12.42	1.23	12.73	1.28	166.93	159.24
$Ti_3N_2(OH)_2$	0.005	0.049	0.430	6.38	6.54	5.83	0.380	0.044	88.49	89.95	2.21	0.29	1.97	0.30	33.47	42.88
Ti_3N_2	0.002	0.024	0.254	5.51	5.43	6.11	0.231	0.021	90.70	90.06	1.41	0.12	1.59	0.11	37.87	29.39
$Ti_3N_2F_2$	0.002	0.024	0.241	2.46	2.41	2.52	0.217	0.022	90.10	90.16	0.55	0.05	0.57	0.05	6.38	5.78
$Ti_3N_2H_2$	0.004	0.039	0.399	7.70	8.17	8.07	0.359	0.036	90.10	90.04	2.90	0.29	2.86	0.31	65.04	67.17
$Ti_3N_2O_2$	0.004	0.037	0.382	6.14	6.33	6.50	0.345	0.033	90.40	89.95	2.25	0.21	2.31	0.22	42.42	40.22
Ti_4C_3	0.003	0.030	0.340	5.37	5.04	5.74	0.310	0.027	91.11	90.14	1.78	0.14	2.03	0.13	33.45	25.20
$Ti_4C_3(OH)_2$	0.005	0.046	0.410	4.89	5.10	4.57	0.364	0.042	88.70	90.02	1.66	0.21	1.49	0.22	20.66	26.09
$Ti_4C_3F_2$	0.002	0.024	0.251	5.24	5.29	5.67	0.227	0.022	90.36	90.02	1.29	0.12	1.38	0.12	32.35	28.03
$Ti_4C_3H_2$	0.004	0.036	0.351	7.15	7.18	7.06	0.315	0.033	89.67	90.03	2.22	0.23	2.19	0.24	49.81	51.56
$Ti_4C_3O_2$	0.003	0.035	0.379	6.67	6.77	7.37	0.343	0.032	90.64	90.13	2.53	0.22	2.75	0.22	54.80	45.96
Ti_4N_3	0.002	0.018	0.195	3.15	3.22	3.67	0.177	0.016	90.83	90.08	0.65	0.05	0.74	0.05	13.66	10.40
$Ti_4N_3(OH)_2$	0.006	0.059	0.570	7.64	7.92	7.74	0.511	0.053	89.69	90.16	3.95	0.42	3.86	0.43	59.71	62.94
$Ti_4N_3F_2$	0.002	0.019	0.199	4.05	4.01	4.31	0.180	0.017	90.39	90.01	0.78	0.07	0.83	0.07	18.69	16.03
$Ti_4N_3H_2$	0.002	0.023	0.238	4.99	4.94	5.36	0.215	0.020	90.52	89.97	1.15	0.10	1.25	0.10	29.01	24.37
$Ti_4N_3O_2$	0.003	0.027	0.286	5.73	5.60	6.14	0.259	0.024	90.59	90.03	1.59	0.14	1.74	0.13	38.03	31.25
$Ti_5C_4(OH)_2$	0.004	0.041	0.345	8.28	7.97	6.83	0.303	0.037	88.02	89.99	2.07	0.30	1.78	0.29	45.80	63.20
$Ti_5C_4F_2$	0.002	0.023	0.229	6.72	7.43	7.35	0.206	0.021	90.04	90.07	1.52	0.15	1.50	0.17	53.94	55.92
$Ti_5C_4O_2$	0.003	0.035	0.363	8.84	9.24	9.58	0.328	0.032	90.33	90.06	3.14	0.29	3.25	0.31	92.06	85.84
$Ti_5N_4F_2$	0.002	0.023	0.255	5.29	5.57	6.11	0.232	0.021	90.80	90.10	1.42	0.12	1.55	0.12	37.76	31.18
$Ti_6C_5F_2$	0.005	0.050	0.381	12.07	12.35	9.67	0.332	0.045	86.99	90.19	3.21	0.55	2.51	0.57	90.58	152.94
$Ti_6N_5F_2$	0.003	0.031	0.283	8.90	8.54	8.07	0.253	0.028	89.17	90.12	2.04	0.24	1.93	0.23	64.74	72.66
$Ti_7C_6F_2$	0.005	0.050	0.390	17.66	18.17	14.24	0.340	0.045	87.15	90.06	4.85	0.82	3.80	0.84	196.49	331.28

$Ti_7N_6F_2$	0.003	0.030	0.259	10.69	10.76	9.49	0.229	0.027	88.47	89.98	2.18	0.29	1.92	0.29	88.67	115.87
$Ti_8C_7F_2$	0.005	0.052	0.355	23.18	22.63	15.59	0.303	0.047	85.24	89.91	4.72	1.07	3.25	1.04	230.50	510.53
$Ti_8N_7F_2$	0.003	0.027	0.230	11.97	11.76	10.55	0.203	0.024	88.27	90.05	2.14	0.29	1.92	0.28	109.74	137.99
$Ti_9C_8F_2$	0.003	0.030	0.252	14.45	15.36	12.92	0.222	0.027	88.02	90.06	2.87	0.42	2.42	0.44	163.49	237.73
$Ti_9N_8F_2$	0.002	0.016	0.156	6.71	8.09	7.83	0.141	0.014	89.94	90.13	1.10	0.11	1.07	0.14	61.14	66.89
$TiCrCO_2$	0.004	0.040	0.452	20.73	20.99	24.28	0.412	0.036	91.20	90.13	10.00	0.75	11.57	0.76	598.71	441.21
$TiHfCO_2$	0.003	0.026	0.281	2.62	2.73	2.89	0.254	0.024	90.58	90.12	0.73	0.07	0.78	0.07	8.38	7.49
$TiHfN(NO)_2$	0.002	0.021	0.231	4.24	3.97	4.51	0.210	0.019	90.98	90.16	0.95	0.07	1.08	0.07	20.66	15.61
$TiMoCO_2$	0.003	0.028	0.307	4.49	4.61	5.12	0.279	0.025	90.95	90.01	1.43	0.12	1.59	0.12	26.52	21.28
TiNbC	0.003	0.034	0.361	4.14	4.31	4.69	0.327	0.031	90.57	89.98	1.53	0.13	1.67	0.14	22.16	18.65
TiVC	0.005	0.049	0.512	2.65	2.74	2.89	0.464	0.044	90.51	90.04	1.34	0.12	1.41	0.12	8.38	7.56
$TiWCO_2$	0.002	0.019	0.216	0.77	0.79	0.90	0.197	0.017	91.07	89.94	0.18	0.01	0.20	0.01	0.83	0.63
$TiZrCO_2$	0.004	0.040	0.462	7.31	7.67	8.58	0.421	0.036	91.25	90.13	3.62	0.28	4.04	0.29	74.50	59.22
V_2C	0.004	0.043	0.476	4.42	4.83	5.27	0.432	0.039	90.96	90.03	2.28	0.19	2.49	0.20	28.07	23.62
$V_2C(OH)_2$	0.006	0.061	0.632	3.68	3.73	3.83	0.571	0.055	90.29	90.11	2.18	0.21	2.24	0.21	14.68	13.91
V_2CBr_2	0.001	0.015	0.152	1.60	1.66	1.74	0.137	0.013	90.32	90.05	0.24	0.02	0.25	0.02	3.04	2.78
$V_2CF(OH)$	0.004	0.042	0.470	7.26	7.45	8.27	0.429	0.038	91.13	90.01	3.55	0.28	3.94	0.29	69.18	55.62
V_2CF_2	0.003	0.031	0.342	2.98	3.04	3.34	0.311	0.028	90.80	90.10	1.04	0.09	1.14	0.09	11.26	9.27
V_2CO_2	0.004	0.044	0.508	4.61	4.77	5.46	0.463	0.040	91.28	90.04	2.53	0.19	2.89	0.20	30.19	22.85
V_2CrCN	0.009	0.095	1.598	7.90	8.05	13.91	1.502	0.086	94.03	90.48	20.90	0.69	36.10	0.71	202.87	64.97
V_2CrCNO_2	0.009	0.095	0.879	14.96	14.99	13.74	0.784	0.086	89.19	90.34	10.77	1.29	9.87	1.29	186.92	224.90
V_2HfCN	0.004	0.043	0.592	5.86	5.98	8.59	0.550	0.038	92.81	90.21	4.72	0.23	6.79	0.23	76.42	35.78
V_2HfCNO_2	0.005	0.048	0.467	11.77	11.91	11.92	0.418	0.044	89.61	90.19	4.98	0.52	4.99	0.53	142.02	142.09
V_2MoCN	0.006	0.066	1.021	6.53	6.93	10.76	0.954	0.060	93.50	90.24	10.26	0.41	15.93	0.44	120.30	48.31
V_2MoCNO_2	0.007	0.070	0.671	12.78	12.90	12.75	0.601	0.063	89.52	90.24	7.66	0.82	7.58	0.83	162.34	166.47
V_2N	0.003	0.031	0.328	2.94	3.14	3.36	0.297	0.028	90.57	90.15	1.00	0.09	1.07	0.09	11.35	9.91
$V_2N(OH)_2$	0.005	0.047	0.493	2.86	3.00	3.19	0.447	0.042	90.55	90.00	1.43	0.13	1.52	0.13	10.28	9.05
$V_2Nb_2C_3$	0.004	0.038	0.524	4.07	4.26	5.87	0.486	0.034	92.72	90.25	2.85	0.15	3.93	0.15	35.57	18.27
V_2NbCN	0.007	0.068	1.052	6.51	7.00	10.98	0.984	0.062	93.51	90.42	10.81	0.43	16.96	0.46	125.60	49.36
V_2NbCNO_2	0.008	0.079	0.679	15.03	15.48	13.67	0.600	0.071	88.33	90.15	8.20	1.11	7.24	1.14	184.06	240.36
V_2NF_2	0.003	0.027	0.286	3.84	3.75	4.07	0.259	0.024	90.59	90.19	1.05	0.09	1.14	0.09	16.67	14.00
V_2NO_2	0.004	0.037	0.411	3.90	4.01	4.49	0.374	0.033	91.05	90.08	1.68	0.13	1.88	0.14	20.44	16.13
$V_2Ta_2C_3$	0.000	0.000	0.004	0.03	0.03	0.04	0.004	0.000	92.21	90.23	0.00	0.00	0.00	0.00	0.00	0.00
V_2TaC_2	0.000	0.001	0.007	8.59	8.75	11.00	0.006	0.001	91.86	90.24	0.07	0.00	0.09	0.00	123.92	76.73
V_2TaCN	0.000	0.001	0.012	6.53	6.67	10.44	0.011	0.001	93.35	90.33	0.12	0.00	0.19	0.00	113.47	44.66
V_2TaCNO_2	0.000	0.001	0.009	12.49	12.95	12.70	0.008	0.001	89.64	90.21	0.10	0.01	0.10	0.01	161.06	168.41
$V_2Ti_2C_3$	0.006	0.059	0.877	523.18	513.75	756.95	0.818	0.054	93.23	90.31	619.05	27.57	912.09	27.07	593375.25	263430.20
V_2TiC_2	0.007	0.067	0.896	6.73	6.92	9.30	0.829	0.061	92.47	90.23	7.70	0.42	10.35	0.43	88.92	48.07
V_2TiCN	0.009	0.089	1.421	6.86	7.25	12.04	1.332	0.080	93.74	90.38	16.03	0.58	26.61	0.62	151.58	52.91
V_2TiCNO_2	0.009	0.093	0.870	14.50	14.16	13.58	0.777	0.084	89.26	90.27	10.54	1.19	10.11	1.17	183.41	199.87
V_2ZrCN	0.006	0.062	0.894	5.94	6.24	9.37	0.832	0.056	93.05	90.31	7.80	0.35	11.72	0.37	91.30	39.12
V_2ZrCNO_2	0.007	0.069	0.654	12.29	12.64	12.33	0.585	0.062	89.50	90.22	7.22	0.78	7.04	0.81	151.67	160.29
V_3C_2	0.004	0.041	0.481	3.55	3.42	4.00	0.440	0.037	91.48	90.16	1.76	0.13	2.06	0.12	16.28	11.63

$V_3C_2(OH)_2$	0.008	0.079	0.596	7.26	7.12	5.52	0.517	0.071	86.75	89.82	2.85	0.51	2.21	0.50	29.41	50.64
$V_3C_2Br_2$	0.002	0.015	0.149	3.59	3.47	3.50	0.134	0.013	89.90	89.88	0.47	0.05	0.47	0.05	12.24	12.03
$V_3C_2Cl_2$	0.004	0.045	0.452	15.94	15.04	15.41	0.407	0.041	90.04	90.14	6.27	0.61	6.42	0.58	238.17	224.92
$V_3C_2F_2$	0.003	0.033	0.330	6.31	6.35	6.35	0.297	0.030	89.98	90.06	1.88	0.19	1.88	0.19	40.30	40.41
$V_3C_2O_2$	0.005	0.049	0.509	10.72	10.24	10.90	0.460	0.044	90.35	90.14	5.01	0.45	5.33	0.43	119.52	104.40
V_3CN	0.008	0.081	1.188	13.53	12.79	20.20	1.107	0.073	93.22	90.35	22.36	0.93	35.33	0.88	426.07	162.59
V_3CNO_2	0.010	0.107	1.062	8.64	8.91	8.92	0.956	0.096	89.97	90.43	8.53	0.86	8.54	0.89	79.66	79.62
V_3N_2	0.002	0.021	0.228	3.13	2.79	3.15	0.207	0.019	90.82	90.16	0.65	0.05	0.73	0.05	10.04	7.71
$V_3N_2(OH)_2$	0.016	0.165	0.960	21.08	21.96	12.57	0.795	0.149	82.77	90.05	9.99	3.27	5.72	3.41	144.98	484.25
$V_3N_2F_2$	0.003	0.027	0.259	5.84	6.56	6.42	0.233	0.024	89.77	90.10	1.49	0.16	1.46	0.18	41.05	43.59
$V_3N_2H_2$	0.004	0.038	0.379	6.94	6.81	6.89	0.341	0.034	90.06	90.07	2.35	0.23	2.38	0.23	47.56	46.29
$V_3N_2O_2$	0.004	0.038	0.391	7.28	6.95	7.37	0.353	0.034	90.28	90.12	2.60	0.24	2.75	0.23	54.61	48.12
V_4C_3	0.003	0.033	0.385	3.86	3.86	4.67	0.352	0.030	91.49	90.20	1.64	0.11	1.99	0.11	22.23	14.89
$V_4C_3(OH)_2$	0.007	0.066	0.519	15.75	16.39	13.34	0.452	0.060	87.23	89.99	6.04	0.98	4.91	1.02	173.29	269.90
$V_4C_3F_2$	0.002	0.025	0.262	5.40	5.46	5.76	0.237	0.022	90.50	90.08	1.36	0.12	1.44	0.12	33.35	29.82
$V_4C_3H_2$	0.002	0.019	0.196	4.43	4.54	4.60	0.177	0.017	90.16	90.03	0.81	0.08	0.83	0.08	21.18	20.64
$V_4C_3O_2$	0.004	0.036	0.394	6.92	6.95	7.60	0.359	0.032	90.90	90.19	2.72	0.22	2.98	0.23	58.24	48.28
V_4N_3	0.002	0.021	0.228	2.60	2.76	3.10	0.207	0.019	90.93	90.12	0.64	0.05	0.72	0.05	9.73	7.65
$V_4N_3(OH)_2$	0.004	0.038	0.364	8.50	8.71	8.34	0.327	0.034	89.65	90.14	2.72	0.30	2.61	0.30	69.19	76.15
$V_4N_3F_2$	0.002	0.018	0.197	4.00	3.87	4.22	0.178	0.017	90.59	90.05	0.75	0.06	0.82	0.06	17.95	14.90
$V_4N_3H_2$	0.001	0.015	0.151	3.80	3.63	3.77	0.137	0.013	90.17	90.00	0.52	0.05	0.54	0.05	14.31	13.07
$V_4N_3O_2$	0.003	0.026	0.283	5.30	5.46	5.92	0.257	0.023	90.81	90.05	1.52	0.13	1.65	0.13	35.31	29.92
$VCrN(NCS)_2$	0.366	1.253	1.651	314.31	103.21	14.22	0.398	0.886	24.11	70.75	5.66	91.49	0.78	30.04	54.49	8337.71
$VCrN(SCN)_2$	0.037	0.354	1.330	51.20	47.45	18.49	0.976	0.317	73.37	89.58	18.04	15.06	7.03	13.96	279.83	2232.92
$VCrNBr_2$	0.027	0.288	1.350	33.80	35.19	17.35	1.062	0.261	78.67	90.62	18.43	9.18	9.08	9.56	264.62	1243.98
$VCrNF_2$	0.003	0.032	0.356	3.08	3.24	3.70	0.324	0.029	90.99	90.06	1.20	0.09	1.37	0.10	13.87	10.59
$VMoN(NCO)_2$	0.011	0.109	0.986	14.90	15.57	14.39	0.876	0.099	88.90	90.30	12.61	1.54	11.66	1.61	205.28	243.51
$VMoN(NCS)_2$	0.242	1.018	1.423	247.17	102.16	15.05	0.405	0.776	28.47	76.23	6.10	79.28	0.90	32.77	72.14	8822.89
$VMoN(OCN)_2$	0.012	0.126	1.066	18.82	17.56	15.59	0.939	0.114	88.13	90.34	14.64	2.01	13.00	1.87	239.34	306.05
$VMoN(SCN)_2$	0.027	0.263	1.124	43.91	42.18	18.87	0.861	0.236	76.61	89.71	16.25	9.95	7.27	9.55	304.76	1771.21
$VMoNBr_2$	0.021	0.218	1.158	30.10	31.41	17.14	0.940	0.198	81.16	90.56	16.11	6.21	8.80	6.47	265.87	990.90
$VMoNCI_2$	0.015	0.159	1.377	16.94	17.88	15.57	1.218	0.143	88.49	90.48	18.97	2.56	16.52	2.71	238.47	321.67
VNbC	0.003	0.033	0.353	1.88	1.96	2.05	0.320	0.030	90.52	90.03	0.66	0.06	0.69	0.06	4.23	3.85
$VNbCF_2$-(model4)	0.004	0.041	0.477	3.72	3.80	4.64	0.436	0.037	91.47	90.24	2.02	0.14	2.47	0.14	21.95	14.49
$VWN(NCO)_2$	0.007	0.067	0.662	12.50	12.49	12.83	0.595	0.061	89.82	90.19	7.63	0.76	7.84	0.76	165.11	156.07
$VWN(OCN)_2$	0.009	0.089	0.788	16.98	16.85	15.37	0.699	0.081	88.67	90.36	10.75	1.36	9.80	1.35	233.65	283.79
$VWNBr_2$	0.014	0.145	0.913	23.09	26.26	16.85	0.769	0.131	84.17	90.54	12.95	3.44	8.31	3.91	265.93	699.73
$VWNCI_2$	0.011	0.116	1.019	16.74	17.35	15.67	0.903	0.105	88.61	90.50	14.15	1.82	12.77	1.89	242.47	302.30
$VWNF_2$	0.002	0.020	0.225	3.35	3.40	3.86	0.205	0.018	91.17	89.92	0.79	0.06	0.90	0.06	15.13	11.61
$W_{1.33}C$	0.498	1.443	2.879	546.38	163.42	32.77	1.436	0.945	49.87	65.51	47.05	154.49	9.43	46.21	595.43	19506.94
$W_{1.33}C(OH)_2$	0.004	0.036	0.394	6.59	7.39	8.32	0.357	0.033	90.76	90.16	2.97	0.24	3.34	0.27	70.04	55.42
$W_{1.33}CO_2$	0.003	0.029	0.342	5.14	5.28	6.40	0.313	0.026	91.50	90.33	2.00	0.14	2.43	0.14	41.83	27.99
W_2C	0.002	0.019	0.222	3.57	3.72	4.41	0.203	0.017	91.54	90.16	0.89	0.06	1.06	0.07	19.75	13.89

$W_2C(OH)_2$	0.003	0.031	0.271	12.13	11.72	10.53	0.240	0.028	88.60	90.03	2.53	0.33	2.27	0.31	109.39	136.84
W_2CCl_2	0.007	0.079	0.787	14.98	15.61	15.80	0.709	0.071	90.02	90.58	11.20	1.11	11.35	1.16	250.15	244.59
W_2CF_2	0.001	0.013	0.138	5.71	5.13	5.44	0.125	0.012	90.34	90.00	0.68	0.06	0.72	0.06	29.84	26.01
W_2CO_2	0.002	0.017	0.198	4.08	4.28	4.94	0.180	0.016	91.22	90.04	0.89	0.07	1.03	0.07	24.76	18.42
$W_2Hf_2C_3O_2$	0.002	0.016	0.154	9.16	9.41	9.43	0.138	0.014	89.79	90.18	1.30	0.13	1.30	0.14	88.97	88.80
W_2HfC_2	0.001	0.009	0.093	2.87	2.76	3.06	0.085	0.008	90.79	90.02	0.26	0.02	0.29	0.02	9.49	7.61
$W_2HfC_2O_2$	0.003	0.025	0.226	13.09	12.27	11.30	0.201	0.023	88.79	90.04	2.27	0.28	2.09	0.26	126.47	149.44
W_2N	0.001	0.013	0.145	3.08	3.01	3.46	0.132	0.011	91.19	89.81	0.46	0.03	0.53	0.03	12.18	9.01
$W_2N(OH)_2$	0.004	0.037	0.293	15.33	14.71	12.36	0.256	0.033	87.46	89.96	3.16	0.49	2.66	0.47	149.34	215.33
W_2NF_2	0.001	0.013	0.131	5.56	5.33	5.57	0.118	0.011	90.28	90.19	0.66	0.06	0.69	0.06	31.23	28.28
W_2NO_2	0.002	0.017	0.185	5.55	5.89	6.46	0.168	0.016	90.71	90.07	1.09	0.09	1.19	0.10	42.16	34.91
$W_2Ti_2C_3O_2$	0.002	0.023	0.228	9.58	9.23	9.40	0.205	0.020	90.12	90.19	1.93	0.19	1.96	0.18	88.51	84.80
$W_2TiC_2O_2$	0.003	0.031	0.299	11.21	11.42	11.10	0.267	0.028	89.56	90.18	2.97	0.32	2.89	0.33	122.86	130.59
$W_2Zr_2C_3O_2$	0.002	0.020	0.195	10.31	9.94	9.63	0.175	0.018	89.65	90.11	1.68	0.18	1.63	0.17	92.33	98.32
W_2ZrC_2	0.001	0.010	0.114	2.90	2.87	3.18	0.104	0.009	90.92	89.94	0.33	0.03	0.37	0.03	10.23	8.23
$W_2ZrC_2O_2$	0.003	0.031	0.278	12.25	12.98	11.79	0.246	0.028	88.74	90.11	2.90	0.37	2.64	0.39	137.32	169.47
W_3C_2	0.002	0.017	0.218	5.32	5.72	7.28	0.201	0.016	92.13	90.23	1.46	0.09	1.86	0.10	54.26	33.03
$W_3C_2(OH)_2$	0.000	0.000	0.003	0.98	0.81	0.84	0.003	0.000	89.63	89.52	0.00	0.00	0.00	0.00	0.70	0.64
$W_3C_2F_2$	0.001	0.012	0.106	9.89	9.18	8.56	0.095	0.010	89.04	89.94	0.81	0.10	0.76	0.09	72.61	83.53
$W_3C_2O_2$	0.002	0.022	0.196	10.29	11.12	10.60	0.175	0.020	88.96	90.06	1.85	0.22	1.76	0.23	111.63	124.85
W_3N_2	0.001	0.010	0.120	4.21	4.34	5.09	0.110	0.009	91.26	90.11	0.56	0.04	0.66	0.04	26.38	18.85
$W_3N_2(OH)_2$	0.000	0.000	0.000	0.02	0.03	0.02	0.000	0.000	87.50	92.31	0.00	0.00	0.00	0.00	0.00	0.00
$W_3N_2F_2$	0.001	0.008	0.076	8.34	7.94	7.84	0.068	0.007	89.26	90.06	0.53	0.06	0.52	0.06	61.36	62.70
$W_3N_2O_2$	0.002	0.019	0.156	14.16	13.94	11.58	0.137	0.017	87.98	90.07	1.59	0.24	1.32	0.23	131.12	193.94
W_4C_3	0.002	0.016	0.219	5.22	5.40	7.35	0.203	0.014	92.66	90.22	1.49	0.08	2.02	0.08	55.54	29.32
$W_4C_3(OH)_2$	0.002	0.016	0.137	10.87	10.57	9.41	0.122	0.014	88.58	90.00	1.15	0.15	1.02	0.15	87.29	111.38
$W_4C_3F_2$	0.001	0.009	0.094	5.09	5.44	5.60	0.085	0.008	90.28	90.12	0.48	0.04	0.49	0.05	31.51	29.83
$W_4C_3H_2$	0.001	0.011	0.121	5.49	5.51	6.36	0.110	0.010	90.95	90.22	0.70	0.05	0.81	0.05	41.10	30.37
$W_4C_3O_2$	0.001	0.013	0.147	6.56	6.72	7.43	0.133	0.012	90.87	90.23	0.99	0.08	1.09	0.08	55.73	45.30
W_4N_3	0.001	0.011	0.128	4.05	4.14	4.86	0.117	0.010	91.64	90.17	0.57	0.04	0.67	0.04	24.02	17.17
$W_4N_3(OH)_2$	0.002	0.020	0.195	11.37	11.74	11.72	0.175	0.018	89.61	90.16	2.05	0.21	2.05	0.22	137.43	138.27
$W_4N_3F_2$	0.001	0.013	0.174	5.89	6.00	8.11	0.160	0.012	92.31	90.33	1.30	0.07	1.76	0.07	67.75	36.12
$W_4N_3H_2$	0.001	0.009	0.098	4.77	4.82	5.52	0.089	0.008	91.06	90.10	0.49	0.04	0.57	0.04	30.95	23.29
$W_4N_3O_2$	0.001	0.010	0.111	4.54	4.62	5.13	0.101	0.009	90.93	90.18	0.52	0.04	0.57	0.04	26.57	21.39
WCrC	0.002	0.019	0.206	2.31	2.27	2.49	0.186	0.017	90.65	90.04	0.46	0.04	0.51	0.04	6.26	5.15
$WCrCO_2$-(model4)	0.002	0.025	0.292	4.40	4.35	5.08	0.267	0.022	91.50	89.99	1.35	0.10	1.58	0.10	26.21	18.90
Y_2C	0.003	0.030	0.320	2.13	2.26	2.45	0.290	0.027	90.72	90.01	0.71	0.06	0.77	0.06	6.07	5.13
$Y_2C(CN)_2$	0.006	0.057	0.612	7.46	7.39	8.08	0.555	0.051	90.69	90.16	4.49	0.38	4.91	0.38	65.98	54.57
$Y_2C(NCO)_2$	0.008	0.082	0.818	11.50	11.86	11.88	0.736	0.074	89.99	90.16	8.75	0.88	8.76	0.90	141.21	141.16
$Y_2C(NCS)_2$	0.019	0.185	1.008	40.52	42.68	23.56	0.823	0.167	81.62	89.99	19.38	7.11	10.70	7.49	504.04	1832.43
$Y_2C(OCI)_2$	0.011	0.110	1.027	14.25	14.52	14.35	0.917	0.100	89.25	90.38	13.16	1.45	13.00	1.48	205.58	211.36
$Y_2C(OCN)_2$	0.008	0.084	0.874	12.20	12.06	12.87	0.790	0.076	90.35	90.17	10.16	0.92	10.84	0.91	166.78	145.35
$Y_2C(OH)_2$	0.003	0.029	0.285	4.28	4.30	4.34	0.256	0.026	89.97	90.13	1.11	0.11	1.12	0.11	18.86	18.53

$Y_2C(SCN)_2$	0.016	0.165	1.151	27.06	29.07	20.42	0.986	0.149	85.66	90.08	20.13	4.32	14.14	4.64	397.15	852.09
Y_2CBr_2	0.009	0.089	0.860	12.38	13.04	13.02	0.771	0.081	89.61	90.24	10.04	1.05	10.02	1.11	169.39	171.11
Y_2CCl_2	0.009	0.096	0.989	10.76	10.81	11.40	0.892	0.087	90.25	90.26	10.17	0.94	10.72	0.94	130.70	116.93
Y_2CF_2	0.003	0.029	0.319	3.56	3.59	3.97	0.290	0.027	90.77	89.97	1.15	0.10	1.27	0.10	15.95	12.88
Y_2CO_2	0.005	0.050	0.595	5.15	5.56	6.59	0.545	0.046	91.52	90.22	3.59	0.25	4.25	0.27	44.12	31.14
Y_2N	0.002	0.025	0.260	2.09	2.06	2.21	0.236	0.022	90.57	89.96	0.52	0.05	0.56	0.05	4.90	4.25
$Y_2N(OH)_2$	0.003	0.028	0.282	4.72	4.52	4.57	0.254	0.025	89.97	90.01	1.16	0.12	1.17	0.11	20.92	20.37
Y_2NF_2	0.002	0.024	0.257	3.29	3.37	3.61	0.233	0.022	90.52	90.10	0.84	0.07	0.90	0.08	13.14	11.40
Y_2NO_2	0.004	0.043	0.506	4.46	4.79	5.69	0.462	0.039	91.41	90.03	2.63	0.19	3.12	0.20	32.91	23.10
Y_3C_2	0.002	0.024	0.253	4.18	3.93	4.38	0.229	0.021	90.62	90.03	1.00	0.08	1.12	0.08	19.40	15.36
$Y_3C_2(OH)_2$	0.000	0.004	0.038	2.80	2.41	2.28	0.034	0.004	89.59	89.85	0.08	0.01	0.07	0.01	5.15	5.70
$Y_3C_2F_2$	0.003	0.027	0.271	7.01	7.16	7.26	0.243	0.025	89.88	89.98	1.77	0.18	1.79	0.18	52.79	51.32
$Y_3C_2O_2$	0.003	0.031	0.281	10.79	11.17	10.14	0.250	0.028	89.03	89.86	2.54	0.31	2.30	0.32	101.62	125.21
Y_3N_2	0.002	0.019	0.202	3.25	3.44	3.74	0.183	0.017	90.52	90.02	0.68	0.06	0.74	0.06	14.11	11.89
$Y_3N_2(OH)_2$	0.003	0.032	0.284	10.09	10.18	9.15	0.252	0.029	88.61	89.84	2.31	0.30	2.07	0.30	82.70	103.71
$Y_3N_2F_2$	0.003	0.030	0.292	7.51	7.93	7.78	0.262	0.027	89.75	90.07	2.04	0.21	2.00	0.23	60.42	63.25
$Y_3N_2O_2$	0.003	0.028	0.255	9.65	9.52	8.71	0.228	0.025	89.23	90.04	1.98	0.24	1.81	0.23	75.02	90.48
Y_4C_3	0.002	0.023	0.252	3.81	3.68	4.17	0.229	0.021	90.90	90.13	0.95	0.08	1.08	0.07	17.61	13.49
$Y_4C_3(OH)_2$	0.000	0.003	0.029	1.99	2.14	2.00	0.026	0.003	89.43	90.11	0.05	0.01	0.05	0.01	3.99	4.64
$Y_4C_3F_2$	0.003	0.026	0.256	8.54	8.03	8.16	0.231	0.023	89.91	90.06	1.88	0.19	1.91	0.18	66.75	64.02
$Y_4C_3O_2$	0.005	0.050	0.519	12.33	12.78	13.24	0.468	0.045	90.29	90.28	6.20	0.58	6.43	0.60	176.04	163.92
Y_4N_3	0.002	0.017	0.181	2.66	2.71	2.95	0.164	0.015	90.77	90.05	0.48	0.04	0.53	0.04	8.79	7.34
$Y_4N_3(OH)_2$	0.002	0.022	0.200	7.01	7.04	6.74	0.178	0.019	89.16	90.04	1.20	0.14	1.15	0.14	45.20	49.57
$Y_4N_3F_2$	0.002	0.025	0.283	5.91	5.83	6.61	0.258	0.023	91.17	90.16	1.70	0.13	1.93	0.13	44.32	33.99
$Y_4N_3O_2$	0.002	0.024	0.252	6.49	6.46	6.93	0.228	0.022	90.47	90.06	1.58	0.14	1.70	0.14	48.43	41.75
$YCrC(NCO)_2$	0.009	0.096	0.915	12.59	12.93	12.90	0.820	0.086	89.56	90.16	10.58	1.11	10.56	1.14	166.49	167.69
$YCrC(NCS)_2$	0.125	0.840	1.514	149.73	95.65	18.00	0.674	0.716	44.51	85.14	12.13	68.44	2.28	43.73	161.06	8606.99
$YCrC(OCN)_2$	0.011	0.117	1.050	14.84	16.22	14.65	0.933	0.106	88.86	90.33	13.67	1.71	12.35	1.87	212.06	265.65
$YCrC(OH)_2$	0.005	0.051	0.522	7.65	7.35	7.54	0.471	0.046	90.18	90.03	3.55	0.34	3.64	0.33	57.04	53.81
$YCrCBr_2$	0.014	0.145	1.144	17.19	19.51	15.94	0.999	0.131	87.30	90.46	15.92	2.56	13.01	2.91	247.54	386.22
$YCrCCl_2$	0.012	0.123	1.304	12.41	12.41	13.44	1.181	0.111	90.54	90.40	15.87	1.38	17.19	1.38	182.32	154.14
$YCrCF_2$	0.004	0.037	0.434	3.90	4.26	5.09	0.397	0.034	91.42	90.17	2.02	0.14	2.41	0.16	26.34	18.32
$YHfN(SCN)_2$	0.013	0.134	0.896	24.42	26.37	18.34	0.762	0.121	85.07	90.17	13.98	3.18	9.72	3.44	319.34	701.73
$YHfNO_2$	0.002	0.021	0.226	4.18	4.22	4.79	0.205	0.019	90.83	90.10	0.98	0.08	1.11	0.08	23.21	17.80
$YMoN(NO)_2$	0.003	0.025	0.278	3.57	3.52	3.87	0.253	0.023	90.88	90.08	0.98	0.08	1.08	0.08	15.14	12.39
$YNbCO_2$	0.003	0.033	0.369	4.28	4.10	4.75	0.336	0.030	90.98	90.17	1.59	0.12	1.85	0.12	22.89	16.70
$YTaCO_2$	0.000	0.000	0.005	3.88	4.32	4.69	0.004	0.000	90.88	90.15	0.02	0.00	0.02	0.00	22.19	18.89
$YTiN(NO)_2$	0.003	0.035	0.395	4.08	4.12	4.66	0.360	0.032	91.04	90.18	1.68	0.13	1.90	0.13	22.00	16.95
$YTiNO_2$	0.003	0.032	0.358	4.15	4.12	4.58	0.325	0.029	90.97	90.01	1.49	0.12	1.66	0.12	21.20	16.92
$YVCO_2$	0.004	0.038	0.415	3.67	3.97	4.49	0.378	0.034	90.90	90.16	1.70	0.14	1.92	0.15	20.47	15.90
$YVNF_2$	0.003	0.030	0.332	3.81	3.96	4.41	0.301	0.028	90.82	90.27	1.33	0.11	1.48	0.11	19.71	15.78
$YZrNO_2$	0.003	0.029	0.322	4.57	4.47	4.98	0.292	0.026	90.87	90.09	1.45	0.12	1.62	0.12	25.08	19.95
Zr_2C	0.003	0.032	0.349	2.75	2.57	2.91	0.318	0.028	90.95	90.07	0.92	0.07	1.04	0.07	8.56	6.55

$Zr_2C(OH)_2$	0.003	0.032	0.318	5.33	5.49	5.59	0.286	0.029	89.95	89.93	1.60	0.16	1.62	0.16	31.30	30.28
Zr_2CF_2	0.002	0.023	0.246	3.35	3.38	3.64	0.223	0.021	90.59	90.18	0.81	0.07	0.88	0.07	13.36	11.41
Zr_2CF_2-(model2)	0.003	0.028	0.317	4.10	3.86	4.43	0.289	0.025	91.17	90.23	1.28	0.10	1.47	0.09	19.91	14.78
Zr_2CF_2-(model3)	0.004	0.036	0.412	3.45	3.36	3.91	0.376	0.033	91.23	90.15	1.47	0.11	1.71	0.11	15.53	11.27
Zr_2CO_2	0.003	0.035	0.403	4.88	4.35	5.27	0.367	0.032	91.20	90.14	1.94	0.14	2.35	0.12	28.39	18.70
Zr_2CrCN	0.004	0.044	0.577	5.36	5.49	7.47	0.534	0.039	92.46	90.26	3.98	0.22	5.42	0.22	57.45	30.25
Zr_2CrCNO_2	0.005	0.049	0.477	10.65	10.87	10.85	0.428	0.044	89.76	90.14	4.64	0.48	4.63	0.49	117.62	118.46
Zr_2HfCN	0.002	0.025	0.298	4.39	4.64	5.65	0.273	0.022	91.68	90.28	1.54	0.10	1.88	0.11	32.51	21.62
Zr_2HfCNO_2	0.003	0.032	0.309	10.76	10.38	10.42	0.276	0.029	89.52	90.04	2.88	0.30	2.89	0.29	108.60	107.43
Zr_2MoCN	0.003	0.034	0.433	5.27	5.06	6.52	0.399	0.031	92.07	90.19	2.60	0.16	3.35	0.15	43.55	25.46
Zr_2MoCNO_2	0.004	0.040	0.394	10.22	10.30	10.35	0.353	0.036	89.74	89.98	3.66	0.37	3.68	0.38	107.28	106.16
Zr_2N	0.002	0.025	0.267	2.27	2.29	2.44	0.242	0.023	90.65	90.18	0.59	0.05	0.63	0.05	5.99	5.25
$Zr_2N(OH)_2$	0.003	0.031	0.304	5.36	5.72	5.53	0.273	0.028	89.87	90.19	1.51	0.16	1.46	0.17	30.50	32.91
Zr_2NbCN	0.003	0.035	0.432	4.76	5.16	6.51	0.397	0.031	91.99	90.31	2.59	0.16	3.27	0.17	43.40	26.84
Zr_2NbCNO_2	0.004	0.042	0.402	10.96	10.61	10.44	0.360	0.038	89.62	90.14	3.76	0.40	3.70	0.39	108.86	112.28
Zr_2NF_2	0.002	0.020	0.217	3.12	3.09	3.24	0.196	0.018	90.58	90.00	0.64	0.06	0.67	0.06	10.56	9.56
Zr_2NF_2-(model2)	0.003	0.033	0.378	3.92	3.67	4.33	0.345	0.030	91.31	90.19	1.50	0.11	1.76	0.10	19.12	13.40
Zr_2NF_2-(model4)	0.003	0.026	0.287	4.17	3.96	4.30	0.261	0.023	90.94	90.17	1.12	0.09	1.22	0.09	18.67	15.62
Zr_2NO_2	0.003	0.029	0.317	4.23	3.92	4.31	0.288	0.026	90.94	90.05	1.24	0.10	1.37	0.09	18.80	15.27
Zr_2TaCN	0.000	0.001	0.007	5.10	4.92	6.24	0.006	0.001	91.88	90.29	0.04	0.00	0.05	0.00	39.89	24.13
Zr_2TaCNO_2	0.000	0.001	0.007	10.08	10.42	10.15	0.007	0.001	89.78	90.10	0.07	0.01	0.06	0.01	102.69	108.98
Zr_2TiCN	0.004	0.042	0.536	5.04	5.18	6.78	0.494	0.038	92.18	90.17	3.35	0.20	4.38	0.20	47.22	26.95
Zr_2TiCNO_2	0.005	0.048	0.471	10.88	10.70	10.45	0.422	0.044	89.75	90.18	4.41	0.47	4.31	0.46	108.91	114.32
Zr_2VCN	0.004	0.041	0.523	4.99	5.22	6.69	0.482	0.037	92.16	90.28	3.22	0.19	4.13	0.20	45.84	27.43
Zr_2VCNO_2	0.005	0.047	0.459	9.66	10.31	10.40	0.413	0.042	89.83	90.16	4.29	0.43	4.33	0.46	108.23	107.14
Zr_3C_2	0.003	0.028	0.317	3.68	3.72	4.43	0.290	0.025	91.29	90.19	1.28	0.09	1.53	0.09	19.99	13.82
$Zr_3C_2(OH)_2$	0.002	0.018	0.168	7.69	7.04	6.54	0.150	0.016	89.38	89.91	0.98	0.11	0.91	0.10	42.41	49.03
$Zr_3C_2F_2$	0.002	0.022	0.218	5.78	5.82	5.84	0.196	0.020	90.03	90.09	1.15	0.11	1.15	0.11	34.09	33.85
$Zr_3C_2H_2$	0.001	0.014	0.133	5.12	5.08	4.88	0.119	0.012	89.66	89.85	0.58	0.06	0.56	0.06	23.74	25.77
$Zr_3C_2O_2$	0.004	0.037	0.375	8.08	8.38	8.76	0.338	0.034	90.08	90.17	2.96	0.28	3.09	0.29	77.17	70.58
Zr_3CN	0.003	0.032	0.380	4.88	4.45	5.58	0.348	0.029	91.65	90.23	1.94	0.13	2.44	0.12	31.90	19.62
Zr_3CNO_2	0.005	0.046	0.477	9.85	10.33	10.70	0.431	0.041	90.35	90.12	4.62	0.43	4.78	0.45	114.99	107.38
$Zr_3N_2(OH)_2$	0.001	0.010	0.096	5.78	5.43	5.19	0.086	0.009	89.42	90.02	0.45	0.05	0.43	0.05	26.75	29.25
Zr_3N_2	0.002	0.018	0.203	3.24	3.12	3.52	0.184	0.017	90.89	90.10	0.65	0.05	0.73	0.05	12.56	9.68
$Zr_3N_2F_2$	0.002	0.017	0.166	5.72	5.65	5.52	0.149	0.015	89.84	90.07	0.82	0.09	0.80	0.08	30.37	31.83
$Zr_3N_2H_2$	0.001	0.015	0.143	5.14	5.11	5.23	0.129	0.013	89.67	90.03	0.67	0.07	0.69	0.07	27.43	26.07
$Zr_3N_2O_2$	0.003	0.030	0.303	7.02	7.32	7.44	0.273	0.027	90.15	90.06	2.03	0.20	2.06	0.20	55.39	53.80
Zr_4C_3	0.002	0.023	0.269	3.68	3.97	4.66	0.246	0.021	91.39	90.15	1.14	0.08	1.35	0.09	22.10	15.86
$Zr_4C_3(OH)_2$	0.002	0.020	0.176	8.31	8.54	7.56	0.156	0.018	88.81	89.92	1.18	0.15	1.05	0.16	56.34	73.09
$Zr_4C_3F_2$	0.002	0.019	0.188	6.07	6.07	6.09	0.169	0.017	90.11	90.01	1.03	0.10	1.03	0.10	37.12	36.81
$Zr_4C_3H_2$	0.002	0.024	0.236	7.53	8.05	7.85	0.212	0.022	89.68	90.13	1.66	0.18	1.62	0.19	61.44	65.31
$Zr_4C_3O_2$	0.003	0.030	0.319	8.42	8.27	8.94	0.289	0.027	90.53	90.12	2.58	0.23	2.79	0.22	80.55	68.22
Zr_4N_3	0.001	0.015	0.165	3.13	3.11	3.43	0.150	0.014	90.91	90.08	0.51	0.04	0.57	0.04	11.87	9.67

$Zr_4N_3(OH)_2$	0.002	0.019	0.171	8.45	8.24	7.73	0.152	0.017	88.85	90.02	1.18	0.14	1.10	0.14	59.29	67.69
$Zr_4N_3F_2$	0.001	0.015	0.147	5.05	5.13	5.27	0.133	0.013	90.14	89.95	0.70	0.07	0.72	0.07	27.90	26.40
$Zr_4N_3O_2$	0.002	0.023	0.243	6.84	6.86	7.24	0.220	0.021	90.48	90.09	1.59	0.14	1.68	0.14	52.68	47.03
$ZrCrNO_2$	0.003	0.032	0.356	4.29	4.17	4.85	0.324	0.029	91.10	90.10	1.57	0.12	1.82	0.12	23.86	17.37
$ZrHfCO_2$	0.002	0.020	0.218	4.30	4.22	4.66	0.198	0.018	90.85	90.09	0.92	0.08	1.02	0.07	21.96	17.77
$ZrMoCO_2$	0.002	0.022	0.242	3.23	3.16	3.57	0.219	0.020	90.81	90.10	0.78	0.06	0.88	0.06	12.92	9.99

APPENDIX C: Adsorption Capacities and Calculated Performance Metrics of MXenes with Large Interlayer Distance at 35°C and 0.1, 1, and 10 bar

MXene Type	CO_2 Adsorption Capacity (mol/kg)			CO_2/H_2 Selectivity			CO_2 Working Capacity		Regenerability (%)		APS		AFM		SSP	
	0.1 bar	1 bar	10 bar	0.1 bar	1 bar	10 bar	PSA	VSA	PSA	VSA	PSA	VSA	PSA	VSA	PSA	VSA
$(CrV)_3C_2$	0.006	0.058	0.642	4.65	4.69	5.22	0.584	0.053	90.91	90.12	3.05	0.25	3.40	0.25	27.60	21.99
$(Mo_{0.66}Y_{0.33})_2CO_2$	0.003	0.028	0.302	2.74	2.82	3.09	0.275	0.025	90.79	90.14	0.85	0.07	0.93	0.07	9.65	8.01
$(TiV)_3C_2$	0.006	0.064	0.677	4.72	4.67	5.02	0.613	0.057	90.61	90.05	3.08	0.27	3.31	0.26	25.40	21.76
$(TiV)C(OH)_2$	0.005	0.047	0.534	3.38	3.47	4.03	0.487	0.042	91.24	90.13	1.96	0.15	2.28	0.15	16.52	12.06
$(TiV)CF_2$	0.004	0.042	0.451	2.83	2.69	2.94	0.409	0.038	90.74	90.07	1.21	0.10	1.32	0.10	8.75	7.22
$(TiV)CO_2$	0.004	0.042	0.459	2.71	2.82	3.12	0.417	0.038	90.84	90.19	1.30	0.11	1.44	0.11	9.85	8.00
$(W_{0.66}Y_{0.33})_2CO_2$	0.002	0.024	0.272	4.08	3.92	4.38	0.247	0.022	91.02	90.16	1.08	0.09	1.21	0.08	19.37	15.28
Cr_2C	0.005	0.051	0.543	2.42	2.43	2.65	0.493	0.046	90.66	90.08	1.30	0.11	1.42	0.11	7.06	5.93
$Cr_2C(OH)_2$	0.004	0.040	0.450	3.05	3.23	3.65	0.410	0.036	91.12	90.12	1.50	0.12	1.69	0.12	13.48	10.53
Cr_2CBr_2	0.008	0.080	1.403	7.68	7.69	14.05	1.323	0.072	94.33	90.45	18.59	0.55	33.96	0.55	207.76	59.17
Cr_2CCl_2	0.009	0.093	1.446	6.19	6.60	10.43	1.353	0.084	93.56	90.36	14.11	0.56	22.31	0.59	113.31	43.84
Cr_2CF_2	0.003	0.033	0.353	2.31	2.40	2.60	0.321	0.029	90.75	90.09	0.83	0.07	0.90	0.07	6.80	5.80
Cr_2CFCl	0.005	0.046	0.517	3.58	3.54	4.00	0.470	0.042	91.03	90.09	1.88	0.15	2.12	0.15	16.17	12.51
Cr_2CH_2	0.003	0.028	0.296	1.83	1.84	1.92	0.268	0.026	90.39	90.10	0.51	0.05	0.53	0.05	3.69	3.38
Cr_2CO_2	0.004	0.043	0.498	3.46	3.50	4.23	0.455	0.039	91.42	90.07	1.93	0.13	2.33	0.14	18.23	12.26
Cr_2CS_2	0.020	0.216	3.231	13.45	14.70	22.57	3.015	0.196	93.32	90.91	68.05	2.88	104.51	3.15	529.78	218.02
Cr_2HfCN	0.004	0.040	0.473	4.57	4.79	5.78	0.433	0.036	91.60	90.21	2.50	0.17	3.02	0.18	34.04	23.09
Cr_2HfCNO_2	0.003	0.033	0.446	5.62	5.45	7.56	0.413	0.030	92.65	90.35	3.12	0.16	4.33	0.16	59.01	29.63
Cr_2MoCN	0.006	0.063	0.779	5.64	5.64	7.03	0.716	0.056	91.96	90.18	5.03	0.32	6.27	0.32	50.50	31.86
Cr_2MoCNO_2	0.004	0.046	0.656	5.52	5.96	8.66	0.610	0.041	93.03	90.31	5.28	0.25	7.67	0.27	77.60	35.84
Cr_2N	0.003	0.032	0.333	1.84	1.93	2.02	0.302	0.029	90.47	90.04	0.61	0.06	0.64	0.06	4.11	3.75
$Cr_2N(OH)_2$	0.004	0.036	0.406	2.97	3.00	3.41	0.370	0.033	91.09	90.05	1.26	0.10	1.44	0.10	11.80	8.98
$Cr_2Nb_2C_3$	0.004	0.036	0.414	3.94	4.15	4.91	0.378	0.032	91.39	90.10	1.86	0.13	2.20	0.14	24.53	17.32
Cr_2NbCN	0.006	0.064	0.794	5.26	5.65	7.13	0.731	0.057	91.99	90.20	5.21	0.32	6.57	0.35	52.03	32.20
Cr_2NbCNO_2	0.005	0.047	0.682	5.94	5.95	8.81	0.635	0.042	93.10	90.22	5.59	0.25	8.28	0.25	80.54	35.41
Cr_2NF_2	0.003	0.027	0.285	2.17	2.10	2.27	0.258	0.024	90.62	90.08	0.59	0.05	0.63	0.05	5.21	4.40
Cr_2NH_2	0.003	0.027	0.286	2.00	1.97	2.08	0.259	0.024	90.54	90.04	0.54	0.05	0.57	0.05	4.33	3.88
Cr_2NO_2	0.003	0.035	0.383	2.51	2.64	2.88	0.348	0.031	90.88	90.11	1.00	0.08	1.09	0.09	8.36	7.01
$Cr_2Ta_2C_3$	0.000	0.000	0.003	3.48	3.71	4.14	0.003	0.000	91.15	90.10	0.01	0.00	0.01	0.00	17.36	13.83
Cr_2TaC_2	0.000	0.000	0.003	2.35	2.30	2.43	0.003	0.000	90.61	90.06	0.01	0.00	0.01	0.00	5.94	5.26
Cr_2TaCN	0.000	0.001	0.009	5.21	5.37	6.63	0.008	0.001	91.83	90.25	0.06	0.00	0.07	0.00	44.93	28.90
Cr_2TaCNO_2	0.000	0.001	0.009	5.56	5.78	8.25	0.008	0.001	92.93	90.28	0.07	0.00	0.10	0.00	70.37	33.54
$Cr_2Ti_2C_3$	0.005	0.055	0.647	4.49	4.63	5.58	0.592	0.049	91.53	90.18	3.30	0.23	3.98	0.24	31.76	21.51
Cr_2TiC_2	0.003	0.033	0.356	2.44	2.59	2.79	0.323	0.030	90.69	90.17	0.90	0.08	0.97	0.08	7.86	6.75
$Cr_2TiC_2(OH)_2$	0.004	0.044	0.566	5.74	5.88	7.43	0.521	0.040	92.15	90.28	3.87	0.24	4.90	0.24	56.52	34.63
$Cr_2TiC_2F_2$	0.006	0.064	0.925	6.21	6.41	9.22	0.861	0.058	93.09	90.29	7.94	0.37	11.43	0.38	87.97	41.22

$Cr_2TiC_2O_2$	0.005	0.051	0.706	5.27	5.60	7.82	0.655	0.046	92.75	90.26	5.12	0.26	7.16	0.27	63.10	31.54
Cr_2TiCN	0.009	0.088	1.126	6.21	6.14	8.12	1.038	0.080	92.15	90.20	8.43	0.49	11.16	0.48	67.85	37.64
Cr_2TiCNO_2	0.006	0.060	0.901	6.41	6.35	9.64	0.841	0.054	93.34	90.33	8.11	0.34	12.30	0.34	96.46	40.31
$Cr_2V_2C_3$	0.005	0.054	0.649	4.64	4.85	5.76	0.594	0.049	91.63	90.08	3.42	0.24	4.06	0.25	33.72	23.67
Cr_2VC_2	0.003	0.032	0.349	2.46	2.58	2.82	0.316	0.029	90.70	90.06	0.89	0.08	0.98	0.08	8.06	6.67
Cr_2VCN	0.009	0.088	1.123	5.89	6.28	8.15	1.035	0.079	92.17	90.22	8.44	0.50	10.96	0.53	68.22	39.69
Cr_2VCNO_2	0.006	0.059	0.880	5.75	6.26	9.45	0.821	0.053	93.31	90.28	7.76	0.33	11.72	0.36	92.75	39.58
Cr_2ZrCN	0.006	0.058	0.698	4.99	5.02	6.17	0.639	0.052	91.67	90.19	3.94	0.26	4.85	0.26	38.83	25.19
Cr_2ZrCNO_2	0.004	0.046	0.638	5.74	5.77	8.20	0.593	0.041	92.84	90.28	4.86	0.24	6.91	0.24	69.53	33.32
Cr_3C_2	0.004	0.045	0.488	3.19	3.30	3.54	0.443	0.041	90.76	90.12	1.57	0.13	1.68	0.14	12.62	10.96
$Cr_3C_2(OH)_2$	0.003	0.033	0.368	4.23	4.14	4.75	0.336	0.029	91.13	90.09	1.59	0.12	1.83	0.12	22.85	17.08
$Cr_3C_2F_2$	0.002	0.023	0.256	3.02	2.96	3.30	0.233	0.021	90.95	90.19	0.77	0.06	0.85	0.06	11.01	8.77
$Cr_3C_2H_2$	0.003	0.033	0.377	3.45	3.66	4.14	0.344	0.030	91.24	90.16	1.42	0.11	1.61	0.12	17.35	13.46
$Cr_3C_2O_2$	0.003	0.031	0.352	3.59	3.57	4.24	0.321	0.028	91.31	90.06	1.36	0.10	1.62	0.10	18.35	12.74
Cr_3CN	0.008	0.083	1.037	5.79	6.01	7.64	0.954	0.075	92.01	90.20	7.29	0.45	9.28	0.47	59.81	36.24
Cr_3CNO_2	0.006	0.067	1.051	6.84	7.08	11.41	0.984	0.060	93.67	90.41	11.23	0.43	18.10	0.44	135.76	50.28
Cr_3N_2	0.002	0.023	0.246	2.22	2.32	2.48	0.223	0.020	90.74	89.98	0.55	0.05	0.59	0.05	6.18	5.43
$Cr_3N_2(OH)_2$	0.007	0.069	1.133	8.08	8.54	14.42	1.064	0.062	93.92	90.49	15.34	0.53	25.91	0.56	217.70	73.39
$Cr_3N_2H_2$	0.003	0.034	0.395	3.51	3.78	4.32	0.361	0.031	91.29	90.16	1.56	0.12	1.78	0.13	18.88	14.39
$Cr_3N_2O_2$	0.003	0.026	0.309	3.91	3.91	4.57	0.282	0.024	91.41	90.19	1.29	0.09	1.51	0.09	21.22	15.30
Cr_4C_3	0.004	0.039	0.430	3.55	3.49	3.93	0.391	0.035	90.90	90.08	1.54	0.12	1.73	0.12	15.65	12.19
$Cr_4C_3(OH)_2$	0.002	0.025	0.289	3.90	3.84	4.37	0.264	0.023	91.27	90.17	1.16	0.09	1.32	0.09	19.39	14.71
$Cr_4C_3F_2$	0.002	0.020	0.214	2.73	2.81	3.14	0.194	0.018	90.77	90.12	0.61	0.05	0.68	0.05	9.96	7.91
$Cr_4C_3H_2$	0.002	0.023	0.255	3.14	3.12	3.55	0.232	0.021	90.94	90.08	0.82	0.07	0.94	0.06	12.76	9.75
$Cr_4C_3O_2$	0.002	0.025	0.286	3.54	3.59	4.22	0.261	0.023	91.27	90.15	1.10	0.08	1.29	0.08	18.08	12.93
Cr_4N_3	0.002	0.024	0.252	2.29	2.30	2.41	0.228	0.022	90.31	90.06	0.55	0.05	0.58	0.05	5.84	5.28
$Cr_4N_3(OH)_2$	0.002	0.022	0.242	3.39	3.43	3.84	0.221	0.020	91.00	90.11	0.85	0.07	0.95	0.07	14.92	11.77
$Cr_4N_3F_2$	0.002	0.016	0.176	2.46	2.50	2.70	0.160	0.015	90.68	90.06	0.43	0.04	0.47	0.04	7.38	6.26
$Cr_4N_3H_2$	0.002	0.019	0.206	2.80	2.84	3.10	0.187	0.017	90.83	90.03	0.58	0.05	0.63	0.05	9.72	8.08
$Cr_4N_3O_2$	0.002	0.020	0.219	2.99	3.01	3.32	0.199	0.018	90.84	90.09	0.66	0.05	0.73	0.05	11.13	9.06
$CrMoCF_2$	0.003	0.032	0.343	2.67	2.72	2.98	0.312	0.029	90.78	90.14	0.93	0.08	1.02	0.08	8.99	7.44
$CrWCF_2$	0.002	0.024	0.261	2.78	2.96	3.34	0.237	0.021	90.97	90.08	0.79	0.06	0.89	0.07	11.32	8.83
Hf_2C	0.002	0.019	0.199	2.33	2.35	2.55	0.180	0.017	90.57	90.03	0.46	0.04	0.50	0.04	6.56	5.52
$Hf_2C(OH)_2$	0.001	0.015	0.162	2.94	2.90	3.31	0.147	0.013	90.91	90.14	0.49	0.04	0.56	0.04	11.14	8.42
Hf_2CF_2	0.001	0.013	0.146	2.48	2.45	2.65	0.132	0.012	90.81	90.03	0.35	0.03	0.38	0.03	7.07	5.99
Hf_2CF_2 -(model2)	0.002	0.015	0.164	2.54	2.57	2.79	0.149	0.014	90.78	90.06	0.42	0.03	0.45	0.04	7.85	6.60
Hf_2CF_2 -(model3)	0.002	0.021	0.217	2.51	2.44	2.58	0.196	0.019	90.48	90.10	0.51	0.05	0.54	0.04	6.72	5.93
Hf_2CF_2 -(model4)	0.002	0.018	0.191	2.42	2.43	2.56	0.173	0.016	90.58	90.04	0.44	0.04	0.47	0.04	6.58	5.90
Hf_2CO_2	0.002	0.019	0.209	2.98	3.13	3.44	0.190	0.017	90.90	90.02	0.65	0.05	0.72	0.06	11.97	9.86
Hf_2CO_2 -(model2)	0.001	0.012	0.134	2.33	2.47	2.65	0.122	0.011	90.80	90.22	0.32	0.03	0.35	0.03	7.08	6.13
Hf_2CO_2 -(model3)	0.002	0.019	0.203	2.58	2.55	2.71	0.184	0.017	90.51	90.02	0.50	0.04	0.53	0.04	7.41	6.50
Hf_2CO_2 -(model4)	0.002	0.022	0.228	2.87	2.76	2.95	0.207	0.019	90.56	90.01	0.61	0.05	0.65	0.05	8.76	7.61
Hf_2CrCN	0.002	0.022	0.250	3.37	3.65	4.11	0.228	0.020	91.04	90.09	0.94	0.07	1.05	0.08	17.13	13.45

Hf_2CrCNO_2	0.002	0.016	0.189	3.87	4.06	4.80	0.173	0.015	91.40	90.12	0.83	0.06	0.98	0.06	23.45	16.58
Hf_2MoCN	0.002	0.019	0.208	3.17	3.33	3.75	0.190	0.017	90.99	90.04	0.71	0.06	0.80	0.06	14.25	11.15
Hf_2MoCNO_2	0.001	0.015	0.169	3.74	4.07	4.73	0.154	0.013	91.32	90.17	0.73	0.05	0.85	0.06	22.71	16.75
Hf_2N	0.001	0.015	0.159	1.99	2.06	2.17	0.144	0.014	90.54	90.06	0.31	0.03	0.33	0.03	4.75	4.28
$Hf_2N(OH)_2$	0.001	0.014	0.158	3.09	3.23	3.66	0.144	0.013	90.98	90.13	0.53	0.04	0.60	0.04	13.58	10.48
Hf_2NbCN	0.002	0.019	0.207	3.16	3.35	3.74	0.188	0.017	90.91	90.15	0.70	0.06	0.78	0.06	14.16	11.32
Hf_2NbCNO_2	0.001	0.015	0.169	3.82	4.13	4.67	0.154	0.013	91.21	90.22	0.72	0.06	0.82	0.06	22.11	17.20
Hf_2NF_2	0.001	0.011	0.118	2.16	2.31	2.54	0.107	0.010	90.75	90.03	0.27	0.02	0.30	0.02	6.50	5.36
Hf_2NF_2 -(model2)	0.001	0.015	0.158	2.54	2.60	2.83	0.144	0.013	90.81	90.06	0.41	0.03	0.44	0.03	8.08	6.77
Hf_2NF_2 -(model4)	0.003	0.027	0.289	3.21	3.34	3.69	0.262	0.024	90.80	90.07	0.97	0.08	1.07	0.08	13.77	11.22
Hf_2NO_2	0.002	0.016	0.180	2.69	2.81	3.12	0.164	0.015	90.86	90.10	0.51	0.04	0.57	0.04	9.87	7.93
Hf_2TaCN	0.000	0.000	0.005	3.28	3.30	3.74	0.005	0.000	90.94	90.15	0.02	0.00	0.02	0.00	14.19	10.90
Hf_2TaCNO_2	0.000	0.000	0.005	4.09	4.13	4.78	0.004	0.000	91.25	90.14	0.02	0.00	0.02	0.00	23.19	17.09
Hf_2TiCN	0.002	0.022	0.241	3.51	3.41	3.92	0.219	0.020	91.01	90.06	0.86	0.07	0.99	0.06	15.63	11.57
Hf_2TiCNO_2	0.002	0.016	0.187	3.99	3.94	4.70	0.171	0.015	91.34	90.13	0.80	0.06	0.96	0.06	22.53	15.49
Hf_2VCN	0.002	0.021	0.236	3.40	3.49	3.86	0.215	0.019	90.93	90.15	0.83	0.07	0.92	0.07	15.06	12.21
Hf_2VCNO_2	0.002	0.016	0.187	4.02	3.98	4.67	0.170	0.015	91.33	90.16	0.80	0.06	0.93	0.06	22.22	15.86
Hf_2ZrCN	0.002	0.018	0.195	3.05	3.22	3.45	0.177	0.016	90.75	90.11	0.61	0.05	0.65	0.06	11.98	10.43
Hf_2ZrCNO_2	0.001	0.015	0.167	3.99	4.00	4.59	0.153	0.013	91.21	90.14	0.70	0.05	0.80	0.05	21.38	15.99
Hf_3C_2	0.002	0.015	0.166	3.00	3.02	3.32	0.151	0.014	90.70	90.03	0.50	0.04	0.55	0.04	11.15	9.15
$Hf_3C_2(OH)_2$	0.001	0.012	0.125	4.03	4.11	4.36	0.113	0.011	90.50	90.08	0.49	0.04	0.52	0.04	19.14	16.95
$Hf_3C_2F_2$	0.001	0.010	0.104	2.91	2.90	3.19	0.094	0.009	90.80	90.02	0.30	0.02	0.33	0.02	10.29	8.40
$Hf_3C_2H_2$	0.001	0.006	0.057	2.07	2.18	2.20	0.051	0.005	90.21	89.94	0.11	0.01	0.11	0.01	4.85	4.79
$Hf_3C_2O_2$	0.001	0.013	0.153	3.82	3.70	4.30	0.139	0.012	91.21	90.14	0.60	0.04	0.70	0.04	18.81	13.63
Hf_3CN	0.001	0.015	0.161	2.94	3.02	3.32	0.146	0.013	90.75	90.04	0.49	0.04	0.53	0.04	11.12	9.18
Hf_3CNO_2	0.001	0.014	0.169	3.93	4.05	4.74	0.154	0.013	91.44	90.18	0.73	0.05	0.86	0.05	22.82	16.42
Hf_3N_2	0.001	0.010	0.111	2.43	2.43	2.67	0.100	0.009	90.67	90.16	0.27	0.02	0.29	0.02	7.20	5.92
$Hf_3N_2(OH)_2$	0.001	0.012	0.122	4.54	4.50	4.76	0.110	0.010	90.48	90.06	0.52	0.05	0.55	0.05	22.79	20.25
$Hf_3N_2F_2$	0.001	0.008	0.085	2.95	2.85	3.12	0.077	0.007	90.72	90.04	0.24	0.02	0.26	0.02	9.82	8.10
$Hf_3N_2H_2$	0.001	0.006	0.066	2.58	2.57	2.68	0.060	0.006	90.38	90.12	0.16	0.01	0.17	0.01	7.24	6.58
$Hf_3N_2O_2$	0.001	0.012	0.129	3.42	3.43	3.88	0.117	0.010	91.04	90.21	0.46	0.04	0.51	0.04	15.25	11.78
Hf_4C_3	0.001	0.008	0.089	2.36	2.39	2.52	0.081	0.008	90.49	90.06	0.20	0.02	0.21	0.02	6.39	5.71
$Hf_4C_3(OH)_2$	0.001	0.009	0.100	3.28	3.20	3.54	0.091	0.008	90.82	90.17	0.32	0.03	0.35	0.03	12.63	10.20
$Hf_4C_3F_2$	0.001	0.008	0.086	3.07	2.99	3.27	0.078	0.007	90.76	90.08	0.25	0.02	0.28	0.02	10.79	8.89
$Hf_4C_3H_2$	0.001	0.005	0.054	2.41	2.51	2.61	0.049	0.005	90.30	90.19	0.13	0.01	0.13	0.01	6.83	6.32
$Hf_4C_3O_2$	0.001	0.011	0.131	3.85	3.94	4.58	0.119	0.010	91.46	90.23	0.55	0.04	0.64	0.04	21.31	15.55
Hf_4N_3	0.001	0.008	0.088	2.38	2.46	2.59	0.079	0.008	90.47	90.07	0.21	0.02	0.22	0.02	6.74	6.07
$Hf_4N_3(OH)_2$	0.001	0.008	0.088	3.66	3.61	4.01	0.080	0.007	90.63	90.07	0.32	0.03	0.36	0.03	16.30	13.04
$Hf_4N_3F_2$	0.001	0.007	0.071	2.62	2.72	2.98	0.064	0.006	90.65	90.09	0.19	0.02	0.21	0.02	8.95	7.45
$Hf_4N_3H_2$	0.000	0.005	0.049	2.31	2.30	2.45	0.044	0.004	90.39	90.05	0.11	0.01	0.11	0.01	6.03	5.28
$Hf_4N_3O_2$	0.001	0.009	0.106	3.48	3.44	3.92	0.096	0.008	91.15	90.12	0.38	0.03	0.43	0.03	15.56	11.84
$HfCrNO_2$	0.002	0.019	0.215	2.74	2.79	3.11	0.196	0.018	90.95	90.13	0.61	0.05	0.68	0.05	9.77	7.81
Mn_2C	0.005	0.050	0.538	2.34	2.45	2.69	0.488	0.045	90.65	90.18	1.31	0.11	1.44	0.12	7.29	6.01

$Mn_2C(OH)_2$	0.004	0.038	0.425	3.08	3.10	3.55	0.388	0.034	91.17	90.14	1.38	0.11	1.58	0.11	12.80	9.64
Mn_2CF_2	0.003	0.028	0.304	2.28	2.33	2.54	0.276	0.025	90.72	90.01	0.70	0.06	0.77	0.06	6.53	5.44
Mn_2CO_2	0.004	0.037	0.414	2.97	2.90	3.16	0.377	0.034	90.98	90.09	1.19	0.10	1.30	0.10	10.06	8.39
Mn_2N	0.003	0.029	0.301	1.73	1.89	2.03	0.273	0.026	90.55	90.12	0.55	0.05	0.60	0.05	4.15	3.59
$Mn_2N(OH)_2$	0.003	0.032	0.357	2.66	2.69	2.96	0.325	0.029	90.92	90.02	0.96	0.08	1.06	0.08	8.85	7.22
Mn_2NF_2	0.003	0.025	0.270	2.03	2.09	2.23	0.245	0.023	90.57	90.14	0.54	0.05	0.58	0.05	5.00	4.38
Mn_2NO_2	0.003	0.032	0.356	2.70	2.74	2.94	0.323	0.029	90.89	90.02	0.95	0.08	1.02	0.08	8.70	7.52
Mn_3C_2	0.004	0.044	0.477	3.23	3.27	3.61	0.433	0.040	90.76	90.11	1.56	0.13	1.73	0.13	13.20	10.68
$Mn_3C_2(OH)_2$	0.003	0.033	0.369	4.23	4.47	5.15	0.336	0.029	91.17	90.24	1.73	0.13	2.00	0.14	26.97	20.15
$Mn_3C_2F_2$	0.002	0.022	0.245	3.03	2.86	3.27	0.223	0.020	91.02	90.19	0.73	0.06	0.84	0.05	10.85	8.10
$Mn_3C_2O_2$	0.003	0.029	0.336	3.72	3.68	4.20	0.306	0.026	91.31	90.15	1.29	0.10	1.46	0.10	17.85	13.56
Mn_3N_2	0.003	0.033	0.344	2.48	2.42	2.57	0.311	0.029	90.49	90.08	0.80	0.07	0.85	0.07	6.66	5.83
$Mn_3N_2(OH)_2$	0.003	0.029	0.315	4.28	4.32	4.63	0.286	0.026	90.92	90.11	1.32	0.11	1.42	0.11	21.61	18.64
$Mn_3N_2F_2$	0.002	0.019	0.210	2.54	2.54	2.84	0.191	0.017	90.84	90.02	0.54	0.04	0.60	0.04	8.15	6.46
Mn_4C_3	0.004	0.038	0.415	3.49	3.53	3.93	0.377	0.034	90.90	90.09	1.48	0.12	1.65	0.12	15.64	12.46
$Mn_4C_3(OH)_2$	0.002	0.025	0.290	4.14	4.18	4.91	0.265	0.022	91.44	90.15	1.30	0.09	1.54	0.09	24.56	17.45
$Mn_4C_3F_2$	0.002	0.018	0.196	2.93	2.91	3.22	0.178	0.016	90.86	90.12	0.57	0.05	0.64	0.05	10.49	8.45
$Mn_4C_3O_2$	0.002	0.023	0.263	3.43	3.51	3.90	0.239	0.021	91.10	90.20	0.93	0.07	1.04	0.08	15.41	12.34
Mn_4N_3	0.002	0.019	0.205	2.47	2.60	2.80	0.186	0.017	90.66	90.16	0.52	0.04	0.56	0.05	7.92	6.81
$Mn_4N_3(OH)_2$	0.002	0.022	0.252	3.97	3.87	4.52	0.229	0.020	91.21	90.18	1.04	0.08	1.21	0.08	20.80	14.97
$Mn_4N_3O_2$	0.002	0.019	0.206	2.86	2.98	3.30	0.187	0.017	90.85	90.07	0.62	0.05	0.69	0.05	11.03	8.91
$Mo_{1.33}C$	0.007	0.074	0.766	3.73	3.75	3.89	0.692	0.066	90.38	90.06	2.69	0.25	2.78	0.25	15.15	14.11
Mo_2C	0.004	0.037	0.396	2.81	2.82	3.00	0.359	0.033	90.66	90.04	1.08	0.09	1.15	0.09	9.08	7.96
$Mo_2C(NCS)_2$	0.019	0.206	1.839	20.37	22.92	20.99	1.633	0.188	88.77	91.00	34.26	4.31	31.38	4.85	435.84	531.94
$Mo_2C(OCN)_2$	0.005	0.048	0.704	6.06	6.21	9.08	0.656	0.043	93.20	90.35	5.96	0.27	8.72	0.28	85.37	38.63
$Mo_2C(OH)_2$	0.002	0.025	0.277	2.74	2.79	3.12	0.252	0.023	90.97	90.09	0.79	0.06	0.88	0.06	9.84	7.83
$Mo_2C(SCN)_2$	0.006	0.064	0.902	8.65	8.62	12.38	0.838	0.058	92.86	90.39	10.38	0.50	14.90	0.50	158.61	74.32
Mo_2CBr_2	0.005	0.054	0.851	7.02	6.94	11.13	0.797	0.049	93.69	90.39	8.88	0.34	14.24	0.33	129.24	48.15
Mo_2CCl_2	0.005	0.055	0.768	5.49	5.50	7.80	0.713	0.050	92.83	90.29	5.56	0.27	7.89	0.27	62.88	30.20
Mo_2CF_2	0.002	0.023	0.250	2.34	2.33	2.51	0.227	0.021	90.68	90.03	0.57	0.05	0.61	0.05	6.36	5.41
Mo_2CF_2 -(model4)	0.004	0.039	0.425	3.18	3.23	3.53	0.385	0.035	90.74	90.12	1.36	0.11	1.49	0.12	12.62	10.44
Mo_2CO_2	0.002	0.025	0.288	3.31	3.19	3.73	0.262	0.023	91.20	90.18	0.98	0.07	1.14	0.07	14.14	10.12
Mo_2CO_2 -(model4)	0.003	0.025	0.276	2.88	2.73	2.99	0.251	0.023	90.86	90.10	0.75	0.06	0.82	0.06	9.00	7.43
Mo_2CrCN	0.005	0.048	0.573	4.84	5.02	6.17	0.525	0.043	91.69	90.21	3.24	0.22	3.98	0.22	38.89	25.34
Mo_2CrCNO_2	0.003	0.034	0.444	5.00	4.91	6.68	0.410	0.030	92.38	90.27	2.74	0.15	3.72	0.15	46.01	24.11
Mo_2CS_2	0.011	0.122	2.026	11.26	12.42	20.74	1.903	0.111	93.97	90.81	39.49	1.38	65.95	1.52	449.68	155.91
$Mo_2Hf_2C_3O_2$	0.001	0.012	0.133	3.74	3.83	4.39	0.121	0.010	91.24	90.06	0.53	0.04	0.61	0.04	19.54	14.69
Mo_2HfC_2	0.001	0.013	0.133	2.15	2.02	2.19	0.120	0.011	90.52	90.07	0.26	0.02	0.28	0.02	4.83	4.06
$Mo_2HfC_2O_2$	0.002	0.017	0.200	3.93	4.11	4.81	0.183	0.016	91.34	90.22	0.88	0.06	1.03	0.07	23.48	16.95
Mo_2HfCN	0.003	0.025	0.291	3.91	3.94	4.46	0.266	0.023	91.25	90.17	1.19	0.09	1.34	0.09	20.16	15.56
Mo_2HfCNO_2	0.002	0.022	0.277	4.52	4.60	5.80	0.255	0.020	92.01	90.25	1.48	0.09	1.86	0.09	34.40	21.24
Mo_2N	0.002	0.024	0.259	2.37	2.31	2.51	0.235	0.022	90.63	90.02	0.59	0.05	0.64	0.05	6.35	5.32
$Mo_2N(OH)_2$	0.003	0.028	0.331	4.26	4.40	5.36	0.303	0.025	91.47	90.15	1.62	0.11	1.98	0.12	29.38	19.44

$Mo_2Nb_2C_3$	0.002	0.025	0.278	3.50	3.69	4.15	0.254	0.022	91.17	90.13	1.05	0.08	1.18	0.09	17.42	13.70
Mo_2NbC_2	0.002	0.016	0.174	2.09	2.22	2.36	0.158	0.015	90.60	90.03	0.37	0.03	0.40	0.03	5.62	4.98
Mo_2NbCN	0.003	0.034	0.400	4.26	4.33	5.09	0.366	0.031	91.41	90.12	1.86	0.13	2.19	0.14	26.39	18.78
Mo_2NbCNO_2	0.003	0.028	0.361	4.74	4.87	6.30	0.333	0.025	92.19	90.28	2.10	0.12	2.72	0.13	40.67	23.74
Mo_2NF_2	0.002	0.017	0.188	2.72	2.79	3.09	0.171	0.015	91.01	89.97	0.53	0.04	0.59	0.04	9.67	7.81
Mo_2NO_2	0.002	0.022	0.256	3.01	3.01	3.49	0.233	0.020	91.20	90.14	0.81	0.06	0.94	0.06	12.35	9.07
Mo_2ScC_2	0.002	0.020	0.214	2.17	2.24	2.39	0.194	0.018	90.64	90.07	0.46	0.04	0.49	0.04	5.74	5.03
$Mo_2ScC_2O_2$	0.002	0.024	0.275	3.97	4.04	4.72	0.251	0.022	91.31	90.21	1.19	0.09	1.39	0.09	22.65	16.37
$Mo_2Ta_2C_3$	0.000	0.000	0.003	3.31	3.41	3.81	0.003	0.000	91.07	90.08	0.01	0.00	0.01	0.00	14.68	11.65
Mo_2TaC_2	0.000	0.000	0.003	2.10	2.11	2.25	0.003	0.000	90.60	90.12	0.01	0.00	0.01	0.00	5.09	4.44
Mo_2TaCN	0.000	0.001	0.007	4.24	4.15	4.90	0.006	0.001	91.35	90.22	0.03	0.00	0.04	0.00	24.40	17.21
Mo_2TaCNO_2	0.000	0.001	0.007	4.55	4.54	5.94	0.006	0.000	92.09	90.14	0.04	0.00	0.05	0.00	36.30	20.65
$Mo_2Ti_2C_3$	0.003	0.035	0.409	4.22	4.13	4.89	0.374	0.032	91.40	90.06	1.83	0.13	2.17	0.13	24.36	17.02
$Mo_2Ti_2C_3(OH)_{1.5}F_{0.5}$	0.003	0.027	0.348	5.03	5.19	6.64	0.321	0.025	92.20	90.32	2.13	0.13	2.72	0.13	45.15	27.02
$Mo_2Ti_2C_3O_{1.5}F_{0.5}$	0.002	0.022	0.261	3.98	3.87	4.69	0.239	0.020	91.56	90.13	1.12	0.08	1.36	0.07	22.40	14.94
$Mo_2Ti_2C_3O_2$	0.002	0.020	0.229	3.62	3.87	4.45	0.209	0.018	91.31	90.23	0.93	0.07	1.07	0.07	20.13	15.07
Mo_2TiC_2	0.002	0.020	0.214	2.34	2.30	2.48	0.194	0.018	90.61	90.00	0.48	0.04	0.52	0.04	6.20	5.26
$Mo_2TiC_2(O_{1.5}F_{0.5})$	0.004	0.039	0.319	6.26	6.22	5.08	0.280	0.035	87.88	89.92	1.42	0.22	1.16	0.22	25.21	38.70
$Mo_2TiC_2(OH)_2$	0.003	0.032	0.386	5.02	5.43	6.65	0.354	0.029	91.78	90.08	2.36	0.16	2.88	0.17	45.15	29.79
$Mo_2TiC_2F_2$	0.004	0.041	0.523	5.06	5.04	6.52	0.482	0.037	92.22	90.16	3.14	0.19	4.06	0.18	43.54	25.41
$Mo_2TiC_2O_2$	0.002	0.025	0.297	3.98	4.06	4.87	0.271	0.023	91.47	90.25	1.32	0.09	1.59	0.09	24.22	16.52
Mo_2TiCN	0.004	0.045	0.536	4.45	4.68	5.67	0.491	0.041	91.54	90.23	2.78	0.19	3.37	0.20	32.77	21.99
Mo_2TiCNO_2	0.003	0.033	0.428	4.98	4.97	6.32	0.395	0.030	92.23	90.32	2.50	0.15	3.18	0.15	40.92	24.70
$Mo_2V_2C_3$	0.003	0.035	0.399	3.93	4.15	4.90	0.365	0.031	91.34	90.14	1.79	0.13	2.11	0.14	24.39	17.31
Mo_2VC_2	0.002	0.020	0.212	2.34	2.30	2.50	0.192	0.018	90.66	89.99	0.48	0.04	0.52	0.04	6.28	5.29
Mo_2VCN	0.004	0.045	0.532	4.46	4.71	5.64	0.487	0.040	91.58	90.08	2.75	0.19	3.29	0.20	32.39	22.29
Mo_2VCNO_2	0.003	0.033	0.422	4.84	4.95	6.31	0.389	0.030	92.21	90.18	2.45	0.15	3.13	0.15	40.78	24.57
$Mo_2Zr_2C_3O_2$	0.002	0.016	0.183	3.64	3.68	4.36	0.167	0.014	91.24	90.11	0.73	0.05	0.86	0.05	19.36	13.57
Mo_2ZrC_2	0.002	0.016	0.172	2.11	2.09	2.26	0.156	0.015	90.58	90.03	0.35	0.03	0.38	0.03	5.13	4.35
$Mo_2ZrC_2O_2$	0.002	0.024	0.285	4.16	4.11	4.95	0.261	0.022	91.58	90.17	1.29	0.09	1.55	0.09	24.95	16.91
Mo_2ZrCN	0.003	0.034	0.387	4.14	4.10	4.70	0.354	0.030	91.29	90.16	1.66	0.12	1.90	0.12	22.36	16.76
Mo_2ZrCNO_2	0.003	0.028	0.355	4.65	4.74	5.99	0.327	0.025	92.10	90.24	1.96	0.12	2.47	0.12	36.76	22.55
Mo_3C_2	0.003	0.027	0.301	3.76	3.58	4.09	0.274	0.024	91.02	90.07	1.12	0.09	1.28	0.08	16.99	12.76
$Mo_3C_2(OH)_2$	0.003	0.029	0.304	7.66	7.34	7.80	0.276	0.026	90.50	90.18	2.15	0.19	2.28	0.18	61.27	53.65
$Mo_3C_2F_2$	0.001	0.015	0.164	3.67	3.74	4.12	0.149	0.013	90.92	90.03	0.62	0.05	0.68	0.05	17.14	14.05
$Mo_3C_2H_2$	0.002	0.021	0.231	3.66	3.72	4.24	0.210	0.018	91.12	90.20	0.89	0.07	1.02	0.07	18.23	13.90
$Mo_3C_2O_2$	0.002	0.023	0.275	4.79	4.76	5.83	0.252	0.021	91.73	90.21	1.47	0.10	1.80	0.10	34.74	22.68
Mo_3CN	0.003	0.034	0.387	4.03	4.16	4.77	0.353	0.030	91.27	90.17	1.68	0.13	1.93	0.13	23.04	17.32
Mo_3N_2	0.002	0.017	0.187	2.67	2.77	3.03	0.170	0.015	90.85	90.13	0.51	0.04	0.56	0.04	9.29	7.69
$Mo_3N_2(OH)_2$	0.003	0.030	0.309	7.95	8.13	8.53	0.279	0.027	90.39	90.14	2.38	0.22	2.50	0.22	73.15	66.30
$Mo_3N_2F_2$	0.001	0.013	0.142	3.54	3.62	3.97	0.129	0.012	90.79	90.02	0.51	0.04	0.56	0.04	15.95	13.12
$Mo_3N_2H_2$	0.002	0.016	0.178	2.96	2.91	3.35	0.162	0.014	91.02	90.08	0.54	0.04	0.63	0.04	11.38	8.47
$Mo_3N_2O_2$	0.002	0.018	0.200	4.24	4.34	4.91	0.182	0.016	91.10	90.32	0.89	0.07	1.01	0.07	24.46	18.91

Mo_4C_3	0.003	0.027	0.302	3.79	3.80	4.45	0.276	0.024	91.19	90.08	1.23	0.09	1.44	0.09	20.13	14.46
$Mo_4C_3(OH)_2$	0.002	0.016	0.176	3.68	3.89	4.43	0.160	0.014	90.99	90.13	0.71	0.06	0.81	0.06	19.93	15.26
$Mo_4C_3F_2$	0.001	0.013	0.140	2.91	2.91	3.26	0.127	0.012	90.81	90.13	0.41	0.03	0.46	0.03	10.74	8.48
$Mo_4C_3O_2$	0.002	0.017	0.194	3.65	3.73	4.41	0.178	0.015	91.37	90.18	0.78	0.06	0.93	0.06	19.80	13.97
Mo_4N_3	0.002	0.016	0.169	2.70	2.77	3.01	0.153	0.014	90.61	90.12	0.46	0.04	0.50	0.04	9.17	7.70
$Mo_4N_3(OH)_2$	0.001	0.014	0.151	3.27	3.16	3.50	0.137	0.012	90.80	90.16	0.48	0.04	0.53	0.04	12.37	9.97
$Mo_4N_3F_2$	0.001	0.012	0.131	2.58	2.57	2.80	0.118	0.011	90.56	90.17	0.33	0.03	0.36	0.03	7.88	6.61
$Mo_4N_3H_2$	0.001	0.009	0.094	2.40	2.46	2.71	0.085	0.008	90.69	90.04	0.23	0.02	0.25	0.02	7.40	6.09
$Mo_4N_3O_2$	0.002	0.016	0.169	3.13	3.05	3.31	0.154	0.014	90.80	90.12	0.51	0.04	0.55	0.04	11.08	9.30
MoCrC	0.003	0.032	0.339	1.91	1.88	2.04	0.307	0.029	90.52	89.99	0.63	0.05	0.68	0.05	4.21	3.52
$MoCrCO_2$ -(model4)	0.003	0.033	0.370	3.09	3.03	3.38	0.337	0.030	90.96	90.09	1.14	0.09	1.27	0.09	11.53	9.18
MoWC	0.002	0.018	0.185	1.91	1.86	1.99	0.167	0.016	90.49	90.08	0.33	0.03	0.35	0.03	3.98	3.45
$MoWC(NCO)_2$	0.003	0.034	0.466	5.56	5.48	7.77	0.432	0.030	92.77	90.29	3.36	0.17	4.76	0.16	62.41	29.98
$MoWC(OCN)_2$	0.004	0.037	0.549	5.88	6.07	9.12	0.512	0.034	93.24	90.37	4.67	0.20	7.01	0.21	86.34	36.99
$MoWC(SCN)_2$	0.005	0.049	0.721	8.05	8.18	12.44	0.672	0.044	93.21	90.47	8.35	0.36	12.71	0.37	160.80	67.01
$MoWCCl_2$	0.005	0.051	0.787	6.41	6.58	10.11	0.736	0.046	93.48	90.31	7.44	0.31	11.42	0.31	106.12	43.45
$MoWCF_2$	0.001	0.014	0.134	0.90	0.92	0.91	0.120	0.012	89.78	89.97	0.11	0.01	0.11	0.01	0.83	0.85
$MoWCO_2$-(model2)	0.002	0.020	0.217	3.06	3.09	3.42	0.198	0.018	91.00	90.11	0.68	0.05	0.75	0.05	11.80	9.55
$Nb_{0.4}V_{1.6}C$	0.073	0.674	4.559	25.56	24.65	16.92	3.885	0.601	85.22	89.20	65.75	14.82	45.14	14.29	271.61	605.05
$Nb_{0.8}V_{1.2}C$	0.022	0.208	1.747	8.77	8.42	7.34	1.539	0.186	88.08	89.56	11.30	1.57	9.84	1.51	52.97	70.65
$Nb_{1.2}V_{0.8}C$	0.011	0.111	1.180	5.11	5.01	5.37	1.069	0.100	90.58	90.07	5.74	0.50	6.14	0.49	29.02	25.08
$Nb_{1.33}C$	2.005	3.362	5.520	934.14	160.61	26.48	2.158	1.357	39.09	40.37	57.15	218.01	9.42	37.48	304.79	11603.47
$Nb_{1.6}V_{0.4}C$	0.007	0.069	0.707	3.42	3.37	3.46	0.638	0.062	90.25	90.16	2.21	0.21	2.27	0.21	12.02	11.35
Nb_2C	0.004	0.036	0.387	2.47	2.51	2.72	0.351	0.033	90.64	90.08	0.96	0.08	1.04	0.08	7.48	6.33
$Nb_2C(OH)_2$	0.003	0.026	0.283	2.90	2.99	3.40	0.257	0.023	90.95	90.01	0.88	0.07	1.00	0.07	11.75	8.99
Nb_2CF_2	0.002	0.022	0.243	2.22	2.43	2.64	0.221	0.020	90.75	90.03	0.58	0.05	0.63	0.05	7.05	5.97
Nb_2CO_2	0.003	0.030	0.328	3.13	2.94	3.33	0.298	0.027	90.90	90.02	0.99	0.08	1.12	0.07	11.22	8.57
Nb_2CrCN	0.005	0.049	0.588	5.01	4.98	6.01	0.539	0.045	91.60	90.19	3.24	0.22	3.91	0.22	36.79	24.80
Nb_2CrCNO_2	0.003	0.031	0.396	4.89	4.88	6.47	0.365	0.028	92.18	90.22	2.36	0.14	3.14	0.14	43.08	23.80
Nb_2HfCN	0.003	0.027	0.302	3.71	3.91	4.49	0.275	0.024	91.14	90.17	1.23	0.09	1.41	0.10	20.41	15.39
Nb_2HfCNO_2	0.002	0.020	0.240	4.54	4.44	5.49	0.220	0.018	91.65	90.27	1.21	0.08	1.49	0.08	30.84	19.63
Nb_2MoCN	0.004	0.038	0.443	4.32	4.45	5.25	0.405	0.034	91.39	90.16	2.13	0.15	2.51	0.16	28.00	19.84
Nb_2MoCNO_2	0.003	0.026	0.319	4.52	4.65	5.95	0.293	0.023	91.94	90.17	1.74	0.11	2.23	0.11	36.25	21.67
Nb_2N	0.003	0.029	0.305	2.08	2.09	2.27	0.276	0.026	90.54	90.04	0.63	0.05	0.68	0.05	5.22	4.37
$Nb_2N(OH)_2$	0.003	0.027	0.305	3.77	3.80	4.43	0.278	0.024	91.25	90.08	1.23	0.09	1.44	0.09	19.96	14.47
Nb_2NF_2	0.002	0.018	0.197	2.46	2.61	2.88	0.179	0.016	90.86	90.00	0.51	0.04	0.57	0.04	8.39	6.83
Nb_2NH_2	0.002	0.018	0.189	1.73	1.65	1.76	0.171	0.016	90.34	90.07	0.30	0.03	0.32	0.03	3.12	2.73
Nb_2NO_2	0.003	0.027	0.299	2.64	2.78	3.12	0.271	0.025	90.87	90.19	0.85	0.07	0.95	0.07	9.86	7.78
$Nb_2Ta_2C_3$	0.000	0.000	0.003	3.42	3.49	3.93	0.003	0.000	91.06	90.12	0.01	0.00	0.01	0.00	15.66	12.22
Nb_2TaCN	0.000	0.001	0.007	4.20	4.31	5.08	0.007	0.001	91.40	90.09	0.03	0.00	0.04	0.00	26.24	18.65
Nb_2TaCNO_2	0.000	0.000	0.006	4.54	4.70	5.80	0.005	0.000	91.90	90.24	0.03	0.00	0.04	0.00	34.30	22.16
Nb_2TiCN	0.005	0.047	0.548	4.56	4.63	5.60	0.501	0.042	91.50	90.12	2.81	0.19	3.40	0.20	32.00	21.44
Nb_2TiCNO_2	0.003	0.030	0.383	4.69	5.02	6.40	0.353	0.027	92.06	90.15	2.26	0.14	2.88	0.15	42.02	25.41

Nb_2VCN	0.004	0.046	0.536	4.66	4.61	5.54	0.491	0.041	91.45	90.20	2.72	0.19	3.27	0.19	31.28	21.21
Nb_2VCNO_2	0.003	0.030	0.378	4.81	4.90	6.27	0.348	0.027	92.02	90.20	2.18	0.13	2.79	0.14	40.27	24.11
$Nb_2W_2C_3$	0.002	0.019	0.213	3.84	3.88	4.53	0.194	0.017	91.24	90.11	0.88	0.07	1.03	0.07	20.88	15.05
$Nb_2Zr_2C_3$	0.003	0.025	0.280	3.49	3.56	3.97	0.255	0.023	91.04	90.03	1.01	0.08	1.13	0.08	15.95	12.73
Nb_2ZrCN	0.004	0.035	0.406	4.26	4.18	4.71	0.371	0.032	91.28	90.11	1.75	0.13	1.96	0.13	22.42	17.46
Nb_2ZrCNO_2	0.002	0.025	0.295	4.51	4.50	5.43	0.271	0.022	91.65	90.11	1.47	0.10	1.77	0.10	30.10	20.27
Nb_3C_2	0.003	0.030	0.333	3.27	3.30	3.68	0.303	0.027	90.91	90.19	1.12	0.09	1.24	0.09	13.71	10.89
$Nb_3C_2(OH)_2$	0.002	0.022	0.236	4.67	4.50	4.87	0.214	0.020	90.69	90.04	1.04	0.09	1.13	0.09	23.91	20.19
$Nb_3C_2F_2$	0.002	0.016	0.181	2.89	3.06	3.42	0.165	0.015	90.90	90.20	0.56	0.05	0.63	0.05	11.86	9.43
$Nb_3C_2H_2$	0.001	0.014	0.146	2.93	2.82	2.98	0.133	0.012	90.59	89.99	0.39	0.03	0.42	0.03	8.91	7.90
$Nb_3C_2O_2$	0.002	0.023	0.266	3.65	3.87	4.43	0.243	0.021	91.31	90.15	1.08	0.08	1.23	0.09	19.90	15.06
Nb_3CN	0.003	0.035	0.401	3.95	4.03	4.62	0.365	0.032	91.15	90.19	1.69	0.13	1.93	0.13	21.63	16.26
Nb_3CNO_2	0.003	0.026	0.320	4.99	4.76	6.06	0.295	0.023	91.93	90.23	1.79	0.11	2.28	0.11	37.69	22.58
Nb_3N_2	0.002	0.018	0.192	2.56	2.62	2.88	0.175	0.016	90.81	90.11	0.50	0.04	0.55	0.04	8.35	6.89
$Nb_3N_2(OH)_2$	0.003	0.027	0.285	6.93	7.08	7.46	0.257	0.025	90.36	90.12	1.92	0.18	2.02	0.18	55.93	50.30
$Nb_3N_2F_2$	0.001	0.014	0.149	3.59	3.53	3.79	0.135	0.012	90.75	90.07	0.51	0.04	0.55	0.04	14.46	12.43
$Nb_3N_2H_2$	0.001	0.015	0.158	2.90	2.99	3.33	0.143	0.013	90.77	90.02	0.48	0.04	0.53	0.04	11.18	8.95
$Nb_3N_2O_2$	0.002	0.019	0.218	3.56	3.57	4.13	0.198	0.018	91.07	90.20	0.82	0.06	0.95	0.06	17.29	12.74
Nb_4C_3	0.002	0.023	0.256	3.36	3.38	3.74	0.233	0.021	91.00	90.16	0.87	0.07	0.96	0.07	14.12	11.45
$Nb_4C_3(OH)_2$	0.002	0.018	0.199	4.87	4.89	5.48	0.181	0.017	90.81	90.24	0.99	0.08	1.11	0.08	30.36	23.96
$Nb_4C_3F_2$	0.001	0.013	0.135	3.37	3.19	3.50	0.123	0.011	90.72	90.10	0.43	0.04	0.47	0.03	12.34	10.13
$Nb_4C_3H_2$	0.001	0.011	0.112	2.66	2.66	2.85	0.101	0.010	90.54	90.15	0.29	0.03	0.31	0.03	8.16	7.10
$Nb_4C_3O_2$	0.002	0.018	0.206	3.65	3.80	4.45	0.189	0.016	91.36	90.09	0.84	0.06	0.98	0.06	20.09	14.48
Nb_4N_3	0.002	0.017	0.183	2.70	2.66	2.84	0.166	0.016	90.52	90.02	0.47	0.04	0.50	0.04	8.13	7.05
$Nb_4N_3(OH)_2$	0.001	0.014	0.157	3.42	3.46	3.78	0.143	0.013	90.82	90.11	0.54	0.04	0.59	0.05	14.42	11.97
$Nb_4N_3F_2$	0.001	0.012	0.128	2.75	2.68	2.89	0.116	0.011	90.58	90.08	0.34	0.03	0.36	0.03	8.41	7.18
$Nb_4N_3O_2$	0.002	0.016	0.180	3.34	3.40	3.82	0.164	0.014	91.07	90.15	0.62	0.05	0.70	0.05	14.74	11.60
$Nb_5C_4(OH)_2$	0.002	0.017	0.185	6.37	6.17	6.63	0.167	0.016	90.59	90.15	1.11	0.10	1.19	0.09	44.33	37.92
$Nb_5C_4F_2$	0.001	0.010	0.106	3.25	3.20	3.45	0.096	0.009	90.72	90.13	0.33	0.03	0.36	0.03	11.97	10.24
$Nb_5C_4O_2$	0.001	0.013	0.156	3.91	3.92	4.59	0.143	0.012	91.40	90.22	0.66	0.05	0.77	0.05	21.45	15.38
$NbCrN(NCO)_2$	0.006	0.059	0.930	6.62	7.31	11.66	0.871	0.054	93.64	90.42	10.15	0.39	16.18	0.43	141.59	54.06
$NbCrN(NCS)_2$	0.042	0.540	2.016	41.54	52.48	20.56	1.475	0.498	73.19	92.14	30.33	26.13	11.88	33.01	345.56	2817.65
$NbCrN(OCN)_2$	0.006	0.057	0.865	6.27	6.37	9.59	0.807	0.052	93.37	90.37	7.75	0.33	11.67	0.34	95.49	40.65
$NbCrN(SCN)_2$	0.007	0.077	1.124	8.97	9.24	13.54	1.047	0.070	93.16	90.48	14.18	0.64	20.77	0.66	189.72	85.65
$NbCrNBr_2$	0.007	0.076	1.393	8.17	8.71	16.46	1.317	0.069	94.53	90.49	21.68	0.60	40.95	0.64	285.49	76.40
$NbCrNCl_2$	0.008	0.082	1.297	6.52	6.97	11.15	1.215	0.075	93.64	90.38	13.54	0.52	21.66	0.56	129.52	48.94
$NbCrNF_2$	0.003	0.033	0.360	3.10	2.85	3.10	0.327	0.030	90.81	90.04	1.01	0.08	1.10	0.08	9.70	8.04
$NbMoN(NCO)_2$	0.004	0.042	0.565	5.25	5.18	7.15	0.523	0.038	92.58	90.34	3.74	0.20	5.16	0.19	52.70	26.79
$NbMoN(NCS)_2$	0.018	0.201	1.877	19.67	22.32	21.49	1.676	0.183	89.30	91.06	36.00	4.08	34.66	4.63	459.60	504.92
$NbMoN(OCN)_2$	0.003	0.028	0.287	6.05	6.16	6.30	0.258	0.025	90.15	90.08	1.63	0.16	1.67	0.16	39.85	37.96
$NbMoN(SCN)_2$	0.006	0.067	0.959	8.75	9.13	13.27	0.892	0.060	93.05	90.47	11.84	0.55	17.21	0.57	182.31	83.74
$NbMoNBr_2$	0.006	0.062	1.092	7.48	7.73	13.78	1.029	0.056	94.30	90.40	14.18	0.43	25.28	0.45	199.22	59.94
$NbMoNCl_2$	0.006	0.065	0.959	5.84	6.22	9.42	0.895	0.059	93.24	90.34	8.42	0.36	12.75	0.39	92.12	38.97

$NbMoN(CN)_2$	0.004	0.036	0.433	3.74	4.05	4.88	0.396	0.033	91.61	90.13	1.94	0.13	2.33	0.14	24.31	16.57
$NbMoNF_2$	0.003	0.030	0.322	2.93	2.88	3.22	0.292	0.027	90.80	90.17	0.94	0.08	1.05	0.08	10.48	8.30
$NbWN(NCO)_2$	0.003	0.033	0.448	5.18	5.41	7.40	0.415	0.030	92.68	90.29	3.07	0.16	4.20	0.17	56.39	29.39
$NbWN(NCS)_2$	0.014	0.160	1.490	20.02	22.74	21.48	1.330	0.146	89.28	91.11	28.57	3.31	26.99	3.76	458.24	523.91
$NbWN(OCN)_2$	0.003	0.036	0.518	5.79	5.82	8.58	0.482	0.032	93.09	90.29	4.14	0.19	6.11	0.19	76.38	33.88
$NbWN(SCN)_2$	0.005	0.050	0.761	8.23	8.38	13.16	0.711	0.045	93.42	90.43	9.36	0.38	14.69	0.39	180.32	70.37
$NbWNBr_2$	0.005	0.052	0.922	7.79	8.03	14.75	0.871	0.047	94.41	90.50	12.84	0.37	23.58	0.39	228.75	64.70
$NbWNCl_2$	0.005	0.050	0.747	5.83	6.44	9.68	0.697	0.045	93.35	90.22	6.75	0.29	10.15	0.32	97.20	41.91
$NbWN(CN)_2$	0.002	0.025	0.278	3.20	3.29	3.67	0.253	0.023	91.00	90.15	0.93	0.07	1.03	0.08	13.63	10.85
$NbWNF_2$	0.002	0.023	0.245	2.89	2.79	3.06	0.223	0.021	90.73	90.12	0.68	0.06	0.75	0.06	9.45	7.77
Sc_2C	0.005	0.048	0.503	1.59	1.70	1.79	0.455	0.043	90.48	90.01	0.82	0.07	0.86	0.08	3.23	2.92
$Sc_2C(CN)_2$	0.005	0.056	0.606	2.84	2.93	3.25	0.550	0.050	90.82	90.12	1.79	0.15	1.98	0.15	10.67	8.64
$Sc_2C(NCO)_2$	0.006	0.062	0.809	5.28	5.44	7.27	0.747	0.056	92.36	90.23	5.43	0.30	7.26	0.31	54.32	29.66
$Sc_2C(NCS)_2$	0.034	0.379	2.485	25.97	29.19	19.75	2.105	0.345	84.74	91.00	41.57	10.07	28.13	11.32	368.42	862.38
$Sc_2C(OCI)_2$	0.009	0.095	1.569	7.28	7.29	12.18	1.474	0.086	93.96	90.37	17.95	0.62	29.97	0.63	154.95	53.17
$Sc_2C(OCN)_2$	0.007	0.069	0.966	5.97	6.45	9.26	0.897	0.063	92.83	90.26	8.31	0.40	11.93	0.44	88.77	41.95
$Sc_2C(OH)_2$	0.004	0.039	0.427	2.61	2.66	2.91	0.388	0.035	90.87	90.04	1.13	0.09	1.24	0.10	8.56	7.10
$Sc_2C(SCN)_2$	0.008	0.080	1.107	6.79	6.67	9.55	1.027	0.072	92.80	90.42	9.81	0.48	14.04	0.47	94.35	44.43
Sc_2CBr_2	0.006	0.066	0.953	5.59	5.88	8.42	0.887	0.060	93.08	90.26	7.47	0.35	10.71	0.37	73.26	34.72
Sc_2CCl_2	0.009	0.088	1.209	5.03	5.40	7.56	1.120	0.080	92.70	90.35	8.48	0.43	11.88	0.46	59.09	29.33
Sc_2CF_2	0.004	0.036	0.386	2.15	2.26	2.40	0.350	0.033	90.64	90.02	0.84	0.07	0.89	0.08	5.82	5.14
Sc_2CF_2 -(model2)	0.005	0.049	0.538	2.87	2.89	3.30	0.488	0.044	90.83	90.01	1.61	0.13	1.84	0.13	11.06	8.37
Sc_2CF_2 -(model3)	0.006	0.059	0.632	2.92	2.86	3.09	0.573	0.053	90.64	90.03	1.77	0.15	1.91	0.15	9.60	8.13
Sc_2CF_2 -(model4)	0.007	0.072	0.781	3.34	3.40	3.73	0.709	0.065	90.83	90.09	2.65	0.22	2.91	0.22	14.08	11.59
Sc_2CO_2 -(model3)	0.006	0.060	0.639	2.76	2.81	3.06	0.580	0.054	90.67	90.13	1.77	0.15	1.92	0.15	9.42	7.93
Sc_2CO_2 -(model4)	0.005	0.046	0.498	2.75	2.68	2.93	0.452	0.041	90.82	90.13	1.33	0.11	1.45	0.11	8.68	7.16
Sc_2N	0.004	0.037	0.383	1.46	1.53	1.59	0.346	0.033	90.35	90.04	0.55	0.05	0.57	0.05	2.52	2.36
$Sc_2N(OH)_2$	0.004	0.037	0.407	2.45	2.67	2.90	0.370	0.034	90.83	90.14	1.07	0.09	1.16	0.10	8.46	7.19
Sc_2NF_2	0.003	0.031	0.331	2.13	2.14	2.28	0.300	0.028	90.62	90.09	0.68	0.06	0.72	0.06	5.21	4.59
Sc_2NF_2 -(model3)	0.006	0.061	0.652	2.91	3.04	3.29	0.591	0.055	90.69	90.11	1.95	0.17	2.11	0.17	10.93	9.29
Sc_2NF_2 -(model4)	0.005	0.047	0.510	2.93	2.77	3.02	0.463	0.042	90.83	90.02	1.40	0.12	1.53	0.11	9.23	7.64
Sc_2NO_2	0.004	0.044	0.477	2.48	2.56	2.80	0.433	0.040	90.69	90.05	1.21	0.10	1.33	0.11	7.91	6.55
Sc_2NO_2 -(model2)	0.004	0.040	0.454	2.87	2.97	3.34	0.413	0.036	91.10	90.04	1.38	0.11	1.56	0.11	11.31	8.84
Sc_3C_2	0.004	0.038	0.398	2.29	2.14	2.31	0.360	0.034	90.46	90.05	0.83	0.07	0.90	0.07	5.38	4.57
$Sc_3C_2(OH)_2$	0.003	0.031	0.331	3.42	3.40	3.66	0.300	0.028	90.52	90.12	1.10	0.10	1.18	0.10	13.53	11.57
$Sc_3C_2Br_2$	0.002	0.018	0.193	3.20	3.13	3.41	0.175	0.016	90.82	90.02	0.60	0.05	0.65	0.05	11.71	9.77
$Sc_3C_2F_2$	0.003	0.025	0.274	2.82	2.73	2.97	0.249	0.023	90.75	90.05	0.74	0.06	0.81	0.06	8.91	7.41
$Sc_3C_2O_2$	0.005	0.046	0.498	3.18	3.25	3.63	0.452	0.041	90.80	90.14	1.64	0.13	1.83	0.14	13.32	10.58
Sc_3N_2	0.003	0.027	0.278	1.83	1.81	1.92	0.251	0.024	90.42	90.09	0.48	0.04	0.51	0.04	3.70	3.26
$Sc_3N_2(OH)_2$	0.003	0.030	0.319	3.65	3.71	3.95	0.289	0.027	90.56	90.06	1.14	0.10	1.22	0.10	15.73	13.77
$Sc_3N_2F_2$	0.002	0.022	0.237	2.52	2.50	2.70	0.214	0.020	90.67	89.97	0.58	0.05	0.63	0.05	7.36	6.22
$Sc_3N_2O_2$	0.003	0.031	0.343	3.00	2.94	3.24	0.311	0.028	90.82	90.19	1.01	0.08	1.11	0.08	10.63	8.63
Sc_4C_3	0.004	0.035	0.373	2.63	2.57	2.72	0.338	0.032	90.50	90.00	0.92	0.08	0.97	0.08	7.43	6.59

$Sc_4C_3(OH)_2$	0.003	0.026	0.271	3.59	3.72	3.92	0.245	0.023	90.47	90.13	0.96	0.09	1.01	0.09	15.45	13.93
$Sc_4C_3F_2$	0.002	0.022	0.230	2.75	2.82	3.02	0.208	0.020	90.58	90.20	0.63	0.06	0.67	0.06	9.21	7.99
$Sc_4C_3O_2$	0.003	0.030	0.332	3.55	3.46	3.92	0.303	0.027	91.09	90.01	1.19	0.09	1.35	0.09	15.61	11.93
Sc_4N_3	0.002	0.021	0.217	1.84	1.83	1.96	0.196	0.019	90.35	89.99	0.38	0.03	0.41	0.03	3.86	3.35
$Sc_4N_3(OH)_2$	0.002	0.023	0.247	3.44	3.39	3.70	0.224	0.021	90.59	90.12	0.83	0.07	0.90	0.07	13.82	11.46
$Sc_4N_3F_2$	0.002	0.018	0.195	2.45	2.52	2.71	0.177	0.017	90.61	90.02	0.48	0.04	0.51	0.04	7.37	6.39
$Sc_4N_3O_2$	0.002	0.025	0.273	2.81	3.04	3.36	0.248	0.023	90.76	90.16	0.83	0.07	0.92	0.08	11.43	9.35
$ScCrC(OCN)_2$	0.007	0.070	1.021	5.75	5.83	8.79	0.951	0.063	93.18	90.26	8.37	0.37	12.63	0.37	80.34	34.03
$ScCrC(OH)_2$	0.005	0.047	0.547	3.35	3.64	4.18	0.500	0.043	91.37	90.28	2.09	0.16	2.40	0.17	17.70	13.36
$ScCrCF_2$	0.004	0.042	0.456	2.74	2.70	2.99	0.414	0.038	90.82	90.04	1.24	0.10	1.37	0.10	9.03	7.29
$ScHfN(SCN)_2$	0.005	0.053	0.722	7.16	7.65	10.53	0.669	0.048	92.65	90.32	7.05	0.37	9.70	0.39	114.34	58.96
$ScHfNO_2$	0.002	0.024	0.260	2.71	2.72	2.94	0.236	0.022	90.71	90.09	0.69	0.06	0.75	0.06	8.73	7.42
$ScNbCO_2$	0.003	0.035	0.381	2.88	2.71	2.99	0.346	0.032	90.78	90.07	1.03	0.09	1.14	0.08	9.02	7.28
$ScTaCO_2$	0.000	0.000	0.004	2.80	2.84	3.17	0.004	0.000	90.81	90.02	0.01	0.00	0.01	0.00	10.16	8.06
$ScTiNO_2$	0.004	0.040	0.443	2.71	2.73	3.07	0.403	0.036	90.94	90.15	1.23	0.10	1.39	0.10	9.51	7.45
$ScVCO_2$	0.004	0.042	0.456	2.58	2.67	2.93	0.414	0.038	90.85	90.16	1.21	0.10	1.33	0.10	8.65	7.15
$ScYC(CN)_2$	0.004	0.039	0.435	3.13	3.04	3.40	0.396	0.036	90.94	90.12	1.35	0.11	1.50	0.11	11.70	9.23
$ScYC(NCO)_2$	0.005	0.050	0.617	4.32	4.49	5.64	0.567	0.045	91.91	90.17	3.20	0.20	4.01	0.21	32.50	20.29
$ScYC(NCS)_2$	0.016	0.170	2.006	14.04	15.41	18.37	1.836	0.154	91.53	90.65	33.73	2.37	40.22	2.61	343.70	239.81
$ScYC(OCI)_2$	0.006	0.061	0.821	4.87	5.09	6.98	0.760	0.055	92.59	90.23	5.30	0.28	7.28	0.29	50.24	26.00
$ScYC(OCN)_2$	0.005	0.053	0.695	4.98	5.00	6.56	0.641	0.048	92.34	90.22	4.21	0.24	5.52	0.24	44.16	25.02
$ScYC(OH)_2$	0.003	0.034	0.382	2.81	2.89	3.26	0.347	0.031	90.97	90.13	1.13	0.09	1.28	0.09	10.77	8.38
$ScYC(SCN)_2$	0.007	0.071	0.951	7.02	7.10	9.74	0.880	0.064	92.55	90.27	8.57	0.45	11.75	0.46	97.73	50.50
$ScYCBr_2$	0.006	0.057	0.796	5.73	5.82	8.18	0.739	0.051	92.87	90.23	6.05	0.30	8.51	0.30	69.12	33.89
$ScYCCl_2$	0.006	0.066	0.834	5.04	4.73	6.00	0.768	0.059	92.10	90.25	4.61	0.28	5.85	0.26	36.88	22.20
$ScYCF_2$	0.004	0.039	0.417	2.59	2.66	2.84	0.378	0.035	90.61	90.12	1.08	0.09	1.15	0.10	8.15	7.10
$ScZrN(SCN)_2$	0.007	0.075	1.045	7.23	8.08	11.47	0.970	0.068	92.84	90.43	11.13	0.55	15.78	0.61	135.86	66.16
$ScZrNO_2$	0.004	0.036	0.392	2.87	2.74	3.12	0.356	0.033	90.81	90.13	1.11	0.09	1.26	0.09	9.86	7.49
Ta_2C	0.000	0.000	0.002	2.82	2.95	3.19	0.002	0.000	90.65	90.13	0.01	0.00	0.01	0.00	10.26	8.76
$Ta_2C(OH)_2$	0.000	0.000	0.002	3.54	3.80	4.46	0.002	0.000	91.26	90.07	0.01	0.00	0.01	0.00	20.27	14.59
Ta_2CF_2	0.000	0.000	0.002	2.57	2.50	2.73	0.001	0.000	90.77	90.11	0.00	0.00	0.00	0.00	7.50	6.21
Ta_2CO_2	0.000	0.000	0.002	3.32	3.17	3.51	0.002	0.000	91.05	90.04	0.01	0.00	0.01	0.00	12.47	9.99
Ta_2CrCN	0.000	0.000	0.004	4.62	4.47	5.34	0.003	0.000	91.44	90.15	0.02	0.00	0.02	0.00	29.08	19.90
Ta_2CrCNO_2	0.000	0.000	0.003	4.35	4.48	5.51	0.002	0.000	91.67	90.19	0.01	0.00	0.02	0.00	30.97	20.10
Ta_2HfCN	0.000	0.000	0.003	3.44	3.62	4.08	0.003	0.000	91.04	90.07	0.01	0.00	0.01	0.00	16.88	13.15
Ta_2HfCNO_2	0.000	0.000	0.002	4.06	4.10	4.82	0.002	0.000	91.32	90.13	0.01	0.00	0.01	0.00	23.63	16.80
Ta_2MoCN	0.000	0.000	0.003	3.88	4.00	4.72	0.003	0.000	91.21	90.10	0.01	0.00	0.02	0.00	22.65	16.02
Ta_2MoCNO_2	0.000	0.000	0.003	4.13	4.17	5.06	0.002	0.000	91.55	90.24	0.01	0.00	0.01	0.00	26.12	17.45
Ta_2N	0.000	0.000	0.002	2.33	2.41	2.61	0.002	0.000	90.63	90.23	0.00	0.00	0.00	0.00	6.85	5.85
$Ta_2N(OH)_2$	0.000	0.000	0.002	4.15	4.12	4.84	0.002	0.000	91.30	90.17	0.01	0.00	0.01	0.00	23.81	16.96
Ta_2NbCN	0.000	0.000	0.003	3.82	3.98	4.48	0.003	0.000	91.14	90.10	0.01	0.00	0.01	0.00	20.34	15.88
Ta_2NbCNO_2	0.000	0.000	0.003	4.05	4.25	5.06	0.002	0.000	91.55	90.17	0.01	0.00	0.01	0.00	26.02	18.20
Ta_2NF_2	0.000	0.000	0.001	3.00	2.79	3.13	0.001	0.000	91.00	90.12	0.00	0.00	0.00	0.00	9.93	7.71

Ta_2NH_2	0.000	0.000	0.001	1.63	1.63	1.69	0.001	0.000	90.30	90.07	0.00	0.00	0.00	0.00	2.87	2.66
Ta_2NO_2	0.000	0.000	0.002	2.91	2.92	3.22	0.002	0.000	90.86	90.08	0.01	0.00	0.01	0.00	10.51	8.54
Ta_2TiCN	0.000	0.000	0.003	4.01	4.17	4.81	0.003	0.000	91.28	90.18	0.02	0.00	0.02	0.00	23.48	17.46
Ta_2TiCNO_2	0.000	0.000	0.003	4.33	4.25	5.24	0.002	0.000	91.54	90.14	0.01	0.00	0.02	0.00	28.04	18.02
Ta_2VCN	0.000	0.000	0.003	3.86	4.08	4.76	0.003	0.000	91.29	90.19	0.01	0.00	0.02	0.00	23.01	16.78
Ta_2VCNO_2	0.000	0.000	0.003	4.15	4.31	5.19	0.002	0.000	91.62	90.25	0.01	0.00	0.01	0.00	27.48	18.69
Ta_2ZrCN	0.000	0.000	0.003	3.65	3.76	4.20	0.003	0.000	91.05	90.16	0.01	0.00	0.01	0.00	17.81	14.16
Ta_2ZrCNO_2	0.000	0.000	0.002	3.94	4.08	4.85	0.002	0.000	91.42	90.24	0.01	0.00	0.01	0.00	23.97	16.75
Ta_3C_2	0.000	0.000	0.002	3.65	3.81	4.28	0.002	0.000	91.10	90.19	0.01	0.00	0.01	0.00	18.53	14.61
$Ta_3C_2(OH)_2$	0.000	0.000	0.002	5.58	5.69	6.18	0.002	0.000	90.74	90.12	0.01	0.00	0.01	0.00	38.48	32.50
$Ta_3C_2F_2$	0.000	0.000	0.001	3.36	3.39	3.90	0.001	0.000	90.97	90.09	0.00	0.00	0.00	0.00	15.44	11.52
$Ta_3C_2H_2$	0.000	0.000	0.001	2.65	2.56	2.73	0.001	0.000	90.45	89.97	0.00	0.00	0.00	0.00	7.50	6.52
$Ta_3C_2O_2$	0.000	0.000	0.002	4.05	3.99	4.76	0.002	0.000	91.45	90.16	0.01	0.00	0.01	0.00	23.05	15.86
Ta_3CN	0.000	0.000	0.002	3.28	3.37	3.73	0.002	0.000	90.85	90.12	0.01	0.00	0.01	0.00	14.04	11.37
Ta_3CNO_2	0.000	0.000	0.002	3.94	4.17	4.94	0.002	0.000	91.46	90.23	0.01	0.00	0.01	0.00	24.83	17.50
Ta_3N_2	0.000	0.000	0.001	3.06	3.05	3.42	0.001	0.000	90.94	90.08	0.00	0.00	0.00	0.00	11.81	9.29
$Ta_3N_2(OH)_2$	0.000	0.000	0.002	7.35	7.80	8.32	0.002	0.000	90.27	90.14	0.01	0.00	0.02	0.00	69.63	61.29
$Ta_3N_2F_2$	0.000	0.000	0.001	3.60	3.86	4.16	0.001	0.000	90.79	90.14	0.00	0.00	0.00	0.00	17.42	15.01
$Ta_3N_2H_2$	0.000	0.000	0.001	2.69	2.64	2.78	0.001	0.000	90.47	90.08	0.00	0.00	0.00	0.00	7.76	6.97
$Ta_3N_2O_2$	0.000	0.000	0.001	3.76	3.90	4.43	0.001	0.000	91.29	90.23	0.01	0.00	0.01	0.00	19.92	15.29
Ta_4C_3	0.000	0.000	0.002	3.78	3.85	4.46	0.002	0.000	91.27	90.11	0.01	0.00	0.01	0.00	20.18	14.87
$Ta_4C_3(OH)_2$	0.000	0.000	0.001	4.87	5.00	5.62	0.001	0.000	91.00	90.11	0.01	0.00	0.01	0.00	31.94	25.11
$Ta_4C_3F_2$	0.000	0.000	0.001	3.37	3.36	3.77	0.001	0.000	90.95	90.15	0.00	0.00	0.00	0.00	14.37	11.29
$Ta_4C_3H_2$	0.000	0.000	0.001	2.48	2.58	2.71	0.001	0.000	90.45	90.12	0.00	0.00	0.00	0.00	7.38	6.69
$Ta_4C_3O_2$	0.000	0.000	0.001	4.02	3.99	4.84	0.001	0.000	91.60	90.16	0.01	0.00	0.01	0.00	23.84	15.92
Ta_4N_3	0.000	0.000	0.001	3.04	2.93	3.23	0.001	0.000	90.76	90.05	0.00	0.00	0.00	0.00	10.52	8.52
$Ta_4N_3(OH)_2$	0.000	0.000	0.001	3.52	3.59	4.06	0.001	0.000	90.90	90.09	0.00	0.00	0.00	0.00	16.74	12.91
$Ta_4N_3F_2$	0.000	0.000	0.001	2.81	2.76	3.01	0.001	0.000	90.65	90.06	0.00	0.00	0.00	0.00	9.17	7.63
$Ta_4N_3H_2$	0.000	0.000	0.001	2.34	2.41	2.58	0.001	0.000	90.53	90.07	0.00	0.00	0.00	0.00	6.71	5.81
$Ta_4N_3O_2$	0.000	0.000	0.001	3.55	3.53	4.14	0.001	0.000	91.24	90.15	0.00	0.00	0.01	0.00	17.40	12.43
$TaCrN(OCN)_2$	0.000	0.001	0.010	5.58	5.71	8.35	0.010	0.001	93.03	90.27	0.08	0.00	0.12	0.00	72.21	32.67
$TaCrN(SCN)_2$	0.000	0.001	0.016	7.59	8.35	12.63	0.015	0.001	93.42	90.40	0.19	0.01	0.29	0.01	165.59	70.53
$TaCrNBr_2$	0.000	0.001	0.022	7.84	8.55	14.93	0.021	0.001	94.33	90.44	0.31	0.01	0.54	0.01	233.32	73.84
$TaCrNCl_2$	0.000	0.001	0.015	6.25	6.72	10.40	0.014	0.001	93.59	90.39	0.15	0.01	0.23	0.01	112.41	45.52
$TaCrNF_2$	0.000	0.000	0.004	2.72	2.66	2.97	0.004	0.000	90.75	90.08	0.01	0.00	0.01	0.00	8.90	7.08
$TaMoN(NCO)_2$	0.000	0.001	0.008	4.69	4.85	6.40	0.007	0.001	92.29	90.23	0.05	0.00	0.06	0.00	42.06	23.62
$TaMoN(NCS)_2$	0.000	0.003	0.032	17.32	19.61	20.71	0.029	0.003	90.38	90.91	0.60	0.05	0.63	0.06	431.50	389.78
$TaMoN(SCN)_2$	0.000	0.001	0.014	9.32	9.52	11.66	0.013	0.001	91.79	90.28	0.15	0.01	0.18	0.01	138.71	90.90
$TaMoNBr_2$	0.000	0.001	0.019	6.62	7.09	12.17	0.018	0.001	94.00	90.40	0.22	0.01	0.37	0.01	155.09	50.67
$TaMoNCl_2$	0.000	0.001	0.013	5.49	5.63	8.36	0.012	0.001	92.96	90.30	0.10	0.00	0.15	0.00	72.57	31.81
$TaMoNF_2$	0.000	0.000	0.004	2.75	2.84	3.02	0.004	0.000	90.73	90.09	0.01	0.00	0.01	0.00	9.21	8.09
$TaWN(CN)_2$	0.000	0.000	0.005	3.15	3.24	3.62	0.005	0.000	91.07	90.13	0.02	0.00	0.02	0.00	13.23	10.52
$TaWN(NCO)_2$	0.000	0.001	0.008	4.67	4.92	6.51	0.008	0.001	92.34	90.25	0.05	0.00	0.07	0.00	43.55	24.38

$TaWNBr_2$	0.000	0.001	0.020	7.09	7.34	13.01	0.019	0.001	94.16	90.45	0.25	0.01	0.43	0.01	177.65	54.04
$TaWNCl_2$	0.000	0.001	0.014	5.95	6.35	9.74	0.013	0.001	93.43	90.34	0.13	0.01	0.20	0.01	98.50	40.68
$Ti_{0.4}Nb_{1.6}C$	0.009	0.090	1.006	5.50	5.50	6.34	0.916	0.081	91.05	90.09	5.81	0.45	6.69	0.45	40.80	30.29
$Ti_{0.8}Nb_{1.2}C$	0.012	0.124	1.523	7.96	7.98	9.84	1.399	0.112	91.83	90.16	13.76	0.90	16.98	0.90	98.86	63.62
$Ti_{1.2}Nb_{0.8}C$	0.028	0.280	2.628	15.92	15.80	15.37	2.349	0.252	89.35	90.11	36.11	3.98	35.14	3.95	235.62	249.38
$Ti_{1.5}Nb_{0.5}C$	0.008	0.083	0.861	3.48	3.44	3.56	0.778	0.075	90.35	89.95	2.77	0.26	2.87	0.25	12.75	11.82
$Ti_{1.6}Nb_{0.4}C$	0.017	0.166	1.428	6.00	5.92	5.14	1.262	0.149	88.37	89.76	6.48	0.88	5.62	0.87	25.92	35.05
$Ti_{10}C_9F_2$	0.001	0.013	0.165	5.11	4.96	6.41	0.151	0.012	91.89	90.27	0.97	0.06	1.25	0.06	42.11	24.57
$Ti_{10}N_9F_2$	0.001	0.009	0.107	3.56	3.80	4.49	0.098	0.008	91.43	90.07	0.44	0.03	0.52	0.03	20.55	14.58
Ti_2C	0.005	0.047	0.498	1.88	1.97	2.10	0.451	0.043	90.48	90.20	0.95	0.08	1.01	0.09	4.44	3.92
$Ti_2C(OH)_2$	0.004	0.041	0.462	2.84	3.16	3.60	0.421	0.037	91.12	90.09	1.51	0.12	1.72	0.13	13.12	10.13
Ti_2CCI_2	0.002	0.025	0.264	1.98	2.15	2.29	0.240	0.022	90.63	90.16	0.55	0.05	0.58	0.05	5.27	4.65
Ti_2CF_2	0.003	0.031	0.338	2.19	2.31	2.50	0.307	0.028	90.69	90.09	0.77	0.07	0.83	0.07	6.28	5.37
Ti_2CF_2-(model2)	0.006	0.059	0.663	3.56	3.57	4.01	0.604	0.053	91.07	90.02	2.42	0.19	2.72	0.19	16.25	12.73
Ti_2CF_2-(model3)	0.007	0.068	0.740	3.48	3.57	4.04	0.673	0.061	90.87	90.10	2.72	0.22	3.07	0.22	16.51	12.81
Ti_2CF_2-(model4)	0.010	0.101	1.166	4.66	4.78	5.72	1.065	0.091	91.37	90.13	6.09	0.43	7.29	0.45	33.37	22.95
$Ti_2CO_{0.11}F_{1.89}$	0.004	0.041	0.441	2.89	2.89	3.15	0.401	0.037	90.73	90.14	1.26	0.11	1.37	0.11	9.98	8.38
$Ti_2CO_{0.44}F_{1.56}$	0.004	0.044	0.482	2.96	3.04	3.37	0.437	0.040	90.82	90.11	1.48	0.12	1.64	0.12	11.51	9.24
$Ti_2CO_{0.67}F_{1.33}$	0.004	0.044	0.486	3.00	3.07	3.42	0.442	0.040	90.87	90.02	1.51	0.12	1.69	0.13	11.84	9.45
$Ti_2CO_{0.89}F_{1.11}$	0.005	0.047	0.520	3.22	3.28	3.61	0.472	0.043	90.88	90.17	1.70	0.14	1.88	0.14	13.14	10.75
$Ti_2CO_{1.33}F_{0.67}$	0.005	0.047	0.515	3.23	3.14	3.57	0.468	0.042	90.92	90.07	1.67	0.13	1.91	0.13	12.94	9.82
Ti_2CO_2	0.004	0.042	0.461	2.63	2.73	3.05	0.419	0.038	90.90	90.11	1.28	0.10	1.43	0.11	9.38	7.46
Ti_2CO_2-(model2)	0.005	0.047	0.527	3.35	3.15	3.54	0.480	0.043	91.02	90.06	1.70	0.13	1.91	0.13	12.69	9.87
Ti_2CO_2-(model3)	0.006	0.057	0.626	3.12	3.11	3.49	0.569	0.052	90.87	90.10	1.98	0.16	2.23	0.16	12.33	9.69
Ti_2CrCN	0.009	0.089	1.106	5.78	5.80	7.44	1.017	0.080	91.98	90.19	7.57	0.46	9.70	0.47	56.73	33.71
Ti_2CrCNO_2	0.005	0.055	0.776	5.78	5.66	8.18	0.721	0.050	92.90	90.23	5.89	0.28	8.51	0.28	69.25	31.99
Ti_2HfCN	0.004	0.040	0.461	4.32	4.39	5.12	0.421	0.036	91.35	90.19	2.16	0.16	2.51	0.16	26.62	19.31
Ti_2HfCNO_2	0.003	0.030	0.388	4.91	4.94	6.42	0.358	0.027	92.22	90.18	2.30	0.13	2.99	0.14	42.28	24.38
Ti_2MoCN	0.006	0.062	0.741	4.98	5.01	6.00	0.679	0.056	91.63	90.15	4.07	0.28	4.88	0.28	36.64	25.11
Ti_2MoCNO_2	0.004	0.042	0.565	5.24	5.25	7.32	0.523	0.038	92.56	90.22	3.83	0.20	5.34	0.20	55.38	27.62
Ti_2N	0.004	0.036	0.370	1.73	1.65	1.76	0.334	0.032	90.39	90.12	0.59	0.05	0.63	0.05	3.10	2.70
$Ti_2N(OH)_2$	0.004	0.038	0.426	3.01	3.02	3.37	0.388	0.034	91.07	90.16	1.31	0.10	1.45	0.10	11.47	9.14
$Ti_2Nb_2C_3$	0.004	0.036	0.410	3.94	3.96	4.63	0.375	0.032	91.25	90.12	1.74	0.13	2.03	0.13	21.81	15.72
Ti_2NbC_2	0.003	0.026	0.280	2.27	2.26	2.47	0.253	0.024	90.62	90.04	0.63	0.05	0.69	0.05	6.17	5.09
Ti_2NbCN	0.006	0.064	0.758	4.97	5.05	6.12	0.695	0.057	91.62	90.18	4.25	0.29	5.16	0.29	38.25	25.56
Ti_2NbCNO_2	0.004	0.043	0.573	5.08	5.27	7.30	0.530	0.039	92.55	90.30	3.87	0.20	5.36	0.21	54.98	27.89
Ti_2NF_2	0.003	0.029	0.305	2.08	2.10	2.29	0.277	0.026	90.62	90.01	0.63	0.05	0.69	0.05	5.27	4.40
Ti_2NF_2-(model2)	0.006	0.058	0.649	3.51	3.67	4.12	0.591	0.052	91.07	90.04	2.44	0.19	2.74	0.20	17.20	13.52
Ti_2NO_2	0.004	0.036	0.398	2.59	2.58	2.88	0.361	0.033	90.89	90.05	1.04	0.08	1.16	0.08	8.38	6.67
Ti_2NO_2-(model4)	0.009	0.088	0.972	3.72	3.81	4.21	0.884	0.079	90.95	90.12	3.73	0.30	4.12	0.31	17.94	14.54
Ti_2NS_2	0.002	0.024	0.262	2.16	2.20	2.39	0.237	0.022	90.67	90.04	0.57	0.05	0.61	0.05	5.77	4.87
$Ti_2Ta_2C_3$	0.000	0.000	0.003	3.76	3.85	4.48	0.003	0.000	91.25	90.20	0.01	0.00	0.02	0.00	20.38	14.85
Ti_2TaC_2	0.000	0.000	0.003	2.20	2.24	2.38	0.003	0.000	90.58	90.08	0.01	0.00	0.01	0.00	5.68	5.04

Ti_2TaCN	0.000	0.001	0.009	4.95	4.80	5.78	0.008	0.001	91.54	90.16	0.05	0.00	0.06	0.00	34.03	22.97
Ti_2TaCNO_2	0.000	0.001	0.007	4.81	5.18	6.98	0.007	0.001	92.41	90.27	0.05	0.00	0.06	0.00	50.11	27.09
Ti_2VC_2	0.003	0.034	0.366	2.55	2.52	2.72	0.332	0.031	90.65	90.02	0.90	0.08	0.97	0.08	7.45	6.32
Ti_2VCN	0.008	0.083	1.014	5.20	5.42	6.72	0.931	0.075	91.80	90.18	6.26	0.41	7.76	0.42	46.18	29.52
Ti_2VCNO_2	0.005	0.054	0.736	5.18	5.44	7.72	0.682	0.048	92.70	90.28	5.27	0.26	7.48	0.28	61.68	29.75
Ti_2ZrCN	0.006	0.058	0.682	4.35	4.53	5.42	0.624	0.052	91.48	90.11	3.38	0.24	4.04	0.25	29.90	20.66
Ti_2ZrCNO_2	0.004	0.041	0.536	5.28	5.10	6.65	0.495	0.037	92.36	90.15	3.30	0.19	4.30	0.18	45.43	25.91
Ti_3C_2	0.004	0.039	0.412	2.43	2.54	2.74	0.373	0.035	90.60	90.01	1.02	0.09	1.11	0.09	7.59	6.46
$Ti_3C_2(O_{0.13}F_{0.83}(OH)_{1.04})$	0.006	0.067	0.860	7.72	7.77	10.05	0.794	0.060	92.24	90.33	7.98	0.47	10.32	0.47	103.58	60.45
$Ti_3C_2(O_{0.1}F_{1.1}(OH)_{0.8})$	0.008	0.080	1.079	9.51	9.40	13.02	0.999	0.072	92.56	90.24	13.00	0.68	18.00	0.67	174.80	88.27
$Ti_3C_2(O_{0.7}F_{1.3})$	0.004	0.038	0.446	4.30	4.33	5.19	0.409	0.034	91.55	90.09	2.12	0.15	2.54	0.15	27.40	18.77
$Ti_3C_2(OH)_2$	0.004	0.038	0.420	4.65	4.77	5.39	0.382	0.035	90.89	90.19	2.06	0.16	2.33	0.17	29.41	22.81
$Ti_3C_2Br_2$	0.002	0.019	0.206	3.48	3.36	3.86	0.187	0.017	91.00	90.09	0.72	0.06	0.83	0.05	15.08	11.23
$Ti_3C_2CI_2$	0.002	0.021	0.229	2.84	2.91	3.23	0.208	0.019	90.88	90.20	0.67	0.05	0.75	0.06	10.58	8.49
$Ti_3C_2F_2$	0.002	0.024	0.267	2.70	2.79	3.10	0.243	0.022	90.87	90.13	0.75	0.06	0.84	0.06	9.70	7.79
$Ti_3C_2O_2$	0.003	0.032	0.366	3.31	3.46	3.97	0.334	0.029	91.17	90.16	1.33	0.10	1.52	0.11	16.02	12.03
$Ti_3C_2Se_2$	0.001	0.013	0.133	2.54	2.57	2.77	0.121	0.011	90.61	90.05	0.33	0.03	0.36	0.03	7.72	6.63
$Ti_3C_2Te_2$	0.001	0.009	0.093	2.55	2.46	2.64	0.084	0.008	90.40	90.06	0.22	0.02	0.24	0.02	7.01	6.03
Ti_3CN	0.007	0.076	0.899	4.84	4.81	5.70	0.822	0.069	91.52	90.17	4.69	0.33	5.56	0.33	33.05	23.09
Ti_3CNF_2	0.007	0.075	1.146	6.57	7.00	11.02	1.071	0.067	93.49	90.44	11.81	0.47	18.59	0.50	126.56	49.36
Ti_3CNO_2	0.006	0.059	0.858	5.79	6.00	8.81	0.799	0.054	93.09	90.24	7.03	0.32	10.33	0.33	80.41	36.16
$Ti_3N_2(OH)_2$	0.003	0.032	0.352	4.28	4.47	4.91	0.320	0.029	90.92	90.04	1.57	0.13	1.73	0.13	24.30	20.04
Ti_3N_2	0.003	0.026	0.276	2.02	2.01	2.15	0.250	0.024	90.50	90.03	0.54	0.05	0.58	0.05	4.67	4.06
$Ti_3N_2F_2$	0.002	0.020	0.215	2.41	2.53	2.85	0.195	0.018	90.78	90.01	0.56	0.05	0.63	0.05	8.25	6.43
$Ti_3N_2H_2$	0.003	0.029	0.325	3.24	3.29	3.70	0.296	0.026	91.07	90.17	1.10	0.09	1.23	0.09	13.86	10.85
$Ti_3N_2O_2$	0.003	0.027	0.302	3.27	3.16	3.51	0.275	0.024	91.08	90.01	0.97	0.08	1.07	0.07	12.44	9.98
Ti_4C_3	0.003	0.031	0.330	2.62	2.63	2.82	0.298	0.028	90.53	90.02	0.84	0.07	0.90	0.07	8.03	6.94
$Ti_4C_3(OH)_2$	0.003	0.026	0.293	3.78	3.93	4.38	0.267	0.024	91.01	90.12	1.17	0.09	1.30	0.10	19.40	15.48
$Ti_4C_3F_2$	0.002	0.020	0.216	2.69	2.71	3.02	0.196	0.018	90.74	90.10	0.59	0.05	0.66	0.05	9.23	7.33
$Ti_4C_3H_2$	0.002	0.016	0.173	2.40	2.30	2.48	0.157	0.015	90.65	89.95	0.39	0.03	0.42	0.03	6.21	5.27
$Ti_4C_3O_2$	0.003	0.026	0.294	3.20	3.39	3.88	0.268	0.024	91.11	90.19	1.04	0.08	1.19	0.08	15.30	11.58
Ti_4N_3	0.002	0.020	0.205	1.98	2.03	2.11	0.185	0.018	90.38	90.03	0.39	0.04	0.41	0.04	4.49	4.12
$Ti_4N_3(OH)_2$	0.003	0.030	0.378	4.45	4.60	5.88	0.348	0.027	92.06	90.20	2.05	0.12	2.61	0.13	35.44	21.25
$Ti_4N_3F_2$	0.002	0.017	0.178	2.55	2.54	2.74	0.161	0.015	90.67	90.03	0.44	0.04	0.48	0.04	7.60	6.45
$Ti_4N_3H_2$	0.002	0.015	0.161	2.38	2.33	2.48	0.146	0.014	90.61	90.06	0.36	0.03	0.39	0.03	6.20	5.39
$Ti_4N_3O_2$	0.002	0.022	0.235	2.97	2.92	3.30	0.214	0.019	90.85	90.09	0.71	0.06	0.80	0.06	11.04	8.53
$Ti_5C_4(OH)_2$	0.002	0.024	0.265	4.48	4.62	5.15	0.241	0.022	90.99	90.19	1.24	0.10	1.39	0.10	26.85	21.40
$Ti_5C_4F_2$	0.002	0.017	0.183	2.91	3.03	3.25	0.166	0.015	90.77	90.13	0.54	0.05	0.58	0.05	10.66	9.21
$Ti_5C_4O_2$	0.002	0.022	0.255	3.62	3.72	4.27	0.233	0.020	91.31	90.25	1.00	0.07	1.14	0.08	18.52	13.84
$Ti_5N_4F_2$	0.002	0.018	0.201	3.30	3.29	3.67	0.183	0.016	91.05	90.08	0.67	0.05	0.75	0.05	13.62	10.80
$Ti_6C_5F_2$	0.002	0.024	0.310	4.75	4.88	6.58	0.287	0.022	92.31	90.30	1.89	0.11	2.55	0.11	44.65	23.90
$Ti_6N_5F_2$	0.002	0.017	0.194	4.08	4.17	4.89	0.177	0.015	91.40	90.12	0.87	0.06	1.02	0.06	24.34	17.40
$Ti_7C_6F_2$	0.002	0.015	0.179	3.92	4.19	5.00	0.164	0.014	91.56	89.96	0.82	0.06	0.98	0.06	25.49	17.67

$Ti_7N_6F_2$	0.001	0.012	0.131	3.70	3.77	4.16	0.119	0.010	91.13	90.19	0.50	0.04	0.55	0.04	17.46	14.26
$Ti_8C_7F_2$	0.001	0.015	0.179	4.63	4.76	5.87	0.163	0.014	91.49	90.25	0.96	0.07	1.18	0.07	35.17	22.73
$Ti_8N_7F_2$	0.001	0.011	0.119	3.58	3.85	4.30	0.109	0.010	91.13	89.98	0.47	0.04	0.52	0.04	18.67	14.92
$Ti_9C_8F_2$	0.001	0.014	0.172	4.29	4.75	5.97	0.158	0.013	91.87	90.25	0.94	0.06	1.18	0.07	36.45	22.82
$Ti_9N_8F_2$	0.001	0.010	0.111	3.51	3.45	4.10	0.101	0.009	91.36	90.08	0.42	0.03	0.49	0.03	17.15	11.89
$TiCrCO_2$	0.004	0.039	0.426	2.75	2.86	3.18	0.388	0.035	90.96	90.13	1.23	0.10	1.37	0.10	10.24	8.24
$TiHfCO_2$	0.002	0.022	0.244	2.89	2.97	3.37	0.222	0.020	91.02	90.10	0.75	0.06	0.85	0.06	11.48	8.86
$TiHfN(NO)_2$	0.002	0.020	0.215	2.40	2.47	2.65	0.195	0.018	90.52	90.09	0.51	0.05	0.55	0.05	7.05	6.13
$TiMoCO_2$	0.003	0.028	0.304	2.53	2.56	2.83	0.277	0.025	90.91	90.04	0.78	0.06	0.87	0.06	8.11	6.58
TiNbC	0.004	0.040	0.412	1.76	1.75	1.82	0.372	0.036	90.35	90.03	0.68	0.06	0.71	0.06	3.34	3.05
TiVC	0.006	0.056	0.579	1.77	1.77	1.88	0.524	0.050	90.38	90.06	0.99	0.09	1.05	0.09	3.57	3.13
$TiWCO_2$	0.002	0.019	0.213	2.51	2.61	2.89	0.194	0.018	90.87	90.00	0.56	0.05	0.62	0.05	8.43	6.83
$TiZrCO_2$	0.004	0.038	0.417	3.07	3.03	3.37	0.379	0.034	90.98	90.11	1.28	0.10	1.42	0.10	11.51	9.15
V_2C	0.005	0.048	0.510	2.25	2.23	2.40	0.462	0.043	90.55	90.07	1.11	0.10	1.19	0.10	5.79	4.98
$V_2C(OH)_2$	0.004	0.042	0.478	3.29	3.32	3.94	0.436	0.038	91.26	90.07	1.72	0.12	2.04	0.13	15.81	11.03
V_2CBr_2	0.002	0.016	0.171	1.91	1.96	2.08	0.155	0.015	90.51	89.93	0.32	0.03	0.34	0.03	4.35	3.87
$V_2CF(OH)$	0.004	0.040	0.440	2.68	2.75	3.08	0.400	0.036	90.94	90.11	1.24	0.10	1.39	0.10	9.63	7.59
V_2CF_2	0.003	0.032	0.345	2.57	2.38	2.66	0.313	0.029	90.78	90.06	0.83	0.07	0.93	0.06	7.18	5.62
V_2CO_2	0.004	0.041	0.456	2.93	3.00	3.37	0.415	0.037	91.02	90.01	1.40	0.11	1.57	0.11	11.46	9.01
V_2CrCN	0.009	0.087	1.091	5.54	6.03	7.62	1.004	0.079	92.00	90.18	7.65	0.47	9.67	0.52	59.44	36.70
V_2CrCNO_2	0.005	0.048	0.659	5.45	5.62	7.75	0.611	0.043	92.70	90.32	4.74	0.24	6.54	0.25	61.98	31.67
V_2HfCN	0.004	0.040	0.459	4.46	4.40	5.13	0.420	0.036	91.40	90.11	2.15	0.16	2.51	0.15	26.77	19.32
V_2HfCNO_2	0.003	0.026	0.325	4.76	4.70	5.88	0.299	0.024	91.95	90.22	1.76	0.11	2.20	0.11	35.34	22.02
V_2MoCN	0.006	0.062	0.741	5.11	5.07	6.28	0.679	0.056	91.65	90.16	4.26	0.28	5.28	0.28	40.34	25.67
V_2MoCNO_2	0.004	0.037	0.481	4.86	5.09	6.62	0.444	0.033	92.31	90.22	2.94	0.17	3.82	0.18	44.97	26.04
V_2N	0.004	0.036	0.376	1.84	1.77	1.90	0.340	0.032	90.51	89.99	0.65	0.06	0.69	0.05	3.65	3.14
$V_2N(OH)_2$	0.004	0.037	0.413	2.73	2.84	3.26	0.376	0.033	91.07	90.06	1.23	0.09	1.41	0.10	10.81	8.08
$V_2Nb_2C_3$	0.004	0.036	0.412	4.00	4.02	4.74	0.376	0.032	91.31	90.11	1.78	0.13	2.10	0.13	22.89	16.20
V_2NbCN	0.006	0.063	0.759	4.85	5.10	6.32	0.696	0.056	91.74	90.18	4.40	0.29	5.46	0.30	40.88	26.18
V_2NbCNO_2	0.004	0.037	0.483	5.25	5.39	6.92	0.445	0.034	92.25	90.33	3.08	0.18	3.96	0.19	49.05	29.15
V_2NF_2	0.003	0.028	0.304	1.98	2.19	2.32	0.275	0.025	90.66	89.98	0.64	0.06	0.67	0.06	5.39	4.84
V_2NO_2	0.004	0.036	0.394	2.72	2.70	2.95	0.358	0.032	90.85	90.13	1.06	0.09	1.16	0.09	8.79	7.26
$V_2Ta_2C_3$	0.000	0.000	0.003	3.40	3.56	4.13	0.003	0.000	91.10	90.15	0.01	0.00	0.01	0.00	17.31	12.73
V_2TaC_2	0.000	0.001	0.006	3.56	3.54	4.00	0.005	0.000	90.97	90.10	0.02	0.00	0.02	0.00	16.22	12.55
V_2TaCN	0.000	0.001	0.009	4.86	5.01	5.96	0.008	0.001	91.60	90.16	0.05	0.00	0.06	0.00	36.19	25.14
V_2TaCNO_2	0.000	0.001	0.006	4.87	4.86	6.33	0.006	0.000	92.14	90.22	0.04	0.00	0.05	0.00	41.08	23.61
$V_2Ti_2C_3$	0.005	0.056	0.651	4.55	4.57	5.42	0.596	0.050	91.46	90.18	3.23	0.23	3.82	0.23	29.85	20.91
V_2TiC_2	0.006	0.064	0.729	3.90	4.09	4.73	0.665	0.058	91.23	90.16	3.14	0.24	3.63	0.25	22.67	16.81
V_2TiCN	0.008	0.082	1.002	5.33	5.53	6.70	0.920	0.074	91.81	90.15	6.16	0.41	7.47	0.42	45.73	30.66
V_2TiCNO_2	0.005	0.048	0.637	4.91	5.37	7.30	0.590	0.043	92.51	90.35	4.30	0.23	5.85	0.25	54.82	29.10
V_2ZrCN	0.006	0.057	0.676	4.44	4.68	5.51	0.618	0.052	91.50	90.11	3.41	0.24	4.01	0.26	30.87	22.03
V_2ZrCNO_2	0.004	0.036	0.459	4.63	4.85	6.25	0.422	0.033	92.06	90.28	2.64	0.16	3.40	0.17	40.02	23.65
V_3C_2	0.004	0.042	0.454	2.99	2.96	3.26	0.412	0.038	90.71	90.13	1.34	0.11	1.48	0.11	10.75	8.76

$V_3C_2(OH)_2$	0.004	0.039	0.448	5.43	5.64	6.49	0.409	0.035	91.24	90.24	2.65	0.20	3.05	0.21	42.69	31.91
$V_3C_2Br_2$	0.001	0.013	0.139	2.79	2.73	2.94	0.126	0.012	90.73	90.06	0.37	0.03	0.40	0.03	8.71	7.45
$V_3C_2Cl_2$	0.003	0.029	0.332	3.76	3.78	4.46	0.303	0.026	91.35	90.10	1.35	0.10	1.59	0.10	20.23	14.32
$V_3C_2F_2$	0.002	0.023	0.261	3.24	3.23	3.68	0.238	0.021	91.05	90.20	0.88	0.07	1.00	0.07	13.76	10.41
$V_3C_2O_2$	0.003	0.032	0.376	3.91	3.76	4.50	0.344	0.029	91.42	90.18	1.55	0.11	1.85	0.11	20.60	14.05
V_3CN	0.007	0.075	0.888	4.98	4.90	5.98	0.814	0.067	91.60	90.16	4.86	0.33	5.93	0.32	36.45	23.99
V_3CNO_2	0.006	0.059	0.857	6.09	6.15	8.97	0.798	0.053	93.12	90.33	7.16	0.33	10.43	0.33	83.22	37.89
V_3N_2	0.002	0.023	0.242	2.05	2.12	2.35	0.219	0.020	90.63	89.97	0.52	0.04	0.57	0.04	5.60	4.51
$V_3N_2(OH)_2$	0.004	0.037	0.408	5.48	5.85	6.45	0.371	0.033	91.03	90.16	2.39	0.19	2.64	0.21	42.07	34.46
$V_3N_2F_2$	0.002	0.019	0.216	3.20	3.06	3.50	0.197	0.018	90.98	90.07	0.69	0.05	0.79	0.05	12.46	9.33
$V_3N_2H_2$	0.003	0.028	0.309	3.35	3.20	3.71	0.281	0.025	91.09	90.18	1.04	0.08	1.21	0.08	14.02	10.18
$V_3N_2O_2$	0.003	0.026	0.297	3.31	3.28	3.82	0.271	0.023	91.21	90.14	1.03	0.08	1.21	0.08	14.85	10.71
V_4C_3	0.003	0.033	0.355	3.03	3.17	3.46	0.323	0.030	90.77	90.01	1.12	0.09	1.22	0.10	12.09	10.12
$V_4C_3(OH)_2$	0.003	0.029	0.351	4.95	5.04	6.07	0.322	0.027	91.63	90.16	1.95	0.13	2.35	0.14	37.53	25.43
$V_4C_3F_2$	0.002	0.020	0.215	2.96	2.98	3.30	0.196	0.018	90.90	90.04	0.65	0.05	0.72	0.05	11.02	8.89
$V_4C_3H_2$	0.002	0.017	0.179	2.53	2.52	2.71	0.162	0.015	90.58	90.04	0.44	0.04	0.47	0.04	7.41	6.37
$V_4C_3O_2$	0.003	0.026	0.300	3.53	3.65	4.27	0.274	0.023	91.34	90.18	1.17	0.09	1.37	0.09	18.50	13.34
V_4N_3	0.002	0.022	0.231	2.22	2.31	2.40	0.209	0.020	90.38	90.04	0.50	0.05	0.52	0.05	5.80	5.37
$V_4N_3(OH)_2$	0.002	0.023	0.256	3.40	3.58	4.09	0.233	0.020	91.14	90.15	0.95	0.07	1.09	0.08	16.96	12.91
$V_4N_3F_2$	0.002	0.017	0.181	2.53	2.52	2.75	0.164	0.015	90.66	90.10	0.45	0.04	0.49	0.04	7.61	6.33
$V_4N_3H_2$	0.001	0.014	0.148	2.22	2.28	2.43	0.134	0.012	90.64	89.92	0.33	0.03	0.35	0.03	5.94	5.21
$V_4N_3O_2$	0.002	0.021	0.232	3.20	3.11	3.42	0.211	0.019	90.92	90.13	0.72	0.06	0.79	0.06	11.84	9.63
$VCrN(NCS)_2$	0.029	0.339	2.615	22.71	27.53	21.86	2.276	0.310	87.03	91.45	49.74	8.54	39.48	10.35	463.42	773.29
$VCrN(SCN)_2$	0.009	0.094	1.406	9.51	9.67	14.79	1.311	0.085	93.30	90.48	19.39	0.82	29.64	0.84	227.24	93.69
$VCrNBr_2$	0.009	0.094	1.719	8.62	9.51	18.26	1.625	0.085	94.53	90.56	29.67	0.81	56.94	0.89	352.13	91.49
$VCrNF_2$	0.003	0.033	0.360	2.52	2.54	2.74	0.327	0.030	90.81	90.07	0.89	0.08	0.96	0.08	7.54	6.43
$VMoN(NCO)_2$	0.005	0.051	0.703	5.52	5.59	7.82	0.652	0.046	92.80	90.32	5.10	0.26	7.14	0.26	63.18	31.28
$VMoN(NCS)_2$	0.022	0.249	2.174	21.12	23.96	21.51	1.926	0.227	88.57	91.25	41.42	5.43	37.18	6.16	456.66	581.53
$VMoN(OCN)_2$	0.005	0.055	0.816	6.05	6.06	9.03	0.760	0.050	93.22	90.37	6.86	0.30	10.23	0.30	84.49	36.69
$VMoN(SCN)_2$	0.007	0.075	1.093	8.60	9.04	13.40	1.018	0.068	93.12	90.40	13.64	0.61	20.21	0.65	186.18	82.22
$VMoNBr_2$	0.007	0.073	1.315	8.08	8.53	15.67	1.242	0.066	94.41	90.47	19.46	0.57	35.75	0.60	258.48	73.24
$VMoNCI_2$	0.007	0.077	1.223	6.66	6.69	11.03	1.146	0.069	93.71	90.36	12.63	0.46	20.82	0.47	127.08	44.78
VNbC	0.004	0.039	0.402	1.72	1.71	1.81	0.363	0.035	90.35	89.99	0.66	0.06	0.70	0.06	3.30	2.94
$VNbCF_2$-(model4)	0.004	0.041	0.447	2.82	2.98	3.30	0.406	0.037	90.76	90.10	1.34	0.11	1.48	0.12	11.02	8.94
$VWN(NCO)_2$	0.003	0.034	0.451	4.87	4.98	6.61	0.417	0.031	92.40	90.25	2.76	0.15	3.66	0.16	44.93	24.85
$VWN(OCN)_2$	0.004	0.041	0.603	6.07	5.99	8.95	0.562	0.037	93.20	90.29	5.03	0.22	7.52	0.22	83.13	35.87
$VWNBr_2$	0.005	0.056	1.006	7.71	8.21	15.15	0.950	0.051	94.42	90.44	14.39	0.42	26.56	0.44	241.54	67.88
$VWNCI_2$	0.006	0.057	0.924	6.68	6.82	11.30	0.867	0.052	93.80	90.36	9.79	0.35	16.20	0.36	133.35	46.69
$VWNF_2$	0.002	0.021	0.224	2.55	2.62	2.86	0.204	0.019	90.83	90.08	0.58	0.05	0.63	0.05	8.24	6.89
$W_{1.33}C$	0.510	1.432	2.626	441.26	129.74	23.76	1.194	0.923	45.46	64.41	28.36	119.68	5.19	35.19	285.08	12108.07
$W_{1.33}C(OH)_2$	0.003	0.026	0.296	3.53	3.82	4.42	0.271	0.023	91.29	90.14	1.20	0.09	1.38	0.10	19.80	14.69
$W_{1.33}CO_2$	0.003	0.027	0.296	3.67	3.56	4.05	0.269	0.024	90.94	90.09	1.09	0.09	1.24	0.08	16.64	12.62
W_2C	0.002	0.020	0.213	2.88	3.07	3.37	0.193	0.018	90.70	90.17	0.65	0.05	0.71	0.06	11.45	9.51

$W_2C(OH)_2$	0.002	0.016	0.190	4.19	4.26	4.93	0.174	0.015	91.36	90.18	0.86	0.06	0.99	0.06	24.72	18.15
W_2CCl_2	0.004	0.043	0.679	6.55	6.62	10.73	0.636	0.039	93.63	90.35	6.82	0.26	11.05	0.26	120.11	43.84
W_2CF_2	0.001	0.011	0.120	2.83	2.87	3.14	0.109	0.010	90.98	90.16	0.34	0.03	0.37	0.03	9.93	8.26
W_2CO_2	0.002	0.016	0.180	2.90	2.94	3.28	0.163	0.015	90.88	90.11	0.54	0.04	0.60	0.04	10.87	8.68
$W_2Hf_2C_3O_2$	0.001	0.009	0.106	3.70	3.85	4.53	0.097	0.008	91.31	90.10	0.44	0.03	0.52	0.03	20.86	14.92
W_2HfC_2	0.001	0.009	0.097	2.16	2.19	2.32	0.088	0.008	90.62	90.04	0.20	0.02	0.22	0.02	5.40	4.81
$W_2HfC_2O_2$	0.001	0.013	0.159	4.61	4.58	5.61	0.145	0.012	91.60	90.21	0.82	0.06	1.00	0.05	32.17	20.97
W_2N	0.001	0.014	0.149	2.62	2.50	2.73	0.135	0.012	90.70	90.06	0.37	0.03	0.40	0.03	7.54	6.23
$W_2N(OH)_2$	0.002	0.017	0.201	4.37	4.80	5.70	0.184	0.015	91.50	90.22	1.05	0.07	1.24	0.08	33.09	23.25
W_2NF_2	0.001	0.010	0.110	2.95	2.78	3.14	0.100	0.009	90.99	90.18	0.31	0.02	0.36	0.02	10.01	7.66
W_2NO_2	0.001	0.013	0.151	3.17	3.20	3.69	0.137	0.012	91.23	90.06	0.51	0.04	0.58	0.04	13.81	10.25
$W_2Ti_2C_3O_2$	0.001	0.013	0.158	3.69	3.85	4.59	0.144	0.012	91.45	90.23	0.66	0.05	0.79	0.05	21.43	14.87
$W_2TiC_2O_2$	0.002	0.017	0.210	4.37	4.58	5.62	0.193	0.016	91.79	90.26	1.09	0.07	1.33	0.07	32.28	21.06
$W_2Zr_2C_3O_2$	0.001	0.012	0.136	3.86	3.93	4.50	0.124	0.011	91.34	90.18	0.56	0.04	0.64	0.04	20.53	15.49
W_2ZrC_2	0.001	0.011	0.117	2.28	2.22	2.44	0.106	0.010	90.61	90.02	0.26	0.02	0.29	0.02	6.00	4.89
$W_2ZrC_2O_2$	0.002	0.016	0.195	4.12	4.04	4.98	0.179	0.015	91.75	90.16	0.89	0.06	1.10	0.06	25.34	16.32
W_3C_2	0.002	0.015	0.176	3.62	3.66	4.45	0.161	0.014	91.25	90.11	0.71	0.05	0.87	0.05	20.19	13.42
$W_3C_2(OH)_2$	0.002	0.018	0.188	8.48	8.24	8.75	0.170	0.016	90.36	90.19	1.49	0.13	1.58	0.13	77.10	67.73
$W_3C_2F_2$	0.001	0.009	0.096	4.35	3.95	4.39	0.087	0.008	90.83	90.10	0.38	0.03	0.42	0.03	19.50	15.48
$W_3C_2O_2$	0.001	0.012	0.140	4.10	4.34	5.09	0.128	0.011	91.39	90.08	0.65	0.05	0.76	0.05	26.31	18.95
W_3N_2	0.001	0.010	0.107	2.94	2.99	3.33	0.097	0.009	90.91	90.14	0.32	0.03	0.36	0.03	11.23	8.98
$W_3N_2(OH)_2$	0.002	0.019	0.191	9.08	9.44	9.59	0.172	0.017	90.00	90.18	1.65	0.16	1.68	0.17	92.14	89.46
$W_3N_2F_2$	0.001	0.008	0.087	3.81	4.15	4.47	0.078	0.007	90.71	90.08	0.35	0.03	0.38	0.03	20.18	17.40
$W_3N_2O_2$	0.001	0.011	0.121	4.56	4.77	5.52	0.110	0.010	91.11	90.22	0.61	0.05	0.70	0.05	30.98	22.86
W_4C_3	0.001	0.015	0.175	3.93	4.05	4.65	0.160	0.014	91.29	90.18	0.74	0.06	0.85	0.06	21.95	16.43
$W_4C_3(OH)_2$	0.001	0.009	0.101	3.82	3.93	4.45	0.092	0.008	91.04	90.08	0.41	0.03	0.46	0.03	20.03	15.52
$W_4C_3F_2$	0.001	0.007	0.078	2.98	2.96	3.20	0.071	0.007	90.76	90.20	0.23	0.02	0.24	0.02	10.31	8.77
$W_4C_3H_2$	0.001	0.009	0.100	3.29	3.33	3.74	0.091	0.008	91.05	90.16	0.34	0.03	0.38	0.03	14.13	11.14
$W_4C_3O_2$	0.001	0.010	0.112	3.50	3.51	4.19	0.102	0.009	91.31	90.13	0.43	0.03	0.51	0.03	17.84	12.30
W_4N_3	0.001	0.011	0.117	3.32	3.22	3.53	0.107	0.010	90.81	90.13	0.38	0.03	0.41	0.03	12.57	10.31
$W_4N_3(OH)_2$	0.001	0.010	0.130	4.30	4.51	5.63	0.120	0.009	91.95	90.27	0.67	0.04	0.84	0.04	32.43	20.40
$W_4N_3F_2$	0.001	0.011	0.132	3.96	3.92	4.70	0.120	0.010	91.39	90.13	0.57	0.04	0.68	0.04	22.47	15.37
$W_4N_3H_2$	0.001	0.008	0.083	3.04	3.09	3.39	0.076	0.007	90.84	90.13	0.26	0.02	0.28	0.02	11.63	9.60
$W_4N_3O_2$	0.001	0.009	0.097	2.87	3.01	3.35	0.088	0.008	90.85	90.15	0.29	0.02	0.33	0.03	11.35	9.11
WCrC	0.002	0.022	0.227	1.87	1.99	2.12	0.205	0.019	90.49	89.97	0.44	0.04	0.46	0.04	4.53	4.01
$WCrCO_2$-(model4)	0.002	0.024	0.263	3.17	3.08	3.43	0.239	0.021	90.99	90.07	0.82	0.07	0.92	0.06	11.93	9.43
Y_2C	0.003	0.034	0.353	1.96	1.89	2.05	0.320	0.030	90.48	89.87	0.65	0.06	0.71	0.06	4.23	3.56
$Y_2C(CN)_2$	0.004	0.039	0.453	3.69	3.75	4.34	0.414	0.035	91.39	90.15	1.80	0.13	2.08	0.13	19.09	14.06
$Y_2C(NCO)_2$	0.004	0.044	0.540	4.33	4.45	5.49	0.495	0.040	91.84	90.17	2.72	0.18	3.35	0.18	30.73	19.89
$Y_2C(NCS)_2$	0.018	0.192	1.585	19.83	20.70	17.59	1.393	0.174	87.89	90.51	24.50	3.60	20.81	3.75	302.97	430.51
$Y_2C(OCI)_2$	0.005	0.052	0.731	5.15	5.50	7.73	0.679	0.047	92.85	90.32	5.24	0.26	7.37	0.28	61.63	30.45
$Y_2C(OCN)_2$	0.005	0.046	0.580	4.59	4.72	5.99	0.534	0.042	92.02	90.25	3.20	0.20	4.06	0.20	36.75	22.35
$Y_2C(OH)_2$	0.002	0.025	0.268	2.47	2.44	2.65	0.243	0.023	90.63	90.06	0.64	0.06	0.70	0.05	7.09	5.93

$Y_2C(SCN)_2$	0.006	0.063	0.829	6.76	6.99	9.42	0.766	0.057	92.41	90.26	7.21	0.40	9.71	0.41	91.24	49.09
Y_2CBr_2	0.004	0.045	0.582	4.71	4.82	6.34	0.537	0.041	92.26	90.25	3.41	0.20	4.48	0.20	41.29	23.31
Y_2CCl_2	0.005	0.055	0.696	4.47	4.51	5.81	0.641	0.050	92.06	90.18	3.72	0.22	4.79	0.23	34.60	20.40
Y_2CF_2	0.003	0.030	0.318	2.58	2.61	2.81	0.288	0.027	90.68	90.12	0.81	0.07	0.87	0.07	7.94	6.81
Y_2CO_2	0.005	0.047	0.514	3.49	3.62	4.04	0.467	0.042	90.89	90.12	1.89	0.15	2.11	0.16	16.54	13.15
Y_2N	0.003	0.028	0.297	1.70	1.78	1.90	0.269	0.026	90.46	90.08	0.51	0.05	0.55	0.05	3.65	3.18
$Y_2N(OH)_2$	0.002	0.024	0.261	2.46	2.51	2.74	0.237	0.022	90.77	90.06	0.65	0.05	0.71	0.06	7.61	6.32
Y_2NF_2	0.002	0.025	0.266	2.42	2.36	2.56	0.241	0.022	90.72	89.98	0.62	0.05	0.67	0.05	6.59	5.56
Y_2NO_2	0.004	0.042	0.452	3.38	3.37	3.65	0.410	0.038	90.72	90.17	1.50	0.13	1.62	0.13	13.46	11.33
Y_3C_2	0.002	0.021	0.229	2.57	2.56	2.82	0.208	0.019	90.72	90.06	0.59	0.05	0.65	0.05	8.03	6.54
$Y_3C_2(OH)_2$	0.002	0.021	0.212	4.03	3.93	4.05	0.191	0.019	90.09	90.01	0.77	0.07	0.79	0.07	16.44	15.41
$Y_3C_2F_2$	0.002	0.020	0.219	3.14	3.23	3.56	0.199	0.018	90.73	90.07	0.71	0.06	0.78	0.06	12.80	10.45
$Y_3C_2O_2$	0.002	0.023	0.247	4.33	4.25	4.72	0.224	0.021	90.75	90.07	1.06	0.09	1.18	0.09	22.55	18.02
Y_3N_2	0.002	0.018	0.196	2.31	2.36	2.54	0.177	0.016	90.70	90.11	0.45	0.04	0.49	0.04	6.49	5.56
$Y_3N_2(OH)_2$	0.002	0.023	0.246	4.27	4.26	4.65	0.224	0.021	90.73	90.08	1.04	0.09	1.13	0.09	21.83	18.17
$Y_3N_2F_2$	0.002	0.020	0.221	3.55	3.40	3.80	0.201	0.018	90.94	90.09	0.76	0.06	0.85	0.06	14.62	11.50
$Y_3N_2O_2$	0.002	0.020	0.214	3.75	3.77	4.18	0.194	0.018	90.72	90.15	0.81	0.07	0.90	0.07	17.70	14.21
Y_4C_3	0.002	0.022	0.236	2.66	2.74	2.90	0.214	0.020	90.62	90.13	0.62	0.05	0.66	0.06	8.46	7.51
$Y_4C_3(OH)_2$	0.002	0.016	0.166	3.67	3.79	3.90	0.149	0.015	90.12	90.05	0.58	0.06	0.60	0.06	15.24	14.38
$Y_4C_3F_2$	0.002	0.018	0.191	3.47	3.50	3.81	0.174	0.016	90.83	90.10	0.66	0.06	0.72	0.06	14.63	12.25
$Y_4C_3O_2$	0.003	0.028	0.348	4.93	4.91	6.09	0.320	0.025	91.89	90.15	1.94	0.12	2.41	0.12	37.83	24.14
Y_4N_3	0.002	0.018	0.184	2.27	2.15	2.29	0.166	0.016	90.31	90.07	0.38	0.03	0.41	0.03	5.30	4.59
$Y_4N_3(OH)_2$	0.002	0.015	0.164	3.29	3.23	3.53	0.149	0.014	90.63	90.08	0.53	0.04	0.57	0.04	12.59	10.42
$Y_4N_3F_2$	0.002	0.021	0.233	3.53	3.46	3.89	0.212	0.019	91.06	90.09	0.82	0.06	0.93	0.06	15.35	11.91
$Y_4N_3O_2$	0.002	0.018	0.199	3.19	3.32	3.73	0.181	0.016	91.01	90.12	0.67	0.05	0.76	0.06	14.05	11.08
$YCrC(NCO)_2$	0.005	0.047	0.604	4.70	4.85	6.18	0.556	0.043	92.16	90.21	3.44	0.21	4.39	0.21	39.11	23.55
$YCrC(NCS)_2$	0.018	0.192	2.070	16.73	17.82	19.99	1.877	0.174	90.72	90.80	37.52	3.11	42.08	3.31	404.50	319.71
$YCrC(OCN)_2$	0.005	0.053	0.724	5.37	5.54	7.40	0.671	0.048	92.67	90.25	4.97	0.27	6.63	0.27	56.21	30.79
$YCrC(OH)_2$	0.003	0.034	0.390	3.23	3.36	3.83	0.355	0.031	91.16	90.14	1.36	0.10	1.55	0.11	14.84	11.31
$YCrCBr_2$	0.006	0.062	0.969	6.70	6.54	10.37	0.907	0.056	93.61	90.38	9.41	0.37	14.93	0.36	112.08	42.60
$YCrCCl_2$	0.007	0.071	0.984	5.33	5.48	7.69	0.913	0.064	92.76	90.19	7.02	0.35	9.85	0.36	61.06	30.15
$YCrCF_2$	0.004	0.036	0.396	2.95	3.05	3.41	0.360	0.032	90.94	90.12	1.23	0.10	1.37	0.10	11.78	9.36
$YHfN(SCN)_2$	0.005	0.047	0.669	6.71	6.75	9.81	0.622	0.043	92.97	90.34	6.10	0.29	8.87	0.29	99.60	45.53
$YHfNO_2$	0.002	0.019	0.212	2.92	2.83	3.14	0.193	0.017	90.91	90.09	0.61	0.05	0.67	0.05	9.98	7.98
$YMoN(NO)_2$	0.002	0.025	0.260	2.43	2.46	2.64	0.235	0.022	90.54	90.11	0.62	0.05	0.67	0.06	7.04	6.06
$YNbCO_2$	0.003	0.032	0.347	2.84	2.84	3.14	0.315	0.029	90.81	90.07	0.99	0.08	1.09	0.08	9.97	8.07
$YTaCO_2$	0.000	0.000	0.004	2.76	2.87	3.12	0.004	0.000	90.73	90.13	0.01	0.00	0.01	0.00	9.85	8.26
$YTiN(NO)_2$	0.003	0.032	0.346	2.81	2.80	3.01	0.314	0.029	90.70	90.11	0.94	0.08	1.01	0.08	9.13	7.84
$YTiNO_2$	0.003	0.031	0.335	2.69	2.75	3.05	0.304	0.028	90.87	90.07	0.93	0.08	1.03	0.08	9.42	7.60
$YVCO_2$	0.004	0.037	0.400	2.85	2.72	3.03	0.363	0.033	90.79	90.00	1.10	0.09	1.23	0.09	9.32	7.34
$YVNF_2$	0.003	0.029	0.319	2.53	2.69	2.97	0.290	0.026	90.94	90.13	0.86	0.07	0.95	0.07	8.91	7.27
$YZrNO_2$	0.003	0.027	0.297	2.74	2.88	3.22	0.270	0.024	90.86	90.15	0.87	0.07	0.97	0.07	10.51	8.33
Zr_2C	0.003	0.035	0.370	2.14	2.27	2.40	0.335	0.032	90.48	90.19	0.80	0.07	0.85	0.08	5.82	5.19

$Zr_2C(OH)_2$	0.002	0.025	0.271	2.86	2.79	3.10	0.246	0.022	90.90	89.96	0.76	0.06	0.85	0.06	9.72	7.74
Zr_2CF_2	0.002	0.023	0.250	2.36	2.34	2.58	0.226	0.021	90.69	90.05	0.58	0.05	0.64	0.05	6.72	5.46
Zr_2CF_2-(model2)	0.003	0.027	0.300	2.66	2.74	3.02	0.272	0.025	90.84	90.09	0.82	0.07	0.91	0.07	9.20	7.52
Zr_2CF_2-(model3)	0.004	0.038	0.406	2.85	2.73	2.92	0.368	0.035	90.56	89.97	1.07	0.09	1.14	0.09	8.56	7.43
Zr_2CO_2	0.003	0.033	0.363	3.00	3.01	3.32	0.329	0.030	90.77	90.14	1.09	0.09	1.21	0.09	11.17	9.09
Zr_2CrCN	0.004	0.041	0.472	3.92	4.06	4.72	0.431	0.037	91.23	90.18	2.03	0.15	2.37	0.16	22.65	16.52
Zr_2CrCNO_2	0.003	0.028	0.336	4.17	4.36	5.37	0.308	0.025	91.67	90.18	1.65	0.11	2.04	0.12	29.49	19.13
Zr_2HfCN	0.002	0.024	0.259	3.31	3.39	3.72	0.235	0.021	90.86	90.19	0.87	0.07	0.96	0.07	13.94	11.52
Zr_2HfCNO_2	0.002	0.019	0.219	3.90	4.23	4.87	0.200	0.017	91.36	90.23	0.97	0.07	1.12	0.08	24.01	18.08
Zr_2MoCN	0.003	0.033	0.368	3.57	3.72	4.24	0.335	0.029	91.10	90.06	1.42	0.11	1.62	0.11	18.26	13.88
Zr_2MoCNO_2	0.002	0.024	0.278	4.07	4.19	5.14	0.255	0.021	91.51	90.06	1.31	0.09	1.60	0.09	26.94	17.63
Zr_2N	0.003	0.028	0.297	1.96	1.92	2.09	0.269	0.025	90.50	90.17	0.56	0.05	0.61	0.05	4.41	3.70
$Zr_2N(OH)_2$	0.002	0.024	0.259	2.76	2.75	3.10	0.235	0.021	90.87	90.04	0.73	0.06	0.82	0.06	9.71	7.56
Zr_2NbCN	0.003	0.033	0.367	3.74	3.74	4.24	0.335	0.029	91.13	90.11	1.42	0.11	1.61	0.11	18.20	14.02
Zr_2NbCNO_2	0.002	0.024	0.283	3.96	4.29	5.09	0.259	0.022	91.51	90.17	1.32	0.09	1.57	0.10	26.41	18.57
Zr_2NF_2	0.002	0.021	0.228	2.26	2.21	2.41	0.207	0.019	90.60	90.13	0.50	0.04	0.54	0.04	5.85	4.89
Zr_2NF_2-(model2)	0.003	0.034	0.363	2.82	2.82	3.08	0.329	0.030	90.69	89.97	1.01	0.09	1.10	0.09	9.56	7.95
Zr_2NF_2-(model4)	0.002	0.025	0.273	2.76	2.70	2.97	0.248	0.022	90.90	90.06	0.74	0.06	0.81	0.06	8.90	7.26
Zr_2NO_2	0.003	0.028	0.300	2.85	2.68	2.94	0.272	0.025	90.78	90.04	0.80	0.07	0.88	0.06	8.75	7.15
Zr_2TaCN	0.000	0.001	0.006	3.59	3.64	4.11	0.005	0.000	91.00	90.15	0.02	0.00	0.03	0.00	17.07	13.27
Zr_2TaCNO_2	0.000	0.000	0.005	3.81	4.21	4.98	0.005	0.000	91.51	90.15	0.02	0.00	0.03	0.00	25.22	17.95
Zr_2TiCN	0.004	0.040	0.452	3.71	3.86	4.42	0.412	0.036	91.14	90.10	1.82	0.14	2.08	0.14	19.81	14.97
Zr_2TiCNO_2	0.003	0.028	0.330	4.55	4.26	5.16	0.302	0.025	91.58	90.18	1.56	0.11	1.88	0.10	27.10	18.00
Zr_2VCN	0.004	0.039	0.441	3.65	3.80	4.35	0.402	0.035	91.10	90.19	1.75	0.13	2.00	0.14	19.18	14.47
Zr_2VCNO_2	0.003	0.027	0.323	4.09	4.26	5.05	0.296	0.025	91.53	90.20	1.49	0.11	1.77	0.11	25.90	18.25
Zr_3C_2	0.003	0.028	0.295	2.84	2.87	3.07	0.267	0.025	90.62	90.07	0.82	0.07	0.88	0.07	9.49	8.23
$Zr_3C_2(OH)_2$	0.002	0.021	0.219	3.89	4.00	4.25	0.198	0.019	90.44	90.07	0.84	0.08	0.89	0.08	18.16	16.03
$Zr_3C_2F_2$	0.002	0.017	0.186	2.93	2.91	3.22	0.169	0.015	90.82	89.99	0.55	0.04	0.60	0.04	10.51	8.47
$Zr_3C_2H_2$	0.001	0.014	0.143	2.52	2.66	2.89	0.130	0.012	90.49	90.14	0.37	0.03	0.41	0.03	8.44	7.13
$Zr_3C_2O_2$	0.002	0.024	0.272	3.63	3.74	4.21	0.248	0.022	91.19	90.21	1.04	0.08	1.18	0.08	17.97	14.01
Zr_3CN	0.003	0.031	0.336	3.25	3.40	3.76	0.305	0.028	90.88	90.08	1.15	0.09	1.27	0.10	14.28	11.64
Zr_3CNO_2	0.003	0.028	0.341	4.18	4.51	5.45	0.313	0.025	91.75	90.28	1.71	0.11	2.07	0.12	30.30	20.47
$Zr_3N_2(OH)_2$	0.002	0.020	0.213	4.40	4.44	4.67	0.192	0.018	90.45	90.06	0.90	0.08	0.95	0.08	21.98	19.73
Zr_3N_2	0.002	0.019	0.203	2.37	2.42	2.53	0.184	0.017	90.63	89.91	0.46	0.04	0.49	0.04	6.45	5.85
$Zr_3N_2F_2$	0.001	0.014	0.151	3.00	2.83	3.07	0.137	0.013	90.75	90.04	0.42	0.04	0.46	0.03	9.50	7.94
$Zr_3N_2H_2$	0.001	0.014	0.144	2.74	2.75	2.97	0.131	0.012	90.54	90.11	0.39	0.03	0.42	0.03	8.90	7.55
$Zr_3N_2O_2$	0.002	0.021	0.230	3.32	3.31	3.85	0.209	0.019	91.03	90.14	0.81	0.06	0.94	0.06	15.10	10.94
Zr_4C_3	0.002	0.023	0.244	3.07	3.01	3.29	0.222	0.020	90.78	90.10	0.73	0.06	0.80	0.06	10.96	9.06
$Zr_4C_3(OH)_2$	0.002	0.016	0.168	3.70	3.76	4.07	0.152	0.014	90.54	90.12	0.62	0.05	0.67	0.05	16.69	14.17
$Zr_4C_3F_2$	0.001	0.014	0.153	2.84	3.02	3.27	0.138	0.013	90.73	90.09	0.45	0.04	0.49	0.04	10.78	9.19
$Zr_4C_3H_2$	0.002	0.016	0.175	3.50	3.41	3.87	0.159	0.014	91.02	90.14	0.62	0.05	0.70	0.05	15.16	11.57
$Zr_4C_3O_2$	0.002	0.020	0.229	3.85	3.84	4.52	0.209	0.018	91.38	90.15	0.95	0.07	1.12	0.07	20.81	14.70
Zr_4N_3	0.002	0.015	0.161	2.38	2.39	2.53	0.146	0.014	90.45	90.06	0.37	0.03	0.39	0.03	6.43	5.69

$Zr_4N_3(OH)_2$	0.001	0.015	0.154	3.59	3.67	4.01	0.140	0.013	90.56	90.02	0.56	0.05	0.61	0.05	16.25	13.49
$Zr_4N_3F_2$	0.001	0.012	0.126	2.69	2.70	2.93	0.114	0.011	90.65	90.06	0.33	0.03	0.36	0.03	8.67	7.27
$Zr_4N_3O_2$	0.002	0.017	0.185	3.42	3.40	3.86	0.169	0.015	91.08	90.11	0.65	0.05	0.74	0.05	15.07	11.59
$ZrCrNO_2$	0.003	0.030	0.330	2.79	2.88	3.24	0.300	0.027	90.94	90.11	0.97	0.08	1.09	0.08	10.66	8.35
$ZrHfCO_2$	0.002	0.019	0.206	2.94	2.72	3.06	0.187	0.017	90.88	90.02	0.57	0.05	0.64	0.04	9.51	7.33
$ZrMoCO_2$	0.002	0.023	0.249	2.37	2.42	2.61	0.226	0.021	90.75	90.07	0.59	0.05	0.63	0.05	6.84	5.89

APPENDIX D: Publications Made within The Scope of this Thesis

- Massoumılari Ş., Doğancı M., Velioğlu S., (2022), “In silico discovery of MXene family for H_2 purification and CO_2 capture”, in preparation.

- Massoumılari Ş., Velioğlu S., (2022), “Potential of MXene adsorbents and membranes for environmental remediation”, in preparation.